Studies of the cosmic radiation using a neutron monitor

I. A. Jenkins

STUDIES OF THE COSMIC RADIATION USING A NEUTRON MONITOR

by

I.A. Jenkins B.Sc.

A thesis submitted to the University of Durham in accordance with the regulations for admittance to the Degree of Doctor of Philosophy.

Department of Physics,
University of Durham.

April, 1974.

C O N T E N T S

ABSTRACT

This thesis is concerned with the production of evaporation neutrons in neutron monitors by the charged particle components of the cosmic radiation at sea level and their detection.

The evaporation neutron detection efficiency of a modified IGY - type monitor is measured using a novel technique which uses stopping negative muons as a source of neutrons, and the result is compared with that expected from previous measurements of other monitors.

Use is made of this result in an experimental study of neutron production by unaccompanied cosmic ray protons, pions and muons in the momentum range 1-30 GeV/c. The experiment has employed an air-gap magnet spectrograph in conjunction with the monitor, and the results of this study are compared with previous work. They confirm previous findings that the yield of evaporation neutrons in monitors from protons and pions is significantly overestimated by the only available theoretical model, and suggestions are made to account for this discrepancy. Within fairly large statistical errors, the measured neutron production by fast muons agrees with the theoretical predictions.

An examination is made of the possibility of using a neutron monitor in conjunction with an air shower detection array to measure the changes in slope of the nuclear active particle (NAP) energy spectrum in extensive air showers (EAS) of energy 10^{17}eV at sea level which may arise due to primary particles of different atomic mass number and fluctuations in the longitudinal development of proton induced showers. Using NAP spectra predicted by a

mathematical model of the EAS development it is found that monitors of conventional design are unlikely to be sensitive to these changes although the total neutron yield per shower could be used as a measure of the expected differences in the NAP flux.

CHAPTER ONE

INTRODUCTION

1-1 General Introduction

There are principally two aspects of research into the cosmic radiation; that concerned with it s production and propagation outside the earth's atmosphere, the astrophysical or origin aspect in which the radiation is used as a tool for investigating a wider range of phenomena and that concerned with it s interaction within the earth's environment, the nuclear or atomic physics aspect, in which the properties of the radiation are of primary interest.

Now, as in the past, cosmic rays offer a unique source of elementary particles for studying interactions of the very highest energy. (The highest energies attainable by artifical acceleration, at present, is $\sim 2 \times 10^{12}$eV). Amongst the energetic cosmic rays are the nuclear active particles (NAPs) which are defined as those particles which interact through the strong nuclear interaction, and include neutrons, protons and pions. The other two main groups of particles constituting the radiation are the soft component (electrons, positrons and photons) and the mu-meson component. Studies of NAPs are of particular importance because of the relatively unknown nature of the strong interaction compared with the electro-magnetic interaction. On the other hand, studies of the electromagnetic interaction between muons and nuclei are also of considerable interest because they give information about the nuclear structure. In both these contexts, the study of the "evaporation" process resulting from interactions between NAPs or muons and nuclei has proved to be a powerful tool.

The charged particle component of the primary cosmic radiation is known to consist principally of atomic nuclei (and in particular hydrogen) and studies of the NAP component of cosmic rays in the atmosphere are likely to yield the most direct evidence on the nature of this primary radiation. A feature of the primary radiation is it s very wide range of energies from about 10^8eV to 10^{20}eV and a consequence of this is that many different techniques are necessary to investigate the properties of the radiation. For energies up to 10^{13}eV, the rate of primaries is sufficiently high to warrant direct studies using satellites and air-borne detectors. Above this point however use has to be made of the magnification effect of large showers of electrons and photons produced after interactions of the primaries with the air nuclei. These showers cover a wide area and can be detected at sea level using arrays of particle detectors. In addition to these extensive air showers (EAS) at sea level, there is a residual flux of cosmic rays resulting from primaries of less energy. At the very lowest energies this flux is subject to considerable variations in time due to the interaction of the primary radiation with, for example, the magnetic fields of the earth and the interplanetary space. Some of these variations have a periodicity of very low frequency ($\sim$ years) and studies of them require stable measuring devices. Ground based detectors have proved themselves suitable for this purpose: the neutron monitor is one such device and is the central concern of this thesis.

1-2 The Development of the Neutron Monitor

This device owes its existence to the observation that a flux of fast neutrons (of energy around 100 MeV) is present in the earth's atmosphere. Since these particles are unstable it was realised that they could not be primary cosmic rays but rather the products of interactions

in the atmosphere. Much of the pioneer work on the origin of these neutrons was carried out by Tongiorgi in the late 1940's using a thermal neutron detector (a Boron Tri-flouride (BF_3) proportional counter), surrounded by a medium to slow them down to thermal energies (some hydrogenous material), and by a target material to simulate the atmospheric production medium. This work established that fast neutrons are produced in successive interactions between the primary radiation and air nuclei and that these neutrons, together with the rest of the NAP component, were responsible for the production of moderate energy (~10 MeV) neutrons via subsequent interactions with other nuclei.

The resulting extra-nuclear cascade was studied quantitatively by Cocconiet al.(1950, 1951) who pointed out that the moderate energy neutrons produced at each stage of the cascade could give information about the development through a thick absorber. Comparison of the measured neutron multiplicity distribution (the distribution of the number of neutrons detected per detected interaction) in a variety of thin absorbers with the observed prong distributions in emulsions revealed that the same mechanism that produces the stars in emulsions was also principally responsible for the production of moderate energy neutrons.

The realisation by Simpson (1948, 1949) that the continuous monitoring of moderate energy neutrons at sea level and at mountain altitudes could give information about the time variations of the low energy (a few GeV) part of the primary spectrum lead to the first installation of a neutron monitor, in 1952. The design followed closely that used by Tongiorgi in that BF_3 counters surrounded by producer and moderator were used for local production and moderation of neutrons. Simpson et al.(1953) demonstrated the need for a protective shield

of moderating material around the monitor to isolate it from the producing and moderating effects of the immediate environment.

A standard monitor for use during the International Geophysical Year was designed by Simpson (1957). This will be referred to here as the SIGY monitor.

A network of these, or very similar, monitors was built up over the world during the ensuing years and has given considerable information about the primary particles and their interaction with the solar system, in the two decades of energy above 1 GeV (Webber, 1962).

A major step in neutron monitor design was made in 1964 when the NM64 high counting rate monitor was introduced. This device ensured an important and continuing role for the neutron monitor for some years to come, in the study of the interaction of the primary radiation with the inter-planetary magnetic field.

1-3 The Response of the Neutron Monitor

It was not until 1964, or well after the IGY type monitors had been established and their results interpreted, that a detailed study of the response of a neutron monitor to the various components of cosmic rays was begun (Hughes et al., 1964) using a monitor of a design developed in the University of Leeds. This IGY type monitor will be referred to as the LIGY. The study involved measuring the neutron detection efficiency of the monitor, and operating it in conjunction with a cosmic ray magnet spectrograph. By measuring the average multiplicity of neutrons detected in the monitor when NAPs of various energies interact in the producing layer, the average number of produced neutrons per interacting NAP in a monitor was found as a function of the NAP energy. It was found that the neutron detection efficiency was low (a few percent) and that the

average multiplicity produced by a 1 GeV proton was about 20 and rose slowly with energy. The same group also studied the production of neutrons by the electro-magnetic nuclear interaction of muons in the lead producer of the monitor.

The results of this work were used by Hughes and Marsden (1966) to calculate the contributions to the total counting rate of a monitor at sea level, made by the various cosmic ray components. They showed that fast neutrons of energy of about 100 MeV were responsible for the vast majority of the produced neutrons, but that protons, pions, muons and EAS particles gave small contributions.

Theoretical interpretations of star production stem from the model suggested by Serber (1947) in which the interaction between the NAP and the nucleus is assumed to take place in two stages; the intra-nuclear cascade within the nucleus, followed by the so called "evaporation" of moderate energy nucleons (principally neutrons but also charged particles) from the excited nucleus in conjunction with the emission of gamma rays. The heavy tracks in the observed star are caused by the evaporation charged particles, mainly protons. The available data on neutron production in single interactions of NAPs with nuclei, were taken by Shen (1968) to predict the neutron yield per incident NAP in lead targets of various thicknesses by using a Monte Carlo computational technique to simulate the extra-nuclear cascade through the target. He found it necessary however, to hypothesise a reduction of 50% in the nominal efficiency of the monitor measured by Hughes et al. in order to obtain agreement with their experimental results.

A comprehensive review of the design and the response of neutron monitors has been given by Hatton (1971) and he pointed out that Shen's hypothesis may not be justified. Although the neutron detection efficiency

may decrease for higher NAP energies, the discrepency between Shen's prediction and the original results of Hughes et al, may be too large to be accounted for by this. This would imply an error in Shen's work.

An important conclusion from Shen's work that is probably not invalidated by the inconsistency between the results of the calculations and the experiment, is that the (exponential) form of the produced neutron multiplicity distribution remains unchanged at high cosmic ray energies, and that the average multiplicity increases monotonically with energy for monitors having producer thicknesses greater than or equal to the IGY and NM64 thickness (150 g cm^{-2} of lead).

It had been suggested by Hughes and Marsden, that the neutron multiplicity distribution measured by a monitor could give information about the time variations of the primary energy spectrum up to at least 100 GeV. They showed that the energy spectrum of NAPs incident on the monitor was directly related to the measured multiplicity distribution and then used a simple model for the interactions of the primary particle in the atmosphere to relate the primary energy spectrum to the sea level spectrum. However, the results from a more sophisticated model (Kodama and Ohuchi, 1968) have been used to show that the fluctuations of the interactions in the atmosphere severely limit the sensitivity of sea level spectrum measurements to changes in the primary spectrum (Hatton 1971).

Although the multiplicity distribution may not give as much information about the steep low energy primary spectrum as at first hoped, Shen's results indicate that the multiplicity distribution measured in EAS could in principle give information about the relatively flat NAP energy spectrum up to very high energies.

1-4 The Present Work

An important aspect of the present work is concerned with the possibility of extending the use of a neutron monitor as an energy measuring device to studies of NAPs in EAS, along the lines outlined above. It has been shown (Hook et al.1970) that the measured average multiplicity of an IGY type monitor arising from NAPs in EAS is greater than that found for unaccompanied NAPs in the cosmic ray beam. This would be expected from the harder NAP energy spectrum found in EAS. Since the probability of a higher multiplicity is larger in EAS, it is possible that the resulting increase in statistical accuracy could enable the shape of the multiplicity distribution measured by a neutron monitor to give information about the shape of the NAP energy spectrum producing the neutrons.

An IGY type monitor has been built in Durham for use in EAS in conjunction with a large magnet spectrograph. This will be referred to as the DIGY monitor. The principal aim of the experiment was to measure the energy spectrum of NAPs directly with the spectrograph, using the monitor as an NAP detector. Unfortunately, as reported by Hook (1972), it proved difficult to identify the tracks of many NAPs in the spectrograph and so allow momentum analysis due to the obscuration caused by the prolific electron-photon component.

However, in view of the uncertainties raised by the work of Shen in relation to the results of Hughes et al.,for the basic performance of monitors, it was thought worthwhile to repeat the earlier experiments to determine the variation of the average neutron multiplicity with NAP energy.

A novel method of measuring the neutron detection efficiency of the DIGY monitor is described (Chapter 3) and the result of the measurement is compared with other measurements. The neutron production by protons and pions is measured and compared with the previous work (Chapter 4) and conclusions are then

drawn in the light of recent calculations of the intra-nuclear cascade/evaporation processes and of the variation of neutron detection efficiency with NAP energy (Chapter 2).

A further topic of considerable current interest is the neutron production by muons at high energies. Although the present experiment was not originally designed for this work, an attempt is made in the work reported in Chapter 5 to measure the probability of neutron production by the muons recorded during the study of NAPs described in Chapter 4, and the results are compared with the earlier experiment of Meyer et al. (1964) and others, over the low energy region where the neutron production mechanism is fairly well understood.

Finally the feasibility of using a neutron monitor in conjunction with an EAS array is considered (Chapter 6), with particular reference to estimating the NAP component and thus the stage of development of showers of energy 10^{17}eV.

Preliminary results of the experimental work described in this thesis are given in Diggory et al. (1971), Dixon et al. (1971) and Hook et al.(1971).

CHAPTER TWO

THE PRODUCTION AND DETECTION OF EVAPORATION NEUTRONS IN A NEUTRON MONITOR

2-1 NEUTRON PRODUCTION

2-1.1 Introduction

The production of evaporation neutrons, from a nucleus involves a two stage process. In the first stage, the excitation stage, an incident particle interacts with the nucleus leaving it in an excited state. The nucleus subsequently de-excites in the second stage, the evaporation stage, principally by emitting nucleons, mainly neutrons. The detection of these evaporation neutrons, provides information about the incident particle and its interaction.

Of all the evaporation neutrons produced in a neutron monitor, most have resulted from interactions by cosmic ray nucleons, and so it is particularly important to understand how nucleons interact with nuclei of various types.

Although the evaporation process is responsible for the majority of detected neutrons, slow cascade and fission neutrons resulting from the initial interaction can also contribute and must be allowed for in interpreting the neutron monitor response.

2-1.2 Neutron Production by Nucleons having energy less than 2 GeV

In the first stage the nucleon loses energy in a cascade within a nucleus, from which cascade nucleons and secondary pions are emitted with energies ranging up towards the initial nucleon energy. A model for this intra-nuclear cascade was suggested by Serber (1947). Monte Carlo calculations based on this model (Metropolis et al. 1958a,b) and Bertini (1963, 1969, 1971, 1972) have been carried out for incident energies up to a few GeV and for a variety of target nuclei having mass numbers in the range $25 \leq A \leq 238$ to predict the numbers and

energy spectra of the emitted cascade particles, and also the excitation energy spectra and other properties of the residual nuclei. Although the calculations of Bertini (1969) incorporated various refinements in the nuclear model such as the diffuseness of the nucleus and allowances for motion of bound nucleons in local potentials, considerable agreement was found with the earlier calculations made in 1958. Of immediate interest in the present work is the relation between incident proton energy and the average excitation energy of the target nucleus, fig. 2.1a, this being the initial condition for the second stage.

The evaporation process was first postulated by Weisskopf (1937) whose ideas were subsequently extended by Le Couteur (1950, 1952). The Fermi gas model of the nucleus has been successful in explaining the features of this process. In these treatments each emitted nucleon leaves the nucleus by virtue of a suitable random fluctuation in its kinetic energy which is sufficiently large to overcome the attractive potential towards the nucleus. After each nucleon has been emitted the nucleus 'cools down' by an amount appropriate to the energy removed by the nucleon, and this will tend to lower the energy of subsequent nucleons. The Monte Carlo method is highly suitable for computing the mean produced numbers and energy spectra of evaporation particles, and has been used by Dostrovsky et al. (1958) for a variety of nuclei having a range of initial excitations from 100 to 700 MeV. Some of their results are shown in fig. 2.1b. Due to the uncertainty in the nuclear model, the energy level density parameter α, which relates the initial nuclear excitation U to the average kinetic energy of the emitted nucleons, was left as a variable and the results given for the extreme values A/10 and A/20 where A is the nuclear mass number. Experimentally

FIG. 2)a

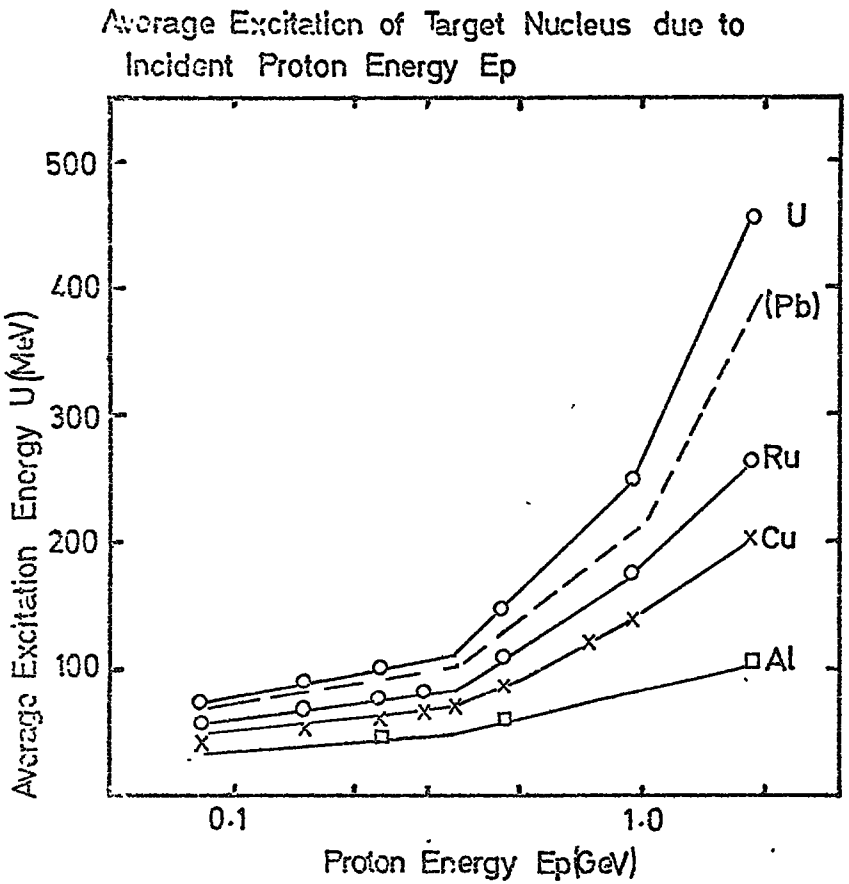
Average Excitation of Target Nucleus due to Incident Proton Energy Ep
Average Excitation Energy U(MeV)
500
400
300
200
100
0·1
1·0
Proton Energy Ep(GeV)
U
(Pb)
Ru
Cu
Al

FIG. 2)b

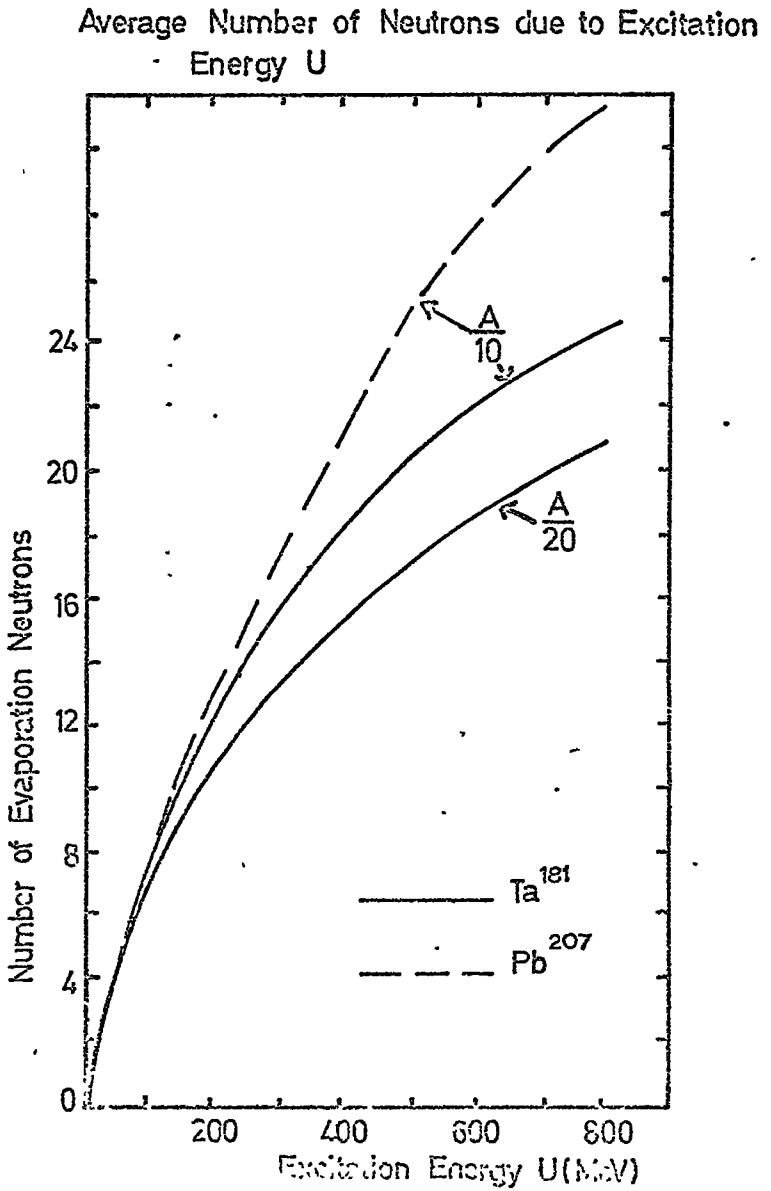
Average Number of Neutrons due to Excitation Energy U
Number of Evaporation Neutrons
24
20
16
12
8
4
0
200
400
600
800
Excitation Energy U(MeV)
A/10
A/20
Ta181
Pb207

(Newton, 1956) and theoretically (Ramamurthy, 1970; Baba, 1970) the high value tends to be preferred although most of the evidence comes from low energy work ($U \lesssim 30$ MeV).

Bercovitch et al. (1960) have measured the average produced neutron multiplicities for proton interactions in thin targets (22 to 44 g cm^{-2}) for various (wide) ranges of proton energy and mass number of target nuclei. In order to compare their results with the combined calculations of Metropolis and Dostrovsky, they found it necessary to correct their measurements for the additional neutrons produced by secondary particles in extra-nuclear cascades through the finite thickness of target. Their corrected results agree with the theoretical prediction particularly if $\alpha = A/20$ is assumed (fig. 2.2a).

The neutron production due to the initial proton interaction alone, has been measured by Vasil'kov et al. (1968) who used $\lesssim 1$ cm thickness of various target materials. The results for 5 g cm^{-2} of lead are shown in fig. 2.2a. together with the corrected results of Bercovitch et al. and the predicted values of Metropolis/Dostrovsky (neglecting slow cascade neutrons). Taken together the two experiments cannot resolve the two theoretical predictions using $\alpha = A/10$ and $A/20$.

Bertini (1972) has extended the Metropolis/Dostrovsky calculations and has calculated the total low energy yield (evaporation and cascade products) expected in the Vasil'kov experiment, using the high value of α. Although the predicted neutron yield agrees fairly well with the experimental results for most of the target nuclei, the prediction for lead is somewhat overestimated (fig. 2.2a).

The predicted evaporation products and residual nuclei were compared with experimental radio-chemical and photographic emulsion results and this revealed some significant differences, particularly

Fig. 2.2 Neutron Production in Proton-Pb Interactions

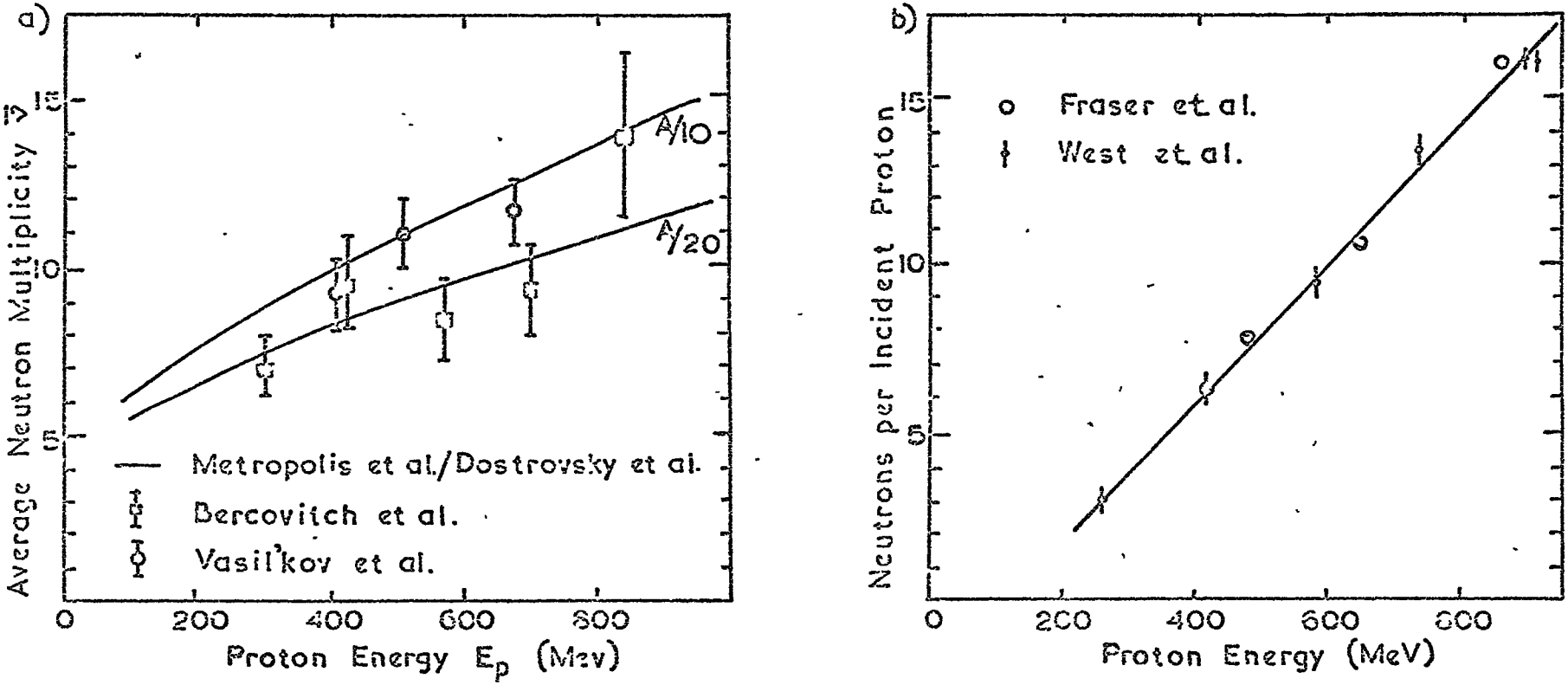

for heavy nuclei. In particular it was evident from both comparisons that the yield of alpha particles and other heavy charged particles was grossly underestimated by the nuclear model. Two reasons were suggested. Direct knockout of alpha particles in the cascade process was not taken into account (Barashenkov, 1969) and the large angular momentum imparted to large nuclei by the incident nucleon which would tend to evaporate more heavy nuclei was not allowed for in the evaporation model (Gilat and Grover, 1971). The size of the discrepancy could mean that the results for neutron production should be about 20% less over the energy range shown in fig. 2.2a. This would result in the calculations predicting a slightly lower neutron yield than that observed by Vasil'kov.

The available experimental data on neutron production in thin targets was summarized by Fraser et al (1965) for comparison with the measured neutron production by $\lesssim$1 GeV protons in very thick targets (where the proton is totally absorbed). A further experiment of the same type by West and Wood (1971) using a beam of protons from a syncrotron incident on a 60 cm thick lead target, has measured very accurately the average neutron yield per incident proton. The two sets of experimental results are shown in fig. 2.2b to be in very good agreement. The calculations derived from the (less accurate) thin target experiments are generally 10-20% higher than those shown, indicating that the results of Vasil'kov are overestimates by this amount. Although the theoretical model of Bertini may be capable of predicting this lower yield with the above mentioned modifications, no detailed calculations have been performed to date.

The Monte Carlo calculations also predict the energy spectrum of the evaporation particles and these are compared in fig. 2.3a,b and c

FIG. 2-3

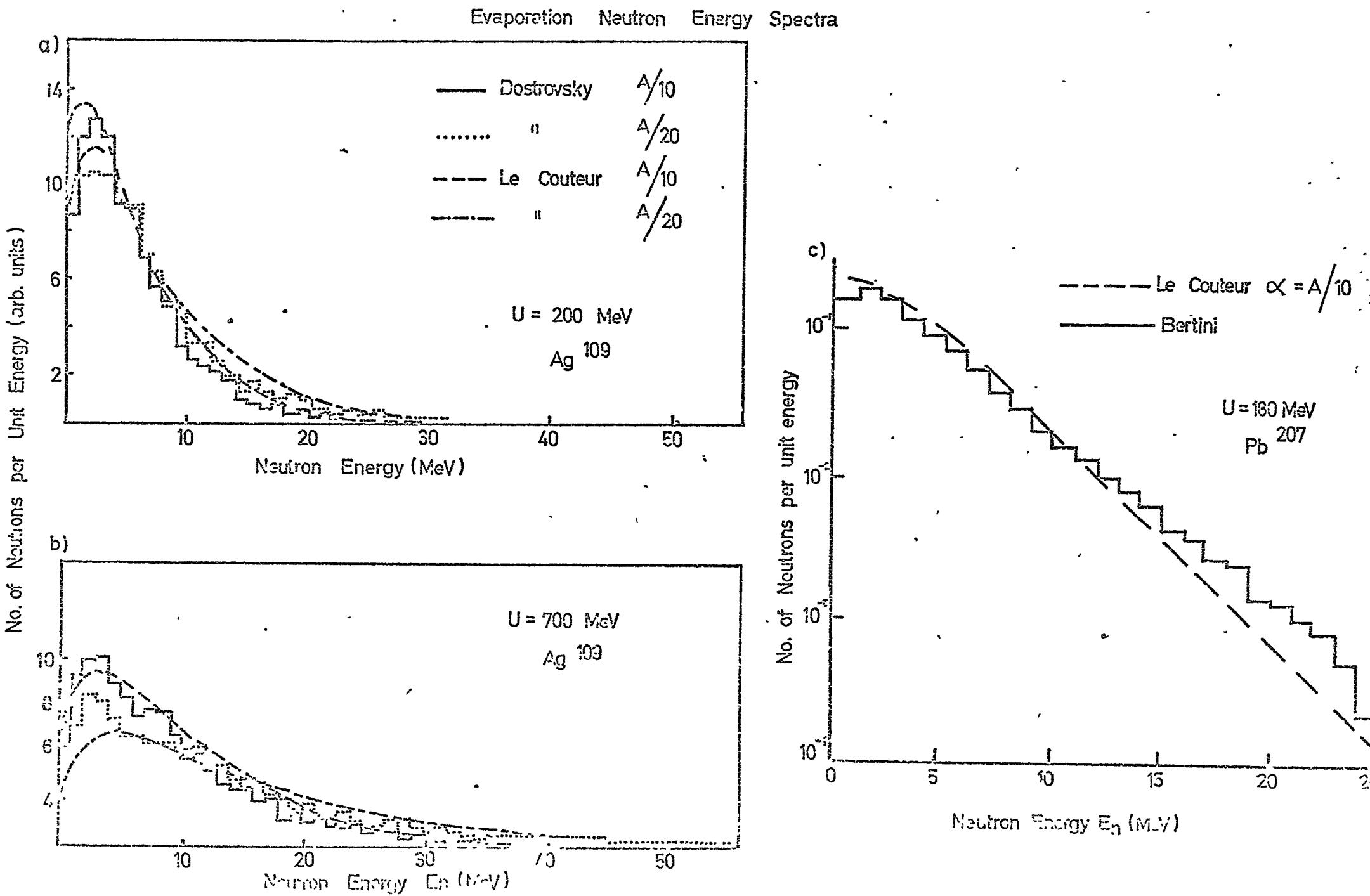
Evaporation Neutron Energy Spectra
a)
Dostrovsky A/10
" A/20
Le Couteur A/10
" A/20
U = 200 MeV
Ag 109
No. of Neutrons per Unit Energy (arb. units)
Neutron Energy (MeV)
b)
U = 700 MeV
Ag 109
Neutron Energy En (MeV)
c)
Le Couteur ∝ = A/10
Bertini
U = 180 MeV
Pb 207
No. of Neutrons per unit energy
Neutron Energy En (MeV)

FIG. 2.3 CONTD.

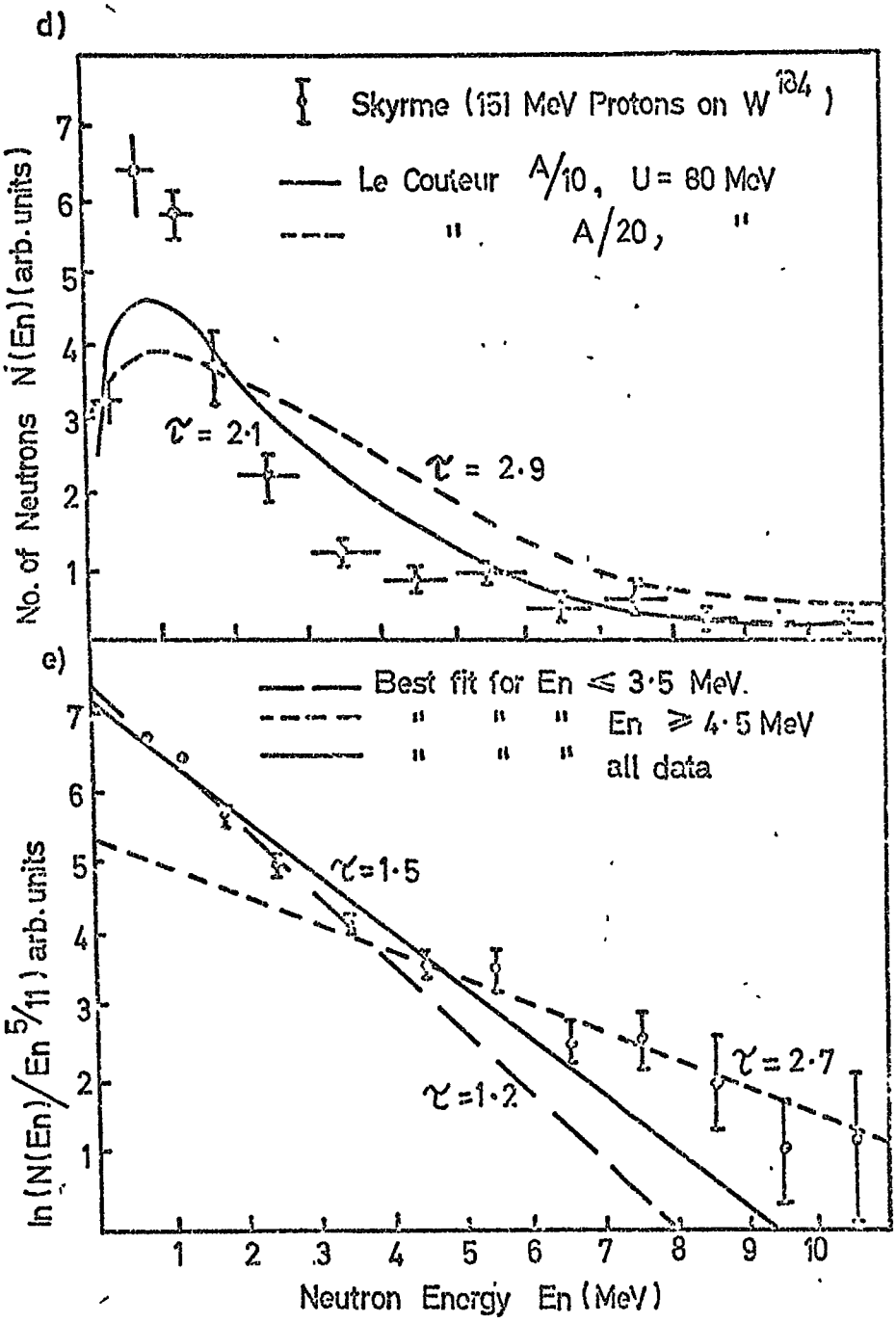
d)
Skyrme (151 MeV Protons on W 184)
Le Couteur A/10, U = 60 MeV
" A/20, "
No. of Neutrons N(En) (arb. units)
τ = 2·1
τ = 2·9
e)
Best fit for En ≤ 3·5 MeV.
" " " En ≥ 4·5 MeV
" " " all data
ln (N(En)/En 5/11) arb. units
τ=1·5
τ=1·2
τ = 2·7
Neutron Energy En (MeV)

with the analytical expression of Le Couteur for neutrons -

$$N(E_n)dE_n = K E_n^{5/11} \exp(-E_n/\tau^*)dE_n \qquad 2.1$$

where E_n is the evaporation neutron energy

K is a constant

τ^* is related to the initial nuclear temperature τ

by $\tau^* = \frac{11}{12}\tau$

and the excitation energy U is related to the temperature by the approximate expression

$$U = \alpha\tau^2 \qquad 2.2$$

where α is the energy level density parameter.

The average energy of the spectrum is

$$\bar{E}_n = \frac{4}{3}\tau \qquad 2.3$$

Equations 2.2 and 2.3 related $\bar{E}_n$ to U so enabling a simple quantitative comparison to be made between Le Couteur's spectrum and those of Dostrovsky and Bertini. Thus the average neutron energies evaporated from Ag^{109} at U = 200 and 700 MeV were found by Dostrovsky to be 5.4 and 9.9 MeV respectively compared with the corresponding Le Couteur values of 5.4 and 10.1 MeV. The difference is $\leq 2\%$.

Similarly the average energy of neutrons evaporated from 750 MeV interactions of protons with lead nuclei calculated by Le Couteur and Bertini are 3.7 and 4.0 MeV respectively.

Skyłme (1962) has measured the spectrum produced by 150 MeV protons on a thin tungsten (A = 184) target and this is compared with that predicted by the calculations of Metropolis/Le Couteur for $\alpha = A/10$ and A/20 in fig. 2.3d. Neither prediction gives a particularly good fit although $\alpha = A/10$ is clearly the better. The same data plotted in a logarithmic form in figure 2. 3e demonstrates the difficulty in finding a single value of τ^*(the "average" temperature) to fit

the data. Skyrme could not account for this in terms of the expected fluctuations in the intra-nuclear cascade and suggested that some of the lower energy neutrons may originate from a cooler surface region of the nucleus. However, Bertini's calculations, using a more realistic nuclear model than Le Couteur's do not indicate that this has much effect on the spectrum (fig. 2.3.c). It is more likely that the average energy of the neutrons is overestimated by Le Couteur due to the underestimation of the alpha particle emission probability suggested by Bertini, since the alpha particles would tend to be emitted early on in the evaporation process whilst the nucleus is relatively energetic.

However, since the total low energy neutron spectrum includes about 20% slow cascade particles according to Bertini (1972) which have a relatively flat energy spectrum (and correspondingly higher average energy) it is possible that Le Couteur's calculated spectrum may be closer than Skyrme's measured spectrum, to that found in a neutron monitor.

2-1.3 Neutron Production by Nucleons having energy greater than 2 GeV

Barashenkov (1961) has made calculations similar to those made by Metropolis but at an energy of 9 GeV assuming an intra-nuclear cascade process, and the results of these agree well with emulsion data. Above this energy however, the nature of the interaction should alter (Shen, 1968; Barashenkov et al. 1971). In the cascade model, the nucleon interacts singly with any nucleon of the nucleus which is passed within the range of the strong nuclear force. However, above a sufficiently high incident nucleon velocity, which is higher for larger nuclei, the thickness of the nucleus will be less than the range of nuclear force

due to the Lorentz contraction and the nucleon will then interact collectively with those nucleons lying along the collision axis. A further consideration at this high particle energy is that the secondary particles will be strongly collimated in the forward direction and so secondary interactions will be severely inhibited. This essentially one dimensional 'tube' model predicts that the value of nuclear excitation and hence average number of evaporation neutrons will approach an assymptotic value as the energy increase which will be lower than the corresponding prediction by a three dimensional intra-nuclear cascade.

Results (fig. 2.4) of photographic emulsion studies by Meyer et al. (1963) and others, have been interpreted by Shen (1967) using a phenomenological 'tube' model, as follows.

According to Powell et al.(1959) and Harding (1949) the following two relationships are indicated experimentally for average emulsion nuclei, Ag and Br, for which $A \approx 70$.

$$N_p \simeq N_b \qquad 2.4$$

where N_p is the number of singly charged evaporation particles emitted by a nucleus after any interaction, and N_b is the corresponding number of black prongs in the observed star.

$$\langle N_b \rangle \simeq \frac{2}{3} \langle N_h \rangle \qquad 2.5$$

where $N_h = N_b + N_g$ is the sum of black and grey prongs in any star, and is conventionally used as a measure of nuclear excitation.

The Monte Carlo calculations of Dostrovsky (1958) predict that for $A \sim 70$ and typical excitation energies of the order of hundreds of MeV, there are equal numbers of singly charged evaporation particles and multiple charged ones, which suggests that $N_p \simeq \frac{1}{2} N_b$, if all the charged particles give rise to visible prongs (c.f.eqn. 2.4). Shen, in noting this inconsistency, made a compromise and assumed $N_p \simeq \frac{3}{4} N_b$ - 2.6.

FIG 24 Variation of Average Number of Heavy Prongs With Nucleon Energy

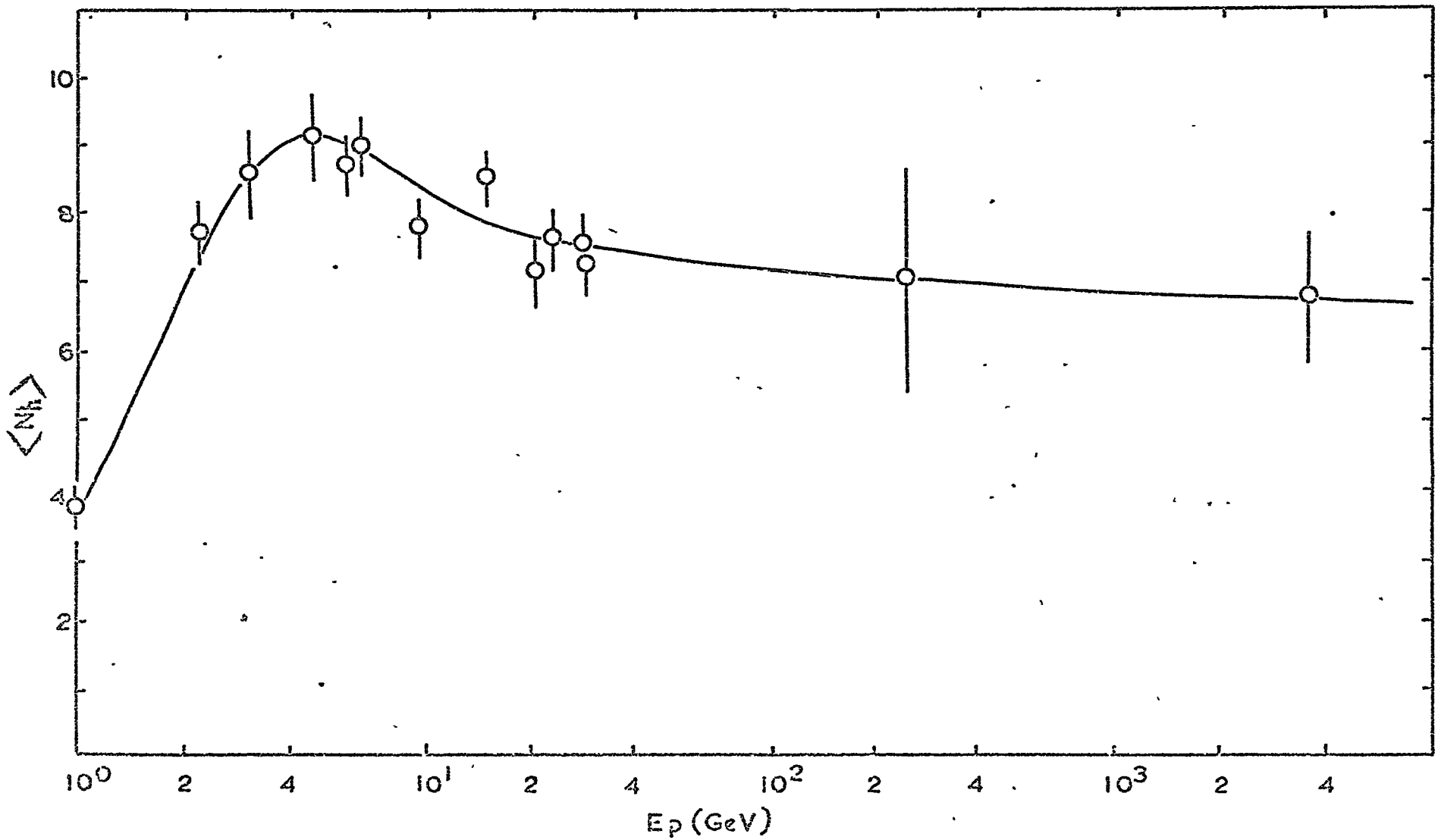

Then using a further result of Dostrovsky relating the number of evaporation neutrons ν to protons N_p (for A = 70 nuclei with excitations of a few hundred MeV).

$$\bar{\nu} = 2 \langle N_p \rangle \qquad 2.7$$

Shen related ν to N_h thus

$$\bar{\nu} = 2 \langle N_p \rangle = \frac{3}{2} \langle N_b \rangle = \langle N_h \rangle \qquad 2.8$$

Because of this simple relationship, it should be expected that $I(\nu;E_p)$, the probability of evaporating ν neutrons after an interaction between a nucleon of energy E_p and a Ag/Br nucleus should have the same functional form as $I(N_h; E_p)$ and that $\bar{\nu}$ behaves in the same way as $\langle N_h \rangle$ as a function of E_p.

The mean number $\langle N_h \rangle$ is found to nearly reach its assymptotic value of seven at $E_p \simeq 30$ GeV (fig. 2.4). The tube mechanism is not expected to dominate the interaction for Ag/Br nuclei until $E_p \sim 200$ GeV and so Shen assumed that the intra-nuclear cascade is effectively one dimensional above 30 GeV for Ag Br due to collimation of secondary particles.

It is clearly important to establish the general character of the interaction as set out above, because when extrapolating the results for nuclei of A = 70 to those appropriate to lead nuclei (A = 208) which is the typical value for the target material used in neutron monitors, the three dimensional interaction must be treated differently from the one dimensional interaction. Metropolis showed that $\bar{\nu} \propto A$ in the 3-D region, which implies that $\bar{\nu} \propto A^{\frac{1}{3}}$ in the 1-D region. For lead nuclei, the 3-D intra-nuclear cascade mechanism should predominate up to 10 GeV; whilst in analogy with the results of Ag Br, the 1-D region begins at 50 GeV. Shen's extrapolation of Meyer's results from A=70 to A =208 is shown in fig. 2.5 . The variation of $\bar{\nu}$ in the intermediate energy region ($10 \lesssim E_p \lesssim 50$ GeV) was obtained simply by interpolation; whilst the behaviour below 1 GeV

FIG.25 Variation of Neutron Multiplicity Produced by a Nucleon of Energy Ep

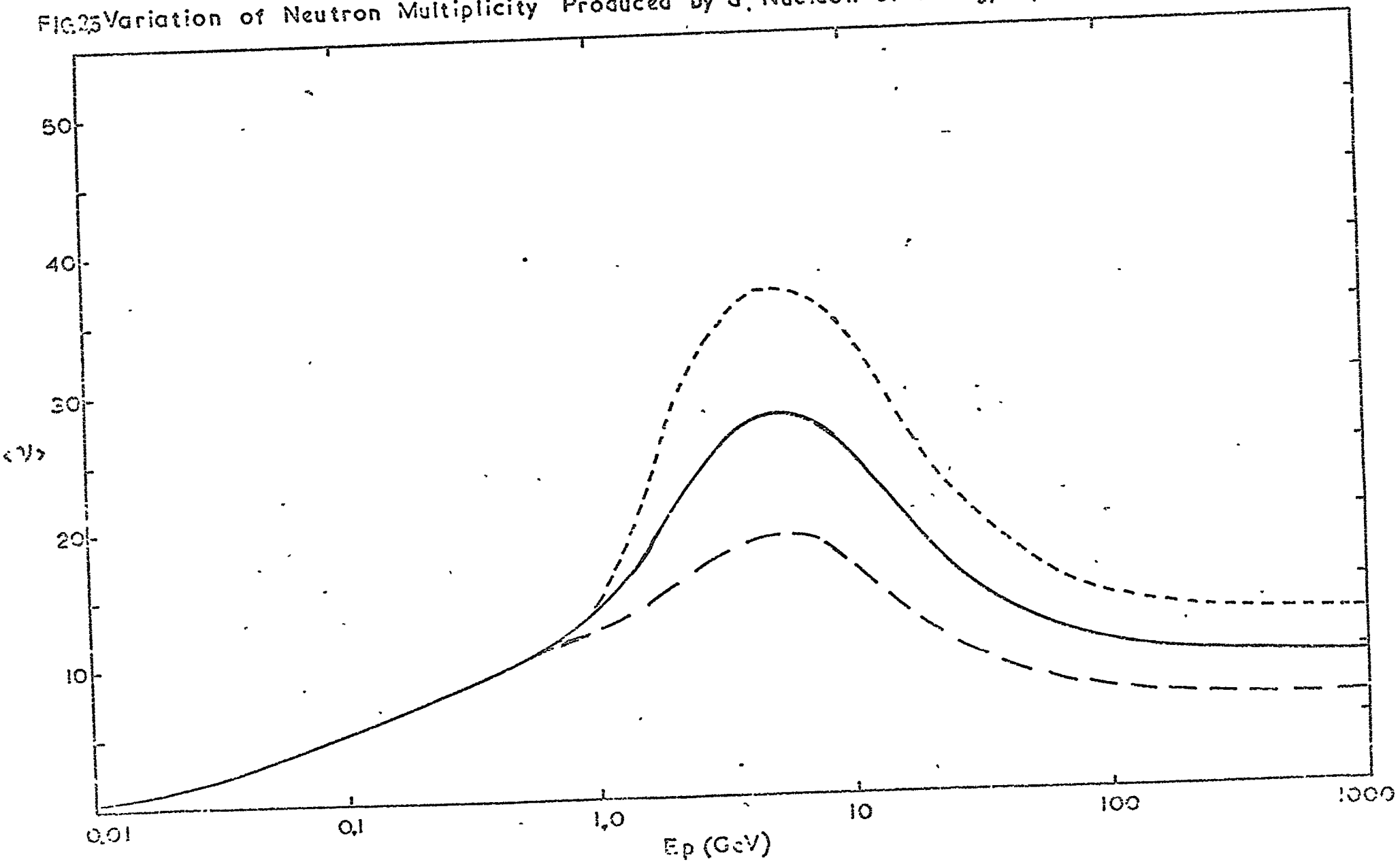

was assumed to follow the data of Bercovitch and the calculations of Metropolis and Dostrovsky. The uncertainty in relating the observed numbers of black prongs to the numbers of evaporation charged particles leads to the corresponding uncertainty in $\bar{\nu}$ above 1 GeV as represented by the dashed curves.

2-2 Neutron Production in a Neutron Monitor

2-2.1 Introduction

The thickness of target material in a neutron monitor is typically 100 g cm^{-2} for vertically incident cosmic rays. Thus the secondary interactions discovered by Bercovitch (1960) become very important in determining the total yield of evaporation neutrons. The next task in the relating of $\bar{\nu}$ to the energy of incident nucleons, is to calculate the numbers of neutrons produced by all the nuclei in the target material which are involved in the extra-nuclear cascade which develops, in general, in each interaction.

2-2.2 Experimental Results

Neutron production in a neutron monitor by single, momentum analysed cosmic rays was first investigated by Hughes et al. (1964) using the LIGY monitor and the Durham Magnetic Spectrograph. Single charged particles traversing an air gap magnet spectrograph and producing a five fold Geiger Counter coincidence, caused the gating system of the neutron monitor to operate, and events were recorded in which one or more neutrons arrived within the gate time. Their experiment recorded the response of the monitor to protons, pions and interacting muons, as well as some muons caused by random coincidences between a non-interacting muon and background neutron pulses arising from low energy cosmic ray nucleons. These different types of event were identified by the charge of the particle and the information

offered by a tray of flash tubes beneath the monitor about the nature of the interaction within the monitor. Data were recorded in the form of neutron multiplicity distributions as a function of the momentum of the particles.

The rate of events due to incident particles of mean energy E in which m neutrons are produced was given by

$$R(m;E) = Q(E) \sum_{\nu=m}^{\infty} I(\nu; E)\, B(m,\nu) \qquad 2.9$$

where $Q(E)$ = rate of interactions,

$$I(\nu;E) = (e^{a} - 1)\, e^{-a\nu} \qquad 2.10$$

is the probability of ν neutrons being produced, as deduced by Cocconi et al.(1950) where

$$\sum_{\nu=1}^{\infty} I(\nu;E) = 1, \qquad 2.11$$

$B(m,\nu) = \binom{\nu}{m} (\epsilon f)^{m}(1 - \epsilon f)^{\nu-m}$ is the (binomial) probability of detecting m neutrons out of ν produced if ϵf is the efficiency of detecting one neutron within the gate time. As pointed out by Geiger (1956), equation 2.9 can be re-written as

$$\log R(m;E) = \log Q(E) + \log (e^{a}-1) + m \log (\epsilon f) - a m - (m + 1) \log (1 - (1-\epsilon f)e^{-a}) \qquad 2.12$$

so a graph of log R against m should be a straight line if the assumption regarding $I(\nu;E)$ is correct. Hughes et al. found this to be so for their data.

The average number of neutrons $\bar{\nu}(E)$ produced was then calculated from their measured average number detected, $\bar{m}$, thus

$$\bar{\nu}(E) = \frac{\sum_{\nu=1}^{\infty} \nu I(\nu;E)}{\sum_{\nu=1}^{\infty} I(\nu;E)} = (e^{a}-1)^{-1} = \frac{\bar{m}-1}{\epsilon f} + 1 \qquad 2.13$$

where $\bar{m} = \frac{\sum_{m=1}^{\infty} m R(m)}{\sum_{m=1}^{\infty} R(m)}$

The value of ϵ used was 3.03% which was determined in a Ra-Be source measurement over the central portion of the monitor upon which the beam of particles from the spectrograph was incident. The value of the gating efficiency f, was obtained from their measured distribution of arrival times of neutrons, taken to be $P(t) = K(1 - \exp(-t/13.5)) \exp(-t/170)$ -2.14 However, their values of $\bar{\nu}$ are systematically inaccurate because

(a) $I(\nu;E)$ should be noramlised from $\nu=0$ to ∞, instead of from 1 to ∞, as suggested by Shen (1968), which leads to the result $\bar{\nu} = (\bar{m} - 1)/\epsilon f$ 2.15

(b) P(t) is more complex than equation 2.14 and leads to an overestimation of f by about 8% (Hatton, 1971). (See fig. 3.7).

(c) It was assumed that $I(\nu;E)$ is a single exponential. Monte Carlo calculations (Shen, 1968) have shown that this may not be true resulting in an underestimation of $\bar{\nu}$.

and (d) Of inaccuracies in the momentum measurement which would lead to an overestimate of the mean kinetic energy at the higher energies, due to the rapidly falling spectrum.

Hatton (1971) has made corrections appropriate to (a) and (b) which have increased $\bar{\nu}$ by ~10% at all energies.

2-2.3 Comparison of Monte Carlo calculations with experimental results

In order to compare his deduction of the average produced neutron multiplicity with the results of Hughes et al, Shen (1968) had to

perform Monte Carlo calculations of the extra-nuclear cascade within the producer, allowing for the production of secondary particles. He calculated the yield of neutrons with energies < 30 MeV from all sources, for a variety of producer thicknesses (less than two interaction lengths) and incident energies (40 MeV to 100 GeV) of neutrons, protons and pions (fig. 2.6) His results for the average thickness of the IGY monitor ($t = 0.75$ interaction lengths) have been compared with Hughes' corrected results (after Hatton, 1971) in fig. 2.7. The large discrepancy could be due to a number of factors:

(a) uncertainty in the monitor efficiency c (see section 2.3)

(b) the interpretation of the emulsion results (fig. 2.5)

(c) systematic errors in the calculation concerned with the effect of slow cascade neutrons

(d) the assumption that $I(\nu)$ is a single exponential.

Fig. 2.7 shows how $\bar{\nu}$, $\bar{\nu}_t$ and $\bar{\nu}_t'$ calculated by Shen for protons incident on a producer thickness $t = 0.75$ interaction length vary with incident energy where $\bar{\nu}$ is the average number of evaporation neutrons, $\bar{\nu}_t$ is the average number of evaporation neutrons plus cascade neutrons less than 30 MeV which have not interacted to produce more evaporation neutrons, and $\bar{\nu}_t'$ is the average number of evaporation neutrons plus all cascade neutrons less than 30 MeV, which are assumed to be thermalised before they have a chance to interact again. The choice between $\bar{\nu}_t$ & $\bar{\nu}_t'$, is a difficult one dependent on the geometry of the monitor. Shen assumed for simplicity that $\bar{\nu}_t$, the upper limit, is the quantity appropriate for comparison with experiment. This may clearly account for part of the discrepancy.

Shen found that the functional form of $I(\nu; E_p, t)$ was not simply of the form $e^{-a\nu}$, for discrete values of E_p and t. On averaging I

FIG. 2.6 Variation of Neutron Multiplicity Produced by a Proton in a Target of Thickness t (Interaction Lengths)

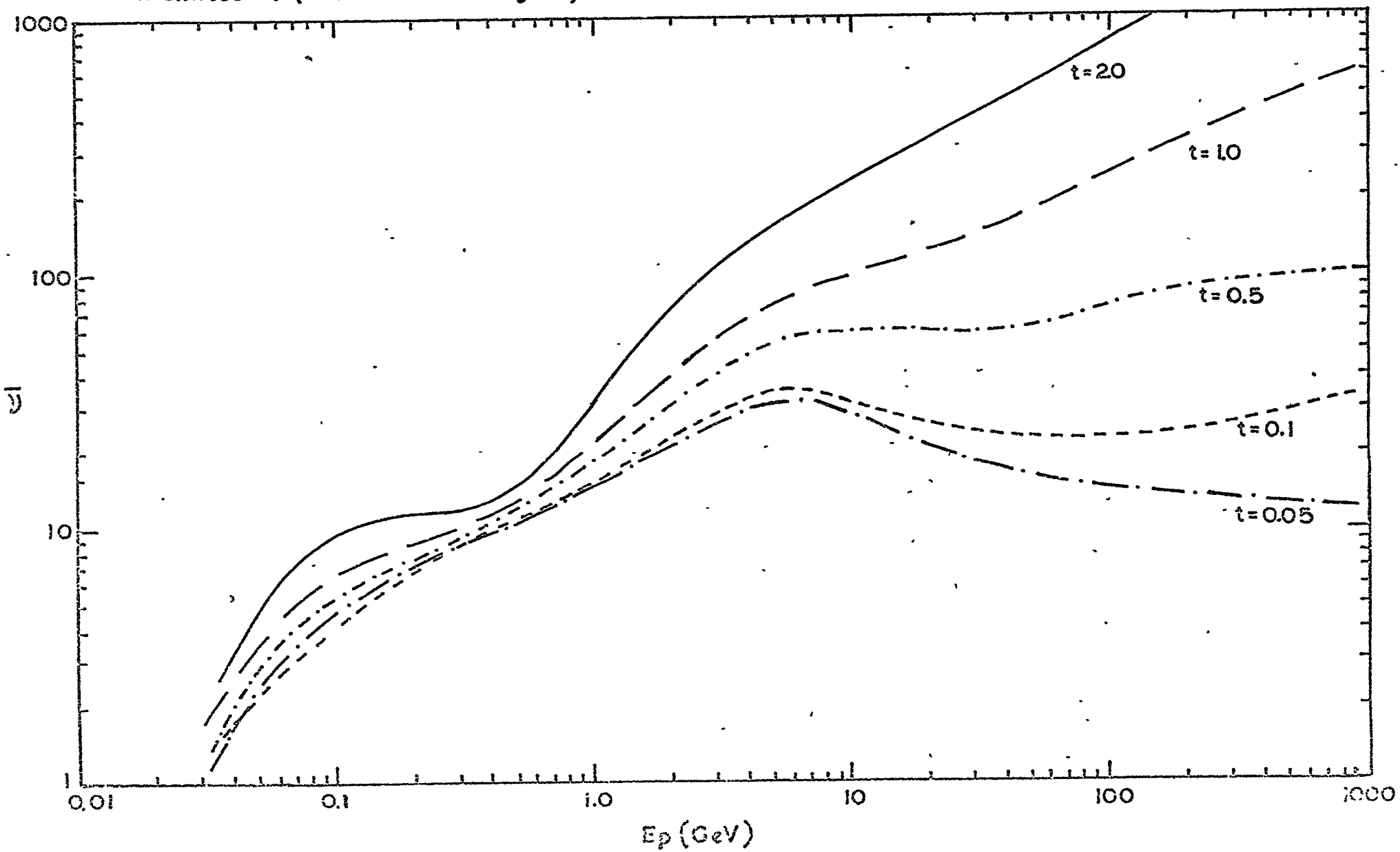

FIG. 2.7 Variation of Average Neutron Multiplicity Produced by Protons in the LIGY Monitor

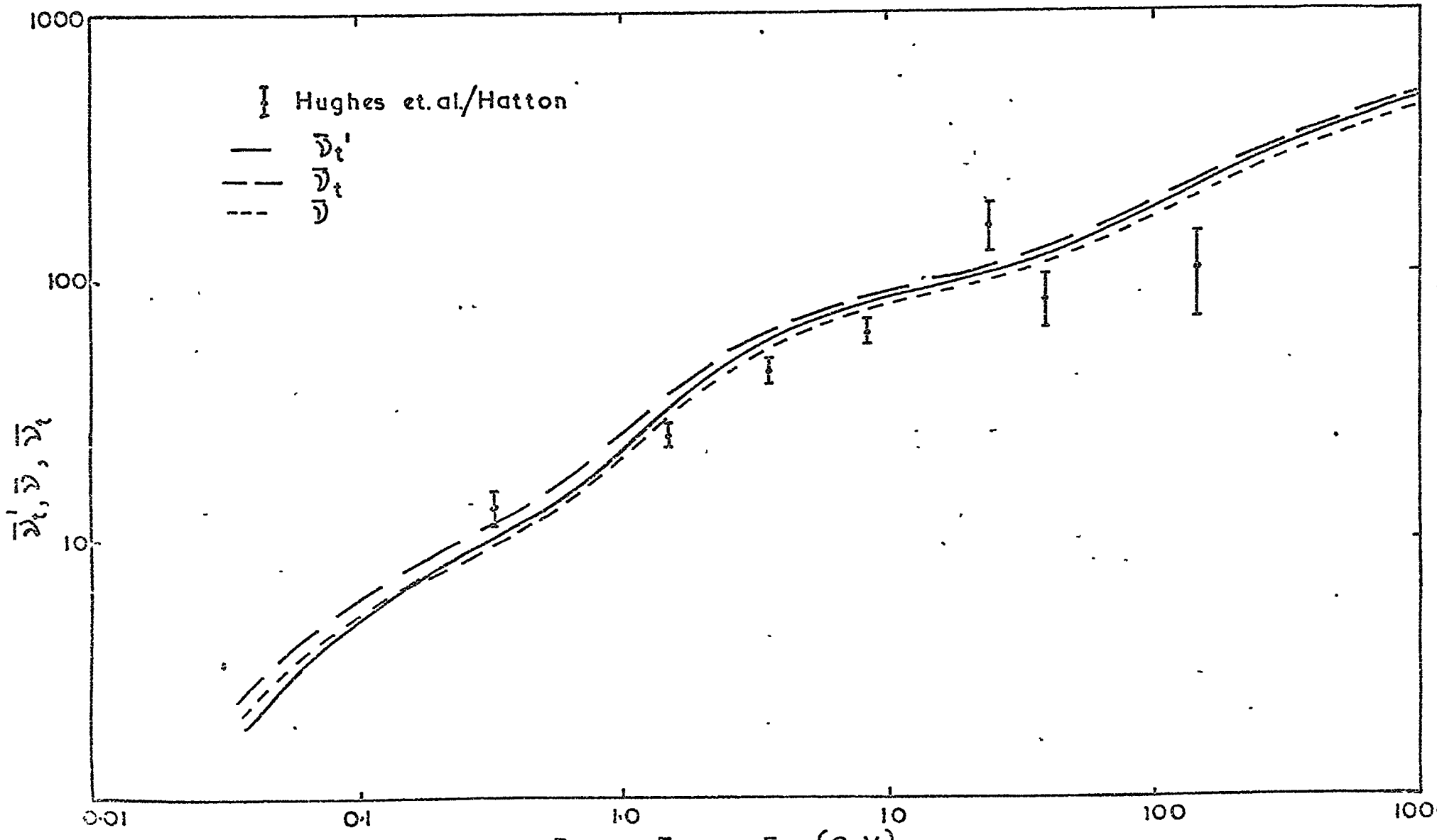

over a range of E_p & t appropriate to the results of Hughes et al. he found that $I(\nu; \bar{E}_p, \bar{t})$ followed much closer an exponential dependence. However, a significant improvement can be made by fitting a double exponential to the theoretically predicted distributions

$$I(\nu; \bar{E}_p, \bar{t}) = K_a e^{-a\nu} - K_b e^{-b\nu} \qquad 2.16$$

which leads to $\bar{\nu} = \frac{\bar{m} - 1}{\epsilon f}\ \alpha(\bar{t}, \epsilon, \bar{E}_p)$ 2.17

where, for $\bar{t} = 0.75$,

$\alpha = 1.00$ { for $E_p \lesssim$ 0.15 GeV and $E_p \gtrsim$ 60 GeV

and $1.0 \lesssim \alpha \lesssim 1.1$ for $0.15 \lesssim E_p \lesssim 60$ GeV

i.e. the results of Hughes et al. would be underestimates by up to 10%.

Shen in considering the effect of a possible overestimation in the average numberof produced neutrons as a result of mis-interpreting the emulsion data, found that the prediction for t = 0.75 interaction lengths could be in error by ± 20% above 1 GeV. It is clear therefore that there is considerable uncertainty in the prediction of $\bar{\nu}$. In the next section we investigate possible errors in the value of the neutron detection efficiency used in the experiment of Hughes et al.

2-3 Efficiency of Detecting Evaporation Neutrons

2-3.1 Introduction.

The evaporation neutrons produced in neutron monitors are conventionally detected using proportional counters filled with BF_3 gas enriched with 90% B^{10}. The neutrons react as follows

$$B_5^{10} + n \rightarrow Li_3^{7} + He_2^{4}$$

The product nuclei have about 2.5 MeV of kinetic energy between them and can produce up to 80,000 ion pairs, making them easily identifiable above the background of cosmic rays passing through the counter. The

cross-section for the above reaction is inversely proportional to the neutron velocity and so the detection process begins by slowing down the evaporation neutrons to thermal energies (a few eV) by elastic scattering within the monitor. Lead, with its high atomic number, is not suitable for this and so some material with a low A value such as paraffin or polyethylene has to be included in the structure.

There are two factors ϵ and f entering into the consideration of the detection efficiency (= ϵf). ϵ is the absolute efficiency of detection and is the effective efficiency when no time limit is set for the thermalising and detection processes. The other factor, f, is the consequence of gating the detection system as a function of time, and is less than 1 except in the limit when the gate width becomes infinitely long. Both ϵ and f depend on the geometry and material in the monitor.

If the probability of detecting a neutron in an interval dt at time t after the interaction is P(t) dt then

$$f(T_1 \rightarrow T_2) = \frac{\int_{T_1}^{T_2} P(t)\,dt}{\int_{0}^{\infty} P(t)\,dt} \qquad \text{for a gate}$$

opening at $t = T_1$ after the interaction and closing at $t = T_2$. Hatton and Tomlinson (1968) found that P(t) will be largely determined by the various thermalising time constants associated with the various parts of the monitor, and can be found by recording the arrival times of neutrons after each interaction. Fig. 3.7 shows the time distribution for the LIGY from Hatton and Tomlinson showing a double exponential; the smaller time constant is associated with thermalisation in the inner paraffin surrounding the BF_3 counters, and the larger time constant is associated with thermalisation in the (outer) paraffin

surrounding the whole monitor.

Unfortunately the thermalising materials or moderators which are usually used in neutron monitors absorb the majority of thermalised neutrons and so the overall efficiency is very low, typically a few per-cent even though careful design can optimise the thickness of moderator (Hatton and Carmichael (1964)).

A substantial increase in efficiency was obtained by Nobles et al. (1967), who replaced the usual lead and paraffin of conventional monitors by bismuth and reactor grade graphite respectively, both of which have lower thermal neutron absorption cross-sections.

Improvements in the efficiency of evaporation neutron detectors have also been made (see for example Kaplan (1958) and Barton (1969)) by the use of a scintillator substance viewed by photo-multiplier tubes which can not only thermalise (if the scintillator is 'loaded' with Gadolinium or similar element) but also detect neutrons through scattered proton scintillations and gamma rays emitted during the slow neutron capture process. Such very high efficiency devices have not been used to cover a large area, as is often required in cosmic ray work, but rather in conjunction with experiments at accelerating machines.

2-3.2 Experimental Measurements

Measurements of efficiencies of neutron monitors have been made using a Ra-Be source (Hughes, 1961) and a plutonium spontaneous fission source (Hatton and Carmichael, 1964), whose energy spectra are shown in fig. 2.8. Hughes found that the efficiency varies throughout the horizontal plane of the monitor being a maximum at the centre.

The efficiency $\epsilon(E_n,x)$ for detecting an evaporation neutron will also depend on its energy E_n and its depth x of production within the

FIG. 2.8 Neutron Energy Spectra

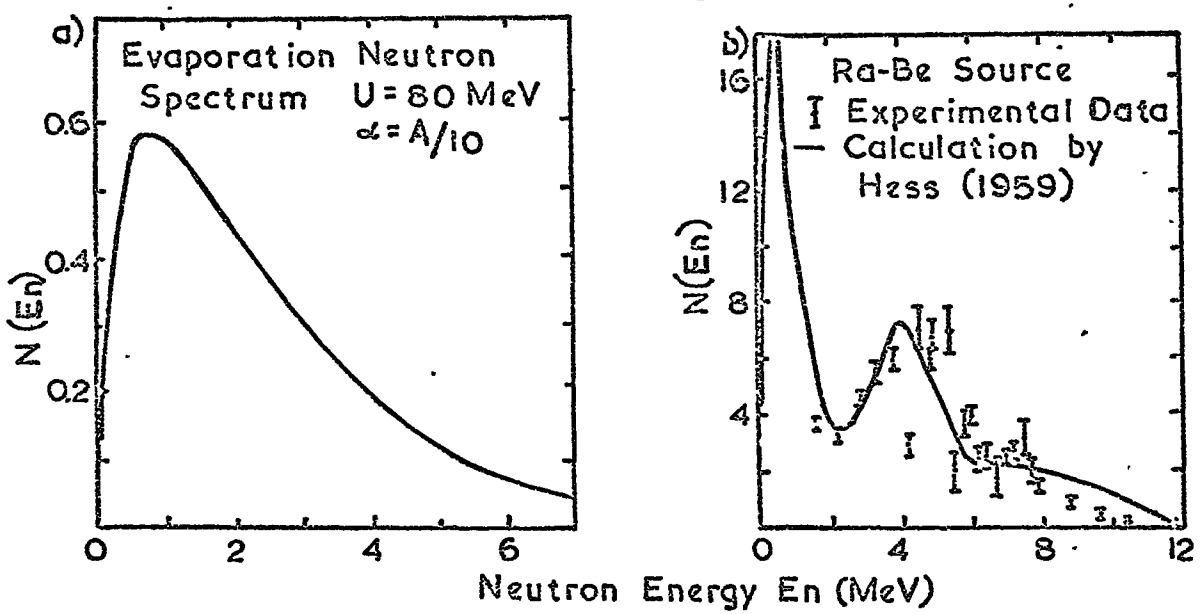

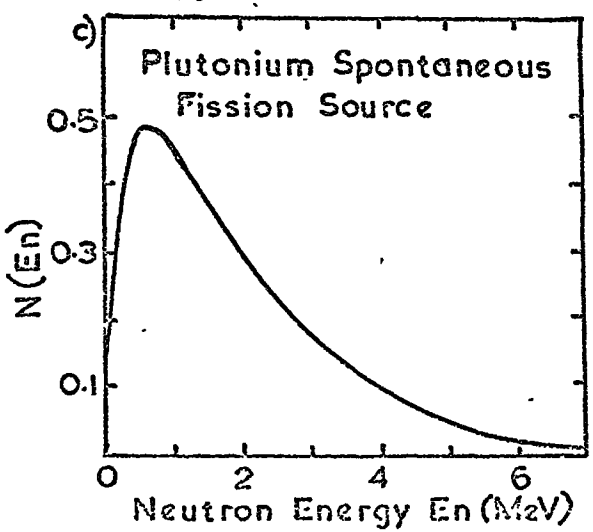

monitor. This means that when a monitor is used to record a certain flux of cosmic rays of a certain type, the energy spectrum of the produced evaporation neutrons, together with the distribution in production as a function of position in the producer must be known in order to relate the averaged efficiency to that measured by a source. Hughes assumed that $\epsilon(E_n,x)$ was not strongly dependent on E_n, that the average energy $\bar{E}_n$ of the source neutrons equalled the average energy of the evaporation neutrons, independent of depth. A value of $\epsilon = 2.1 \pm 0.1\%$ has been attributed to the average efficiency of the LIGY for all cosmic ray induced evaporation neutrons. The results of Treiman and Fonger (1952) showing the production of neutrons as a function of depth due to the cosmic ray flux at sea level, indicate that the third approximation is justified, but Monte Carlo simulations of the detection process (Pearce and Fowler 1964) have shown that the same may not be true of the assumption regarding the dependence on the neutron energy.

In the simulation, a cylindrically symmetric arrangement of one infinitely long unit (i.e. one BF_3 counter surrounded by its inner moderator, producer and reflector in amounts equal to that used in a monitor) was considered. This was done for two actual monitors, the standard (Simpson) IGY and the NM64 monitor. The histories of many evaporation neutrons produced at varying distances from the centre, and of varying initial energies, were followed and the resultant detection efficiency determined. This predicted efficiency is not directly comparable with the actual monitors because in reality

(i) monitors are not infinitely long and

(ii) some tens of per-cent of the neutrons detected by one counter have been produced and/or thermalised around an adjacent counter

according to Hatton and Carmichael (1964). The variation of efficiency with energy for this ideal, long counter geometry is shown in fig 2.9. The decrease in efficiency with increasing energy was attributed by the authors to the decrease with energy of the nucleon-nucleon elastic cross-section which is responsible for the thermalisation. Hatton (1971) has calculated that for a typical energy of incident nucleon (150 MeV), for which the calculations of Metropolis and Le Couteur predict an evaporation neutron energy spectrum given by fig. 2.8a, the correction that should be made to ϵ is negligible for the LICY, indicating that the Ra-Be source closely approximates the actual spectrum even though its average neutron energy is some 40% too high. The equivalent calculation forthe Pu source measurement however shows the value of ϵ to be in error by + 14% inspite of its apparent similarity to the theoretically predicted spectrum. This indicates that the correction to be applied to the source measurement is highly sensitive to the precise form of the energy spectrum, especially where the reflector thickness is as thin as that of the NM64. Since

(i) the Ra-Be source spectrum is open to some considerable doubt (Hess, 1959)

(ii) in deriving the theoretical evaporation energy spectrum for nuclear interactions, evaporation neutrons from secondary excited nuclei have been neglected which would alter the energy spectrum,

and (iii) Le Couteur's spectrum used by Hatton is an approximation , there must be considerable uncertainty in the absolute efficiency for neutron detection.

2-3.3 Variation of Efficiency with incident nucleon energy.

The results of Metropolis et al's calculations (fig. 2.1) show that the average excitation of the target lead nucleus is increasing with the incident nucleon energy at the upper limit of 1.8 GeV energy

FIG. 2.9 Variation of Detection Efficiency with Neutron Energy

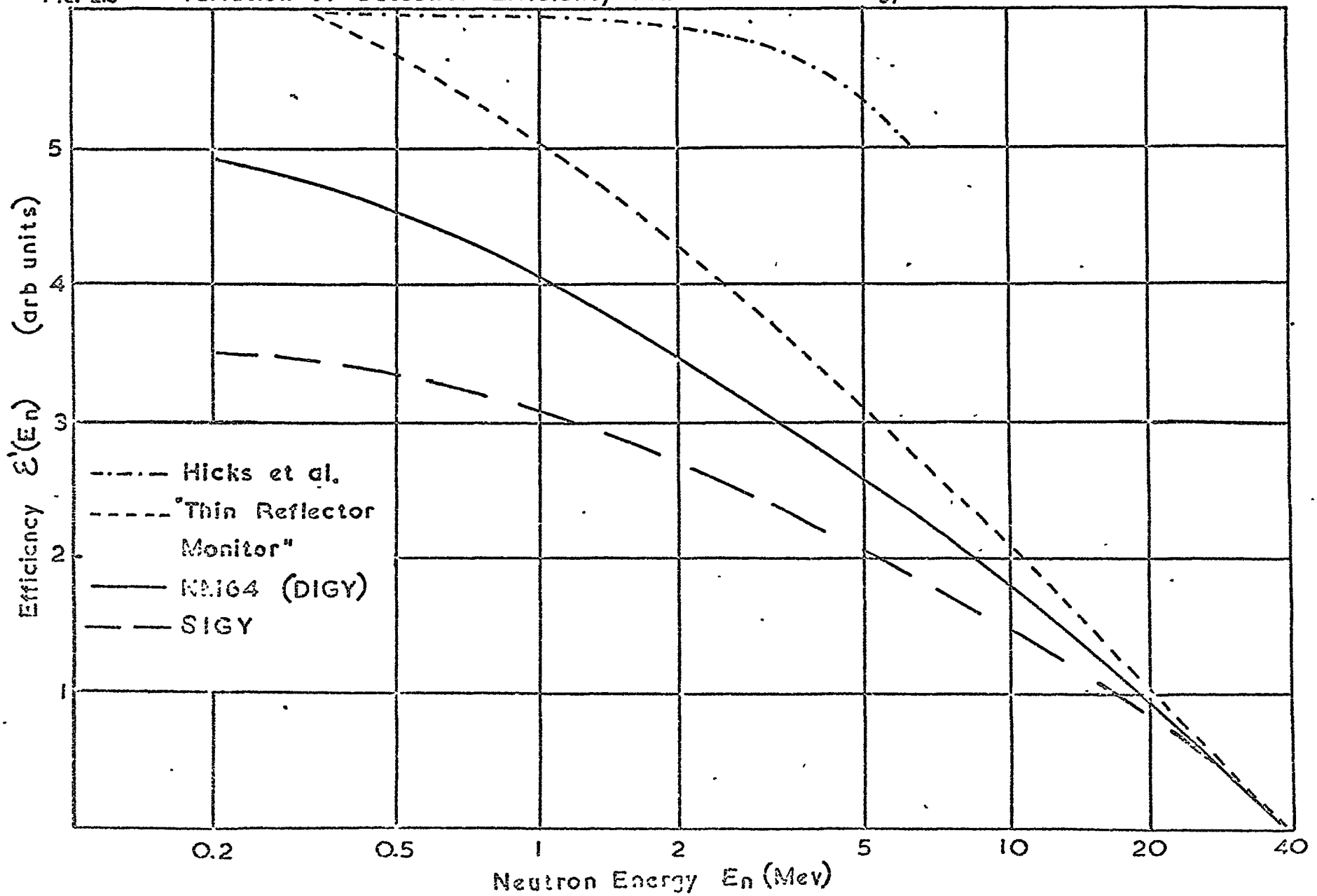

which they considered. This increase should continue whilst the 3-D intra-nuclear cascade dominates the interaction, i.e. up to ≃10 GeV. The results of Le Couteur (equations 2.2, 2.3) show that the mean energy of evaporation neutrons increases with increased nuclear excitation, so this should lower the detection efficiency in accordance with the predictions of Pearce and Fowler (fig. 2.9). On the other hand, secondary particles from the initial interaction may cause other nuclear excitation of characteristically less energy and the evaporated neutrons from these will have correspondingly higher probabilities of detection. The maximum variation in efficiency may be roughly estimated by considering only the initial excitation.

The dependence of average excitation energy on nucleon energy is only known below 1.8 GeV. However, it is possible to sketch the variation of average excitation energy $\bar{U}$ with nucleon energy E_p above 1 GeV by using the results of calculations by Dostrovsky (fig. 2.1) to relate U to the average number of neutrons produced $\bar{\nu}$, and Shen (Fig. 2.5) to relate $\bar{\nu}$ to E_p. There will be a possible error in $\bar{U}$ of $\pm$ 50 % due to uncertainties in $\bar{\nu}$ above 1 GeV, although there is very good agreement with Metropolis up to 1.8GeV (see fig. 2.10).

Assume the energy spectrum of evaporation neutrons due to incident nucleon energy E_p (giving average initial nuclear temperature $\tau = \frac{12}{11}\tau^*$) to be given by equation 2.1. Then neglecting ionization losses before the interaction the mean efficiency of detecting any evaporation neutron is

$$\bar{\epsilon}(\tau^*) = \frac{\int_0^\infty N(E_n;\tau^*)\ \epsilon'(E_n)\ dE_n}{\int_0^\infty N(E_n;\tau^*)\ d\,E_n} \qquad 2.18$$

where $\epsilon'(E_n)$ is the mean efficiency of detecting an evaporation neutron of energy E_n produced in the monitor. This has only been calculated here

FIG. 2.10

Variation of Average Nuclear Excitation Energy with Energy of Nucleon

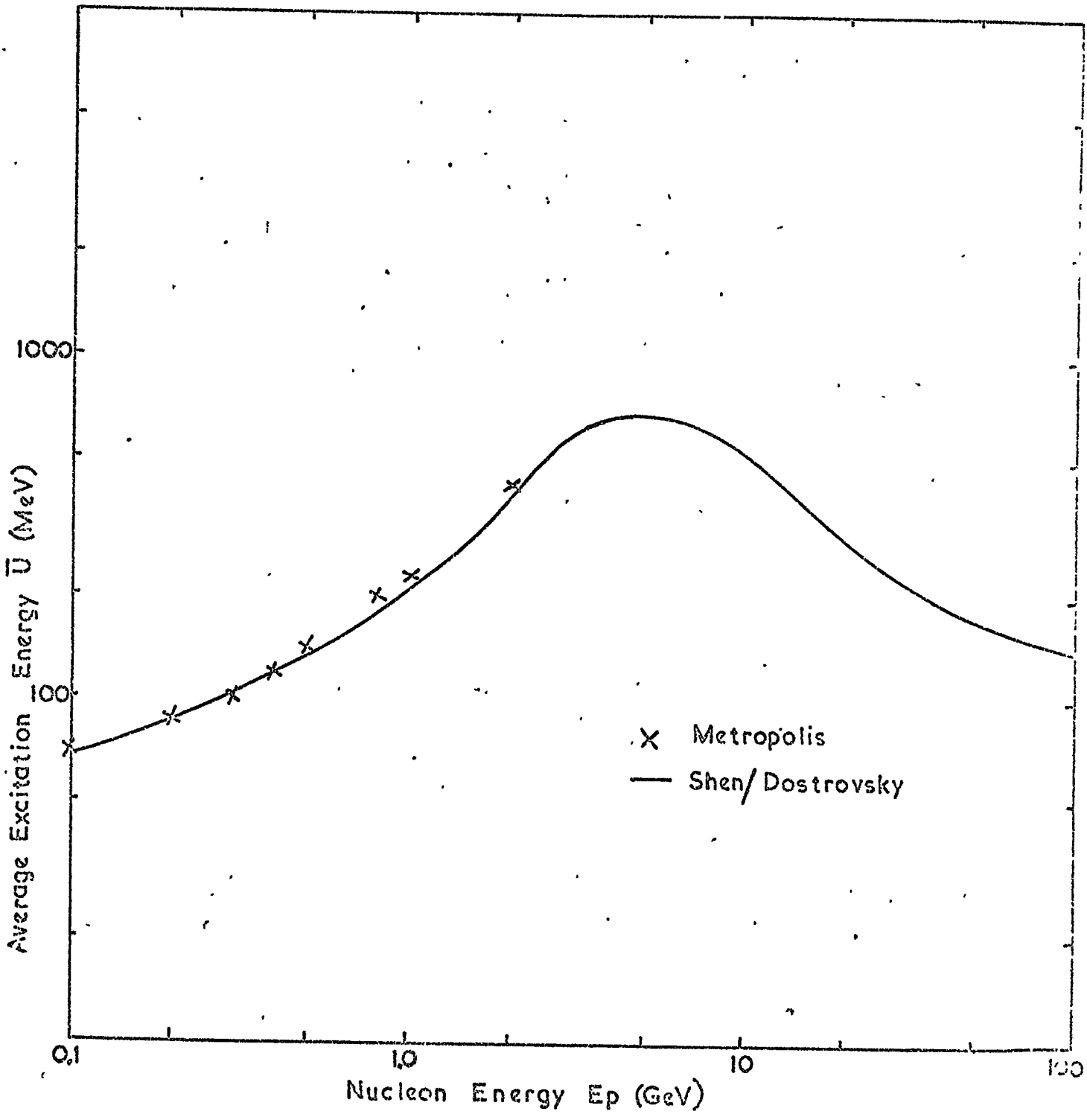

for two simplified geometries (Pearce and Fowler) but this is sufficient to show roughly how $\bar{\varepsilon}'(\tau)$ varies in a typical monitor. To test the sensitivity on $\bar{\varepsilon}'(\tau)$ of variations in $\varepsilon'(E_n)$, values of $\bar{\varepsilon}'$ were also calculated for a hypothetical thin reflector monitor where the relative leakage of 'high' energy evaporation neutrons is about twice as great as in the SIGY (see fig. 2.9). The results of computing equation 2.18 are shown in fig. 2.11.

The variations of average efficiency with the energy E_p of incident nucleons, for the SIGY and NM64 monitors have been found from figs. 2.10 and 2.11 using equation 2.2 where α has been taken as A/10. The results of this approximate treatment are shown in fig. 2.12 (curves a and b). Both graphs have been normalised to the experimental source measurement of the LIGY at E_p = 150 MeV. It is evident that the decrease in efficiency is not very sensitive to the different monitor designs.

The actual variations will be less than those calculated due to the secondary interactions and ionization losses. Shen's predictions for varying thicknesses of lead (see fig. 2.6) show that for a thickness of 18cm (one inelastic interaction length), these secondary interactions contribute an ever increasing fraction of the total neutron yield; roughly 50% at 3 GeV, rising to 80% at 10 GeV and 95% at 100 GeV. The first estimate of the effect that these secondary interactions will have on the excitations of the nuclei can be made by finding out for a given incident energy (a) the average numbers of cascade nucleons and created charged pions together with their distributions in energy and (b) the evaporation neutron yield from these secondaries and surviving incident nucleon in the extra-nuclear cascade.

For example, in theenergy region $0.1 < E_p < 5$ GeV there are a

FIG 2.11 Variation of Efficiency With Nuclear Temperature

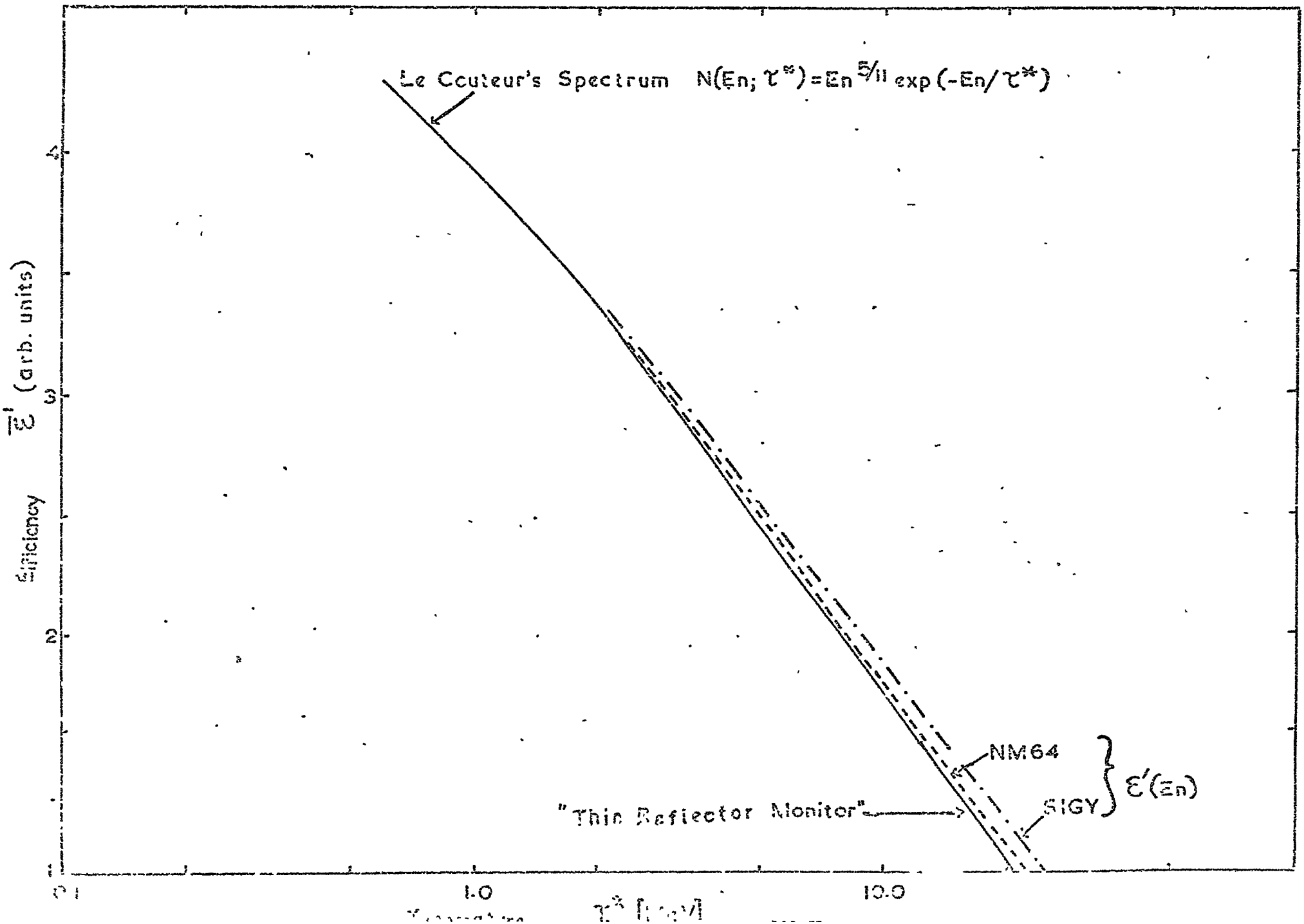

FIG 2.12 Variation of Efficiency with Energy of NAP

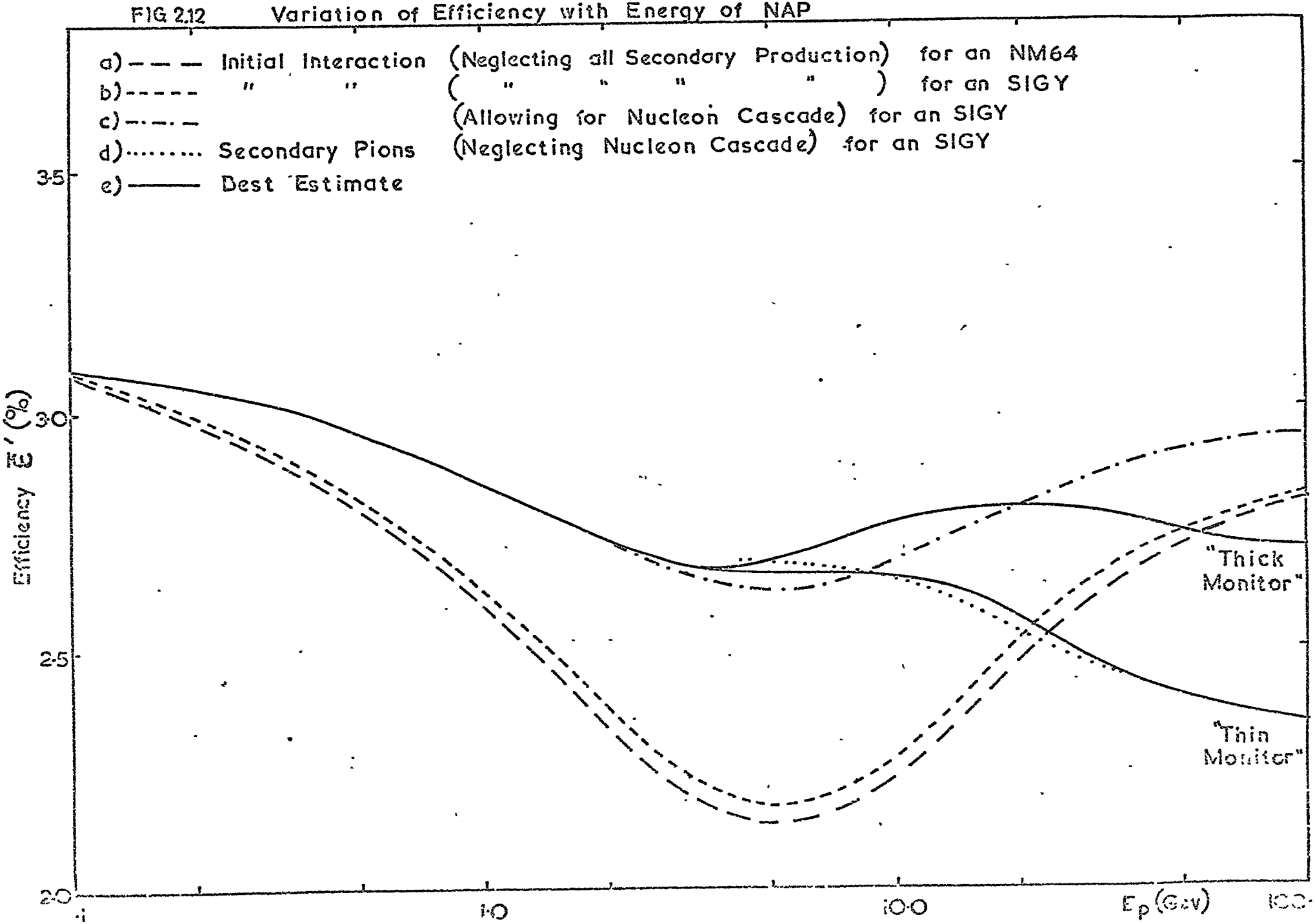

negligible number of pions produced but a spectrum of cascade nucleons with typical energy (Shen, 1968) of 100 MeV. These, together with the surviving incident nucleon which has a similar energy to the cascade nucleons, give rise to as many evaporation neutrons as the first interaction (fig. 2.6). Thus neglecting tertiary interactions, it can be estimated that the decrease in efficiency $\bar{\epsilon}(E_p)$ over this range will be only half of that calculated on the basis of the initial interaction.

For nucleon and pion energies greater than 5 GeV the average number of cascade nucleons per inelastic interaction is proportional to the average number of evaporation neutrons produced (Shen, 1968) and so these cascade nucleons should roughly double the neutron yield at all energies. It would be expected therefore that (neglecting pion production) the variation in $\bar{\epsilon}(E_p)$ is only half that calculated in fig. 2.12 over the whole of the energy range, (curve c, for the SIGY only).

At energies above 50 GeV almost all ($\gtrsim$90%) of the evaporation neutrons arise from secondary pion interactions and their nucleon cascades. The energy spectrum of these pions at production is given approximately by the CKP formula, neglecting the backward cone

$$\frac{dN}{dE_\pi}(E_p) = \frac{1}{\bar{E}_\pi} \exp\left(-E_\pi/\bar{E}_\pi\right) \qquad 2.19$$

where $\bar{E}_\pi$ is the average pion energy, estimated from data quoted by Shen (1968). These pions can be thought of as giving rise to an effective excitation energy given by

$$\bar{U}'(E_p) = \frac{\int_0^\infty \frac{dN}{dE_\pi}(E_p)\ \bar{\nu}(E_\pi)\ \bar{U}(E_\pi)\ dE_\pi}{\int_0^\infty \frac{dN}{dE_\pi}(E_p)\ \bar{\nu}(E_\pi)\ dE_\pi} \qquad 2.20$$

(Neglecting ionization losses)

Where $\bar{U}(E_\pi) \cong \bar{U}(E_p)$ in fig. 2.10.

$\bar{U}$ has been calculated for several values of incident nucleon energy above 20 GeV and the corresponding variation of $\bar{\epsilon}(E_p)$ is shown in fig. 12 curve d for the SIGY. As previously mentioned, these values of $\bar{\epsilon}(E_p)$ should be underestimates due to the effect of the low energy cascade nucleons resulting from the pion interactions. It is difficult to assess the extent of this effect due to the reduced depth of producer presented to this next generation of secondaries, and results in the underestimation not being as great as at 3 GeV. Therefore the variation of $\bar{\epsilon}(E_p)$ in $0.1 < E_p < 100$ GeV is given (curve e) for (i) a thin monitor (i.e. where the neutron yield from pion-produced nucleons is negligible), and (ii) a thick monitor (where this neutron yield is as great as from the "initial" secondary pion interactions). In the region 3 GeV to 20 GeV the variation of $\bar{\epsilon}(E_p)$ has been obtained by interpolation.

The general feature of the variation of efficiency is a decrease to a minimum at energies of about 5 GeV due to the increase in excitation energies of the target nuclei; followed by a further, slower decrease until about 100 GeV due to the effect of the secondary pions, which having average energies of a few GeV tend to give higher nuclear excitations.

However, there is a major source of uncertainty in the variation of the average excitation energy $\bar{U}$ for $E_p \gtrsim 2$ GeV as well as the relatively minor ones concerned with the "evaporation and slow cascade neutron" spectrum and the effect of secondary interactions.

The maximum error in the change in efficiency between $E_p = 0.1$ and 5 GeV due to the possible error in $\bar{U}$ is $\pm$ 30%.

It has been pointed out earlier that the Le Couteur spectrum assumed here gives higher values for the average neutron energy than

that measured at E_p = 150 MeV, and this could cause an error in the estimated decrease in efficiency. Unfortunately there appears to have been no direct experimental measurement made of the spectrum at higher energies so this error can only be estimated from the error at lower energies.

The value of $\bar{\epsilon}(E_p)$ at E_p = 150 MeV has been calculated using the spectrum of Skyrme shown in fig. 2.3d. This value was only 3% higher than that expected from the Metropolis/Le Couteur adopted in the present work, for $\alpha = A/10$. The difference at higher energies may be of the same order, because the results of Pearce and Fowler indicate that the sensitivity of the monitor to changes in the spectrum does not increase as $\bar{E}_n$ increases. The slope of the evaporation spectrum (see fig. 2.3a,b) decreases at approximately the same rate as the slope of $\epsilon'(E_n)$ in fig. 2.9 (i.e. $\approx 1/\bar{E}_n$), so that as E_p increases, although the neutron spectrum increases in width, the relative fall in efficiency over the spectrum remains the same. Therefore, assuming the spectrum of evaporation neutrons produced by, say, a 5 GeV nucleon is as well represented by the corresponding Le Couteur expression as the measured Skyrme spectrum is by the Le Couteur spectrum in fig. 2.3d, then a similar overestimate of $\bar{\epsilon}(E_p)$ would be expected at 5 GeV. It follows that the error in the decrease in effiency between 0.1 and 5 GeV would be even less than this.

The presence of ionization losses should reduce the decrease in efficiency (due to the loss of energy of the incident nucleon, before it interacts) by only a small amount because $\bar{\nu}$ for protons and neutrons are virtually the same for $E_p > 1$ GeV.

The corresponding effect of ionization loss by the secondary particles should not be very important because for $E_p < 5$ GeV the

majority of the evaporation neutrons are produced by secondaries having no charge (neutrons) whereas above about 20 GeV most secondaries are pions of average energy $\gtrsim 1$ GeV which should lose only a small fraction of their energy before interacting.

Considerable uncertainty lies in the effect of the secondary interactions which contribute half of the neutron yield at 5 GeV. It would be possible to obtain a more reliable, quantitative, estimate of the evaporation spectrum by extending the calculations of Shen to include the distribution of nuclear excitations and a detailed treatment of the thermalising of the cascade neutrons. However, in the absence of this, it can be concluded that the efficiency for detecting evaporation neutrons produced in a neutron monitor by nucleons with energies of a few GeV may be about 15% lower than that for detecting neutrons from 100 MeV nucleons. This would account for a large proportion of the discrepancy in fig. 2.7.

With this uncertainty in both ϵ and $\bar{\nu}$, it is appropriate to try and obtain a surer estimate of the efficiency, and to use it to measure $\bar{\nu}$ in a similar experiment to that of Hughes et al. to reduce statistical errors and any systematic errors in the method of analysis.

In the next chapter a new method of measuring the efficiency is described together with its application to an IGY-type monitor. This will be followed in chapter 4 by a description of the use of this monitor to measure the number of neutrons produced by protons and pions.

CHAPTER THREE

THE EXPERIMENTAL EQUIPMENT

The neutron monitor used in this experiment is a development of the IGY type and will be referred to as the Durham IGY (DIGY). It was designed for use as an NAP detector in studies of NAPs in extensive air showers (EAS) in conjunction with a spectrograph and an array of water Cerenkov detectors. The original aim was to record simultaneously a neutron monitor response, one or more momentum analysable tracks in the spectrograph which impacted on the monitor, and an EAS falling nearby. By studying the interactions of the momentum measured particles in the monitor by means of a tray of flash tubes underneath, it was hoped to unambiguously identify most of the NAPs. Unfortunately as reported by Hook (1972), it proved very difficult to distinguish visually the NAP tracks from the copious electron-photon component. Although the present work is concerned with another aspect of cosmic ray studies, that of unaccompanied NAPs, it should be remembered that the design of the experimental equipment stems from the earlier work described by Hook. The equipment is shown in figs. 3.1 and 2.

3-1 The Durham Neutron Monitor (DIGY)

3-1.1 The Design

The results of Shen (1968) demonstrated that $\bar{\nu}_t$ and the ratio $\Delta \bar{\nu}_t(E_p)/\Delta E_p$ increase generally as the thickness of producer increases (see fig. 2.6) due to the greater probability of absorbing the energy of the incident particle through secondary and higher interactions. This reduces the statistical errors in $\bar{\nu}_t$, by increasing the probability of detecting an NAP, particularly for high values of E_p as are found in air showers, provided the efficiency of neutron detection does not decrease. For thicknesses greater than about two interaction lengths it becomes very difficult to calculate $\bar{\nu}(E_p)$ accurately because it

Fig. 3.1 The Modified Air Gap Spectrograph.

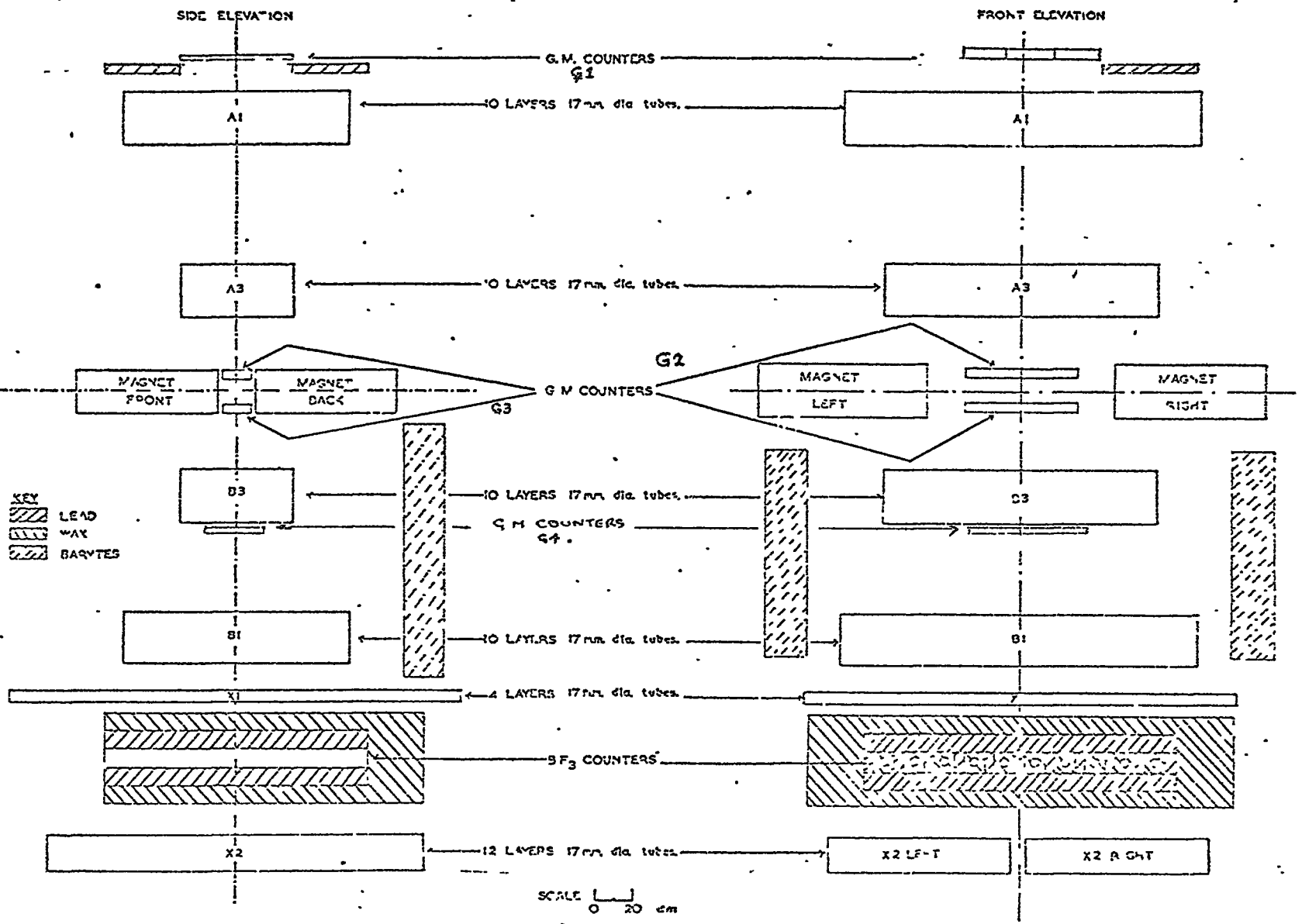

FIG. 32 The DIGY Neutron Monitor

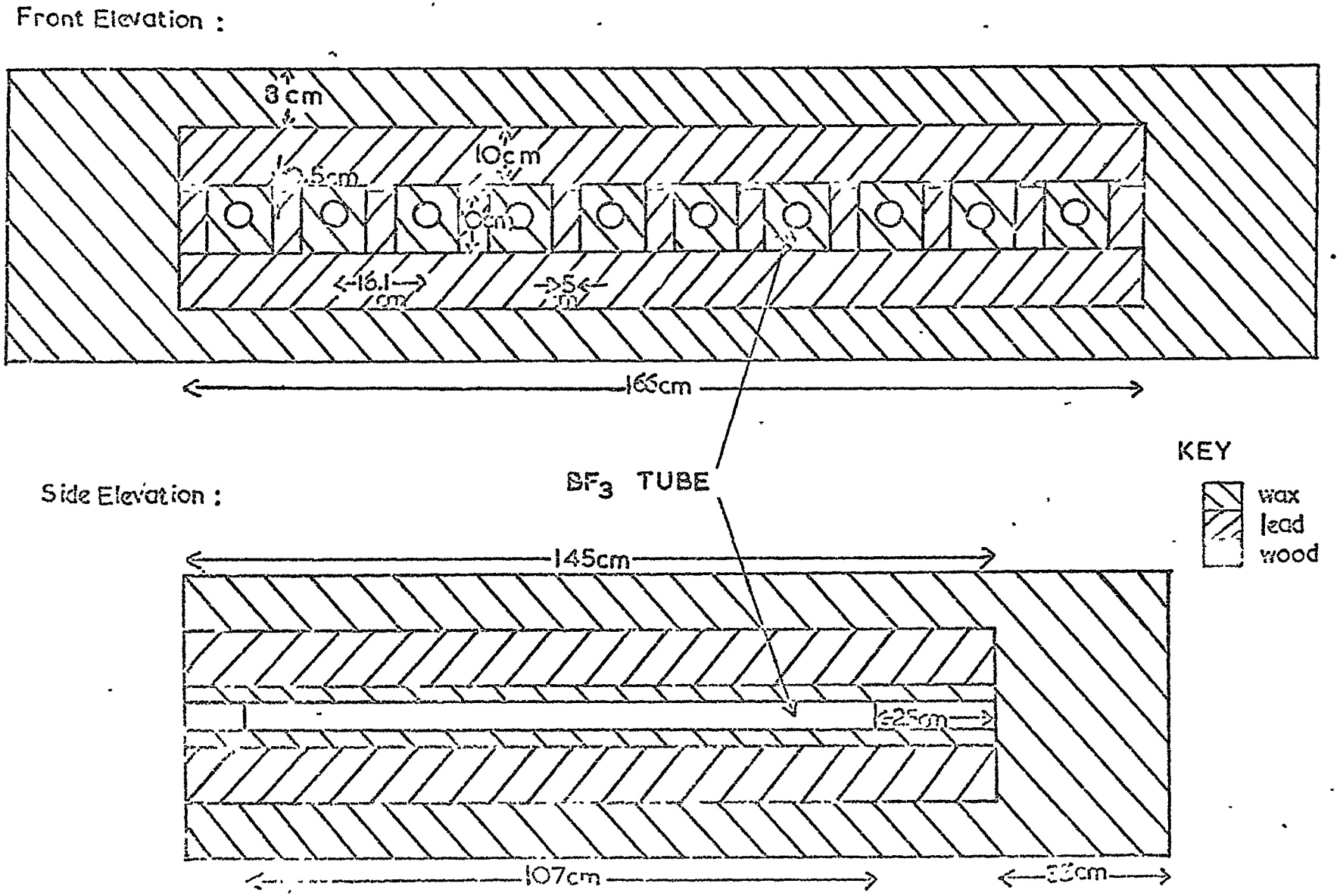

is no longer possible to assume a one dimensional approach (Shen, 1968). Further, any increase in producer thickness will tend to decrease the average solid angle subtended by the inner moderator to the producer and increase the volume accessible to the neutrons, thus reducing the neutron detection efficiency. For these reasons it was decided to have an average thickness of lead producer equal to 1.3 interaction lengths for nucleon/nucleus interactions, almost double the 0.75 interaction lengths of the SIGY and LIGY. Compared to the LIGY, the sensitive area was increased by having ten longer BF_3 counters, each of effective length 107cm and their detection efficiency was enhanced by the use of a higher gas pressure. The outer reflecting layer of paraffin was reduced considerably to 8 cm in order to reduce the vertical dimension, but the resulting loss of evaporation neutrons should be very small (Hatton and Carmichael, 1964). A summary of the design features of a selection of monitors (partly taken from Hatton 1971) is shown in table 3.1.

3-1.2 Auxiliary Electronics

It was anticipated that good spatial resolution across the monitor would help to differentiate in an EAS between the neutrons produced by two or more NAP candidates impacting on the monitor. To this end each counter in the monitor was individually hodoscoped, having its own amplifier, discriminator, multiplicity recorder and data-recording facilities. The amplifier/discriminator unit for each channel was built in an all-enclosing, earthed copper box and placed near to the BF_3 tube, in order to minimise the danger of radiative pick-up from the nearby flash tube pulsing system. The circuit diagram for one channel is shown in fig. 3.3. The BF_3 counter was operated with an EHT of -4.1kV applied to the outer copper electrode. This rather high value was chosen in order to differentiate more between the

TABLE 3.1

A Comparison of Monitor Designs

		SIGY	LIGY	DIGY	OTTAWA IGY	NM64
Number of Counters per Channel		6	6	1	1	6
Counters	Active length cm	86.4	41	107	69	191
	Diameter cm	3.8	5.1	5.1	6.35	14.8
	Pressure cm Hg	45	40	70	56	20
	Average Depth g cm^{-2}	153	153	268	285	156
Producer	Area per channel m^2	0.94	0.72	0.24	0.17	6.21
	Length Parallel to counters cm	102	76	145	61	207
Average Thickness of Moderator cm		3.2	3.3	3.2	5.4	2.0
Average Thickness of Reflector cm		28	28	8	13	7.5
Approximate Counting Rate †	Per Channel per hr	12,000	9,000	6,000	6,000	250,000
	Per m^2 of producer per hr.	12,800	12,000	25,000	35,000	40,000
Average Efficiency		0.022*	0.021	0.021*	0.034*	0.050

† The average rate over the solar cycle at high latitude, sea level and at normal atmospheric pressure.

* Estimated values from the relative counting rates.

Fig. 3.3 The Proportional Counter Electronic System.

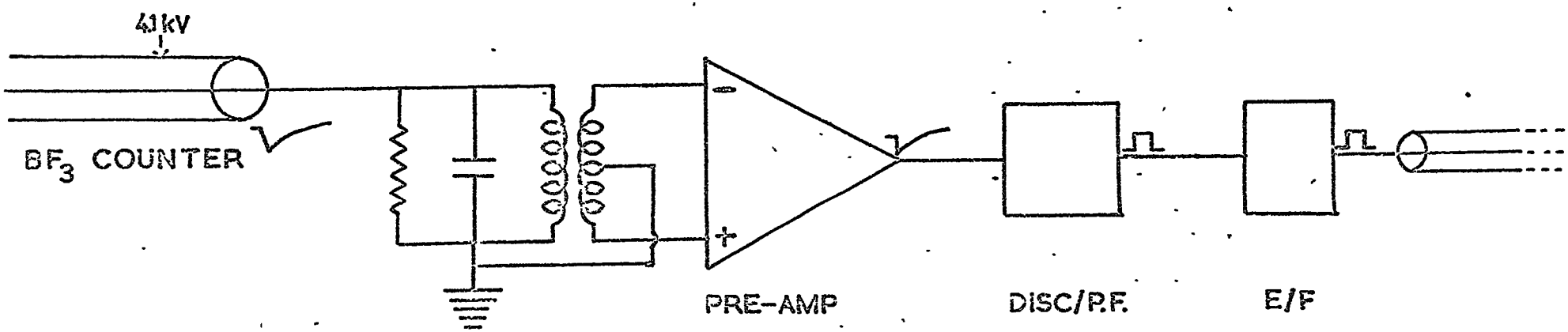

detected neutron pulses and the radiative pick-up. This pick-up was also partially filtered away from the counter output by the resistor/capacitor combination, whose values were found empirically. The negative signal from the inner electrode was fed into the primary of a matching transformer which gave positive and negative outputs from two oppositely wound secondaries. These two outputs were fed into the inverting and non-inverting inputs of a differential amplifier, SGS type$_\mu$ A702A) which produced a negative output signal. This was fed into a discriminator/pulse-forming circuit (SGS type$_\mu$ A710A) which produced a 4V positive, 6 μsec long square pulse for input pulses greater (negatively) than the discriminator level. The discriminator level was chosen on the basis of the pulse height distribution obtained from the discriminator input, a typical example of which is shown in fig. 3.4. It was estimated that 90% of the genuine neutron pulses were greater than the discrimination level and that the noise contribution from cosmic ray traversals of the BF_3 tube, was negligible. The dead time of the amplifier/discriminator was just the length of the square output pulse and would give rise to a negligible fractional loss of neutrons due to overlap ($\lesssim$1%). The square pulses were fed along several meters of 68Ω co-axial cable to a digital scaling unit shown in fig. 3.5 for use in conjunction with the operation of the spectrograph. The signals were gated by an SCR unit (whose only purpose was to prevent pulses induced by the high voltage flash tube pulsing system from entering the scaling unit) before passing through the neutron monitor (NM) gate which was activated by a pulse of accurately known delay (40μsecs) and length (300μsecs). Both gates could be controlled by, say, the Geiger-Muller counters in the spectrograph. The pulses from each counter were counted by a 4-bit binary counter so that the gated multiplicity in each channel could be recorded and displayed in binary form, using bulbs situated in the field of view of the

Fig. 3.4 The Pulse Height Distribution from a Proportional Counter.

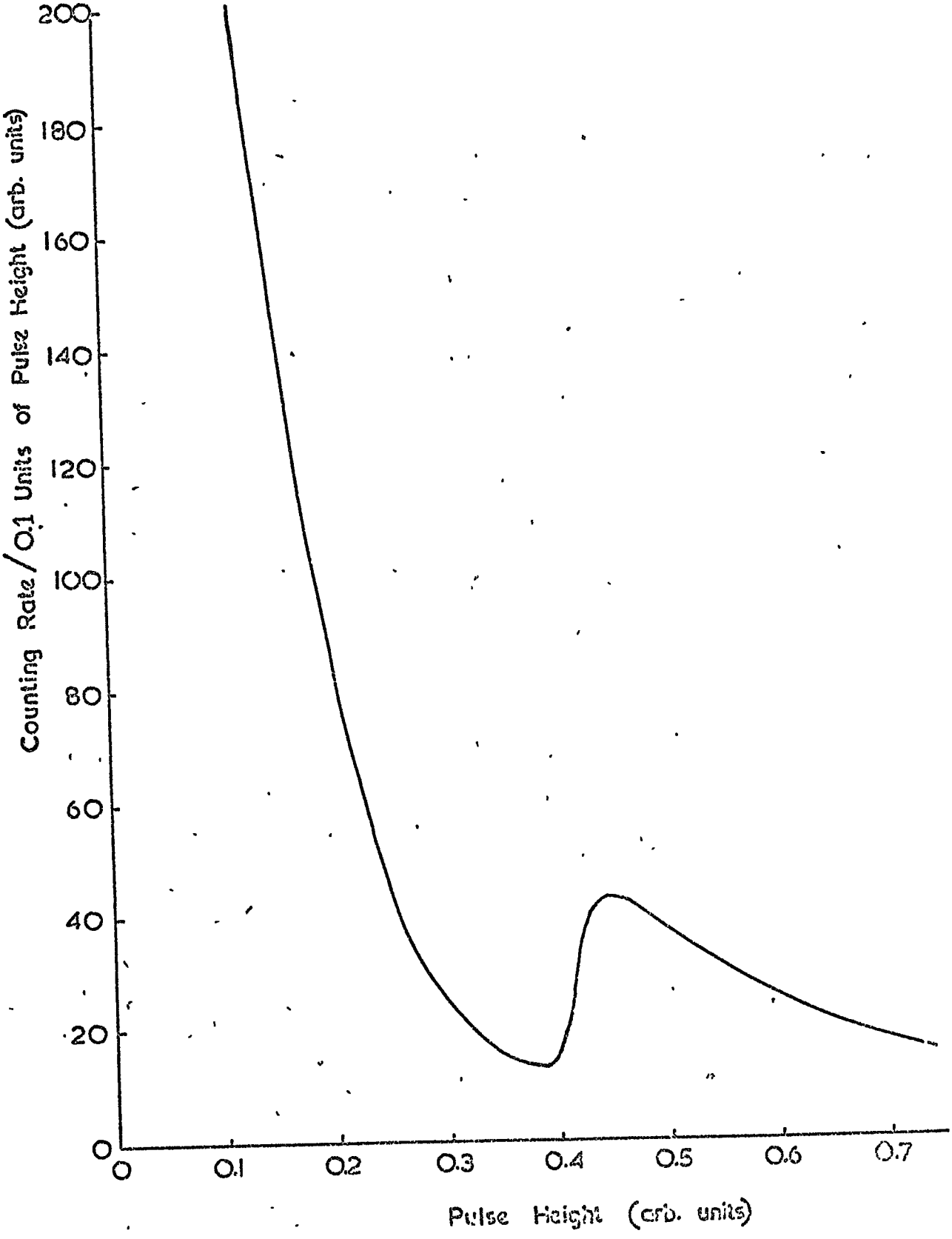

Fig 3.5 The Neutron Multiplicity Recording System

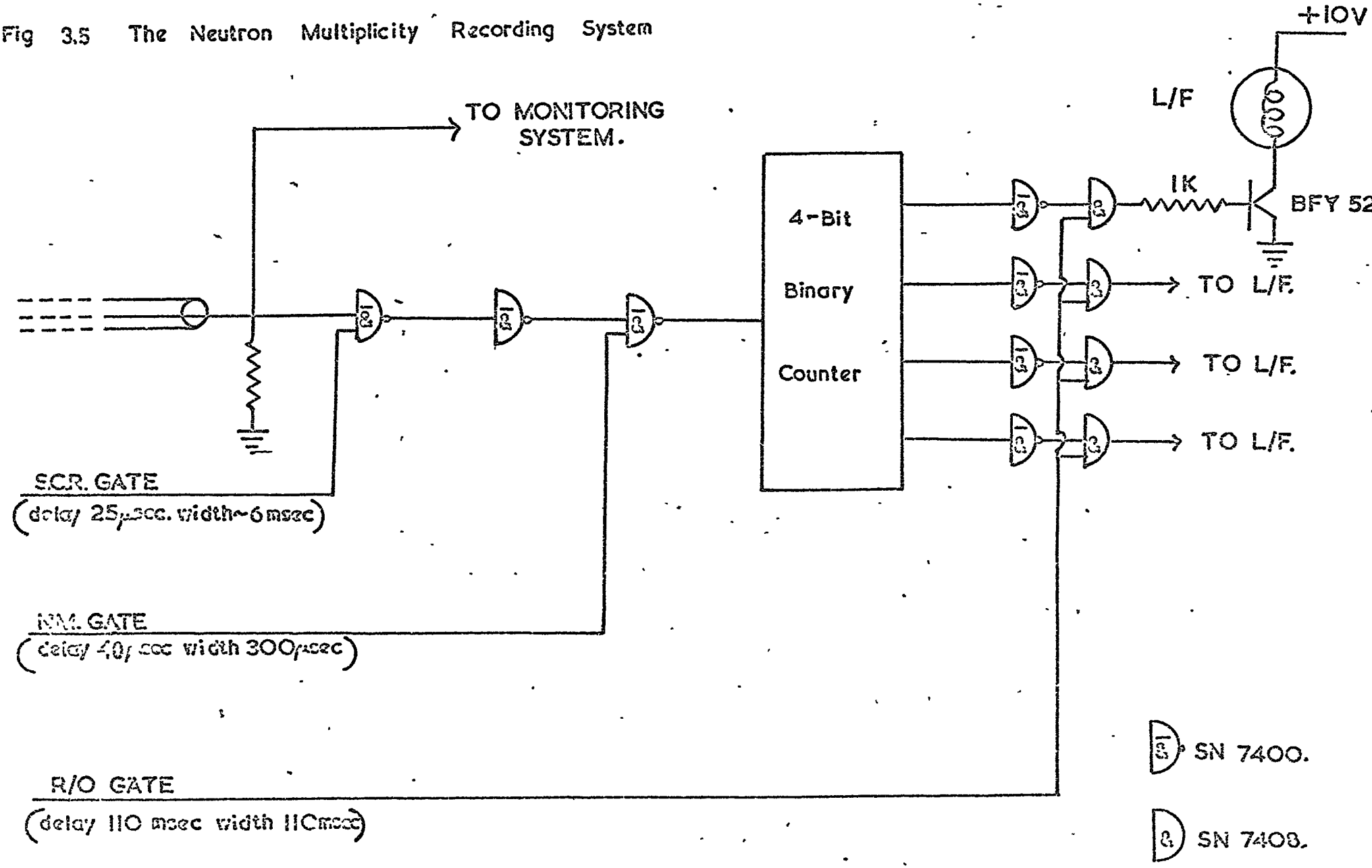

spectrograph recording cameras. An illuminated bulb represented binary '0' and so, since the most likely multiplicity is zero most of the bulbs were tested in each event. It should be noted that the maximum number that could be read out was 15, and multiplicities greater than this would be read out as m-16.

Each of the ten channels was fed into a coincidence circuit (fig. 3.6) which added the pulses, gated them with the NM gate, and sent a 1msec long output pulse to the spectrograph control panel (see section 3.3) if there was at least one neutron within the gate time.

The multiplicities in each channel for each event were recorded by two cameras which were also used to record simultaneously the information on the particle momentum and charge in the spectrograph. In addition, the total multiplicity for each event and the times of detection of the neutrons after some predetermined time could be recorded on a cathode ray oscilloscope (CRO)

3-1.3 Checks of the Equipment

When the monitor was used in conjunction with the spectrograph it was necessary to gate the multiplicity recorders against pulses from radiative pick-up on the BF_3 tubes produced by the flash- tube pulsing system. An SCR gate was used on the inputs to the ten binary counters, which only opened 40μsecs after the flash-tubes were pulsed. To check that the gate was preventing this pick-up from entering the multiplicity recorders, the spectrograph and monitor were operated together for 48 hrs with the EHT of the monitor BF_3 counters off but all other power supplies on (including the amplifiers and discriminators of the monitor). No events were recorded during this time in which the flash-tubes were pulsed about 30K times.

Another potential source of spurious counts from the BF_3 counters was from their EHT supply. Due to the high value used (~4kV) normal EHT coaxial plugs carrying the signal along the inner connection, with

Fig. 3.6 The Neutron Counter Event Selector.

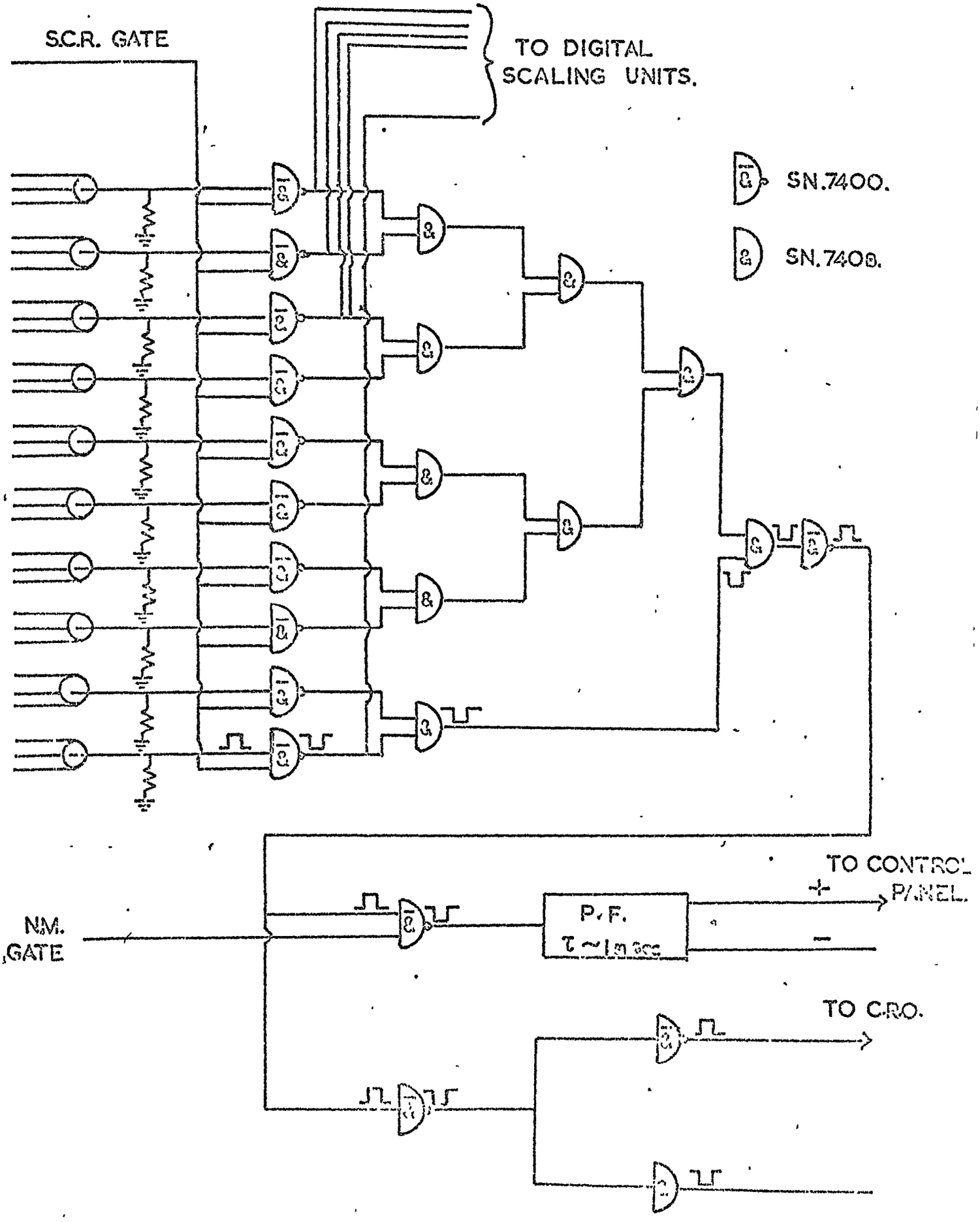

the EHT on the outer casing, could not be used to supply the counters because of slight breakdown across the insulator onto the signal wire which produced pulses of a few mV. A satisfactory alternative was found by supplying the EHT in a cable far removed from the signal wire and connected to the counter by a battery clip. A comparative check on the performance of this monitor has been made by measuring the real and apparent time distributions for the arrival of neutrons (fig. 3.7 and 3.8). The real time distribution (zero time is the time of the interaction) in the range 40 - 340μsec was obtained from all the events classified as protons or pions in the work described in Chapter 4. An oscilloscope was triggered at the time of interaction and any subsequent neutrons recorded by the monitor, appeared on the trace against a calibrated scale, to be photographed by a camera. It is seen that the resulting time distribution is very similar to that obtained from the LIGY (Hatton and Tomlinson, 1968), although there is evidence of a slightly steeper slope. Considering the similarity in design of the inner moderator and BF_3 counter, a similar distribution is to be expected.

The apparent time distribution was recorded in a similar way except that the oscilloscope was triggered by the neutrons themselves (zero time being the time of arrival of first neutron). In this way the arrival times of second and subsequent neutrons after the first, were measured. It is seen that this time distribution agrees with the corresponding one for the LIGY up to 400μsecs except for a slightly steeper slope, as found for the real time distribution. However, between 400μsecs and 1000μsec the DIGY appears to be about 50% less than the LIGY. This can be interpreted, after Hatton and Tomlinson, as meaning that the thinner reflector of the DIGY is only half as efficient as that of the LIGY. However in view of the small contribution to the total counting rate that these reflected neutrons make, the net

FIG. 3.7 The Distribution of Real Detection Time of Neutrons Produced by NAP's in the DIGY

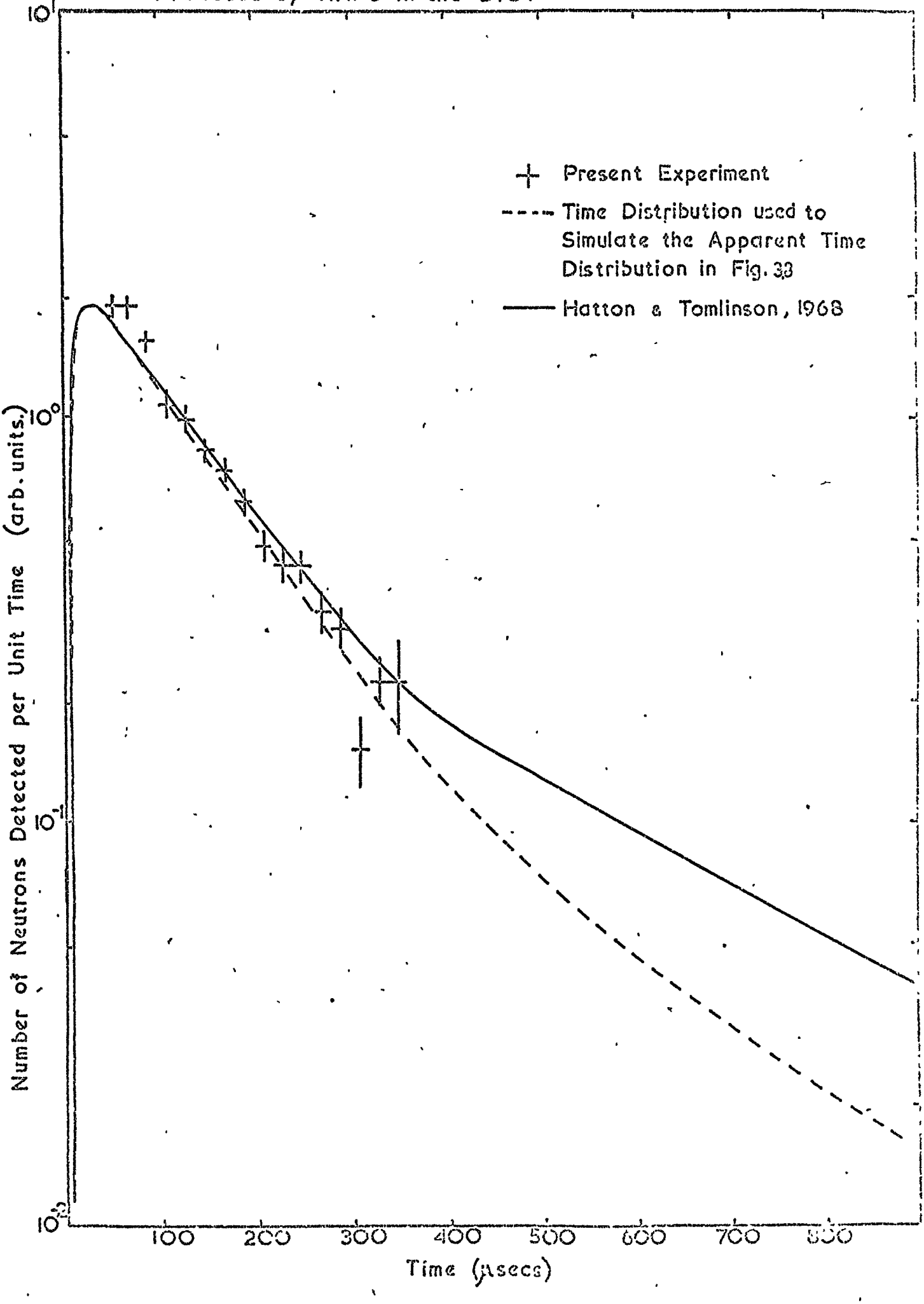

Fig. 3.8 The Distribution of Apparent Detection Time of Recorded Neutrons.

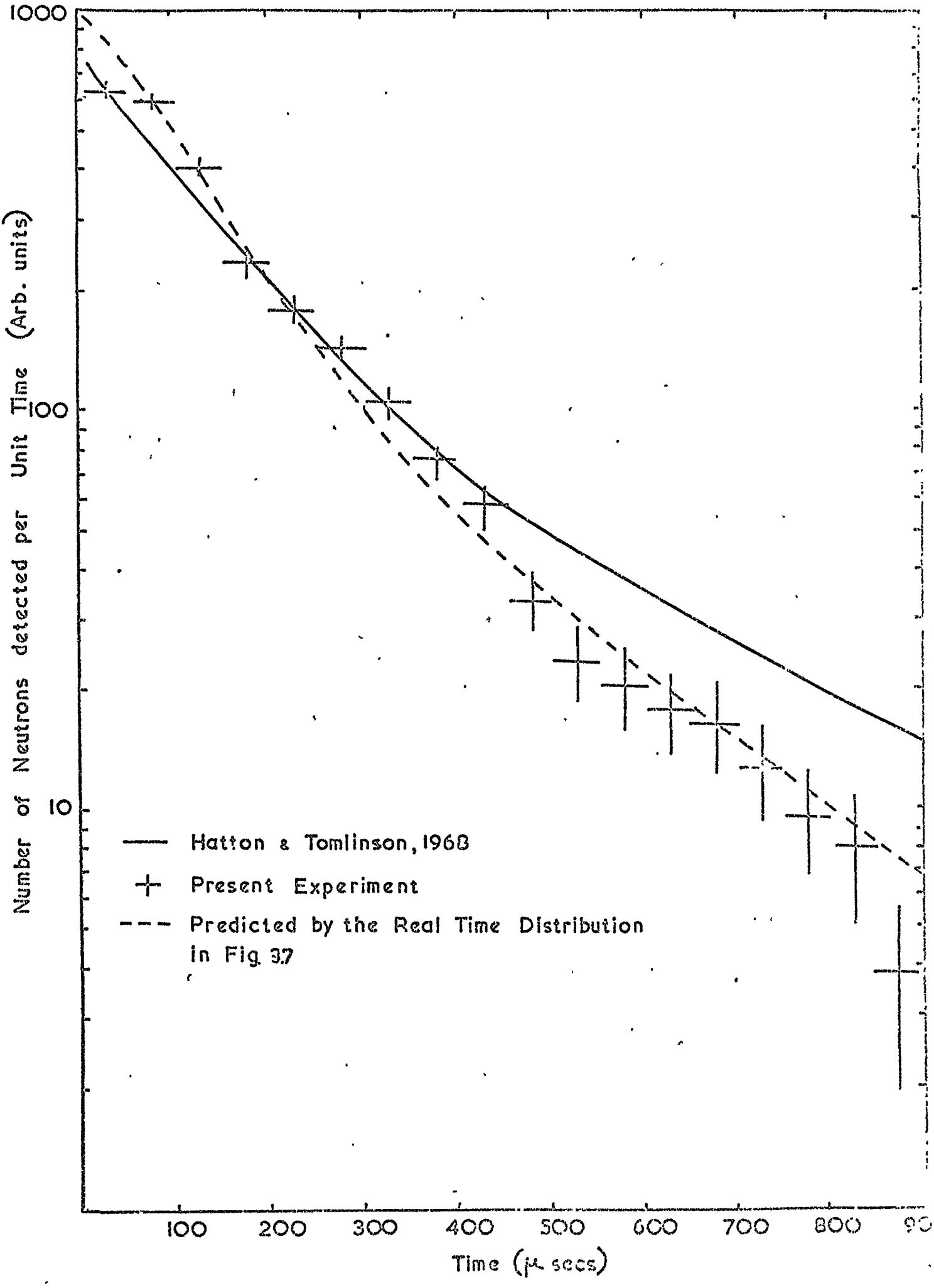

loss in efficiency is only about 5%.

The real time distribution of the DIGY has not been measured beyond 340μsec, or less than 40μsec, but it can be found from the apparent time distribution in the manner of Hatton and Tomlinson, assuming a distribution of arrival time t of the first neutron in events of multiplicity m, given by $e^{-tm/\tau}$ where τ is the mean lifetime of evaporation neutrons in the monitor. It has been shown that the observed apparent time distribution of the DIGY is consistent with the real time distribution given in fig. 3.7, assuming τ=150 sec, and using the distribution in multiplicities P(m) found for the DIGY. It was found that the predicted apparent time distribution was not very sensitive to the possible uncertainties in τ or P(m).

The counting rates of each channel were indicated by ten separate rate-meters which allowed a convenient and effective check on its daily performance, a serious fault in any of the ten channels being immediately obvious. The multiplicity distributions and count rates for each channel have been obtained using a multiplicity recorder and are shown in table 3.2. The neutron gate in the multiplicity recorder was delayed by 25μsec and was 350μsec, in length, so that its results could be roughly compared with the spectrograph scaling units. In the above measurements the gate was triggered by the first neutron so that the gating efficiency f has been obtained from the apparent time distribution and it was found to have a value of 0.70.

The multiplicity distribution for the whole of the monitor, obtained in a similar way is shown in fig. 3.9. Theaverage multiplicity $\bar{m}$ appropriate to f=1 is~1.34.

There is evidence in table 3.2 that channels 4 and 6 may be about 20% less efficient than the others; both the counting rates and the average multiplicities being significantly lower than the others. The

TABLE 3.2

Multiplicity Distribution and Counting Rate of each Channel of the DIGY.

Channel	1	2	3	4	5	6	7	8	9	10
Average Detected multiplicity m	1.10	1.11	1.09	1.08	1.09	1.07	1.10	1.10	1.12	1.11
Counting Rate $hr.^{-1}$	3023	3700	3729	2920	3529	3072	3985	4031	3934	3439

Fig. 3.9 The Multiplicity Distribution of Neutrons recorded by the DIGY Monitor in the Cosmic Ray Beam compared with that for a Leeds L.I.G.Y. Monitor.

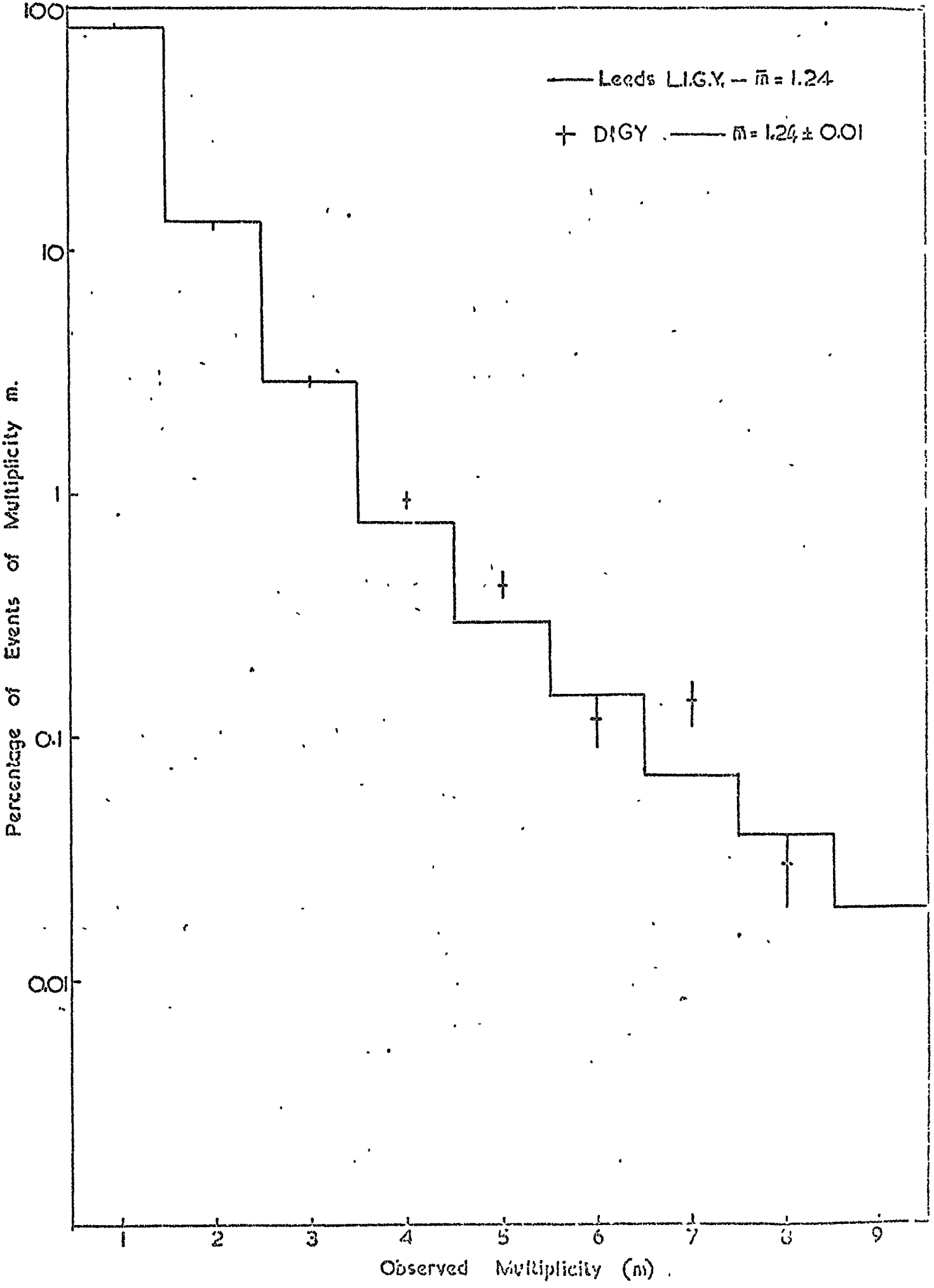

lower counting rates of the outer channels would be expected because of the reduced amount of producer contributing to the count rate of these channels. The monitors performance with individual interacting cosmic rays selected and measured by the spectrograph can give a clearer indication of the variation of efficiency across the monitor. The distribution in number of neutrons detected in each channel for a few hundred events classified as protons and pions (see chapter 4) interacting in the monitor over a restricted width, is shown in fig. 3.10. It is seen that although the frequency of responses from channels 4 and 6 may be relatively low the distribution in lateral impact of the detected incident protons andpions over the monitor indicates no irregularity in the acceptarce function of the monitor; the dip in impacts over channel five being due to the rejection of protons andpions which pass near the gap of the flash tube tray under the monitor (see section 4.4.2). It would seem that the diffusion of the evaporation neutrons across the monitor may have smoothed out any small change in counter efficiency.

A more detailed study of the response of the monitor to evaporation neutrons produced by interacting particles, particularly stopping negative muons, is described in section 3.2.

3-1.4 The Cosmic Ray Beam Count Rate

Due to the similarity in design between the LIGY and DIGY (see table 3.1) it is possible to roughly estimate the efficiency of the DIGY relative to that of the LIGY (which is known from the work of Hughes etal(1964)) by comparing their counting rates when exposed to the same flux of cosmic rays.

The relative contributions from the various components of this flux, to the total count rates of the NM64 and LIGY, have been calculated by Hughes and Marsden (1966), Harman and Hatton (1968) and more recently

Fig. 3.10 . The Uniformity of the Response of the Neutron Monitor.

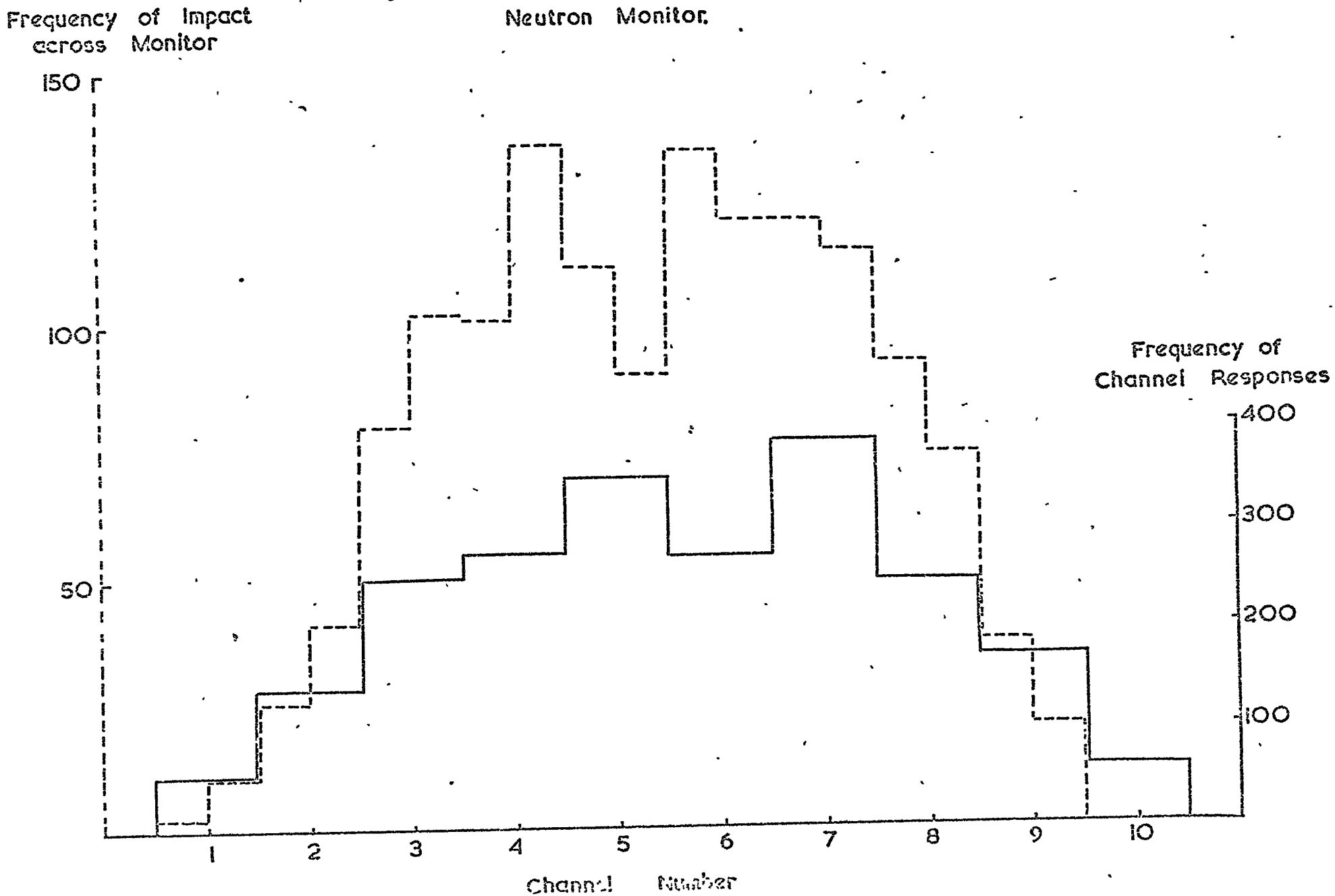

by Hatton (1971) (see table 3.3). Unfortunately, the energy spectrum of the principal component, neutrons, is the least known of all the components, but they are nevertheless thought to be responsible for most of the counts in both NM64 and LIGY. Since the second most important component, protons are similar to neutrons, to a first approximation the other components may be neglected.

Using an assumed neutron spectrum N(E)dE and average produced evaporation neutron multiplicity $\bar{\nu}(E)$ (Shen (1968), Hughes et al.(1964)) the median energies of the nucleons contributing to the count rates of the monitors have been calculated allowing for attenuation of the cosmic ray flux in the outer reflector (Hatton, 1971). The difference (160 MeV for the LIGY compared with 130 MeV for the NM64) was partly attributed to the different reflector thicknesses (11" and 3" respectively) which would mainly affect the low energy neutron contribution. This would have the effect of lowering theaverage produced multiplicity of the events detected by the NM64.

The multiplicity distribution of the DIGY should be affected in a similar way, not only because of its 3" reflector, but also because of its thicker producer which increases the fraction of (lower multiplicity) muon contributions (Hatton 1971). However, the problem is complicated by the presence of the spectrograph (principally a large mass of iron) underneath whichthe DIGY was built and operated, and the large solid angle subtended by nearby land masses. The effect of these would be to reduce the flux of cosmic rays incident on the monitor so a three counter model of the DIGY was built well away from large objects such as the large mass of iron in the spectrograph, so that the effect of these objects on the count rate could be found. The rate of the centre counter was compared with that of a counter in the standard, ten counter model under the spectrograph, and was

TABLE 3.3

The Relative Contributions to the Total Counting Rate of a Monitor.

	LIGY	NM64
Neutrons	0.79	0.76
Protons	0.07	0.06
Pions	0.01	0.01
Stopping Muons	0.04	0.03
Interacting Muons	0.02	0.02
Background	0.06	0.12

found to be 50% higher. There was an uncertainty of about 5% in the measurements of the centre counter of the mini-monitor regarding the choice of reflector thickness at the sides. In addition, the unavoidable presence of nearby buildings may have reduced the count rate by about 10%.

In order to relate the efficiencies of the DIGY and LIGY through their counting rates it is necessary to correct forthe different attenuations of the cosmic ray flux by the different reflector thicknesses. Hatton and Carmichael (1964) have measured the variation of counting rate with reflector thickness for a two counter NM64 monitor and found a maximum rate at 2" thickness. The decrease in rate as the thickness increases was attributed primarily to the attenuation of the nucleonic component of the cosmic ray flux, & secondarily to the absorption of evaporation neutrons produced outside the monitor. Assuming the count rate of the DIGY behaves in the same way as the NM64, there would be a decrease of 25% in the count rate if the reflector thickness was increased from 3" to the LIGY thickness of 11"; of which ~2% would be responsible to the absorption of externally produced evaporation neutrons.

The number n of evaporation neutrons detected per sec per m^2 of (horizontal) producer surface area, is related to the number N produced per sec per m^2 of producer by the expression

$$n = \epsilon N \qquad 3.1$$

where ϵ is the average efficiency of detecting an evaporation neutron of any energy.

Using a result of Treiman and Fonger (1952), the total neutron production in a slab of lead of thickness t, due to the cosmic radiation is approximately

$$N \propto f' \int_0^t \exp(-Z/L)\, dZ \qquad 3.2$$

where $L = 320$ g cm^{-2}

and f' is the attenuation of radiation in reflector, which has the value 0.75 for the LIGY compared with the attenuation of the DIGY, as mentioned earlier.

Evaluating the integral 3.1 for $t = 150$ and 270 we relate the expected production rate N_D of the DIGY when clear of the spectrograph to the production rate N_L of the LIGY thus

$$N_D \approx \frac{N_L}{f'} \cdot \frac{0.57}{0.375} = 2.0\ N_L \qquad 3.3$$

Using the observed counting rates/m^2 in the table 3.1 we get the estimated efficiency of the DIGY

$$\epsilon_D = \frac{N_L}{N_D}\frac{n_D}{n_L}\epsilon_L \approx \frac{1}{2.0} \cdot \frac{26.0}{12.0}\epsilon_L \approx 0.021 \qquad 3.4$$

This result indicates that the efficiency of the DIGY is very similar to the efficiency of the LIGY used in the work of Hughes et al. (1964). The effect of the high pressure counter in increasing the efficiency of the monitor (Hatton and Carmichael) was almost exactly compensated by the choice of discrimination level in the DIGY which was biased against 10% of the genuine neutrons. One of the actual low pressure BF_3 counters used in the LIGY of Hughes et al. has been placed in the DIGY and operated with a discrimination level that was $\sim 100\%$ efficient in selecting neutrons. It was found to give the same count rate per length of counter as the high pressure ones, operated inefficiently.

The effects of the thinner reflector of the DIGY and the possible malfunctioning of channels 4 and 6 would be to lower its efficiency by about 5% in both cases. A possibly more important factor determining the efficiency is the thickness of producer, which alters the density of neutrons and the mean solid angles presented by the inner thermaliser/

counters to the lead producer. This differs in the two monitors. However, its effect is very difficult to predict quantitatively, because on the one hand , the mean solid angle subtended by the thinner producer in the LIGY will be higher, leading to a higher efficiency; but on the other, this may be over-compensated by the greater end corrections of the shorter monitor. It would therefore appear coincidental that the two monitors have closely similar efficiencies.

As a check on this method of estimating the efficiency of the DIGY, the values of n and average reflector thickness in table 3.1 have been used to predict the efficiencies of the other monitors. Using $\epsilon = 2.1\%$ for the LIGY, values of 2.2%, 3.4% and 5.7% were obtained for the SIGY, Ottawa IGY and NM64 monitors, in good agreement with the values quoted by Hatton (1971). The Ottawa monitor (Fenton, Fenton and Rose, 1958) is an IGY type design incorporating similar features to the DIGY having a comparable thickness of producer, gas pressure and reflector thickness. It s higher estimated efficiency is not unexpected in view of the large size and length, relative to producer, of the inner moderator and counter, which therefore subtend a larger solid angle to the producer than those in the DIGY.

3-2. Measurement of Absolute Efficiency of the DIGY

3-2.1 Introduction

One of the sources of evaporation neutrons which are detected in a monitor is the process by which a negative muon slows down by ionization within the producer and becomes captured in an electron orbit of a lead atom. It has a high probability of cascading into the inner K- shell and interacting with the nucleus according to

$$p^+ + \mu^- \rightarrow n + \nu_\mu \qquad 3.5$$

Most of the rest mass energy of the muon is removed by the neutrino leaving the nucleus with an excitation energy of about 15 MeV. The subsequent de-excitation, principally by emission of evaporation particles (~0.5% proton, ~99% neutrons) has been carefully studied by several authors using devices with neutron detection efficiencies of the order of 0.5, which are also rather insensitive to the energy of the evaporation neutrons. The resulting value of $\bar{\nu}_{\mu^-}$, the average number of neutrons emitted per de-excitation, is known to an accuracy of 4% (MacDonald, 1965), so that if the monitor's response to negative muons stopping in the monitor is known, it is possible to accurately calculate its efficiency for detecting these evaporation neutrons.

3-2.2 The Experiment

In the experiment to be described in Chapter 4, the monitor was operated in conjunction with a magnet spectrograph in a similar way to the experiment of Hughes et al. (1964).

The minimum momentum of a muon to pass vertically through the thickest part of the DIGY (340 g cm^{-2}) is 530 MeV/c. Amongst the events recorded on film were a large number of single particles with deflections appropriate to momenta less than 700 MeV/c, negative charge, no emerging track underneath the monitor and with impacts on the monitor close to the channel containing the detected neutron(s). These events were classified as stopping negative muons. During the experiment in which there were 8.13×10^5 4-fold coincidences between the Geiger counters in the spectrograph (predominantly single muons), the number of events in the stopping μ^- category was 1157, the number of detected neutrons $n_{\mu^-} = 1170$, with an arrival time distribution shown in fig. 3.11. The results have been corrected for accidental coincidences between a stopping muon giving no detected neutron, and a neutron from the overall monitor background count rate of 11 sec^{-1}. which accounted for about 10% of the

FIG. 311 The Distribution of Real Detection Time of Detected Neutrons Produced by Stopping μ^- in the DIGY

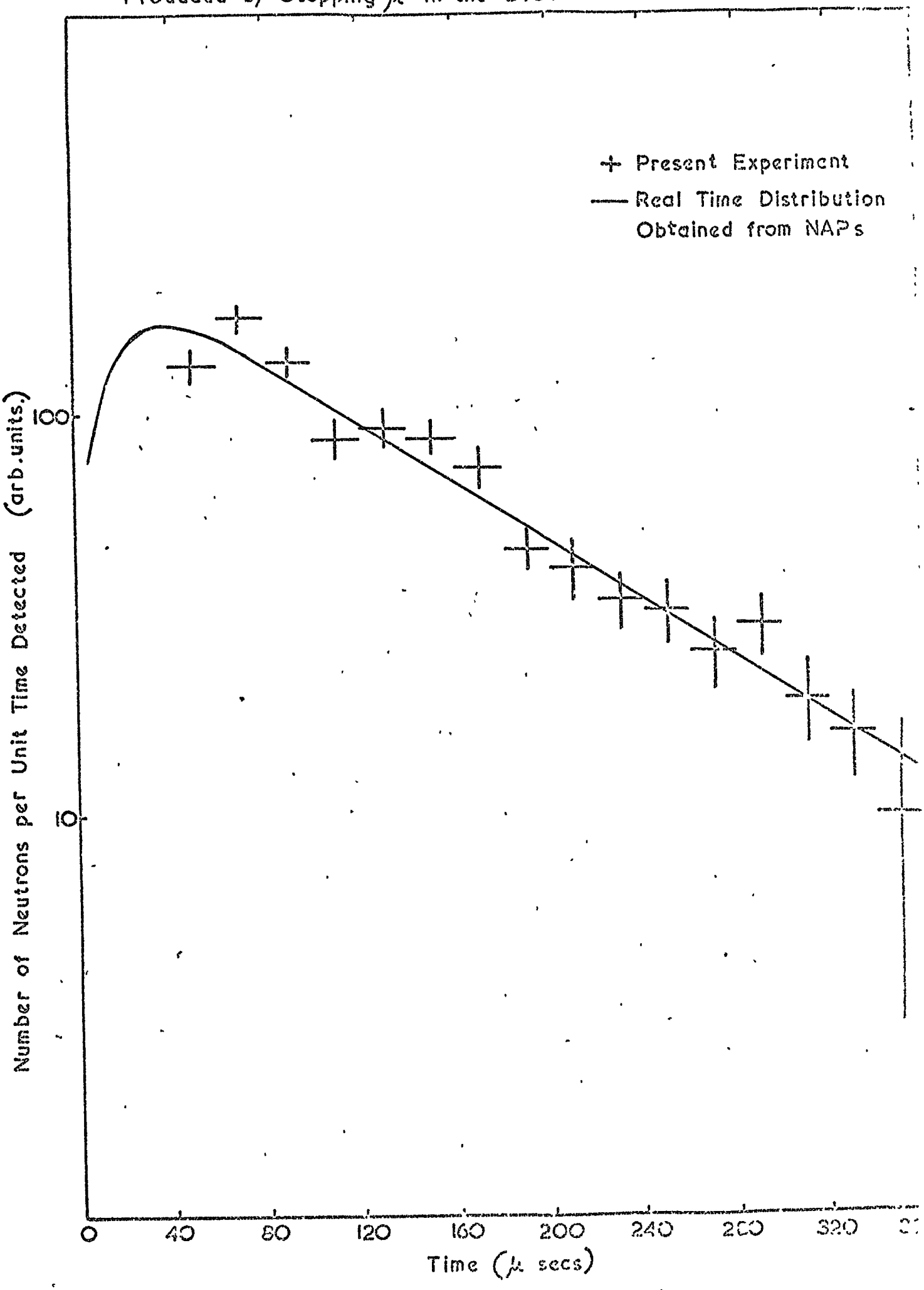

events recorded. The corrected time distribution is very similar to the real time distribution found for protons and pions, thus justifying the use of the same gating efficiency f (=0.7) as in the NAP work in chapter 4.

3-2.3 Number of negative muons stopping in the monitor during the Experiment

The number of negative muons with apparent magnetic deflection $\Delta\psi > 4.2^{o}$ (corresponding to momenta < 0.7 GeV/c) that stopped in the monitor during the experiment was calculated in two independent ways. The first used the vertical muon sea-level spectrum of Allkofer et al. (1971) (fig. 3.12) correcting for the reduced acceptance of the spectrograph for low momentum (and hence large magnetic deflection) particles, angular coulomb scattering and interaction and other measurement losses in the flash tube trays. The absolute number of stopping muon candidates was found by normalising the measured number of the 8.13×10^{5} 4-fold Geiger coincidences which were single muons with momenta ≥ 1 GeV/c to the Allkofer integral intensity at 1 GeV/c.

The number of negative muons that stopped in the lead producer with a measured deflection in the range $(\Delta\psi_i - \Delta\psi_j)$ is

$$I_{\Delta\psi j}^{\Delta\psi i} = T\ A\ L_f \int_{\Delta\psi_j}^{\Delta\psi_i} \int_{p_{min}}^{p_{min}} S'(p)\ W(p,\Delta\psi)\ dp\ d(\Delta\psi) \qquad 3.6$$

where $S'(p)$ is the differential momentum spectrum of muons weighted with the probability of being stopped in the lead,

L_f is the probability of a recorded particle being identified, accepted and having a measureable momentum,

A is the acceptance of the spectrograph for infinite momentum particles,

T is the total sensitive on-time during the run,

and $W(p,\Delta\psi)$ is the weighting factor function for muons and is the

FIG. 3.12 The Differential Muon Spectrum

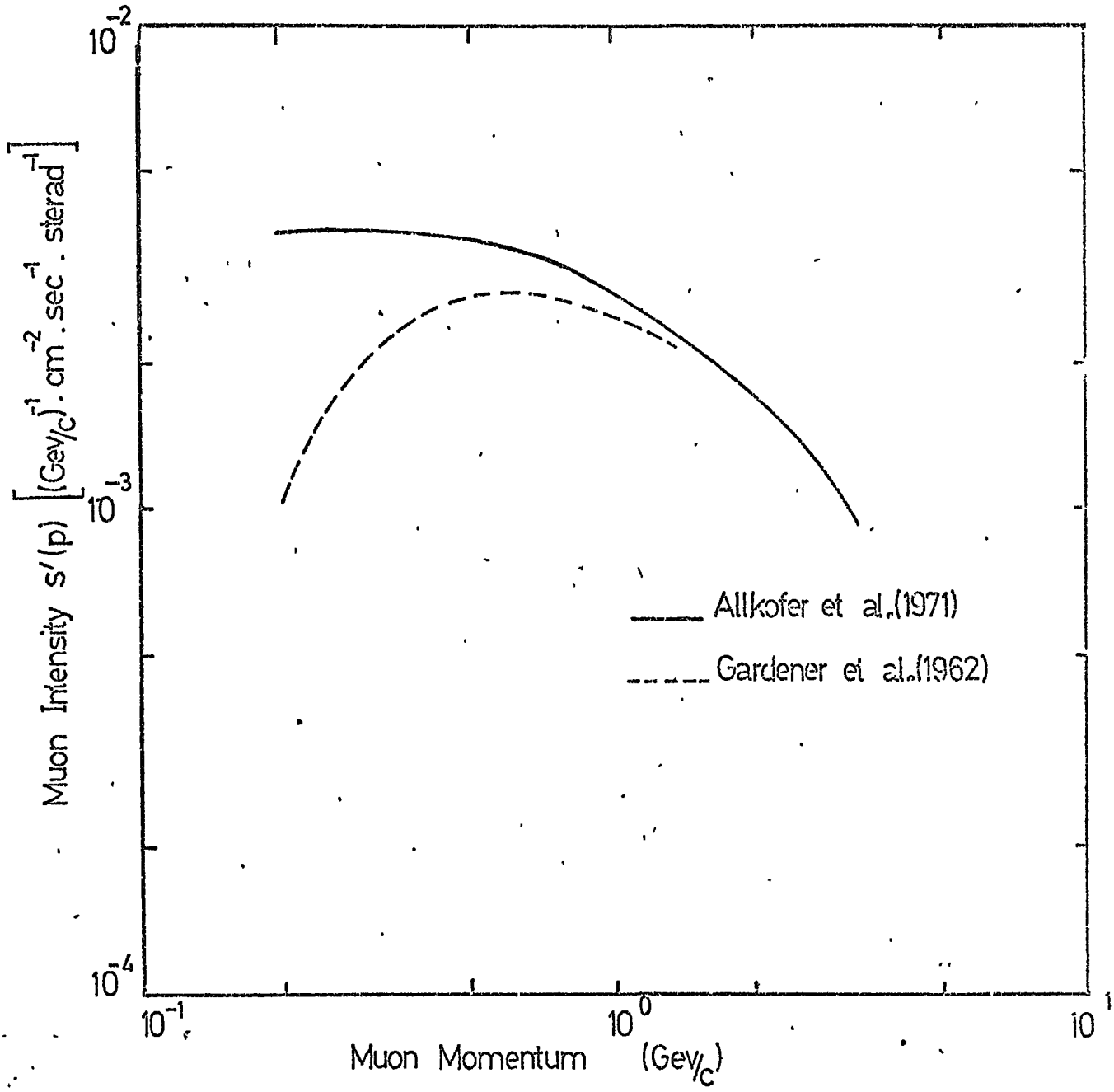

probability of a muon of momentum p recorded by the spectrograph of having a measured deflection $\Delta\psi$. This is given by

$$W(p,\Delta\psi) = \int\int_{\psi_0 \phi_0} A(\psi_o,\Delta\psi)B(\psi_o)C(\phi_o)D(\phi_o)\ P(p,\Delta\psi)d\psi_o\ d\phi_o \qquad 3.7$$

where $A(\psi_o,\Delta\psi)$ is the probability of the particle, incident at angle ψ_o (as projected onto the deflection measuring plane) and being deflected through $\Delta\psi$, of being accepted by the spectrograph in this plane,

$B(\psi_o)$ is the probability of the accepted particle being incident at angle ψ_o (in the measuring plane),

$C(\phi_o)$ is the probability of the particle being accepted by the spectrograph in the back-front plane (perpendicular to the measuring plane),

$D(\phi_o)$ is the probability of the accepted particle being incident at angle ϕ_o in the back-front plane,

and $P(p,\Delta\psi)$ is the probability that the incident particle will have a measured deflection $\Delta\psi$ and is given by equations 3.15 and 3.16.

Functions A and C were obtained from geometric constructions of a scale model of the spectrograph.

The probability L_f arises through spectrograph inefficiencies, and consists of contributions from

(i) Ambiguous tracks in the momentum measurement flash tube trays, manifested as F events (see sect. 4.3). About $(8 \pm 1)\%$ of the single particle events recorded by the spectrograph had an extra track in one of the momentum measurement trays. By triggering the spectrograph randomly it was deduced that virtually all these tracks were unrelated to the triggering particle. Since the F events were ignored in the analysis, 8% of stopping muon candidates were lost.

(ii) Ambiguous tracks in the sub-monitor flash tube tray (X2). By the same process as (i), particles which stop in the monitor ($\bar{X}2$ events) may appear to pass through the monitor and be classified as X2 events (with an X2 track). It was found by random-triggering that 10% of events would have a spurious track in X2, of which 20% would be accepted by the analysis procedure so that 2% of the $\bar{X}2$ events will be wrongly classified as X2 events. This estimate has been substantiated by the number of low momentum muons ($\lesssim$0.6 GeV/c) which appear to pass through the monitor.

(iii) A small fraction (5%) of the single particles recorded by the spectrograph had an insufficient number of flashed tubes to allow accurate track fitting. These events were ignored in the analysis.

(iv) Calculations show that the probability of a 350 MeV/c muon interacting in the 50 g cm^{-2} of glass in the spectrograph is 10%, where an interaction is defined as a knock-on process producing an electron with more than 6 MeV (The approximate minimum energy necessary to produce a visible knock-on track).

(v) Events were rejected if the particle impacted on the monitor near the gap of the sub-monitor flash tube tray (see section 3.3.6). It was found that 5% of all events irrespective of $\Delta\psi$, were rejected for this reason.

Thus $L_f = (.92)(.98)(.95)(.90)(.95) = 0.73$ 3.8

The acceptance A was calculated by recording the rate of muons with momentum >1 GeV/c (see section 5-3.2) and normalising the 76 cm Hg atmospheric pressure rate to the absolute rate given by Allkofer et al.. (1971) after corrections for spectrograph losses had been made (i, iii-v above, where the knock-on interaction loss was calculated for a 5 GeV/c muon to be 15%). It should be noted that corrections (i),(iii) and (v) are

exactly self-cancelling when calculating $I^{\Delta\psi_i}_{\Delta\psi_j}$; that correction (iv) should be fairly accurate and self-cancelling to a degree; and that the remaining correction (ii), is very small. Therefore the error in I due to L_f should be small.

The resulting value for A is 54.1 $cm^2 str$ ($\pm$ 10%), where the error is due to the statistical uncertainty in the measured rate of muons $>$1 GeV (6%) and the measurement of Allkofer et al. at 1 GeV (7%).

The sensitive on-time T has been found to be 1.56×10^6 secs and includes losses due to the paralysis time of the instrument and catastrophies such as damage to films, spectrograph failures etc.

The monitor presents two different thicknesses of lead (226 and 340 g cm^{-2}) to vertically incident particles, with relative weights 2:1, and it has been assumed that all muons with range between R and (226 + R) (or momentum p in the range $0.225 < p < 0.45$ GeV/c) are stopped, whilst only one third of the muons with range between (226 + R) and (340 + R) ($0.45 \leq p \leq 0.6$ GeV/c) will be stopped (where R = 55 g cm^{-2} Pb is the minimum range necessary for a muon to traverse the distance from the centre of the spectrograph to the top of the lead producer).

The differential momentum spectrum $S'(p)$ of Allkofer was weighted by 1 and $\frac{1}{3}$ in these two ranges. The upper limit of momentum is that appropriate to the maximum thickness of lead presented to a particle incident at $\sim 15^\circ$ (in both planes) to the vertical, this being a typical figure observed in practice.

The absolute $\Delta\psi$ distribution of stopping muons (+ & -) calculated by equation 3.6 is shown in table 3.4(a), together with the integral number with $\Delta\psi \geq 4.2^\circ$ ($p \lesssim 0.7$ GeV/c). A check can be made on the weighting factor function by comparing this $\Delta\psi$ distribution with that actually detected (after a suitable normalisation). This is done in

TABLE 3.4

Distribution of $\Delta\psi$ for Stopping Muons

	Number of Muons per $\Delta\psi$ interval $I_{\Delta\psi_i}^{\Delta\psi_j}$ ($X10^{-4}$)				
$\Delta\psi^\circ$	40 — 19.7	19.7 — 9.8	9.8 — 4.2	4.2 — 2.95	$I_{\geq 4.2^\circ}$
a	0.011	1.23	4.06	0.308	5.31 (±0.5)
b	0.055 (±0.018)	1.30 (±0.08)	3.96 (±0.14)	0.45 (0.04)	5.31*
c	0.27 (±0.2)	2.40 (±0.6)	3.20 (±0.6)	0.53 (±0.4)	5.87 (±0.9)

*Normalised to a

table 3.4 (b) where the $\Delta\psi$ distribution of the $\bar{X}2$ events with a neutron monitor response is found to be in excellent agreement with prediction. The principal sources of errors in this determination are the shape of the low energy muon spectrum (7%), the measured fraction of muons detected by the spectrograph with momentum $\geq$1 GeV/c (6%) and the weighting factors (unknown but probably small). Note that the result is independent of the absolute muon intensity.

The second method of estimating the number of stopping muons removes these uncertainties, and simply involves analysing the muon runs described in Section 5-3.2 and multiplying the fraction of triggers which are $\bar{X}2$ events with $\Delta\psi \geq 4.2^{o}$ and satisfy all the analysis requirements, by the total number of GM triggers (8.13×10^{5}) during the sensitive on time. This method however, requires a much larger statistical sample of events in the muon runs to reduce the error in $I_{\geq 4.2^{o}}$. The absolute $\Delta\psi$ distribution predicted by this method is shown in table 3.4(c). The errors are too large to compare the $\Delta\psi$ distribution, but the value of $I_{\geq 4.2^{o}}$ is in good agreement with the first method.

Using the mean of these two estimates, and a muon charge ratio at an appropriate momentum $(N(+)/N(-) = 1.28 \pm .025$ (Owen and Wilson, 1951) the effective number of negative muons which stopped in the lead producer of the monitor duringthe NAP run is $I_{\mu\text{-}L} = 2.45 \times 10^{4}$.

The neutron yield due to low energy negative pions has been estimated from the pion/muon ratio given by Brooke et al.(1964), assuming that the pions produce about 10 neutrons per interaction. They should give less than 1% of the neutron yield attributed to stopping negative muons. The neutron yield due to protons, coulomb scattered to appear to have a negative charge is also negligible since the measured ratio of positive

to negative particles with $\Delta\psi > 4.2^{o}$ has been found to be only about 5% and so a negligible proportion of the classified negative particles will be of the opposite charge.

A negligible number of muons will stop in the paraffin wax of the monitor, predominantly in the two 8. cm thick reflectors. It is estimated that the fractions of muonsstopped by the monitor which are stopped in the reflector and inner moderator are only 5% and 3% respectively.

3-2.4 The fraction of stopping negative muons which are absorbed by the nucleus

The time taken for the muon to stop and cascade into the K shell ($\sim 10^{-9}$secs) is negligible compared with the nuclear absorption and spontaneous decay life times (τ_A and τ_D respectively) (Tennent, 1960). The total probability, per unit time, of the muon's disappearance is given by

$$\frac{1}{\tau^-} = \frac{1}{\tau_D} + \frac{1}{\tau_A} \qquad 3.9$$

τ_A^{-1} increases rapidly with Z for light nuclei, but slower for heavy nuclei. This has been interpreted (Wheeler, 1949) as due to the variation of nuclear charge density in the region traversed by the muon. For large radii the charge density due to protons, decreases inside the K shell causing the slower increase in τ_A^{-1} with Z. Good agreement between experiment and theory has been obtained (Primakoff, 1955) for this variation and Tennent has tabulated the weighted mean of observed values of τ^-, (76.2 $\pm$ 2.5 and 2,000nsecs for lead and paraffin respectively).

Thus the fractions of stopping muons which are absorbed in lead F_L, and paraffin F_P are given by

$$F_{L,P} = \frac{\tau_{L,P}^{-}}{\tau_{A(L,P)}} = 1 - \frac{\tau_{L,P}^{-}}{\tau_{D}} = \begin{cases} 0.965 \pm .001 \text{ for lead} \\ 0.1 \pm .001 \text{ for paraffin} \end{cases}$$

3.10

3-2.5 The average number $\bar{\nu}_{\mu^-}$ of neutrons produced per absorption

Kaplan et al.(1958) and MacDonald et al.(1965) have studied the emission of neutrons from lead nuclei using a similar technique. Muons were fired at a variety of target materials ranging from Al to Pb, which were surrounded by a high efficiency evaporation neutron detector - a cadmium-seeded liquid scintillator tank viewed by photomultiplier tubes and surrounded by a thick paraffin reflector. Stopping events, which were selected by demanding an anti-coincidence with detectors behind the target, opened a gate from the neutron detector for a few tens of μ secs (the mean life time of the neutrons being of the order of 10μ secs in this particular detector) and the number of detected evaporation neutron pulses were recorded.

The efficiency of the detector was found by replacing the target with a Cf^{252} fission neutron source of average energy 3.87 ± 0.08 MeV. Monte Carlo simulations of the detection process in a similar detector (Hicks et al., 1956) indicate that the efficiency of detecting an evaporation neutron is not very sensitive to its energy (see fig. 2.9), due to the large size of the thermaliser/detector. Repeated checks of the efficiency had to be made throughout the two experiments due to the deterioration of the scintillator solution, which caused the efficiency to drop. For example, in the experiment of Kaplan et al. the efficiency fell from 0.60 to 0.49 giving a mean of 0.545. The results of MacDonald et al. give a value $\bar{\nu}_{\mu^-} = 1.709 (\pm 4\%)$ for the average number of evaporation neutrons emitted per absorbed stopping muon in lead.

3-2.6 The variation of the DIGY's efficiency with neutron energy

The number n_{μ^-} of evaporation neutrons detected by the DIGY due to I_{μ^-} muons stopping in the lead producer of the monitor is related

to the average efficiency $\bar{\epsilon}_{\mu^-}$ for detecting these neutrons by

$$n_{\mu^-} = I_{\mu^-L}\, \bar{\nu}_{\mu^-}\, F_L\, f \bar{\epsilon}_{\mu^-} \qquad 3.11$$

Putting in the values of n_{μ^-}, I_{μ^-L}, $\bar{\nu}_{\mu^-}$ F_L and f evaluated previously, we get $\bar{\epsilon}_{\mu^-} = 0.0414$ ($\pm$ 13%). The error in $\bar{\epsilon}_{\mu^-}$ being principally due to I_{μ^-L}. (Stopping events in the paraffin give a negligible contribution to n_{μ} - since $I_{\mu^-P}\, F_P / I_{\mu^-L} F_L < 1\%$).

As pointed out in section 2-3.2 the efficiency depends on the energy spectrum of the evaporation neutrons produced and also on the position of production within the monitor. It is therefore necessary to assume a function $\epsilon'(E_n)$ for the DIGY, for the variation of efficiency with evaporation neutron energy E_n equivalent to the results of Pearce and Fowler (1964) for the SIGY and NM64. In this respect the DIGY should be more similar to the NM64 than the SIGY due to its thin outer reflector which according to Pearce and Fowler gives rise to the relatively higher fall in efficiency of the NM64 as E_n increases. For this reason, the variation in efficiency of the DIGY is assumed here to be the same as in the NM64.

The energy spectrum of neutrons produced by nuclear absorption of negative muons was measured by Hagge et al.(1964) in conjunction with the experiment of MacDonald et al.(1965). They assumed a spectrum of the form

$$N_{\mu^-}(E_n) \alpha\ E_n \exp(-E_n/\Theta_n) \qquad 3.12$$

and used a value of $\Theta_n = 0.75$ ($\pm$ 0.25) to get a rough fit to the experimental data.

More recently, considerable interest in the mechanism of muon capture has lead to several experiments being made to measure the neutron spectrum. One such experiment by Evseev et al.(1970) has studied

the spectrum of neutrons in the range 1.5 to 13 MeV from lead nuclei. This spectrum, shown in fig. 3.13, demonstrates that, in the case of lead at least, the principal yield of neutrons is from evaporation but that there is a small probability of direct neutron emission in which the neutron produced in equation 3.5 is emitted without exciting the nucleus.

This process produces the high energy tail of the spectrum. The evaporation spectrum was fitted by Evseev et al. by

$$N_{\mu^-}(E_n) \propto E_n^{5/11} \exp(-E_n/\tau^*) \qquad 3.13$$

where $\tau^* = 1.15\ (\pm 0.1)$ MeV.

In view of the small contribution made by the high energy tail, this simplified spectrum will be used in this work.

The average efficiency $\bar{\epsilon}(\tau^*)$ of detecting evaporation neutrons having an energy spectrum $N(E_n;\tau^*)$ given by Le Couteur (equation 2.1 and 2.2) can now be calculated thus:-

$$\bar{\epsilon}(\tau^*) = \frac{\int_0^\infty N(E_n;\tau^*)\ \epsilon'(E_n)\ dE_n \Big/ \int_0^\infty N(E_n;\tau^*)\ dE_n}{\int_0^\infty N_{\mu^-}(E_n)\ \epsilon'(E_n)\ dE_n \Big/ \int_0^\infty N_{\mu^-}(E_n)\ dE_n} \cdot \bar{\epsilon}_{\mu^-} \qquad 3.14$$

The value of $\bar{U}$ appropriate to the median energy ($\sim$ 150 MeV) of the nucleons contributing to the monitor count rate is 80 MeV (Metropolis) for which $\tau^* = 1.81$, assuming $\alpha = A/10$. The corresponding value of the efficiency $\bar{\epsilon}$ is 0.0376.

3-2.7 Variation of efficiency over the producer volume

The above value is appropriate to the region of the monitor within which the negative muons were restricted to impact by the acceptance of the spectrograph. Hughes (1961), and Hatton and Carmichael (1964) showed that the efficiency falls near the edges so the overall efficiency is less than 0.376. The variation of efficiency of the DIGY over the horizontal

FIG. 3.13 Neutron Energy Spectrum from Muon Absorption in Lead Nuclei

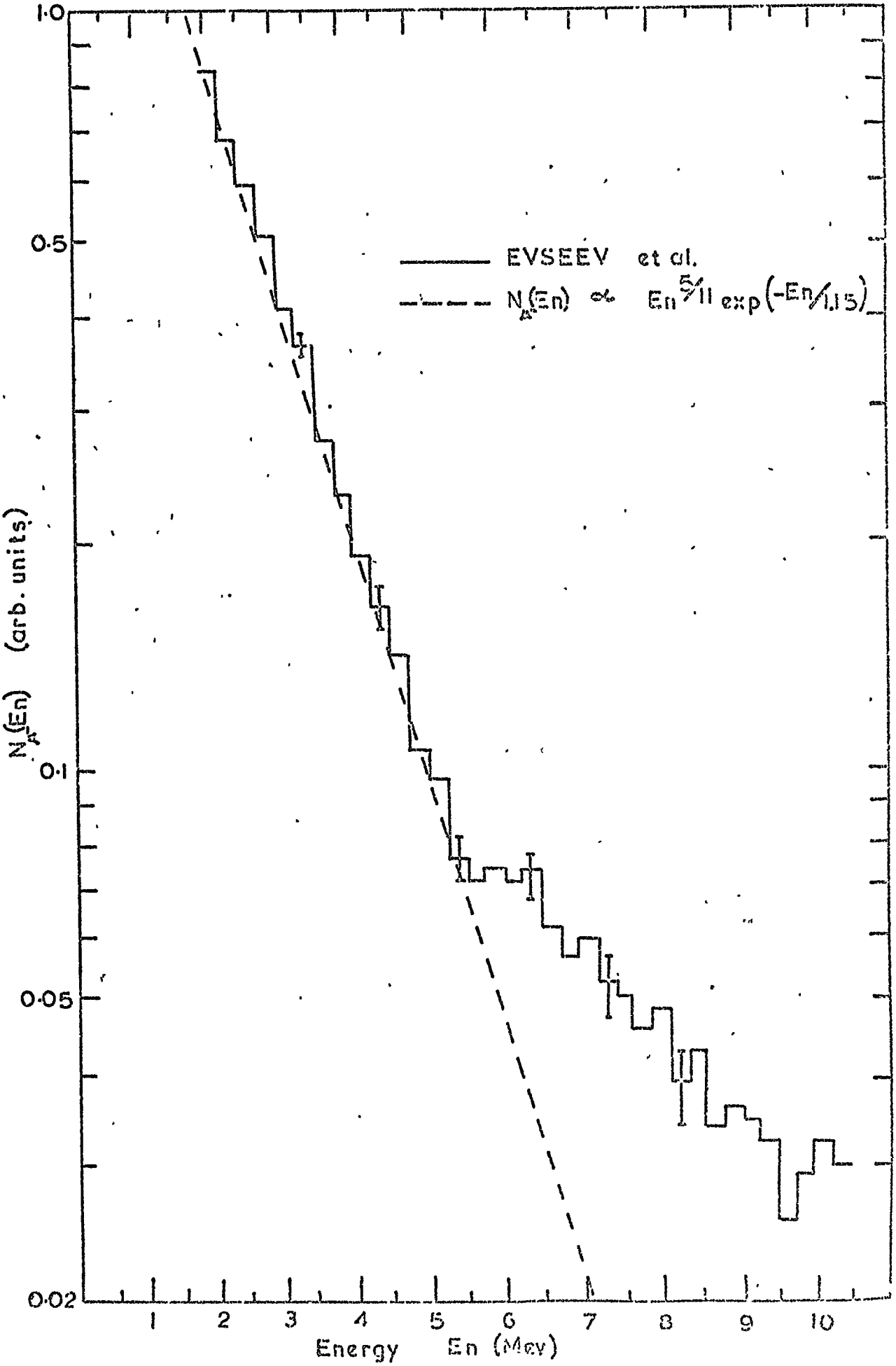

plane has been estimated in fig. 3.14 from the source measurements of Hughes, and Hatton and Carmichael for the LIGY. and the NM64. The variation over the producer, of the flux (or acceptance) of stopping muons has been calculated for the direction parallel to the BF_3 counter axis, using a scale drawing of the spectrograph under the assumptions that the muons suffer no coulomb scattering in traversing the spectrograph, and that the muon flux incident on the spectrograph is isotropic. The error due to the ignoring of the scattering should be negligible ($\lesssim$ 1%). This acceptance function is shown in fig. 3.14a. The variation in acceptance in the direction perpendicular to the counter axis has been obtained by recording muons with the spectrograph and plotting the distribution of impacts on the monitor of low (<1 GeV) momentum muons (fig. 3.14b). Although the errors on this acceptance function are large only a small error will be introduced into the efficiency correction because the change in efficiency across the monitor is very small.

The variation of rate of production of neutrons with depth should be small for both the slow μ^- and interacting nucleons, and has been neglected here.

The average over the whole surface of the DIGY has been calculated to be 0.0242 by averaging the function for the DIGY in fig. 3.14.

3-2.8 Discussion of errors and comparison with other measurements

The main uncertainty in this determination of the efficiency lies in the estimation of $I_{\mu^-} L$.

The result is not particularly sensitive to the uncertainties in energy spectra of evaporation neutrons, nor to the assumptions about $\epsilon'(E_n)$. The effect of the possible errors in the spectra have been estimated by evaluating equation 3.14 for the limits of error of γ^* (as measured by Evseev for stopping muons) and for the spectrum given

FIG. 3.14

Variation of Efficiency and Spectrograph's Acceptance Function Over the Monitor in the Horizontal Plane.

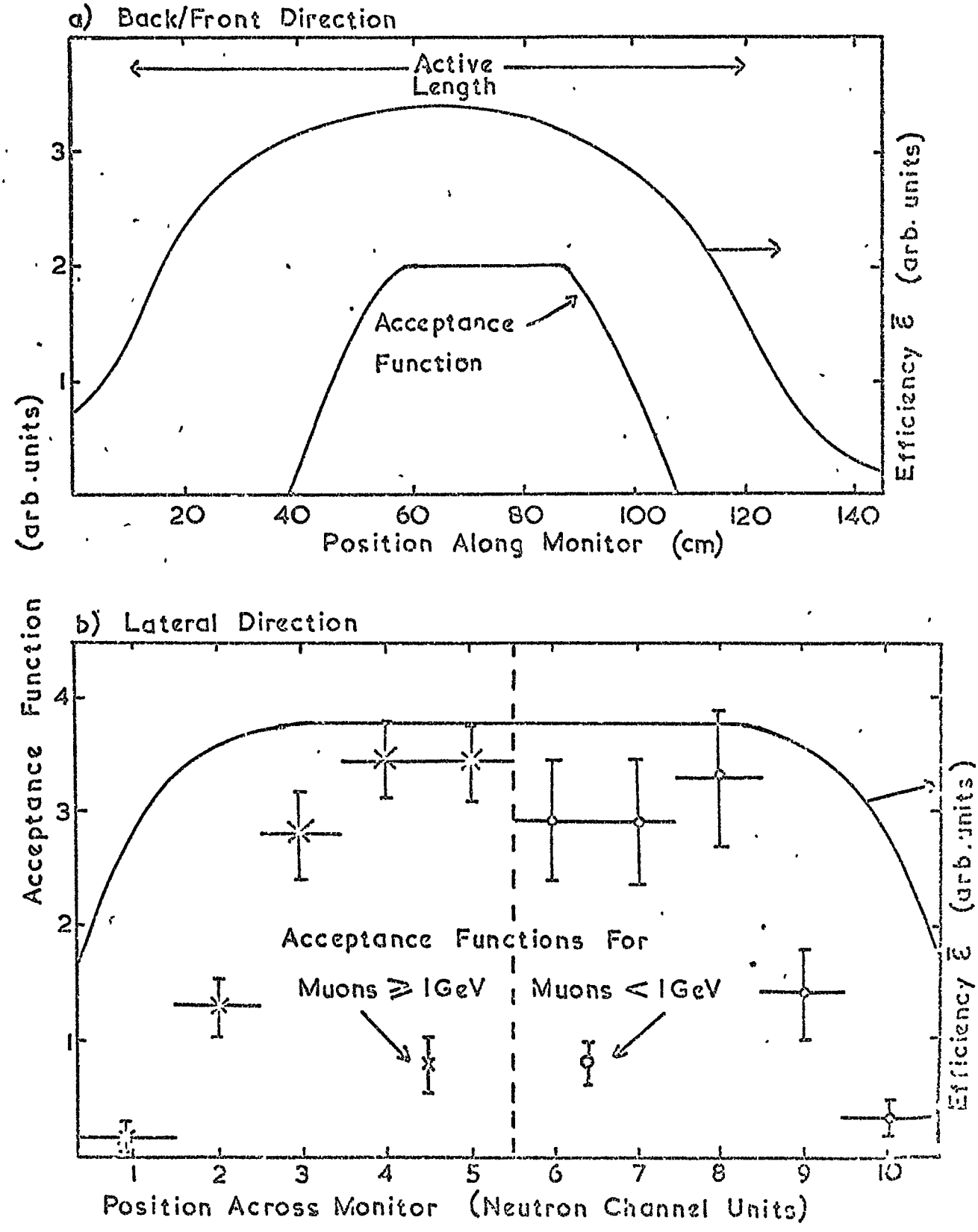

by Skyrme for 150 MeV protons (fig. 2.3). In both cases, the estimated efficiency changed by less than 3%. The effect on the spectrum of the uncertainty in the median sea level nucleon energy of the DIGY, and the low energy secondary nucleons produced by these nucleons should be small because the excitation energy is not a strong function of E_p in this region (fig. 2.1a). To test the sensitivity on $\bar{\epsilon}(E_p)$ of variations in the function $\epsilon'(E_n)$, values of $\bar{\bar{\epsilon}}(\tau^*)$ were calculated (fig. 2.11) assuming two other functions for $\epsilon'(E_n)$(fig. 2.9); onebeing the SIGY prediction of Pearce and Fowler, the other corresponding to a monitor where the relative leakage of 'high' energy evaporation neutrons is about twice that in the SIGY. The fact that the resulting change in $\bar{\bar{\epsilon}}(\tau^*)$ is negligible for $\tau^* < 2$ MeV , is because the evaporation neutrons produced at these low excitation energies have too low energies to escape through the reflector.

Therefore the best estimate of the efficiency of detecting neutrons produced by a $\gtrsim$150 MeV nucleon is 0.024 with an error of $\pm$ 13%.

This value is slightly higher than the estimate (equation 3.4) of 0.021, based on the relative counting rates of various monitors. However, considering the approximations made in the comparative estimate, the new measurement is not inconsistent with the other measurements of monitor efficiencies (Hughes; Hatton and Carmichael) all of which have a similar size of error to that given here.

It is hard to decide which of the efficiency measurements is more reliable than another. The present method has the advantage that the measurement is carried out with no geometrical alterations to the monitor and is weighted towards the experimental conditions, i.e. the measured efficiency is automatically averaged over the volume of the producer and moderator in a way that may closely approximate to the production of neutrons by cosmic rays. Also compared to the Ra-Be source measurements

the present method has an obvious advantage in that it is using a source of neutrons more similar to those which the monitor normally detects, being produced by the same mechanism.

On theother hand the present method suffers from having a spectrum of cosmic rays as it s source of neutrons - with consequent statistical uncertainties in the flux and uncertainties in the interaction of this flux with the spectrograph. In particular, the lower energy limit of muons which can pass through the spectrograph and be accepted as an event, is particularly difficult to estimate. (It should be noted that if the muon spectrum had a form similar to that measured by Gardener et al. (1962) (fig. 3.12) the estimated efficiency would have been considerably higher.)

In conclusion, there is certainly no evidence for the commonly quoted value of efficiency for the LIGY monitor being too high, as suggested by Shen. On the contrary, the figure of 0.03 given by Hatton may be a slight underestimate.

The best estimate of the DIGY has been taken as the mean of the two estimates given here (0.024, 0.021), the increased weight of the two source measurements compared with the one "stopping muon" measurement, being roughly counteracted by the uncertainties in comparing efficiencies of the three monitors.

3-3 The Spectrograph

3-3.1 Introduction

This spectrograph was designed for use in studies of the momentum spectra of nuclear active particles in air showers. A detailed description of it has been made elsewhere (Hook, 1972), so only the main features will be described here.

An important design specification was to minimise the amount of matter in the spectrograph in order to reduce the probability of the NAP's, protons and pions, interacting in the spectrograph. For this reason an air-gap

magnet was used. Another important factor in the design was the low intensity of both unaccompanied NAP s, and NAP s in extensive air showers. This required a detector with a large area and solid angle of acceptance, and was fullfilled in this case by the use of trays of Geiger-Müller (GM) counters in conjunction with a neon flash-tube visual detector array viewed by cameras. A diagram of the spectrograph as used in the main part of the work is shown in fig, 3.1. Charged single particles traversing the spectrograph were selected by demanding a coincidence between at least one GM counter in each of the trays G1, G2, G3 and G4. It was known that only about 1% of these single particles would be NAPs, the remainder being muons (Brooke et al., 1964) so the method used by Brooke et al. of selecting the required NAPs was adopted here incorporating multiple pulsing of the flash tubes and shuttered cameras. The sequence of events is as follows:-

(1) The single particle triggers the GM counters which causes the flash tubes to be immediately pulsed, a 2.1 sec paralysis to be imposed on the system, and the gate between the neutron monitor and the multiplicity recorders opened after a short time delay (40 μ secs),

(2) The neutron multiplicities recorded in each channel during the 300 μ sec gating time are stored before,

(3) The camera shutters are opened whilst the flash tubes are repeatedly pulsed, to allow the films to record the initial track (retained by virtue of the after-flashing property of flash tubes (Coxell and Wolfendale, 1960), and the displayed neutron multiplicities together with a clock showing British Standard Time, fiducial lights on the flash tube trays and the identifying film and frame numbers for that event,

(4) The shutters are closed before the films are advanced and the frame number incremented by one,

(5) The multiplicity recorders are re-set to zero and the paralysis is removed.

If no neutron is recorded during (2), then steps (3) and (4) are not carried out. The time sequence of operations is shown in fig. 3.15 and the electronic control circuit is shown in fig. 3.16.

The events recorded in this way included a large number of muons; some being genuine interactions in the monitor whilst others were random coincidences between a particle fulfilling the GM counter coincidence and the background count rate of the monitor.

3-3.2 The Magnetic Field.

The momentum of a single particle has been determined from its deflection in the magnetic field of the spectrograph assuming a horizontal uniform field (of flux 0.3 tesla due to a constant current of 20 amps flowing in the windings), perpendicular to the deflection measurement plane and completely contained in the air gap volume of 0.1 m^3. The magnetic flux density in and around the air-gap has been measured using a calibrated Hall-effect probe and it has been shown (Hook, 1972) that the effect of the non-uniformities is negligible.

3-3.3 The Visual Detectors

Four trays of neon flash tubes A1, A3, B3 and B1 were used for measuring the deflection, the A trays enabling the incident trajectory of the particle to be obtained, whilst the B trays gave the deflected trajectory. The dimensions are given in table 3.5. Aluminium electrodes placed between each layer of tubes were connected to a high voltage pulsing system which could pulse the trays seven times at intervals of about 10 msecs. An interval of time of about 2 secs was necessary for re-charging the system after the discharging. The operation of the flash tubes in this mode has been checked by Hook who found that the loss in efficiency due to the non-unit probability of after-flashing is only 5%.

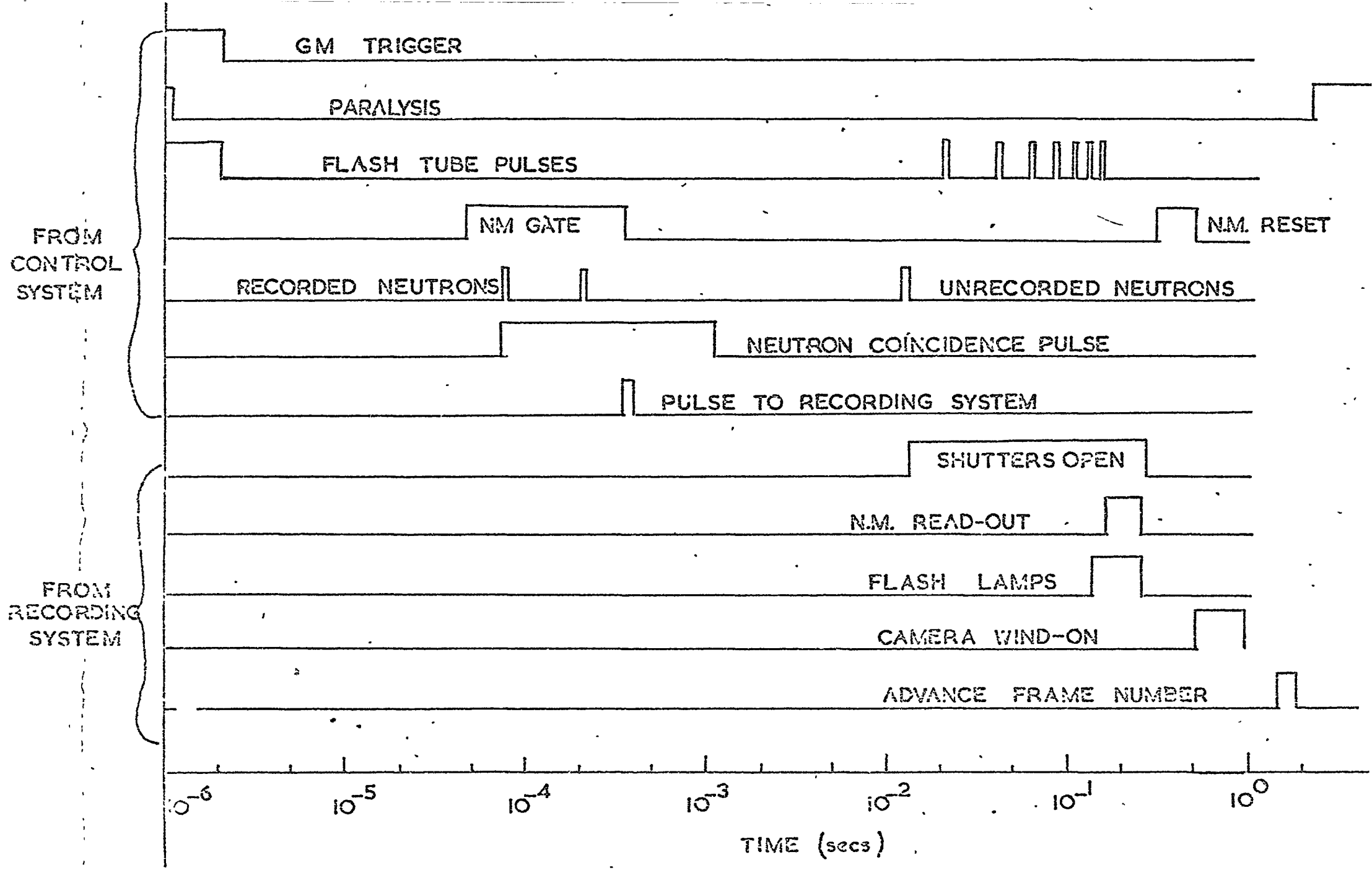

Fig. 3.15 The Time Sequencing of the Control System.

Fig. 316. Block Diagram of the Control Circuit.

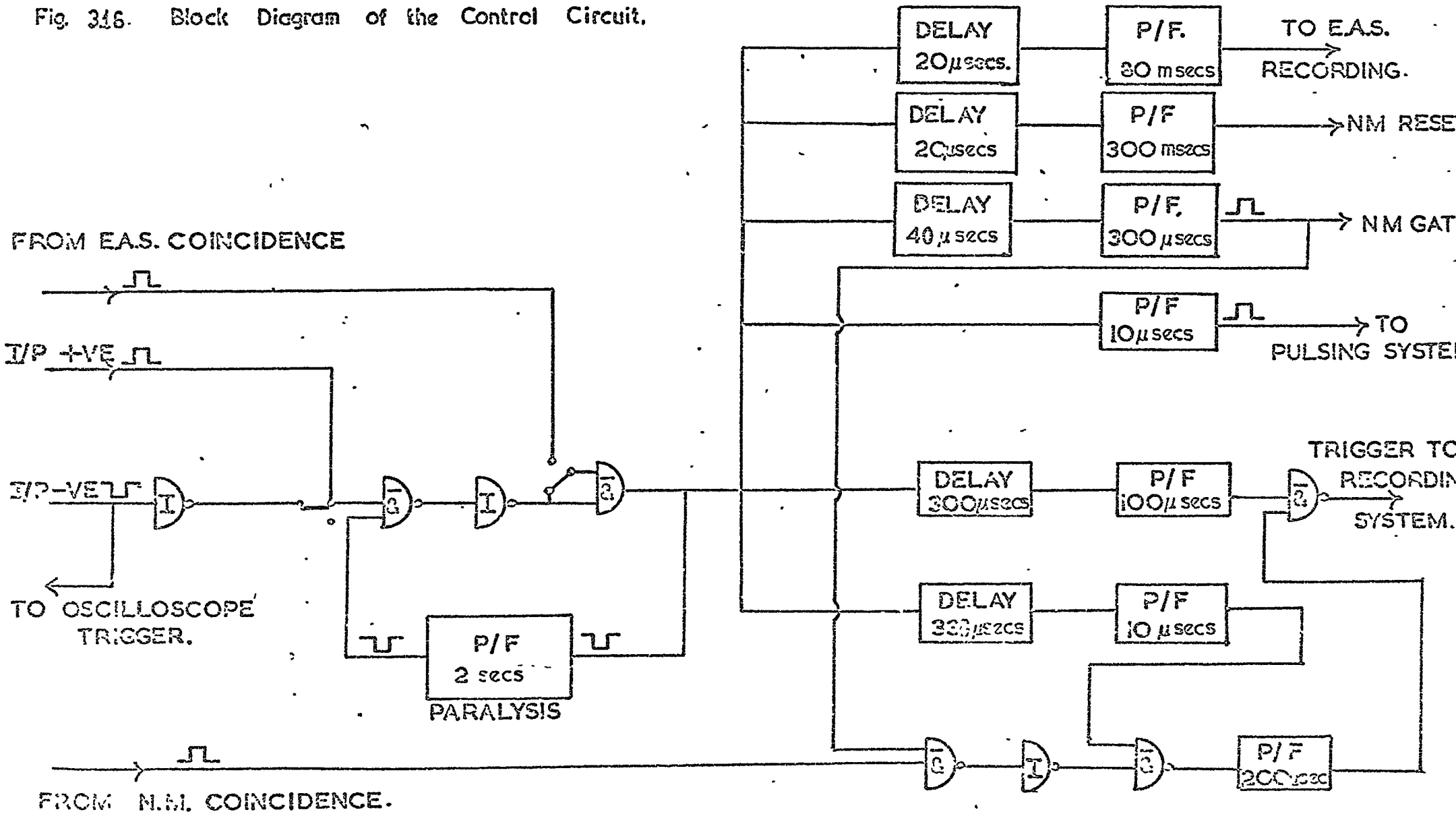

TABLE 3.5

The Flash Tube Trays

Tray	A1	A3	B3	B1	X1	X2
The Flash Tubes	Internal and External diameter = 1.6 and 1.8cm respectively Neon gas pressure = 60 cm Hg.					
Number of Tubes	990	760	760	990	400	1284
Number of Layers	10	10	10	10	4	12
Pitch of Layers (cm)	3.2	3.2	3.2	3.2	$\lesssim$ 1.8	$\lesssim$ 1.8
Pitch of Tubes (cm)	1.907	1.907	1.907	1.907	$\approx$ 1.8	$\approx$ 1.8
Length of Tubes (cm)	120	120	60	60	250	200
Tube support	Supported at each end in accurately machined slots in rectangular duralumin tubing				Close-packed self supporting	
Arrangement of Electrodes	Between each layer				Between every two layers	

Trays of neon flash tubes X1 and X2 were used to help the distinguishing of the NAPs and muons by observing the way in which the particles interacted in the monitor. The X2 tray was constructed in two halves which were placed as close together as possible. The effect of the gap of about 10 cm between the edge flash tubes in each half, was allowed for in the selection procedure, which was based on the lateral scatter of the particle after having passed through the monitor. The accuracy of these flash tube locations (1mm) was sufficient to measure the deviation of the average momentum muon recorded in this work (~3 GeV/c) to an accuracy limited by the tube and array size. The X1 tray was used purely to indicate the presence of charged particles incident on the top of the monitor and so the flash tube location accuracy was not as important as in the other trays. The dimensions of these trays are given in table 3.5. These trays were connected to a similar pulsing unit to the one supplying the momentum measurement trays.

3-3.4 The Single Particle Selection System

The upper-most tray (G1) of Geiger-Müller (GM) counters consisted of three adjacent sets of ten adjacent counters (20th Century Ltd., G60) (length 0.6m diameter 3cms) placed horizontally and parallel to the axis of the flash tubes. The outputs from the three sets were fed into a mixing unit which produced a standard pulse whenever any one of the thirty counters was discharged.

Each of the trays G2 and G3 consisted of 11 G60 counters arranged in two close packed layers with their axis horizontal and perpendicular to those in G1. A coincidence unit gave a standard output pulse in the event of a simultaneous discharge of a counter in each tray.

The G4 tray consisted of 10 G60 counters placed horizontally and perpendicular to those in G1. It's output was pulse-formed in the same way as that of G1.

The shaped pulses from G1, G2 + G3 and G4 were fed into a coincidence unit which, during the single particle work, gave an output pulse in the event of simultaneous discharges of GM counters in each of the four trays. The performance of the GM counters was checked by monitoring on a ratemeter, the rates of pulses from G1, G4 and from the coincidence between G2 + G3.

3-3.5 The Recording of Information

Two Shackman automatic 35mm cameras were used to record on Ilford HP4 film the visual information in the spectrograph, one for the upper (A) half and onefor the lower (B) half of the spectrograph. These two cameras were fitted with venetian blind type shutters which were fully open 13msecs after the detection of a neutron coincidence.

A third camera (C) (without shutters) was used to record the detection times and multiplicity of the neutrons from the neutron monitor on an oscilloscope, as mentioned in 3-1.3. The CRO time base was set at 50μsec/cm and triggered by every 4-fold GM coincidence. In order to reduce the fogging effect of these frequent sweeps of the trace (only 1% of which would produce a neutron) the lower part of the scale was blanked off, thus obscuring the bare sweep, and only displaying the positive ungated neutron pulses from the mixed neutron coincidence unit.

3-3.6 Computer Track Fitting

Re-construction of the path of the particles was performed using a track fitting program, assuming the path to be a straight line in each half of the spectrograph; the track in each half being fitted independently.

The initial estimate of the position of the track is obtained by least-squares analysis and gauss fits on the coordinates of the centres of the flash tubes, and of the gaps in layers with no flashed tubes. These are followed by a path-fit procedure whereby the track is varied step-wise over small ranges of angle ($\pm$ 0.5^{o}) and transverse position ($\pm$0.4cm), the

goodness of fit being assessed using three criteria in turn. First the number of flashed tubes traversed by the track is maximised, then the length (BMIN) of track traversing unflashed tubes is minimised and finally the length (BMAX) of track traversing flashed tubes is maximised. This procedure is carried out for both arms of the spectrograph and for all combinations of tubes in the event of there being more than one flashed tube in a layer. Using the resulting two best fits the angular deflection $\Delta\psi$, and the apparent momentum p and charge for this deflection are calculated. The approximate impact across the neutron monitor is also calculated by dividing the monitor into 80 cells along a line level with the top of the inner moderator, and finding which cell the track falls into.

Tracks are rejected which do not fulfil certain conditions regarding the goodness of fit, indicating human errors in track enumeration or interactions of the particle within the spectrograph.

The parameters used for rejection purposes are:-

(a) the number of ignored flashed tubes (not traversed by the track),

(b) the efficiency (defined as BMAX/(BMAX+ |BMIN|)) of the track,

(c) the difference Λ between the intersection points Y_o and Y_1 of the upper and lower tracks respectively with the horizontal line, perpendicular to the axis of the flash tubes, in the middle of the magnet. and (d) the intersection points of the tracks with the GM trays.

It was found that interactions or wrongly enumerated flash tubes would be noticed either by abnormally high values of (a) and (c); a low value of (b); or a value of (d) outside the geometrical limit of the trays.

The angle and centre of gravity of the best straight line through the illuminated X2 flash tubes (if any) are obtained using the flashed tubes' centres in a least squares fit; and the actual amount of lead traversed by the particle in the monitor is calculated for those events

with tracks in X2.

The actual lateral displacement of the particle in X2 is compared with that expected for a muon of momentum p passing through the calculated thickness of lead, and the probability of the particle being a muon is calculated (see section 3-3.7(ii)). The event is 'flagged' if the X2 track does not intersect with the spectrograph track within the monitor; or if the X2 track, expected on the basis of a particle being a muon, would fall in or near the gap between the two halves of the flash tube tray.

3-3.7 The Estimation of Errors in Track Fitting

(i) The Momentum Measurement

In the absence of measurement and reconstruction errors, magnetic field non-uniformities, and interactions of the particle with the spectrograph, the momentum p of the particle is related to its magnetic deflection $\Delta\psi_m$ by

$$p = \frac{K}{\Delta\psi_m} \qquad 3.15$$

where K is a constant depending on the magnetic field (=2.95 for a current of 20amps). However, in practice the probability $P(\Delta\psi;\Delta\psi_m)$ of observing a deflection in the range $(\Delta\psi,\Delta\psi+d\Delta\psi)$ can be assumed to be given by:-

$$P(\Delta\psi;\Delta\psi_m)d\Delta\psi = \frac{1}{\sigma\sqrt{2\pi}} \exp\left(-\frac{[\Delta\psi-\Delta\psi_m]^2}{2\sigma^2}\right) d\Delta\psi \qquad 3.16$$

where $\sigma^2 = \sigma_c^2 + \sigma_T^2$ is the standard deviation of the distribution and is made up from a contribution σ_c due to particle scattering, and a contribution σ_T due to measurement errors. When a charged particle of momentum p (GeV/c) and velocity β (in units of c) traverses x radiation lengths of material, the r.m.s. angle of scatter (in degrees) is given by

$$\sigma_c = \frac{0.148\sqrt{x}}{p\beta} \qquad 3.17$$

In the limit as p becomes very large, $P(\Delta\psi;\Delta\psi_m)$ depends only on σ_T, or is independent of p. A useful indication of the limit of accurate high momentum measurements is the so called maximum detectable momentum (mdm) defined as that p for which $\Delta\psi_m = \sigma_T$. An accurate knowledge of σ_T is necessary to extend momentum measurements meaningfully beyond the mdm. It has been shown by Hook (1973, private communication) that σ_T has a value of $(0.15 \pm 0.04)^o$, corresponding to an mdm of 20 GeV/c for a magnet current of 20 amps.

The track-fitting program has been tested (Hook, 1972) by generating artificial events in one of the arms of the spectrograph, and then analysing them by the program. It was found that with the usual angular path-fit steps of 0.05^o, the program reconstructed the tracks with angles accurate to 0.1^o. It would therefore appear that the angular measuring error of the spectrograph is about 0.11^o.

(ii) The Particle Identification

The angular displacement viewed in two dimensions of muons of incident momentum p, after traversing a thickness t g cm^{-2} of lead is described by a gaussian (for small t) with a root mean square (measured in radians) given by

$$\sigma_c = 5.81.10^{-3} \frac{t^{0.5}}{\beta p} \qquad 3.18$$

where β is the velocity of the muons (in units of the velocity of light).

The resulting mean lateral scatter in the middle of the X2 tray is $r\sigma_c$ (fig. 3.17).

The lateral displacement of these muons immediately below the monitor is also given by a gaussian with a mean (in cm) given by

$$\sigma_L = 3.36.10^{-3} \frac{t^{1.5}}{p} \qquad 3.19$$

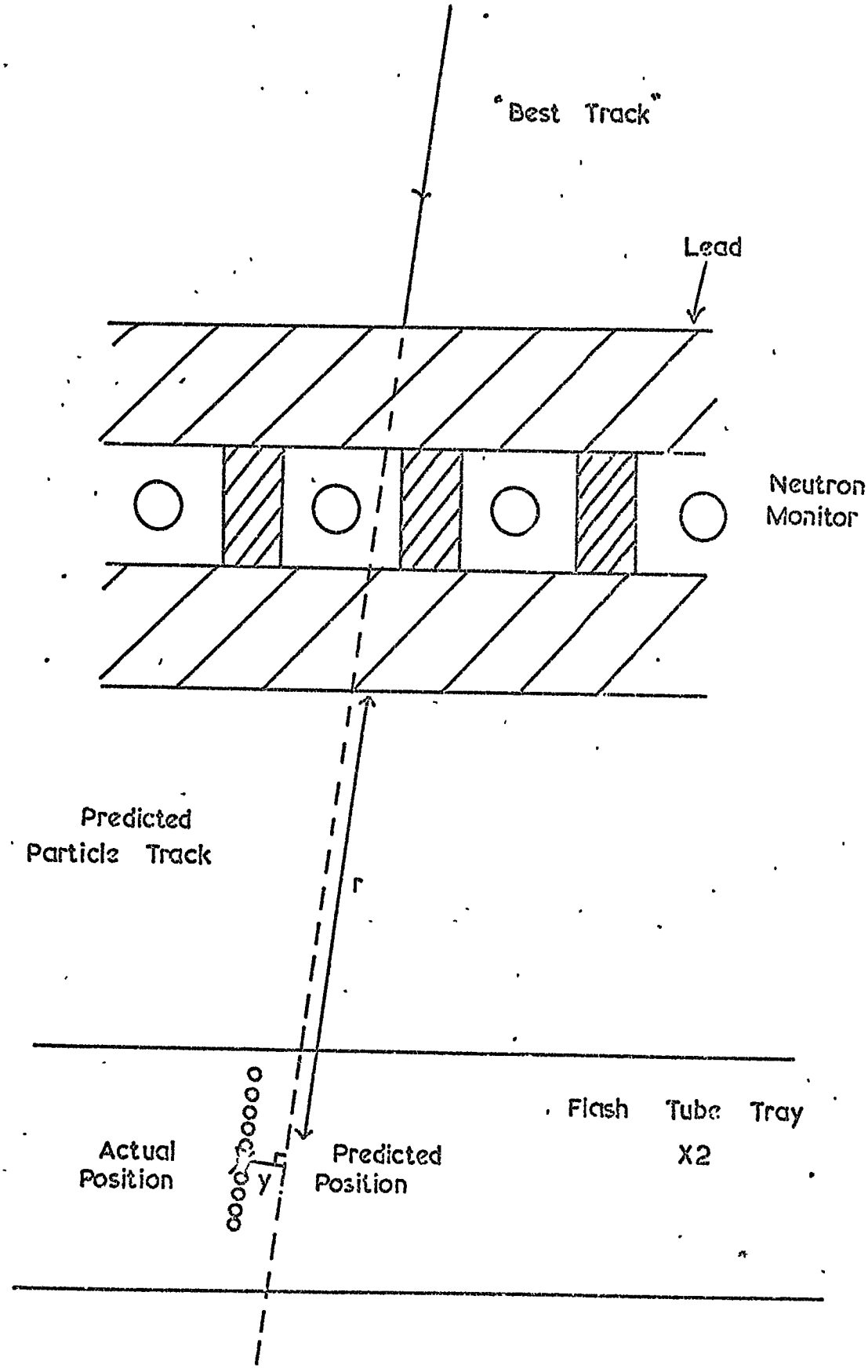

Fig. 3.17 The Scattering of Particles in the Neutron Monitor.

It has therefore been assumed that the total lateral scatter y in X2 is also a gaussian with a mean given by

$$\sigma_{cx} \approx \sqrt{(r^2 \sigma_c^2 + \sigma_L^2)} \qquad 3.20$$

The measured scatter will be greater than this due to track location errors. Assuming a gaussian measurement error distribution with a mean of σ_{NX}, the measured average scatter will be given by

$$\sigma_x = \sqrt{\sigma_{NX}^2 + \sigma_{cx}^2} \qquad 3.21$$

The distribution of measured lateral scatter (in units of σ_{cx}) of about 300 cosmic ray muons ($\geq$1 GeV/c), detected and computer-analysed has been found in fig. 5.5 (solid line) to be closely gaussian. Similar distributions for smaller ranges of muon momentum have been used to make several estimates of σ_{NX} (which is independent of momentum). The resulting mean value of σ_{NX} is 1.0 cm, with a standard deviation of 0.34 cm.

This value would be expected to be considerably higher than the flash tube location error ($\pm$ 0.1cm) because of the short height of the tray and the relatively large diameter of the flash tubes, but since, in the absence of a refined track fitting procedure such as is used for the momentum measurement, the best resolution of the position of the track in each layer is $\sim \pm$ 1 cm (the radius of the tubes) this estimate of the measurement error seems to be rather high. Checks of the enumeration accuracy reveal no significant errors which could cause an overestimation.

As the muon momentum increases, σ_x tends to be dominated by σ_{NX}. The value of momentum for which $\sigma_{NX} = \sigma_{CX}$ is about 3 GeV/c and this gives a useful estimate of the upper limit of the range of momentum over-which muons can be reliably identified. However, in view of the

high probability of an overestimation of σ_{NX}, it would seem likely that reliable identification of muons is possible at twice this momentum. At the maximum detectable momentum of the spectrograph (20 GeV/c) the measurement error σ_{NX} is up to ten times the average coulomb scatter σ_{CX} and so most of the muons will have a measured scatter less than $10\sigma_c$.

CHAPTER FOUR

NEUTRON PRODUCTION BY PROTONS AND PIONS

4-1 Introduction

The purpose of the work described in this chapter is to determine the variation of evaporation neutron production from lead nuclei with the energy of the interacting nuclear active particle (NAP). As in the case of the previous work by Hughes et al. (1964), the NAPs recorded are mainly positively charged protons, but with a small contribution of both positive and negative pions. The yield of kaons and anti-protons in proton collisions are small compared with that of pions at a few hundred GeV ($<10\%$ according to Antipov et al. (1971)) and their survival probabilities are also smaller than that of pions, so that they may be ignored in this analysis.

Apart from the reduction in statistical errors, the present experiment should be an improvement over that of Hughes et al. because an allowance has been made for the variation of average neutron detection efficiency with NAP energy.

4-2 The Experiment

The spectrograph and monitor were operated together in the mode described in 3-3.1 with events being recorded on film when the single particle GM-counter coincidence (a GM event) was followed by at least one neutron being detected within the gate, which opened 40μsec after the coincidence and closed at 340 μsec (an NM event).

The rate of these NM events was about $10hr^{-1}$ compared with the single particle GM coincidence rate of about 900 hr^{-1}.

All three recording films were changed daily whilst the equipment was being checked and the films were immediately developed to ensure

that the cameras were recording the visual information clearly. At the beginning and end of each daily run the various event counters, British standard time and the magnet current were noted; and the time and date marked on the continuous record of the magnet current. The GM counters and the monitor BF_3 counters were checked at these times using the rate-meters, and any abnormalities noted and corrected. The magnetic field was reversed daily in order to minimise the effect of any assymetry in the acceptance of the spectrograph which may distort the apparent charge of a particle.

The equipment was operated in this manner from Dec. 1970 to Feb. 1971 for a total of 986.8 hrs. Of this, 553.5 hrs were lost due to equipment failures, damage to films and (principally) the dead time of the equipment (equal to 2.1 sec per GM coincidence), and so the actual sensitive time was 433.3 hrs. During this sensitive time 8.13×10^5 GM and 1.03×10^4 NM, coincidences were recorded (after the losses had been subtracted) whilst the magnetic field was maintained at 20.0 ± 0.6 amps. Corresponding to a field integral of 167 kG.cm.

4-3 The Extraction of Data

Each set of three films from the spectrograph was inspected and the following information noted for each event.

1. The film and event numbers
2. British standard time
3. The neutron multiplicity in each neutron channel
4. The number of tracks in each flash tube tray
5. Evidence of any interactions in the spectrograph
6. The arrival times of the neutrons.

Each event was then assigned to one of the following categories:

(A) "B event" - a momentum-analysable track (a single track in each

of the four momentum measurement trays), and no more than one track in the (sub-monitor) X2 tray.

(B) "F event" - a "B event" accompanied by other tracks which were not momentum-analysable (shorter tracks which do not pass through each momentum measurement tray).

(C) "EAS event" - two or more momentum analysable tracks which may or may not be accompanied by other tracks.

(D) "B(P) event" - a "B event" with more than one track in X2

(E) "F(P) event" - an "F event" with more than onetrack in X2

(F) "Dense event" - many tracks but none analysable

(G) "Reject event" - an event with either (a) no analysable track because

(i) a single particle interacted in the spectrograph

or (ii) the spectrograph was triggered by chance coincidences in the GM-telescope;

or (b) a fault in the spectrograph or in the neutron read-out as indicated by a large discrepency between that indicated on films A and B, and that recorded on film C (as opposed to the occasional (about one in a hundred) small difference which would be accounted for by the finite resolution of the pulses on the CRO timebase viewed by camera C).

The spectrograph records of the "B" and "F" events were projected and the row numbers of the illuminated flash tubes in each layer punched onto a set of three computer cards, together with the identifying film and event numbers the nominal signed value of magnet current, the neutron multiplicity in each channel as read out on A and B frames, and the arrival times of the neutrons. In this way all the available information about the events (except for British standard time B.S.T) was stored on computer cards.

The A and B frames of the "B(P)", "F(P)" and "EAS" events were enlarged and printed onto photographic paper so that closer inspections could be made. The extension of each spectrograph track into X2 was drawn graphically and the nearest X2 track marked accordingly. The tracks of these events (selecting the marked X2 track only) were then enumerated onto punched cards in a similar way to the "B"'s and "F"'s except that a transparent overlay was used to indicate the tube positions. In this way all the available information about these events was stored on computer cards except for B.S.I. and the extra X2 tracks. "Dense" and "Reject" events received no further treatment. Table 4.1 gives the fraction of the total data that fell into each of these categories.

Each event was analysed by the computer track fitting program and the results recorded in print and on a computer card, which when combined with the other three cards formed a set containing almost all the available information about that event. A few events were rejected due to interactions in the spectrograph which had not been noticed in the initial scan. These were added to the "Reject (a)" category. A further fraction of the events (5%) were not analysed due to there being a small number of flashed tubes in a track, which would increase the $\Delta\psi$ measurement error.

4-4 Identification of Protons and Pions

4-4.1 Introduction

There are four distinct processes that can give rise to a single particle event with a response from the monitor:-

(a) a strong nuclear interaction between protons or pions and a nucleus in the monitor

(b) an electromagnetic interaction of a fast muon with a nucleus in the monitor

TABLE 4.1

Category of Event	Name	Fraction of Event %
A	B	49
B	$F_,$	4
C	EAS	<1
D	B(P)	7
E	F(P)	<1
F	Dense	15
G	Reject	25

(c) an electromagnetic interaction of a slow, stopping, negative muon with a monitor nucleus

and (d) an accidental coincidence between the single particle (GM) trigger (usually produced by a muon that passes through the monitor without interacting) and the monitor (which counts neutrons produced by low energy cosmic ray neutrons by process (a)).

There are four sources of information that have been used in the identification of these processes.

I The apparent momentum and charge of the particle (determined from its deflection in the spectrograph),

II The number and position of tracks emerging from the monitor,

III The distance between the monitor impact of the particle and the position of the channel (s) that detected the neutrons,

and IV the arrival times of the neutrons.

The muon momentum corresponding to a range in lead equal to the maximum thickness (340 g cm^{-2}) presented by the monitor to vertical particles is 530 MeV/c. The corresponding mean deflection $\Delta\psi_m$ in the magnetic field (when the energising current is 20 amps) is about 5^o with a measurement error (principally due to coulomb scattering in the flash tubes in this case) of $\pm 0.7^o$. This indicates that there should be few stopping muons having deflections less than 3^o, and so proton and pion candidates are only selected if they are deflected by less than 3^o (corresponding to a momentum $\gtrsim$ 1 GeV).

4-4.2 $\bar{X}2$ events (with no track in the X2 tray)

A feature of the events in category (b) and the majority of those in (d), is that the incident particle is not absorbed by the monitor, whereas the more strongly interacting protons and pions (NAP s) with energies in the region of interest here ($\sim$ 5 GeV), have a high

probability of being completely absorbed, together with their interaction products. Thus any event with $|\Delta\psi| < 3^{o}$ and no track in X2 is almost certain to be an NAP; and small corrections can be made for muonic contamination due to the following causes:-

1. A particle emergent underneath the monitor may pass through the gap between the two halves of the X2 tray,

2. A slow (momentum <0.6 GeV/c) accidental muon in category (d) may be coulomb scattered to appear to have $|\Delta\psi| < 3^{o}$ and then, stopped in the monitor.

3. A slow negative muon in category (c) may be similarly scattered and then stopped in the monitor.

Events in which the projection of the incident track falls within 3 cm of the edge of the X2 tray, are rejected to eliminate cause 1.

The number of accidental events and the fraction of these which would be classified as an NAP ($\bar{X}2; |\Delta\psi| < 3^{o}$) have been calculated (see section 5-3.2) by analysing events without the monitor coincidence. Similarly the number of genuine stopping negative muon interactions having $|\Delta\psi| < 3^{o}$ and whose neutrons are detected, has been estimated. In both these cases the fraction of non NAP events in the $|\Delta\psi| < 3^{o}$; $\bar{X}2$ category is very small ($\lesssim$ 1%).

4-4.3 X2 Events - (with track in the X2 tray)

Events with X2 tracks can be due to either muons or NAP's. The 2-D projection, in the measurement plane, of the lateral scatter y (fig. 3.17) of the incident particle after traversing the monitor, is found and events are assumed to be NAPs if y is large compared with that expected for an accidental muon of the same momentum. An arbitrary upper limit of $8\sigma_{cx}$ (see sect. 5-3.2) has been chosen for

the scatter of muons in categories (b) and (d); and all events with $y > 8\sigma_{cx}$ have been assumed to be NAPs.. In the case of more than one track in X2 the parent particle is assumed to be that track with the minimum value of y. This is justified because in a proton-nucleus inelastic interaction the proton is usually left with significantly more energy than any of the secondaries (Shen, 1968). Assuming that all the product particles have the same distribution in transverse momentum, the proton should emerge closest to the incident trajectory. In the case of pion-nucleus interactions the incident pion is not known to survive but the choice of the nearest secondary should not introduce a significant bias in the particle selection.

It will be shown (see section 5-3.3) that a small fraction of NAP s have $y < 8\sigma_{cx}$. This can be understood in terms of the effect of the 2-D projection and should not introduce a significant bias. It will also be shown that small numbers of interacting and accidental muons are classified as NAPs, particularly at momenta greater than 20 GeV/c due to the error in track location in X2, and the over-estimation of the momentum above the mdm, thus underestimating σ_{cx}. Both these factors tend to classify muons as NAPs and small corrections have been made for them. In order to reduce the small correction due to the accidental muons, the NAP s were only selected if the impact distance (the minimum distance between the impacting particle and the nearest edge of the nearest neutron monitor channel giving a response), was less than 20 cell widths. The impact distance distribution for those events (assumed to be 100% NAP) in the $(\bar{X}2; |\Delta\psi| < 3^{o})$ category is shown in fig. 4.1 together with the calculated impact distance distribution for accidental muons (see section 5-3.2). It can be seen that almost all the genuine NAP s have impact distances less than 20 cell widths whereas only about one

FIG. 41

The Distribution of Impact Distance in the Neutron Monitor

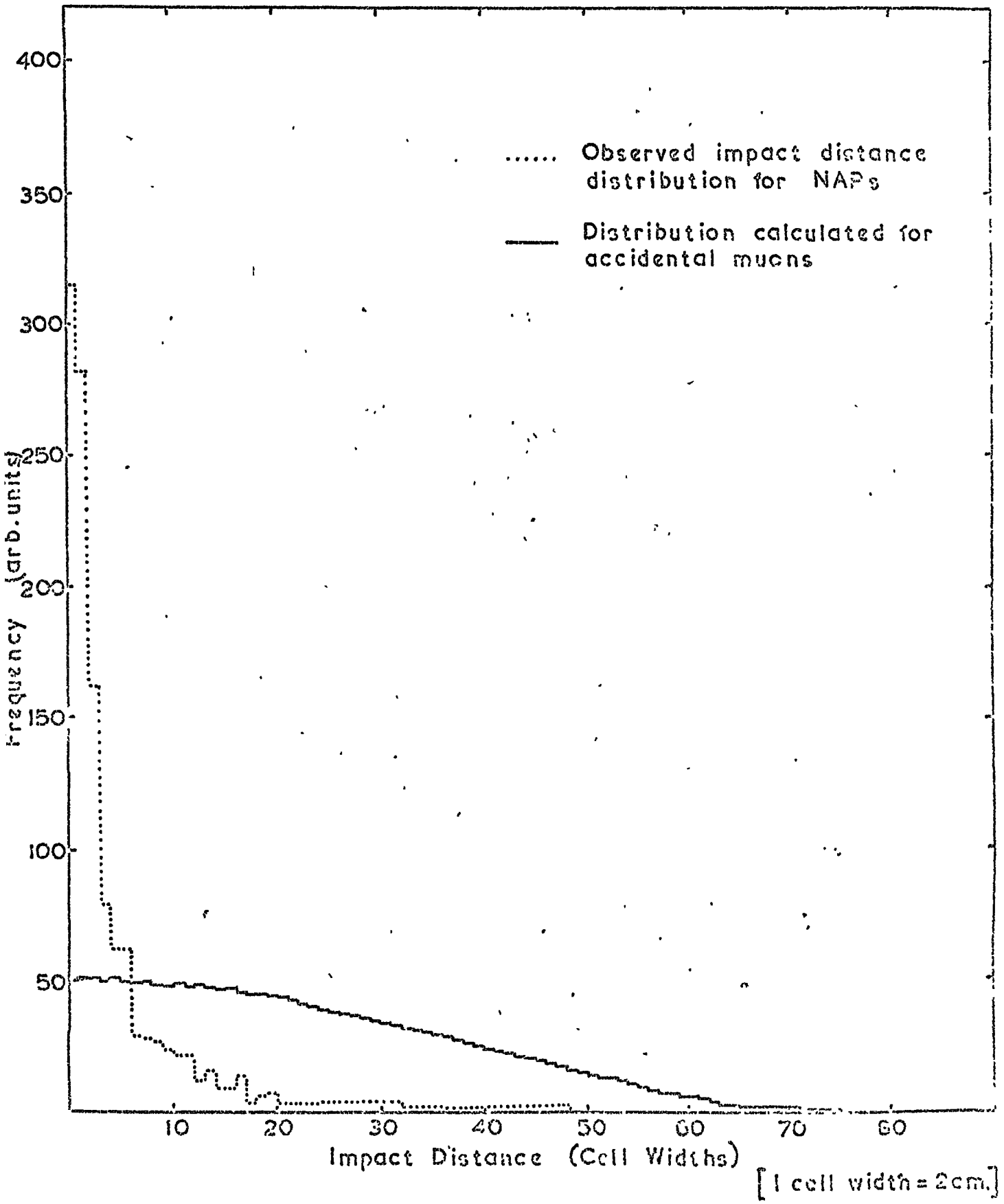

half of the accidental events fall within this limit.

4-5. The Experimental Results

The measured multiplicity distributions for the NAP s in categories (A) and (D), (i.e. unaccompanied momentum-analysable particles with any number of X2 tracks) are shown in table 4.2 for different charges and ranges of deflection $|\Delta\psi|$ in the magnetic field of the spectrograph The different contributions from the $\bar{X}2$ (without X2 tracks) and X2 (with X2 track(s)) events are given thus

$$\Omega(\chi)$$

where Ω represents the number of $\bar{X}2$ events

χ represents the number of X2 events

The resulting average multiplicities $\bar{m}$ for each deflection bin and charge are calculated before and after the small corrections for muonic contamination.

4-6 The Variation of Mean Multiplicity of Produced Neutrons $\bar{\nu}$ with Incident Particle Energy

4-6.1 The Measurement of particle energy

It has been assumed, after Hughes et al., that the charge ratio of positive and negative pions is unity and that there are no anti-protons over the energy range considered. The neutron multiplicity distribution, in a given deflection bin, attributable to protons has therefore been taken as the distribution of positive NAPs (protons and positive pions) minus the distribution of negative NAPs (negative pions).

The approximate average momentum for each deflection bin of a particle can be found (neglecting spectrograph errors) by assuming the momentum p of the particle to be given by equation 3.15, and then finding the mean value of p for each bin. These approximations become increasingly inaccurate as p approaches the mdm (20 GeV/c) when there will be

Table 4.2 The Detected Neutron Multiplicity Distributions Produced by Positive and Negative NAPs

Charge	Positive					Negative				
$\Delta\psi^\circ$ / Multiplicity	2.95	1.97	0.98	0.42	0.20	0	0.20	0.42	0.98	1.97	2.95
1	142(4)	257(24)	149(34)	17(13)	7(4)	4(7)	10(3)	22(4)	22(3)	25(0)	
2	40(2)	131(12)	84(20)	14(11)	5(3)	3(2)	4(1)	4(1)	5(1)	5(0)	
3	13(0)	48(3)	42(16)	11(8)	2(0)	3(1)	2(1)	4(2)	1(0)	2(0)	
4	4(0)	19(1)	23(5)	8(6)	2(0)	2(0)		1(1)	2(0)		
5		7(1)	10(2)	2(2)	4(0)	1(1)	0(2)	1(0)			
6	1(0)	1(0)	3(2)	2(4)				0(1)			
7		1(0)	4(0)	2(1)		1(0)	1(1)				
8		1(0)	2(2)	2(1)							
9				1(0)	1(0)	1(0)		1(0)			
12						1(0)	1(0)				
13			1(1)								
14							0(1)				
15					0(2)						
21			0(1)								
$\bar{m}_{uncorr}$	1.41	1.70	2.18	2.89	3.70	3.34	3.04	1.95	1.41	1.28	
$\bar{m}_{corr}$	1.41	1.70	2.18	2.90	3.76	3.45	3.12	2.00	1.47	1.33	

high contributions to the bins of high apparent momentum from particles with lower momenta, and a considerable "spill over" of particles of one charge into the other. For this reason the momentum of the particles with $|\Delta\psi| < 0.2^{\circ}$ has been taken as 20 GeV/c.

Using these assumptions the average kinetic energy for each bin has been calculated and a further small correction made for the energy loss by the NAPs in traversing the distance from the centre of the spectrograph magnet to the top of the Pb layer in the monitor. This is given in table 4.3. In order to estimate the error in the estimation of momentum near the mdm the deflection distributions for positive and negative NAP s have been used after the method of Hook (1972) to derive the momentum spectrum (N(p)dp) of the protons detected during the experiment, and this has been used to calculate the mean momentum $\bar{p}$ of protons in each $\Delta\psi$ bin $(\Delta\psi_i \rightarrow \Delta\psi_j)$, integrated over the whole spectrum weighted with the probability $P(\Delta\psi,p)d\Delta\psi$ of a proton of momentum p being deflected to have a deflection in $(\Delta\psi,\Delta\psi+ d\Delta\psi)$ (see also section 3-2.3). Thus the average momentum is given by:-

$$\bar{p}\ (\Delta\psi_i \rightarrow \Delta\psi_j) = \frac{\int_{p_{min}}^{\infty}\int_{\Delta\psi_i}^{\Delta\psi_j} N(p)P(\Delta\psi,p)\ p\ dp\ d\Delta\psi}{\int_{p_{min}}^{\infty}\int_{\Delta\psi_i}^{\Delta\psi_j} N(p)P(\Delta\psi,p)\ d\ p\ d\Delta\psi} \qquad 4.1$$

It was found that although the effect of the correction is very small less than 10 GeV/c, it sets an upper limit of about 15 GeV/c for the NAP energy in this work.

4-6.2 The measurement of mean multiplicity

In table 4.3 the average multiplicities $\bar{m}$ for each deflection bin have been calculated for those events attributed, in turn, to protons and negative pions.

Table 4.3 The Average Neutron Multiplicity of Protons and Pions

Particle	Protons					Pions				
$\Delta\psi^{o}$	2.95	1.97	0.98	0.42	0.20	0.0	0.20	0.42	0.98	1.97	2.95
$\bar{E}p$ (GeV)	0.5	1.30	3.70	9.0	19	20	11.0	4.40	1.90	1.0	
$\bar{m}$	1.44	1.72	2.20	2.84	7.00	3.38	3.12	2.00	1.47	1.33	
$\pm$(standard deviation)	0.06	0.05	0.10	0.12	2.12	0.61	0.67	0.27	0.16	0.12	
$\bar{\nu}$ (a)	18.0	29.4	49.0	75.1	245	97.1	86.5	40.8	19.2	13.5	
$\bar{\nu}$ (b)	18.6	32.1	56.3	86.0	278						
K_a		0.110	0.034	0.019							
K_b		0.108	0.028	0.018							
a		0.038	0.021	0.012							
b		0.057	0.045	0.033							
α'		1.125	1.146	1.060							

The "spill over" of particles near the mdm tends to reduce (a) any difference in $\bar{m}$ between positive and negative particles and, (b) the statistical sample of the protons.

It can be seen in table 4.3 that although $\bar{m}$ for protons near the mdm increases considerably compared with that for positive NAPs in table 4.2, there is a large error in this value.

The average produced neutron multiplicity $\bar{\nu}$ for each deflection cell of both particles has been calculated from the measured average detected multiplicity $\bar{m}$ under the assumption that the probability of ν neutrons being produced in interactions of mean energy $\bar{E}_p$ is given by

$$I(\nu; \bar{E}_p) = (1 - e^{-a}) e^{-a\nu} \qquad 4.2$$

where $\sum_{\nu=o}^{\infty} I(\nu; \bar{E}_p) = 1$.

After Shen (1968), this gives the average produced neutron multiplicity as

$$\nu(\bar{E}_p) = \frac{\sum_{\nu=o}^{\infty} \nu\, I(\nu; \bar{E}_p)}{\sum_{\nu=o}^{\infty} I(\nu; \bar{E}_p)} = (e^a - 1)^{-1} \qquad 4.3$$

Assuming that the probability of detecting m of the ν neutrons is given by

$$B(m,\nu) = \binom{\nu}{m} (\epsilon(\bar{E}_p)\, f)^m (1 - \epsilon(\bar{E}_p) f)^{\nu-m} \qquad 4.4$$

where f is the gating efficiency , the probability of a detected multiplicity m in interactions of average energy $\bar{E}_p$ is

$$R(m;\bar{E}_p) \propto \sum_{\nu=m}^{\infty} I(\nu;\bar{E}_p)\, B(m,\nu) \qquad 4.5$$

and the average multiplicity is

$$\bar{m}(\bar{E}_p) = \frac{\sum_{m=1}^{\infty} m\, R(m;\bar{E}_p)}{\sum_{m=1}^{\infty} R(m; \bar{E}_p)} = 1 - \frac{(\epsilon(\bar{E}_p)\, f)\, e^{-a}}{1-(1-\epsilon(\bar{E}_p)\, f)e^{-a}} \qquad 4.6$$

whence $$\bar{\nu}(\bar{E}_p) = \frac{\bar{m}(\bar{E}_p) - 1}{\epsilon(\bar{E}_p)\, f} \qquad 4.7$$

Using the values of $\bar{m}$ in table 4.3, values of $\bar{\nu}$ have been calculated for two different assumptions about $\epsilon(\bar{E}_p)$; (a) that $\epsilon(\bar{E}_p) = \epsilon(\bar{E}_p = 150\ \text{MeV}) = 0.035$ as deduced by the mean of the stopping μ^- and the neutron source measurements (section 3-2.8)., and (b) that $\epsilon(\bar{E}_p)$ is given by fig. 2.12(e) normalised to $\epsilon = 0.035$ at $\bar{E}_p = 150$ MeV (for protons only). The results are given in table 4.3.

The gating efficiency f has been taken to be 0.70 being that appropriate to a gate opening and closing at 40 and 340 μsec respectively, after the interaction.

To check the assumption in equation 4.2, plots of log $R(m; \bar{E}_p)$ against m have been plotted. Combining equation 4.2, 4.4 and 4.5 we get

$$R(m;\bar{E}_p) \propto \sum_{\nu=m}^{\infty} e^{-a\nu} \frac{m!}{\nu!(\nu-m)!} (\epsilon f)^m (1-\epsilon f)^{\nu-m} \qquad 4.8$$

so that

$$\log R(m; \bar{E}_p) \propto m \log(\epsilon f) - a - \log\left(1 - (1-\epsilon f)e^{-a}\right) \qquad 4.9$$

Thus the plots for interactions of mean energy $\bar{E}_p$, and average detected multiplicity $\bar{\nu}$ should be a straight line. These are shown in fig. 4.2 for protons. It is clear that in general $R(m,\bar{E}_p)$ is not a single exponential function. A much better fit to the points can be obtained using a double exponential expression as shown, which would follow from $I(\nu; \bar{E}_p)$ being a double exponential of the form

$$I(\nu; \bar{E}_p) = K_a \exp(-a\nu) - K_b \exp(-b\nu) \qquad 4.10$$

The corresponding expression for $R(m;\bar{E}_p)$ is given by

$$R(m;\bar{E}_p) = \sum_{\nu=m}^{\infty} B(m,\nu)\left(K_a e^{-a\nu} - K_b e^{-b\nu}\right)$$

$$= K_a' \left[\frac{(\epsilon f)\, e^{-a}}{1-(1-\epsilon f)e^{-a}}\right]^m - K_b' \left[\frac{(\epsilon f)e^{-b}}{1-(1-\epsilon f)e^{-b}}\right]^m \qquad 4.11$$

where $K_a' = \dfrac{K_a}{1-(1-\epsilon f)e^{-a}}$ etc.

Rough visual fits to the points in fig. 4.2 have been made corresponding to values of K_a, K_b, a and b given in table 4.3 It was noted that for:-

(a) $m \gg 1$ $\quad R(m; \bar{E}_p) \approx K_a' \left[\dfrac{(\epsilon f)\, e^{-a}}{1-(1-\epsilon f)e^{-a}}\right]^m$ $\qquad 4.12$

(b) $m = 0$ $\quad R(m; \bar{E}_p) = K_a' - K_b'$

or $\quad R(0;\bar{E}_p) = \dfrac{K_a}{1-(1-\epsilon f)e^{-a}} - \dfrac{K_b}{1-(1-\epsilon f)e^{-b}}$

and that due to normalisation

(c) $\quad 1 = \dfrac{K_a}{1-e^{-a}} - \dfrac{K_b}{1-e^{-b}}$ $\qquad 4.13$

Thus the slope of log R against m for $m \gg 1$ gives the value of a (equation 4.12). The value of b was obtained in a similar way after subtraction of the actual distribution from equation 4.12. The normalisation constants K_a and K_b where found from the simultaneous equations 4.13, $R(0;\bar{E}_p)$ being found by extrapolating the experimental points as shown in fig. 4.2.

After Shen, the average produced multiplicity is given by

$$\bar{\nu} = \frac{K_a e^{-a}}{(1-e^{-a})^2} - \frac{K_b e^{-b}}{(1-e^{-b})^2} \qquad 4.14$$

The resulting values of α', the ratios of these values of $\bar{\nu}$, to those calculated assuming a single exponential, are given in table 4.3.

4-7 Discussion of Results

The variation of $\bar{\nu}$, the average produced number of neutrons (<30 MeV), with energy E_p of proton incident on a lead layer of average

FIG.4·2.

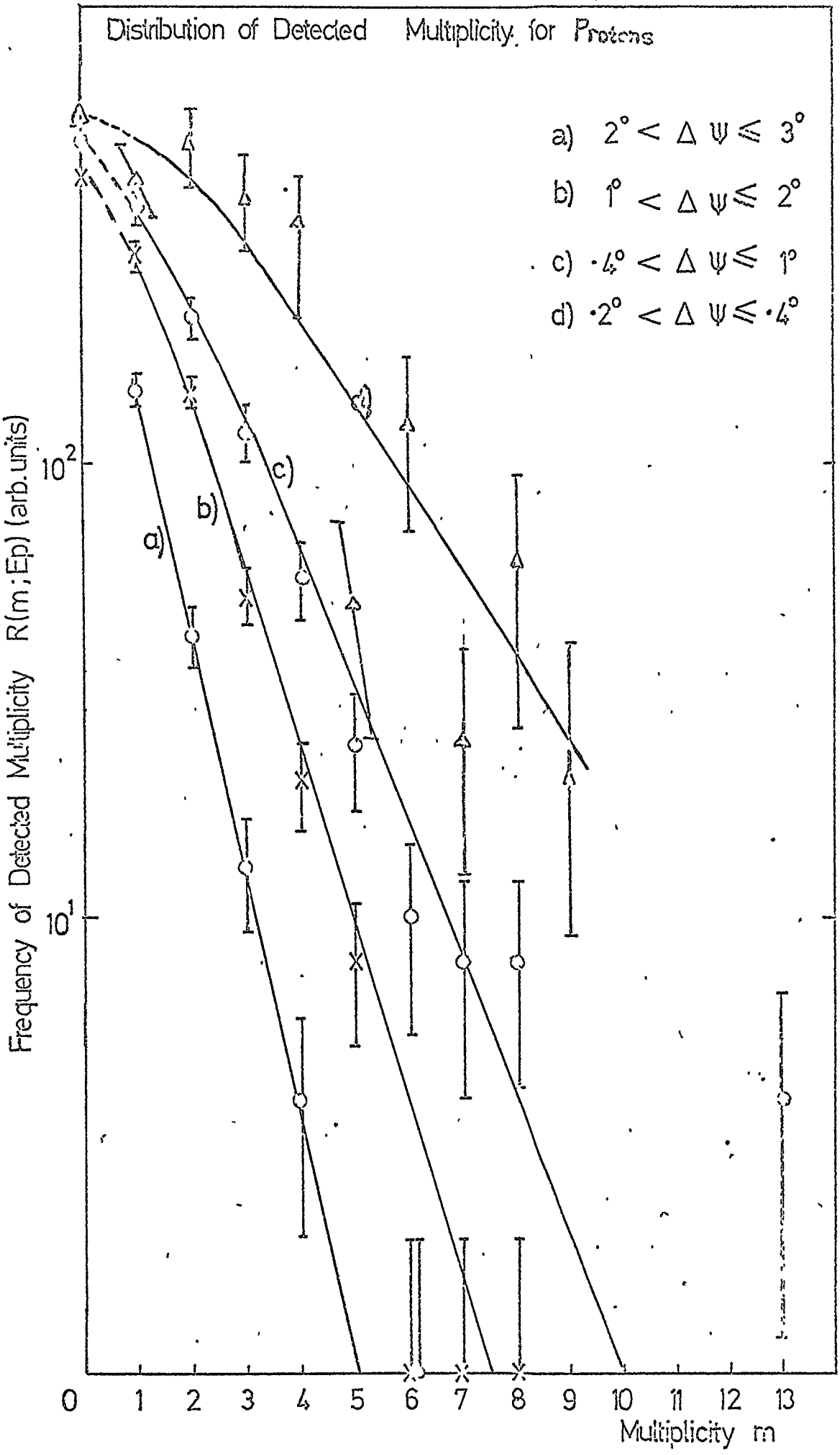
Distribution of Detected Multiplicity for Protons
a) 2° < Δ Ψ ≤ 3°
b) 1° < Δ Ψ ≤ 2°
c) ·4° < Δ Ψ ≤ 1°
d) ·2° < Δ Ψ ≤ ·4°
Frequency of Detected Multiplicity R(m;Ep) (arb.units)
10²
10¹
0 1 2 3 4 5 6 7 8 9 10 11 12 13
Multiplicity m

thickness t = 1.3 interaction lengths is shown in figures 4.3 and 4.4. To allow for the uncertainty in the effect of the cascade neutrons mentioned in section 2-2.3 a shaded area is drawn bounded by the lines corresponding to $\bar{\nu}$(lower) and $\bar{\nu}_t$ (upper) and has been obtained by averaging the results of Shen (1968) for various thicknesses t. Also shown are the values of $\bar{\nu}$ calculated in table 4.3 for positive and negative particles (protons and pions respectively) for the cases in which the efficiency ϵ is constant (fig. 4.3) and varies with E_p (fig. 4.4), protons only.

To compare the results of the present experiment with those of Hughes et al. (1964), the experimentally determined ratio $\bar{\nu}_{1.3}/\bar{\nu}_{0.75}$ for the same mean proton energies as estimated in the two experiments is compared in fig. 4.5 with that predicted by Shen. The values of $\bar{\nu}_{0.75}$ are those given by Hatton (1971) whilst the values of $\bar{\nu}_{1.3}$ are those obtained without any correction for the variation of $\epsilon(E_p)$ and have been interpolated at appropriate energies for purposes of comparison.

A feature of the results of the present experiment is a consistently lower set of values for $\bar{\nu}$ than that predicted by Shen for energies above 0.5 GeV. The discrepency in fig. 4.3 is slightly larger than that noted by Hatton (1971) and, for protons, is about 40% less than Shen's predicted $\bar{\nu}_t$. Although the low energy experimental value is in good agreement with $\bar{\nu}_t$, this may be fortuitous because at these low energies the calculation tends to underestimate the neutron yield, according to Shen.

It can be seen in fig. 4.5 that the uncorrected data for the present experiment are about 15% less than those expected from the experiment of Hughes et al. assuming the calculations of Shen are accurate enough to relate the neutron yields from the two thicknesses of lead. In fact, if these calculations greatly overestimate the neutron yield for energies

Variation of Neutron Multiplicity with Energy FIG. 4.3

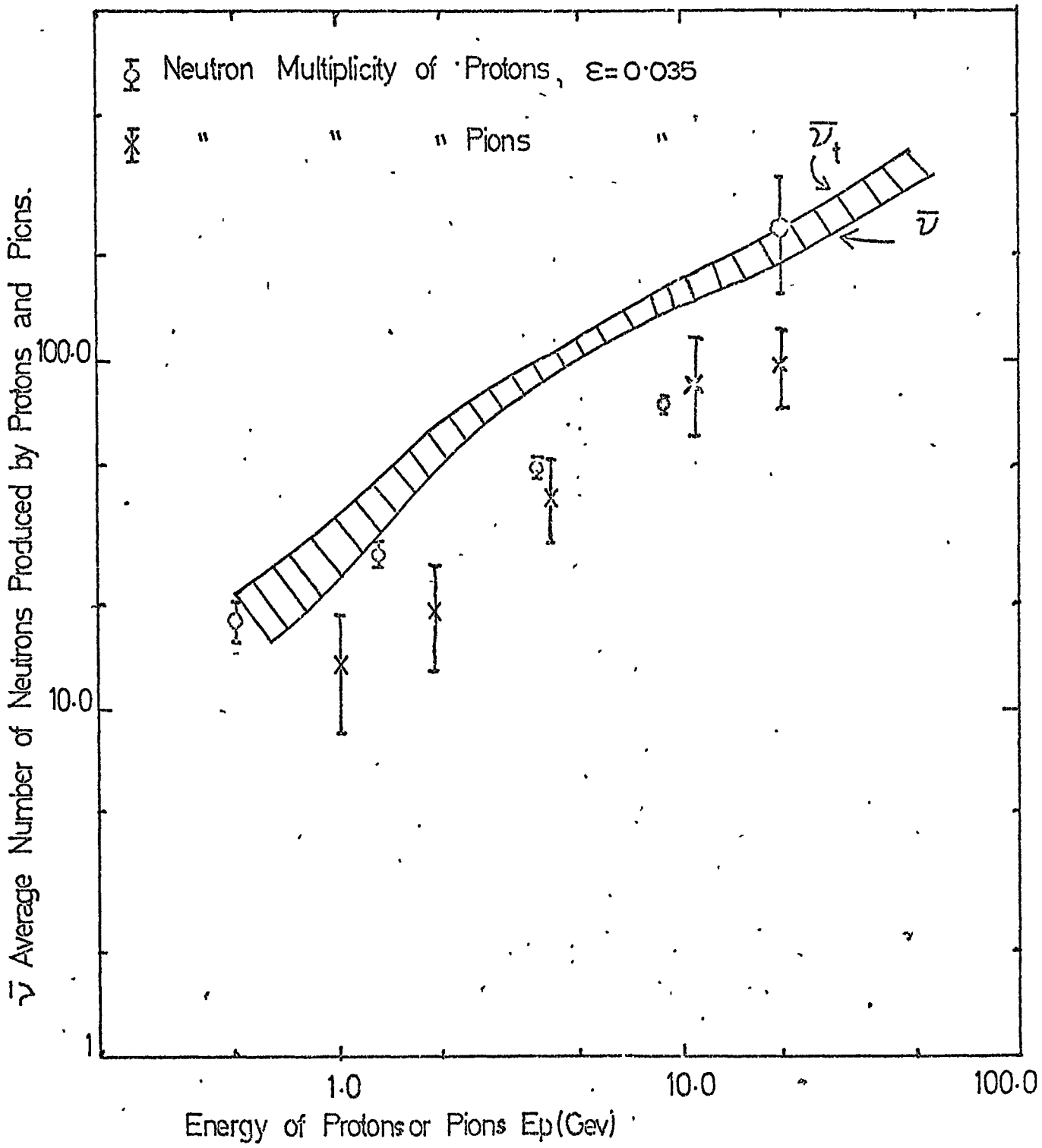

Variation of Neutron Multiplicity with Energy FIG. 4.4

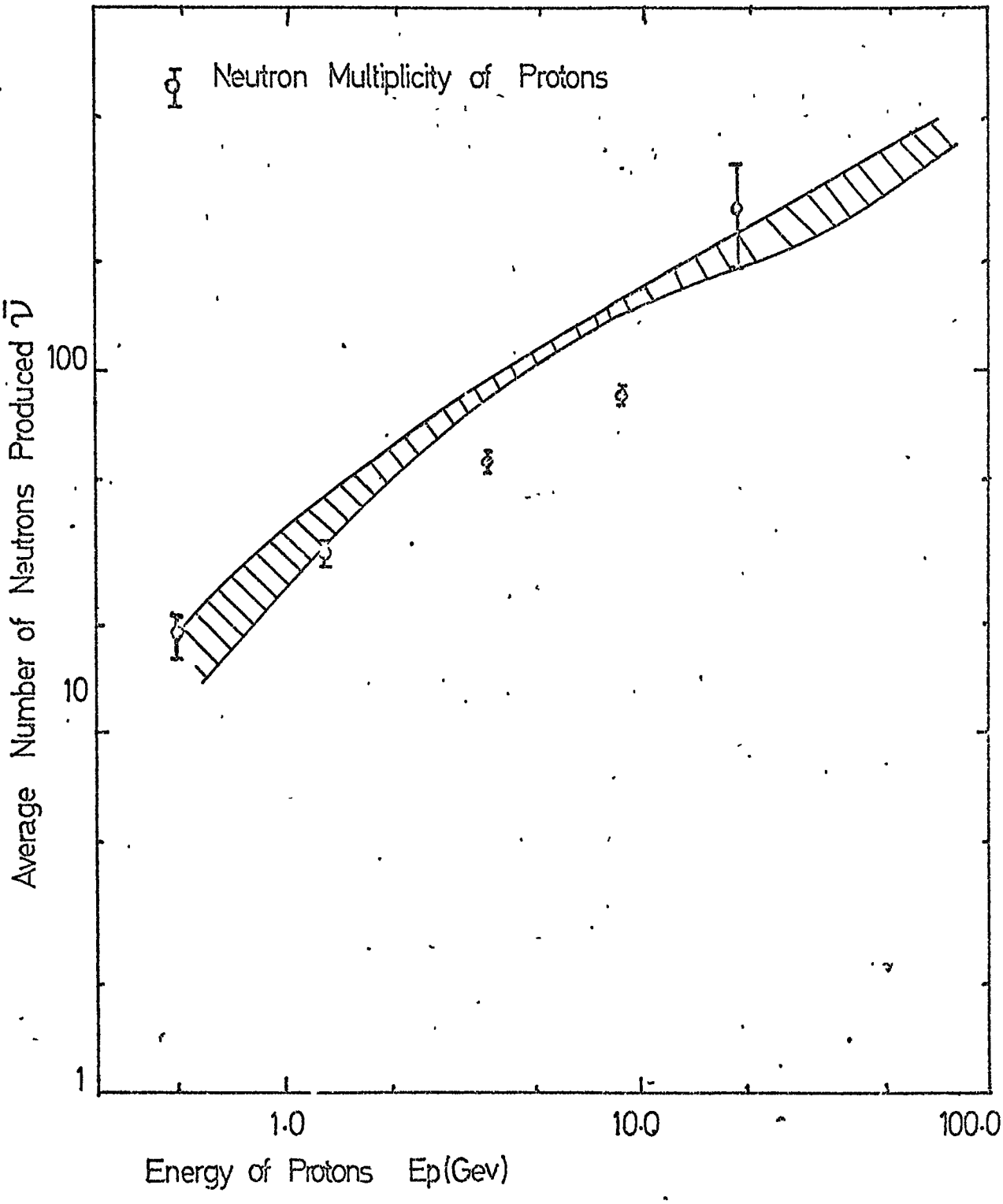

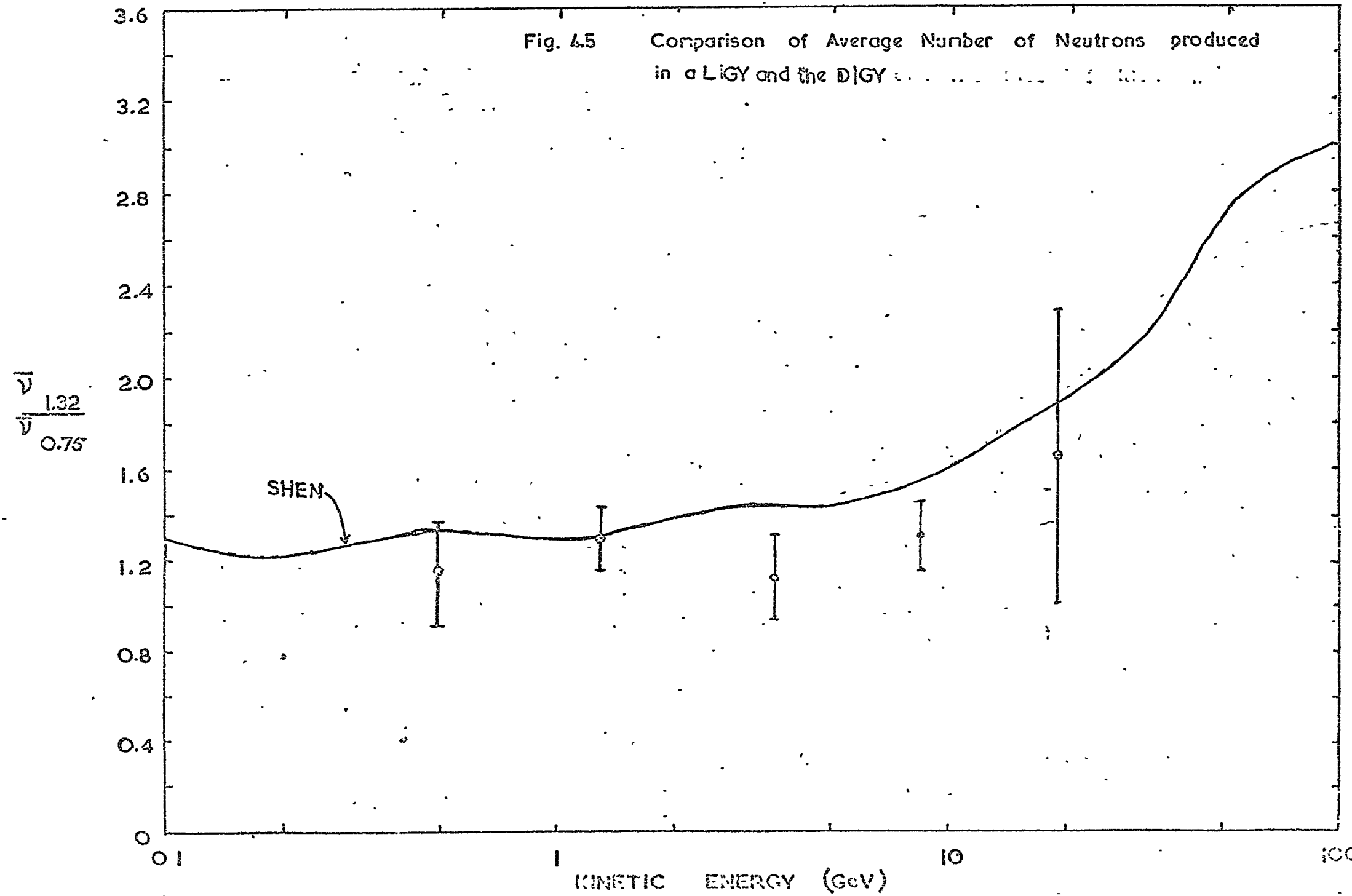
Fig. 4.5 Comparison of Average Number of Neutrons produced in a LIGY and the DIGY
$\frac{\bar{\nu}_{1.32}}{\bar{\nu}_{0.75}}$
3.6
3.2
2.8
2.4
2.0
1.6
1.2
0.8
0.4
0
SHEN
0.1
1
10
100
KINETIC ENERGY (GeV)

above 0.5 GeV as suggested by figs. 4.3 and 3.7, the predicted ratio $\bar{\nu}_{1.3}/\bar{\nu}_{0.75}$ above 0.5 GeV would tend to be too low due to the greater contribution of neutrons from the low energy secondaries in the thicker producer. Although this result could indicate an inconsistency in $\bar{m}$ between the two sets of data, a plausible explanation, given the compromise that had to be made in section 3.2.8 between the two estimates of the DIGY's efficiency, is that the relative efficiency of this monitor assumed in the present experiment is toohigh by the same amount. This would account for why the discrepency in fig. 4.3 is larger than expected from the previous experiment.

The results of fig. 4.4 indicate that the estimation of variation in efficiency considered in section 2-3.3 can account for a significant proportion (~20%) of the discrepency at the higher energies in fig. 4.3, whilst having relatively little effect on $\bar{\nu}$ at low energies where there is good agreement.

Not included in fig. 4.4 is the effect of the double exponential form of the neutron production spectrum, which is substantiated in this experiment for the first time. The approximate correction factors α' for $\bar{\nu}$ are generally higher than those predicted by Shen for a thinner monitor, but the experimental errors are very large and should only be taken as qualitative confirmation of Shen's results. In agreement with the prediction of Shen, the double exponential form is not perceptible at low energies ($\lesssim$ 0.5 GeV) and so the increase in $\bar{\nu}$ is only expected at higher energies. The effect of this is therefore similar to the effect of the variation of efficiency noted in fig. 4.4, increasing $\bar{\nu}$ preferentially at higher energies and by a similar amount (~10%).

However, these two factors can account for less than half of the discrepency, and the uncertainty in $\bar{\nu}$ represented by the shaded area

cannot account for the rest.

The suggestion by Hatton that the discrepency between results of Hughes et al. and Shen could be largely due to the mis-interpretation of emulsion data for energies greater than 1 GeV and the effect of the variation in efficiency with energy, may not be true because the results of the present experiment (fig. 4.4) indicate that Shen's calculations overestimate $\bar{\nu}$ significantly at about 1 GeV inspite of a correction for the latter effect. To reconcile this, it would be necessary to assume a decrease in the absolute effieincy of the DIGY of some 35% or considerably more than the errors of the efficiency measurements and the variation of efficiency with energy, and would be inconsistent with efficiency measurements of other monitors.

It has been pointed out in section 2-1.2 that the intra-nuclear cascade calculations which form the base of Shen's data at this energy, may overestimate the neutron yield in lead nuclei by as much as 20% (West and Wood, 1971). If this is so the neutron yield $\langle\nu\rangle$ per inelastic interaction assumed by Shen and shown in fig. 2.5, may be lower by this amount below 2 GeV, and so the neutron yield $\bar{\nu}$ per incident interacting proton shown in figs. 2.7, 4.3 and 4.4 would be down by a similar amount over this energy range.

Therefore, below 2 GeV, it would appear to be more likely that there is a large (~20%) systematic error in the theoretical neutron yield rather than in theabsolute neutron detection efficiency, and that the discrepency in fig. 4.3 below 2 GeV can be explained as being due to roughly equal systematic errors in the theoretical predictions and in the experimental values.

The general agreement between theory and experiment of the increase of $\bar{\nu}$ with proton energy above 2 GeV, indicates that the general features

of Shen's calculations are correct and, in particular, that the one dimensional-type model for the nucleon-nucleus interaction is a true representation. However, the absolute difference in neutron yield indicates that the interpretation of emulsion data has led to a significant overestimation which cannot be accounted for by uncertainties in the neutron detection efficiency at high energies. The estimation of momentum measurement error near the mdm indicates that the proton momenta measured by Hughes et al. with a similar spectrograph to the one in this experiment, may be seriously overestimated at their mdm (~150 GeV). This is unlikely to change the above conclusion though because $\bar{\nu}$ is a slowly changing function with energy.

The results of Bertini (1972) indicate that the neutron yield from nuclei may be increasingly overestimated by conventional intranuclear cascade calculations as the size of the nucleus increases above A ~ 60. This would throw doubt on Shen's simple extrapolation technique of deriving $\langle\nu\rangle$ for lead from $\langle N_n \rangle$ for emulsion nuclei and could explain why Shen found good agreement with the intranuclear calculations of Metropolis/Dostrovsky at 1.8 GeV. If, as seem likely, the Metropolis/Dostrovsky value of $\bar{\nu}$ is too high at 1.8 GeV, Shen's $\langle\nu\rangle$ above 1 GeV would also be too high and can account for a substantial part of the discrepency in fig. 4.3

There are indications in fig. 4.3 of there being a lower produced neutron multiplicity from (negative) pions than from protons although the difference is only statistically significant at the 30% level (i.e. there is a 30% probability of $\bar{\nu}$ for pions being equal to $\bar{\nu}$ for protons). In making his predictions for the neutron yield from pions in lead, Shen assumed the same $\langle\nu\rangle$ as in fig. 2.5, arguing that the effect of the increased interaction mean free path (mfp) of pions

in nuclear matter should be cancelled by the effect of the increase in the rate of production of secondaries. More recent experimental measurements of pion interactions in emulsions (Barashenkov et al., 1970) indicate no significant difference in $\langle\nu\rangle$ between pions and protons up to 6 GeV (see fig. 4.6), thus verifying Shen's assumption. The resulting values of $\bar{\nu}$ for pions, calculated by the extra-nuclear-cascade program, assuming the same mfp in lead for pions and protons differed very little from those for protons, so no significant difference between pions and protons would be expected in fig. 4.3.

There is no indication of this effect in the results of Hughes et al., although their statistical errors are larger than those in the present experiment. No source of experimental bias has been found which could have caused the observed discrepency; the bulk of the data (particularly at low energies) consists of $\bar{X}2$ events (table 4.2) which are not susceptible to any biases in the X2 track selection criteria, and the low momentum cut-off excludes virtually all the stopping negative muons.

The assumption that the mfp's in lead for protons and pions are the same needs to be questioned. Evidence from π^-p and p-p interactions suggests that this mfp of pions may be about 15% greater than that of protons at a few GeV (Giacomelli, 1970). This would reduce the ability of the monitor to absorb the energy of the pions, resulting in a lower $\bar{\nu}$. However the mfp would have to be considerably longer than that of protons to account for the observed difference in $\bar{\nu}$.

4-8 Conclusions

Within the uncertainty in relative efficiency of the LIGY and DIGY monitors, the results of the present experiment for neutron production by protons are in good agreement with those of Hughes et al..

FIG. 4.6 Variation of Average Number of Heavy Prongs

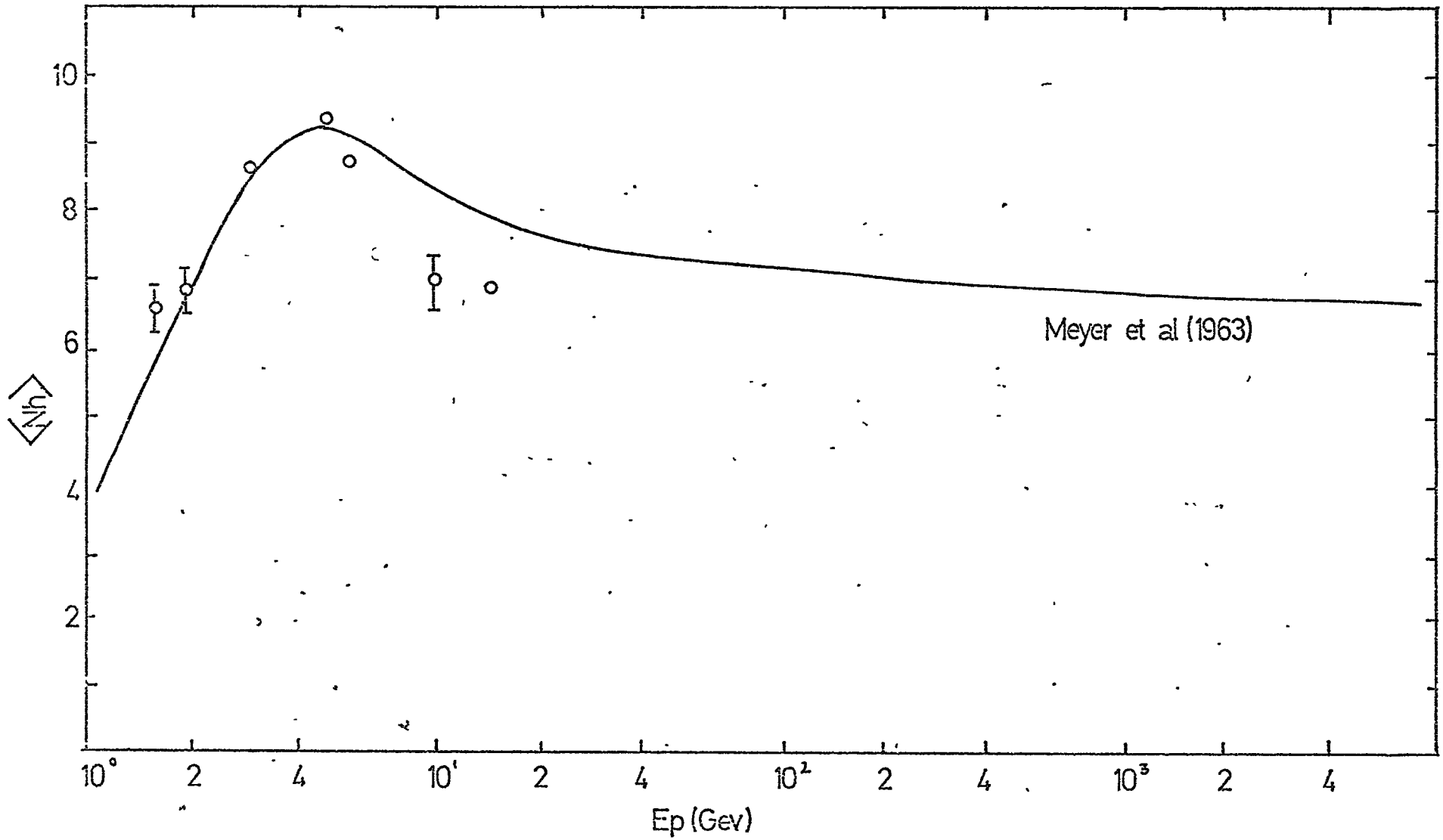

The double exponential production spectrum for neutrons predicted by Shen has been substantiated qualitatively.

About halfof the large discrepency between Shen's calculations and the two experimental results above 0.5 GeV can be accounted for by the effect of the double exponential spectrum and the variation of detection efficiency with NAP energy.

Contrary to Hatton's suggestion, the remaining discrepency cannot be attributed solely to the misinterpretation by Shen of emulsion data because intra-nuclear cascade calculations which form a basis of his calculations below 1 GeV are unable to account for the observed values of $\bar{\nu}$ below 2 GeV. There is evidence elsewhere that conventional intra-nuclear cascade calculations consistently overestimate the yield of evaporation neutrons from heavy nuclei and so Shen's calculations are likely to be overestimates too. The work of West and Wood indicates that the scale of the overestimation is large enough to account for the remaining discrepancy between Shen's predictions, and the results of Hughes et al. and the present work.

Within this uncertainty in the absolute value of $\bar{\nu}$ the calculations of Shen appear to be capable of explaining the general rise of $\bar{\nu}$ with increasing NAP energy measured by the two experiments.

There is evidence in the present work that the neutron production by pions is smaller than that by protons. There appears to be no other evidence for this in previous work and no theoretical justification for the observed difference which is only statistically significant at the 30% level.

CHAPTER FIVE

NEUTRON PRODUCTION BY FAST MUONS

5-1 Introduction

There is interest in the process of neutron production by fast muons both in the nuclear physics and the astrophysical aspects. Several cosmic ray experiments deep underground have been made in recent years to measure the sea level energy spectrum of very high energy muons (>1 TeV) using the rock cover as an energy analyser. It is of great importance to determine the rate of energy loss in matter of muons at these energies so that these measurements can be related accurately to the sea level flux.

The rate of energy loss by cosmic ray muons of energy E_μ can be approximated (Barrett et al., 1952) by

$$\frac{-dE_\mu}{dx} = a + bE_\mu$$

The first term gives the contribution from ionization and excitation and dominates for $E_\mu \lesssim 1$ TeV whilst the second term contains contributions from bremsstrahlung, pair production and photonuclear interactions, and becomes increasingly important at very high energies. Although the photonuclear contribution is the smallest it is also the least well known and so limits the degree of certainty of interpretation of the underground measurements.

At rather lower energies it is possible to measure this energy loss and hence obtain information about the nuclear interaction by comparing the measured energy spectrum at sea level with that at depths underground.

The nuclear interaction of high energy muons was discovered in underground emulsion studies by George and Evans (1950) who detected the characteristic nuclear "stars". The production of evaporation neutrons in these interactions was subsequently established by de Pagter et al. (1960). The limitation in underground studies is the lack of muon energy resolution, but sea level studies of muon interactions using large spectrographs

(Meyer et al., 1964; Allkofer et al., 1968) have enabled the variation of $\bar{\nu}\sigma$ (the nuclear cross section×produced neutron multiplicity product) with muon energy to be measured up to a few hundred GeV.

The present experiment investigates muons in the energy range 1-15 GeV, a region where the photonuclear cross section is now well known (Caldwell et al., 1969); the purpose of this measurement being the verification of other cosmic ray measurements in this region, so making the cosmic ray studies at higher energies more reliable. Also it is hoped that the present experiment, using a thickness of lead producer intermediate between those used in other experiments (Allkofer et al. and, Bergamasco et al.) may clarify the effect of the producer thickness on the average produced neutron multiplicity $\bar{\nu}$.

5-2 The Photonuclear Cross-section

Neutron production by muons has been interpreted as due to the interaction between the electromagnetic field of the muon and the nucleus. There are two distinct ways by which this interaction takes place, the direct and the indirect mode. In the first the muon interacts directly with the nucleus via the virtual photons associated with the muon. In the other, the interaction is between the nucleus and real photons generated by electromagnetic cascades initiated by the knock-on, pair production or bremsstrahlung processes.

5-2.1 The Direct Neutron Production

The product of the muon-nuclear cross-section and the average produced neutron multiplicity for a muon of energy E_μ is given (Allkofer et al., 1968) by

$$\bar{\nu}\sigma_{(E_\mu)}^{(\mu,n)} = \int_{k_{min}}^{E_\mu - m} \int_{\tau_{min}}^{\tau_{max}} N(E_\mu, k, \tau)\sqrt{(\tau)}\ \bar{\nu}\sigma_{(k)}^{(\gamma,n)}\, dk d\tau \qquad 5.1$$

where N is the virtual photon spectrum given by Kessler (1960)

$\sqrt{(\tau)}$ is the electromagnetic form factor of nucleons given by Daiyasu et al. (1962)

k is the energy of the photon

and τ is modulus of the squared 4-momentum transfer.

The variation of $\bar{\nu}\sigma_{(k)}^{(\gamma,n)}$ the mean multiplicity-photonuclear cross section product, with photon energy is given for lead in fig. 5.1. Allkofer et al. investigated the effect of three different assumptions regarding $\bar{\nu}\sigma_{(k)}^{(\gamma,n)}$ for $k > 1$ GeV:-

I $\quad \sigma_{(k)}^{(\gamma,n)} = \text{constant}$ (Castagnoli et al. 1967),

II $\quad \sigma_{(k)}^{(\gamma,n)} \sim k^{-1}$ in $1 \text{ GeV} < k \leq 5 \text{ GeV}$
$\quad\quad \sigma_{(k)}^{(\gamma,n)} = \text{constant}, k > 5 \text{ GeV}$ (Hogdson et al. 1968),

III $\quad \sigma_{(k)}^{(\gamma,n)} \sim k^{-1}$ in $k > 1$ GeV (Jameel, 1965).

In all three cases $\bar{\nu}$ was assumed (Roos, 1961) to vary as

$$\bar{\nu} \alpha\ k^{\frac{1}{4}} \quad \text{for } k > 0.3 \text{ GeV}$$

The results of computing equation 5.1 for these three cases are shown in fig. 5.2 as curves I, II and III.

5.2.2 The Indirect Neutron Production

The muon-nuclear cross section and multiplicity product for the knock on process is given by Allkofer et al. as

$$\bar{\nu}\sigma_{(E_\mu)}^{(\mu\rightarrow e,n)} = \int_{E_e\,min}^{E_e\,max} \int_{k_{min}}^{E_e} \phi_{coll}(E_\mu, E_e)\, g_o(E_e,k)\, \bar{\nu}\sigma_{(k)}^{(\gamma,n)}\, d E_e\, dk \qquad 5.2$$

ϕ_{coll} is the probability of a muon of energy E_μ transferring energy in range $(E_e, E_e + dE_e)$ to an atomic electron after traversing unit thickness of lead, and g_o is the track length of shower photons produced by the knock-on electron. Both ϕ_{coll} and g_o were taken from Rossi (1956).

The result of this computation is given in fig. 5.2 as curve IV It was found that this result was not sensitive to the assumptions about

FIG. 5.1

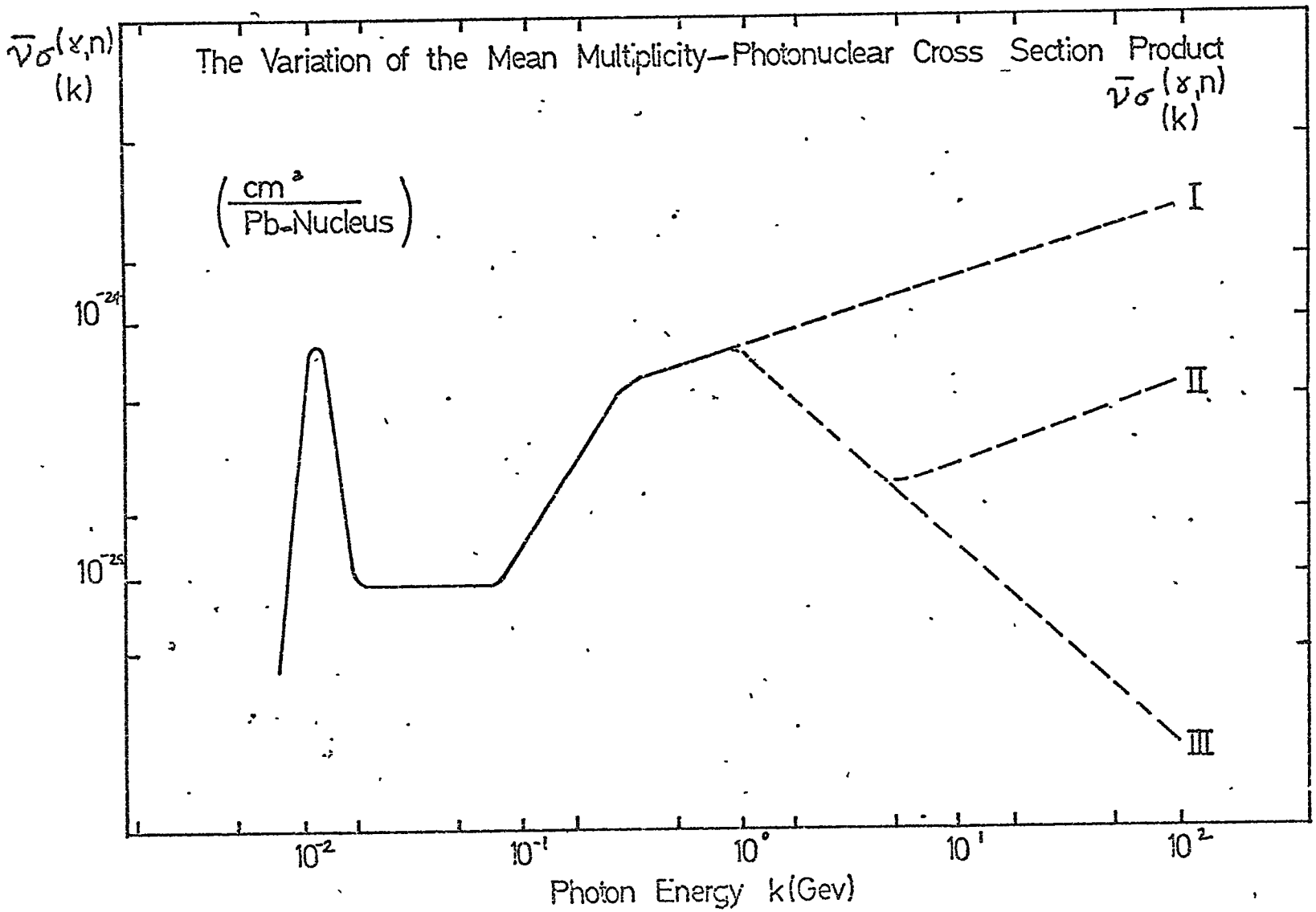
$\bar{\nu}\sigma(\gamma,n)$ (k)
The Variation of the Mean Multiplicity–Photonuclear Cross Section Product
$\bar{\nu}\sigma(\gamma,n)$ (k)
$\left(\frac{cm^2}{Pb\text{-}Nucleus}\right)$
10^{-24}
10^{-25}
I
II
III
10^{-2}
10^{-1}
10^{0}
10^{1}
10^{2}
Photon Energy k(Gev)

FIG. 5.2

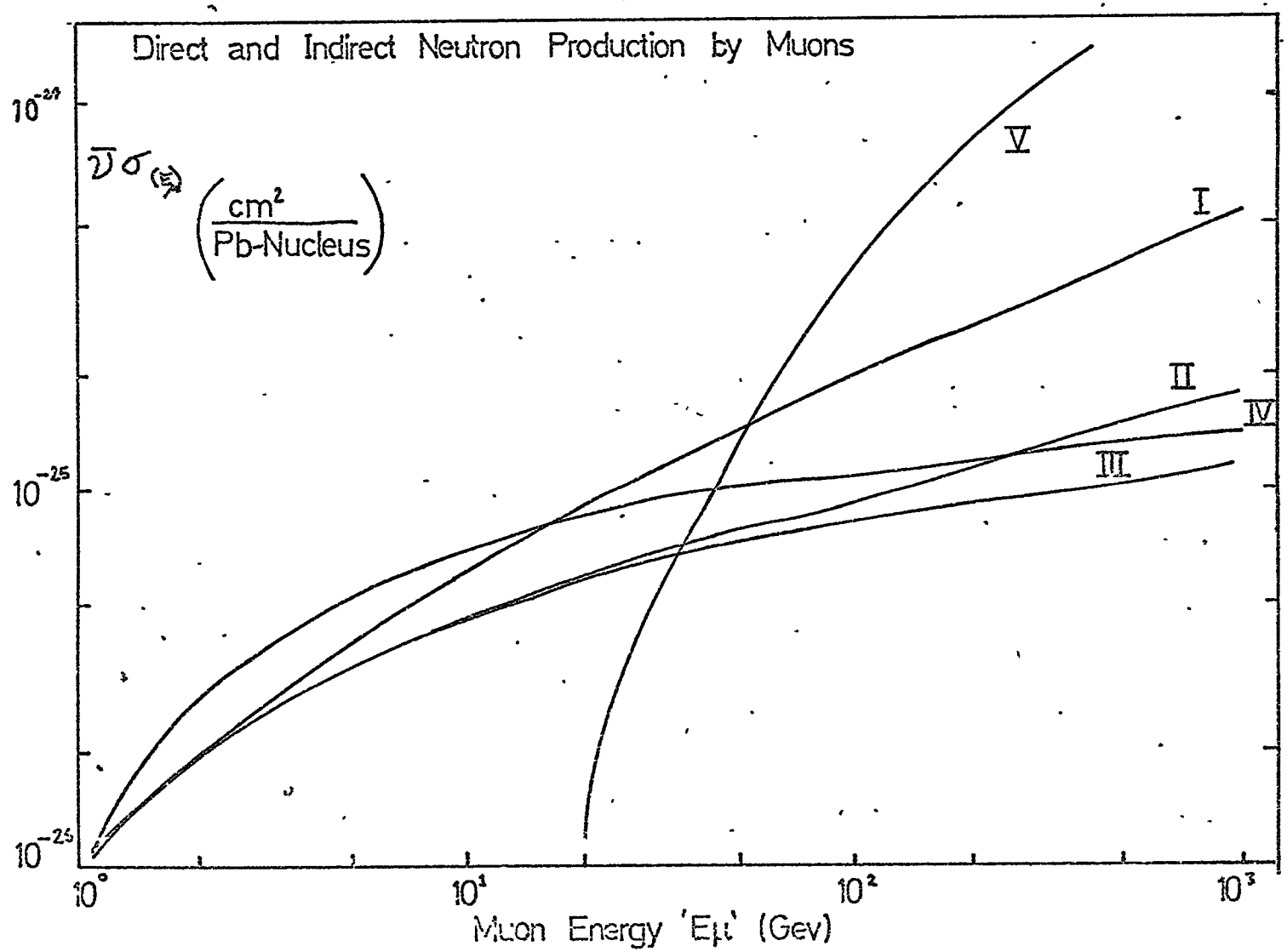
Direct and Indirect Neutron Production by Muons
$\bar{\nu}\sigma_{(E_\mu)}$
$\left(\frac{cm^2}{Pb\text{-}Nucleus}\right)$
10^{-24}
10^{-25}
10^{-25}
V
I
II
IV
III
10^0
10^1
10^2
10^3
Muon Energy 'Eμ' (Gev)

$\bar{\nu}\sigma(k)^{(\gamma,n)}$ for k> 1 GeV due to the lower average energy of photons in this process.

The total neutron production for these two processes is given in fig. 5.3 for the three cases I, II and III.

Bergamasco et al. (1973) have performed calculations for neutron production allowing for bremsstrahlung and pair-production, using Caldwell's more recent data on the photo-nuclear cross-section (which is very similar to assumption I of Allkofer et al).

The contribution from bremsstrahlung and pair production is seen in fig. 5.2 (curve V) to be dominant for E_μ> 100 GeV. The resultant contributions from these various processes are shown in fig. 5.3 (curves I' (Direct and knock-on) and IV (Direct and knock-on, bremsstrahlung and pair production)). The combined contribution for knock-on and direct interaction as calculated by Bergamasco et al. agrees with that by Allkofer et al. but the bremsstrahlung and pair-production contribution becomes increasingly more important as E_μ increases above 10 GeV, As pointed out by Bergamasco et al. this limits the use of measurements of neutrons production by high energy muons as a tool to investigate nuclear structure via the direct interaction.

5-2.3 Experimental Measurements at Sea Level

Two previous experiments have been performed using a neutron monitor to investigate the photonuclear cross-section at high energies using a magnet spectrograph for measuring the muon energy.

The first (Meyer et al., 1964) was similar in many respects to the present experiment in that an air gap magnet spectrograph with Geiger-Müller counters and a flash tube array having an mdm of 150 GeV/c was used; and the muons were selected from data which predominantly consisted of protons (see Hughes et al; Brooke et al., 1964). It differed particularly in the design of neutron monitor which was the standard Leeds monitor (LIGY).

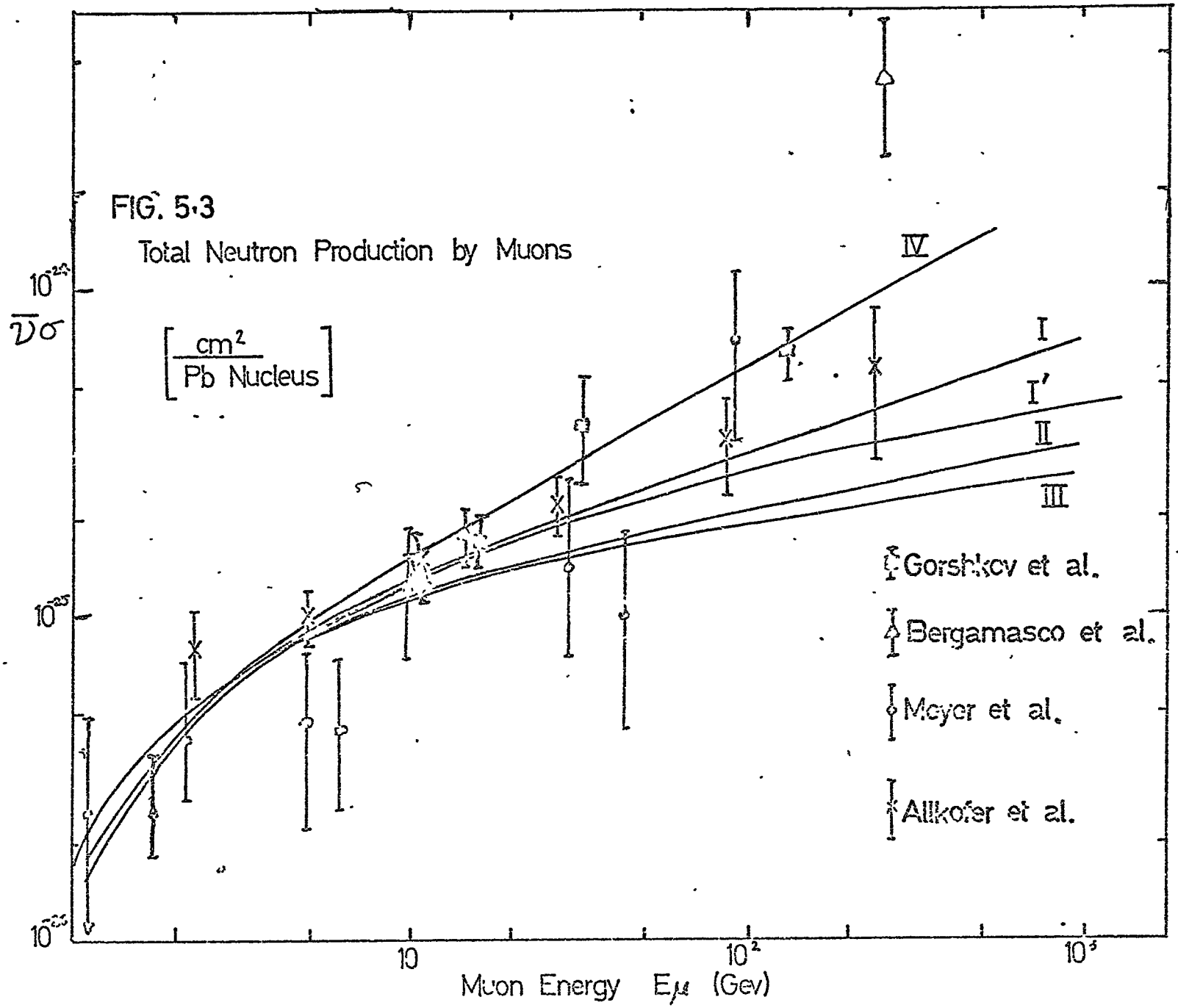
FIG. 5.3
Total Neutron Production by Muons
$\bar{\nu}\sigma$
$\left[\frac{cm^2}{Pb\ Nucleus}\right]$
10^{-24}
10^{-25}
10^{-26}
IV
I
I'
II
III
Gorshkov et al.
Bergamasco et al.
Meyer et al.
Allkofer et al.
10
10^2
10^3
Muon Energy E_μ (Gev)

This experiment suffered from large statistical uncertainties in both the number of interacting muons and the number of accidental muons caused by chance coincidences of non-interacting muons with the background count rate of the monitor. The hadron contamination was a further possible source of error.

The more recent experiment by Allkofer et al. (1968) effectively reduced the number of accidental muons and likelihood of contamination by hadrons by placing the monitor under 1500 g cm^{-2} of solid iron magnet and the whole experiment inside a concrete bunker with walls and roof 600-800 g cm^{-2} thick. This reduced the flux of hadrons to small proportions lowering the monitor background count rate from a normal 200 min^{-1} to 13 min^{-1}, and reducing the number of accidental events in the measurement correspondingly. A solid iron magnet spectrograph utilizing six double gap spark chambers and four scintillator counters, and having an mdm of 2,000 GeV/c, was used in conjunction with a 6 counter standard IGY monitor (SIGY). The monitor gate was opened 20 μsec after the passage of the particle through the spectrograph and shut after 250 μ sec, the neutron multiplicity being recorded for each event.

It can be shown that the product of muon-nuclear cross-section and mean produced multiplicity $\bar{\nu}\sigma$ is related to the number n of neutrons detected after the passage of N_μ penetrating muons by

$$\bar{\nu}\sigma = \frac{A}{N_o t \epsilon f} \frac{n}{N_\mu} \qquad 5.3$$

where A = 207 is the atomic number of the monitor's producer

$N_o = 6.02 \times 10^{23}$ is Avogadro's Number

t = average thickness of producer (=150g cm^{-2} for vertical particles in the SIGY and LIGY)

and ϵf = neutron detection efficiency (ϵf = 0.021 has been used in the two previous experiments, for all muon energies).

The results of these two experiments using the above values are shown in fig. 5.3. The results of Allkofer et al. agree well with prediction I (assuming a virtually constant photonuclear cross-section above 1 GeV but neglecting bremsstrahlung and pair-production), agree rather less well with prediction IV (including bremsstrahlung and pair production) at high energies but give a bad fit to cases II and III. The Meyer et al. results (obtained only from negative muons in order to minimise hadron (principally proton) contamination) are consistently lower but have significantly larger errors.

Allkofer et al. have calculated the average produced neutron multiplicity $\bar{\nu}$ assuming an exponential neutron production spectrum, and found a general increase from 5 to 50 as the muon energy increased from 2 to 250 GeV. This disagreed with Meyer et al. who found a constant $\bar{\nu}$ within the large experimental errors.

5-2.4 Experimental Measurements Underground

Several experiments have been performed underground, at depths ranging from 40 mwe to 4,300 mwe.

Bergamasco (1970) used two neutron monitors at 40 mwe, each having five BF_3 counters and a lead producer thickness of 150 g cm^{-2}, placed next to a liquid scintillator tank. A plastic scintillator muon telescope accepted muons from two directions (corresponding to two depths, 60 and 110 mwe) and interactions were identified by the pulse sequences in the liquid scintillator. Each coincidence caused a gate to be opened and the neutrons from the monitors counted. A Ra-Be source was used to measure the neutron detection efficiency and gave a reported result of 0.05. The results were corrected for background coincidences and for pion interactions, and $\bar{\nu}\sigma$ evaluated using equation 5.3.

A similar experiment by Bergamasco et al. (1973) at 4,300 mwe utilised a larger, non-standard neutron detector. This consisted of twenty eight

BF_3 counters, each 40 cm long, having a gas pressure of 70 cm Hg, embedded in a (100 x 100 x 40) cm^3 paraffin block. The lead target had dimensions (80 x 100 x 35)cm^3 and was placed 24 cm above the paraffin block.

A $2m^2$ scintillator telescope selected vertical muons and opened a 2 millisecond long neutron gate, allowing the neutron pulses to be counted. The absolute neutron detection efficiency was measured using a Ra-Be source, and the variation with neutron energy using a Monte Carlo calculation in a similar manner to Pearce and Fowler (1964). The maximum efficiency, at 15 MeV, was 0.006, falling gradually to 0.003 at 50 MeV, but falling very sharply below 10 MeV. The very low value of the efficiency, particularly less than 10 MeV could be due to the large distance between the producer and moderator.

The neutron energy spectrum from the high energy muon interactions was assumed to be composed of an evaporative component (due to the lower energy photons) and a flat spectrum (due to the high energy photons) and an estimate was made of their relative contributions from considerations of the photonuclear cross section and the bremsstrahlung photon spectrum. This resulted in the expression for the efficiency

$$\langle\epsilon\rangle \approx 0.85\langle\epsilon_{evap}\rangle + 0.15\langle\epsilon_{flat}\rangle \qquad 5.4$$

$$= 0.0021\ (\pm\ 0.0005)$$

where $\langle\epsilon_{evap}\rangle = 0.0019$ assuming a nuclear temperature of 1.5MeV

and $\langle\epsilon_{flat}\rangle = 0.0031$

This compares with a value of 0.0038 ($\pm$ 0.0007) obtained using the Ra-Be source.

The measured values of $\bar{\nu}\sigma$ for the two experiments are shown in fig. 5.3 plotted at the values of mean muon energy appropriate to the two experiments. Although the low energy point is in good agreement,

the high energy point is particularly high compared with Allkofer et al.'s sea-level measurements. It would be expected to be somewhat higher due to the extra yield of neutrons that would result from the extra-nuclear cascades in the thicker producer (392 g cm^{-2} c.f. 150 g cm^{-2}). The results for the average produced neutron multiplicity are, however, in more reasonable agreement with Allkofer et al. being $\bar{\nu}$ = 10 at 15 GeV and $\bar{\nu}$ = 100 at 275 GeV and so cannot account for the difference. As pointed out by Bergamasco et al. the uncertainties in efficiency at these energies are particularly great and could be onecause of the discrepency between the two.

A similar set of experiments by Gorshkov et al. 1971a and Gorshkov et al. 1971b has been performed at depths of 40 mwe and 150 mwe using a monitor of lead producer thickness 170 g cm^{-2}. By accepting muons from two directions, results were also obtained for 80 mwe and 800 mwe. Their results for $\bar{\nu}\sigma$ are seen in fig. 5.3 to be in good agreement with those of Allkofer et al.

5-3. The Present Experiment

5-3.1 Introduction

The experimental arrangement and procedure were the same as in the work concerned with the neutron production by protons and pions, and are described in the previous chapter. The data for the muon work were taken from the same sample, namely the events falling in categories A and D (i.e. unaccompanied, momentum-analysable tracks with any number of X2 tracks).

5-3.2. The Selection of Muons and Removal of Accidental Muons

Events were initially selected which had $|\Delta_\psi| < 3^o$, at least one X2 track which was only slightly deviated and an impact on the monitor within 20 cells (1 cell = 2 cm wide) of a channel detecting a neutron.

A muon loses a very small fraction of its energy in an interaction (Kessler (1960)) and is practically certain to emerge from the monitor. Further, the probability of a low four-momentum transfer is very high and makes a slight angular deflection similarly likely (Meyer et al.1964) A maximum limit of the lateral scatter as measured in the X2 flash tube tray, of interacting muons must be assumed in order to remove the effects of the protons and pions which have characteristically larger scatter.

The distribution in y, the lateral scatter (in units of σ_{cx}, the typical value of scatter expected for a muon - see section 3-3.7) for all events with $|\Delta\psi| < 3^{o}$, a monitor response, a nearest impact distance 20 cells and oneor more X2 tracks, is shown in fig. 5.4, for both positive and negative particles. There is evidence for there being two superimposed groups of particles, one predominantly below $8\sigma_{cx}$, the other above the same.

To investigate the effects of accidental events on this distribution, the spectrograph has been operated without requiring a response from the neutron monitor, although in all other respects identical to the normal spectrograph and monitor mode. The events recorded in this, so called, muon mode have been analysed in the same way as the normal events into the categories A to G (section 4.3). Shown in table 5.1 is a summary of the events recorded.

The distribution in y for the muons in categories A and D, with $|\Delta\psi| < 3^{o}$ is given in fig. 5.5 and shows that very few ($\approx 3\%$) of the muons have scatters greater than $8\sigma_{cx}$. The large fraction of muons with values of y greater than σ_{cx} can be explained in terms of the measurement errors in the spectrograph and X2 flash tube tray (section 3-3.7). Assuming that the interacting muons should not be scattered much more than the non-interacting ones it would seem reasonable to attribute the majority of those events with $y < 8\sigma_{cx}$ to interacting and non-

FIG. 5.4

The Distribution in Lateral Scatter in the Neutron Monitor

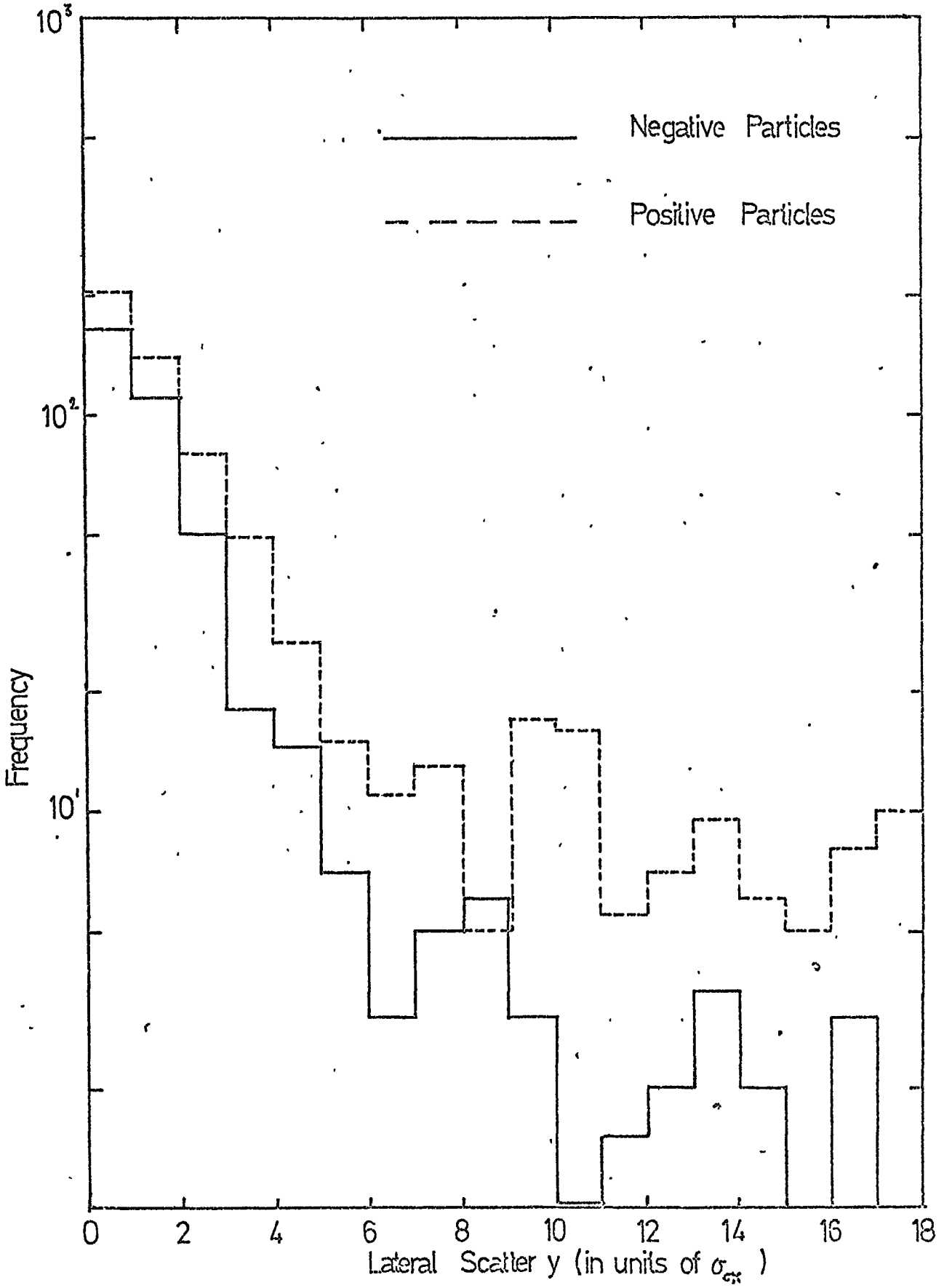

TABLE 5.1

Category of Event	Name	Fraction of Events %
A	B	75
B	F	7
C	EAS	1
D	B(P)	3
E	F(P)	1
F	Dense	1
G	Reject	15

FIG. 5.5

The Distribution in Lateral Scatter of Muons in the Neutron Monitor

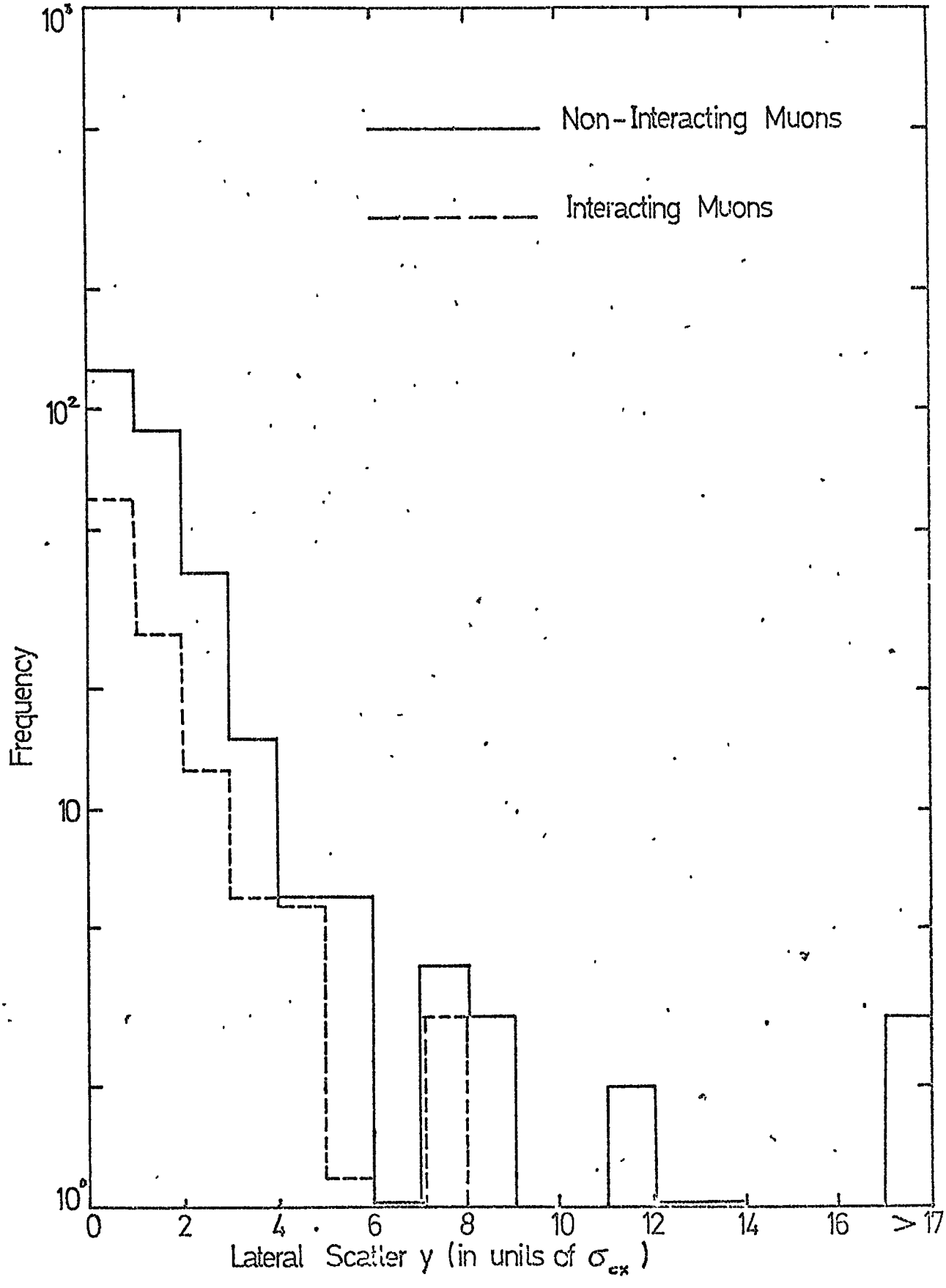

interacting muons, and the rest to interacting protons and pions, as assumed by Meyer et al..

The absolute number of accidental muons in fig. 5.4 has been calculated and subtracted from the total. The remaining distribution is assumed to consist of interacting muons ($< 8\sigma_{cx}$), protons and pions. The number of accidental muons μ_{acc} is given by

$$\mu_{acc} = \frac{R.\Delta t\, M\, i.a.}{\bar{m}_{acc}} \qquad 5.5$$

where M = number of single particle triggers (GM s) with or without a response from the monitor

Δt = the monitor gate width (secs)

R = background count rate of the monitor (sec^{-1})

i.a = fraction of accidental events which satisfy the analysis requirements (i.e. those in categories A and D, $|\Delta\psi| < 3^{o}$) and only includes that fraction i which have impact distances within the chosen limit. The factor a has been found from table 5.1.

and $\bar{m}_{acc}$ = average neutron multiplicity for the accidental events.

During the experiment in which the interacting muons were recorded,

$R = 11\ sec^{-1}$

$\Delta t = 300\mu sec$

$M = 8.13 \times 10^{5}$

and $\bar{m}$ was found to equal 1.12.

The expected impact distribution for the accidental events has been calculated (fig. 4.1) using the variation of muon flux over the monitor found in the muon-mode experiment, and the relative count rates from each channel given in table 3.2 (normalised to a total of R = 11 sec^{-1}). It has been found that i = 27 and 48% of the events fall within a range 10 cells and 20 cells respectively.

The numbers of negative and positive accidental muons have been calculated assuming a muon charge ratio of 1.28 (Owen and Wilson, 1951) over the whole of the momentum range.

5-3.2 Proton and Pion Contamination of the Muon Sample

Using the distributions in y for positive and negative particles with the correction for accidental events, it is possible to roughly estimate the numbers of positive and negative NAP s (protons and pions) having $y < 8\sigma_{cx}$, by making the following assumptions:-

1. The muon charge ratio is 1.28 (=N(+)/N(-),
2. the muon-nuclear cross-section is independent of charge,
3. the y distribution of pions has the same shape as that of protons,
4. there are no interacting muons with $y > 8\sigma_{cx}$.

Then charge ratio r of NAP s in each range of y is the charge ratio of NAP's with $y > 8\sigma_{cx}$ (using 3 and 4) which is

$$r = 9.7 \text{ from fig. } 5.4.$$

Therefore assuming 2 we can equate the numbers of positive and negative interacting muons (allowing for the charge ratio), in each of the eight ranges of y less than σ_{cx} by

$$(N^- - x)\,1.28 = N^+ - xr \qquad 5.6$$

where N^- and N^+ are the numbers of particles in each y range and x is the number of negative NAP s in each y range.

The results of this simple analysis indicate that there are about 10 negative NAP s and 100 positive NAPs in the muon sample.

The resulting interacting muon y-distribution is very similar to that obtained for accidental muons (fig. 5.5) as expected. The actual number of interacting muons (of both charges) is estimated to be 260 of which 114 are negative, only about one half of the number of accidental muons removed from fig. 5.4.

To further improve the selection of interacting muons over the accidental ones, only those events which have impact distances less than 10 cell widths have been used. The effective number N_μ of muons incident on the monitor during the experiment is then given by

$$N_\mu = M \cdot a \cdot j \qquad 5.7$$

where j is the fraction of interacting muon events selected under the impact criterion and has been found from the distribution in impact distances for NAP s given in fig. 4.1, to be 0.85.

In view of the large proton contamination of the positive interacting muons (~70%), the photonuclear cross-section has only been investigated using negative muons, where the correction for negative pions is relatively small (~10%).

5-4 The Experimental Results

The number N of events with X2 tracks, having $y < 8\sigma_{cx}$ and impact distances less than 10 cell widths, and the resulting number n of neutrons are given in table 5.2 for various ranges of magnetic deflection $|\Delta\psi|$. Also shown are the values of these quantities attributed to muon interactions i.e. after the pion and accidental muon contaminations have been subtracted. The relative numbers N_μ of muons in each deflection range, incident on the monitor during the experiment has been found from the muon deflection spectrum derived from the muon-mode events.

The integral muon momentum spectrum derived from this deflection spectrum and shown in figure 5.6 without any momentum measurement corrections being applied, agreed very well with the spectrum given by Allkofer et al. (1971) and Hayman and Wolfendale (1962), after normalisation of the absolute intensities.

The neutron time distribution for the events with and without the correction for the accidental muons (which are characterised by a flat

Table 5.2 Neutron Production by Muons

$\Delta\Psi^\circ$	3.0	2.0	0.98	0.42	0.2	0.09	0
Mean Energy E_μ (GeV)	0.9	1.8	4.0	9.4	20	-	
Number of Incident Muons N_μ ($\times 10^{-4}$)	2.70	3.94	4.84	1.89	0.25	0.47	
Number of events recorded (N)	29	61	78	35	5	6	
Number of neutrons recorded (n)	39	75	108	48	6	7	
Number of events recorded after correction	1.4	22	30.6	16.2	2.0		
Number of neutrons recorded after correction	7.2	29	515	24	2.4		
$\bar{m}$ (after correction)	5.1	1.3	1.7	1.5	1.23		
Average produced multiplicity $\bar{\nu}$	167(±59)	12.2(±3.3)	28.6(±6.7)	20.4(±7.5)	9.4(±10)		
n/N_μ (after correction)	2.60	7.19	10.40	12.42	9.43		
$\sigma\bar{\nu}$	1.35(±0.48)	3.74(±1.01)	5.4(±1.27)	6.46(±2.37)	4.90(±5.2)		

Fig. 5.6 The integral Muon Momentum Spectrum recorded with the present instrument (no corrections for instrumental noise have been made.)

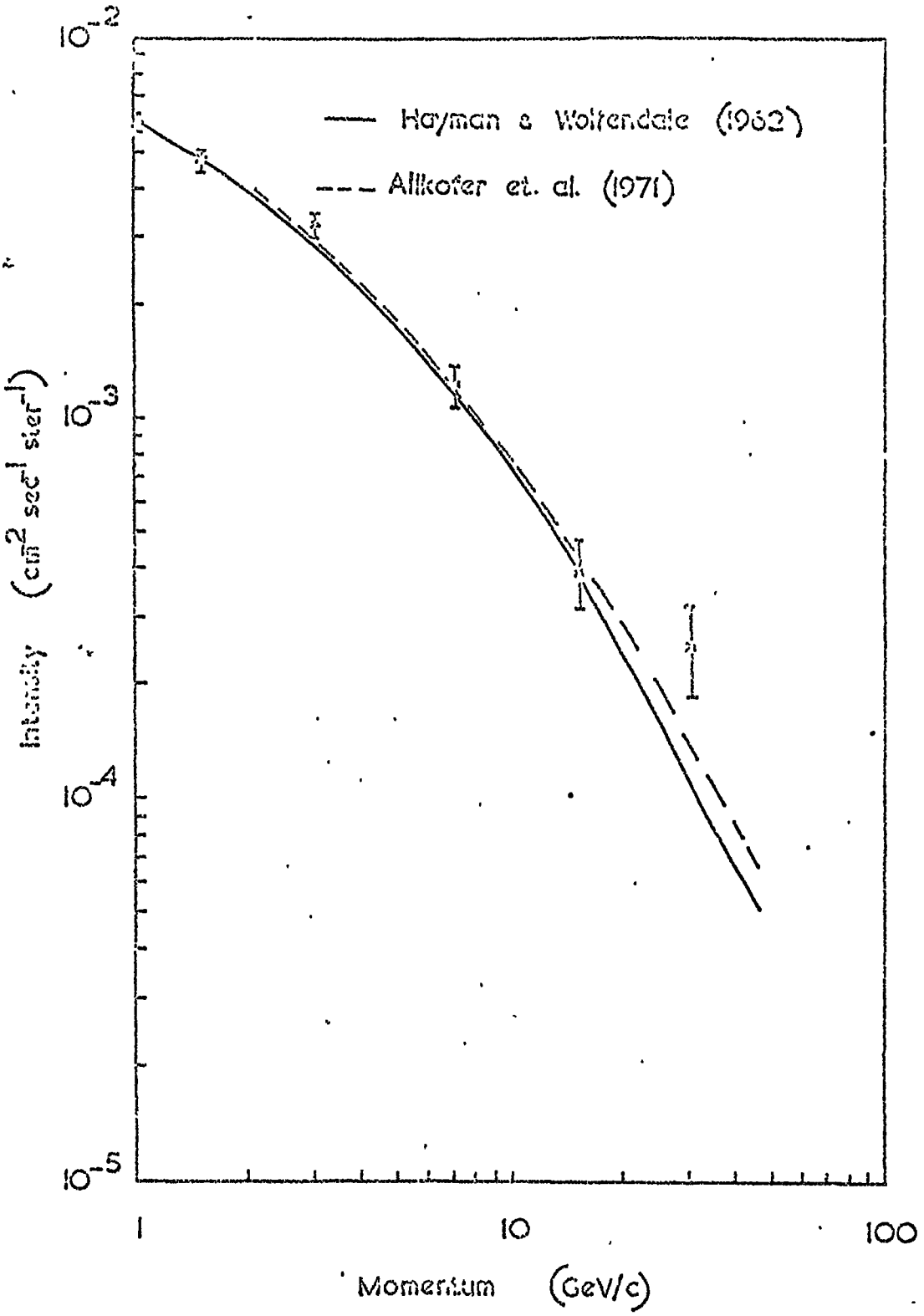

time distribution) is shown in fig. 5.7. The agreement of the corrected distribution with that obtained for NAP s (fig. 3.7) demonstrates that the effect of the accidental events has been accounted for correctly.

The product of muon cross-section σ and mean produced multiplicity $\bar{\nu}$ for each $\Delta\psi$ range has been calculated (table 5.2) using

$$\bar{\nu}\sigma = \frac{A}{N_o t\, \epsilon(E_\mu) f} \cdot \frac{n}{N_\mu} \quad \text{cm}^2/\text{Pb nucleus} \qquad 5.8$$

where $A = 207$

$N_o = 6.02.10^{23}$

$t = 270$ g cm^{-2}

$f = 0.70$

and $\epsilon(E_\mu) = 0.035$.

The mean multiplicity $\bar{\nu}$ has been calculated from

$$\bar{\nu} = \frac{(\bar{m} - 1)}{\epsilon(E_\mu) f} \qquad 5.9$$

where $\bar{m}$ is the average detected multiplicity after corrections for background events and pions.

The results are given in table 5.2.

The choice of $\epsilon(E_\mu)$, being that appropriate for evaporation neutrons produced by low energy (~100 MeV) cosmic ray neutrons, is justified because the nuclear excitation by the two processes should be similar, given that they produce a similar value of $\bar{m}$ (1.24 for cosmic ray neutrons compared with the values in table 5.2). At this low energy the nuclear excitation is rather insensitive to the primary energy (fig. 2.1) and justifies a constant efficiency in the first instance. It is apparent that the large errors in $\bar{m}$ do not allow a meaningful estimate to be made of the variation of efficiency with muon energy.

FIG. 5.7

Real Time Distribution of Neutrons Produced by Interacting Muons

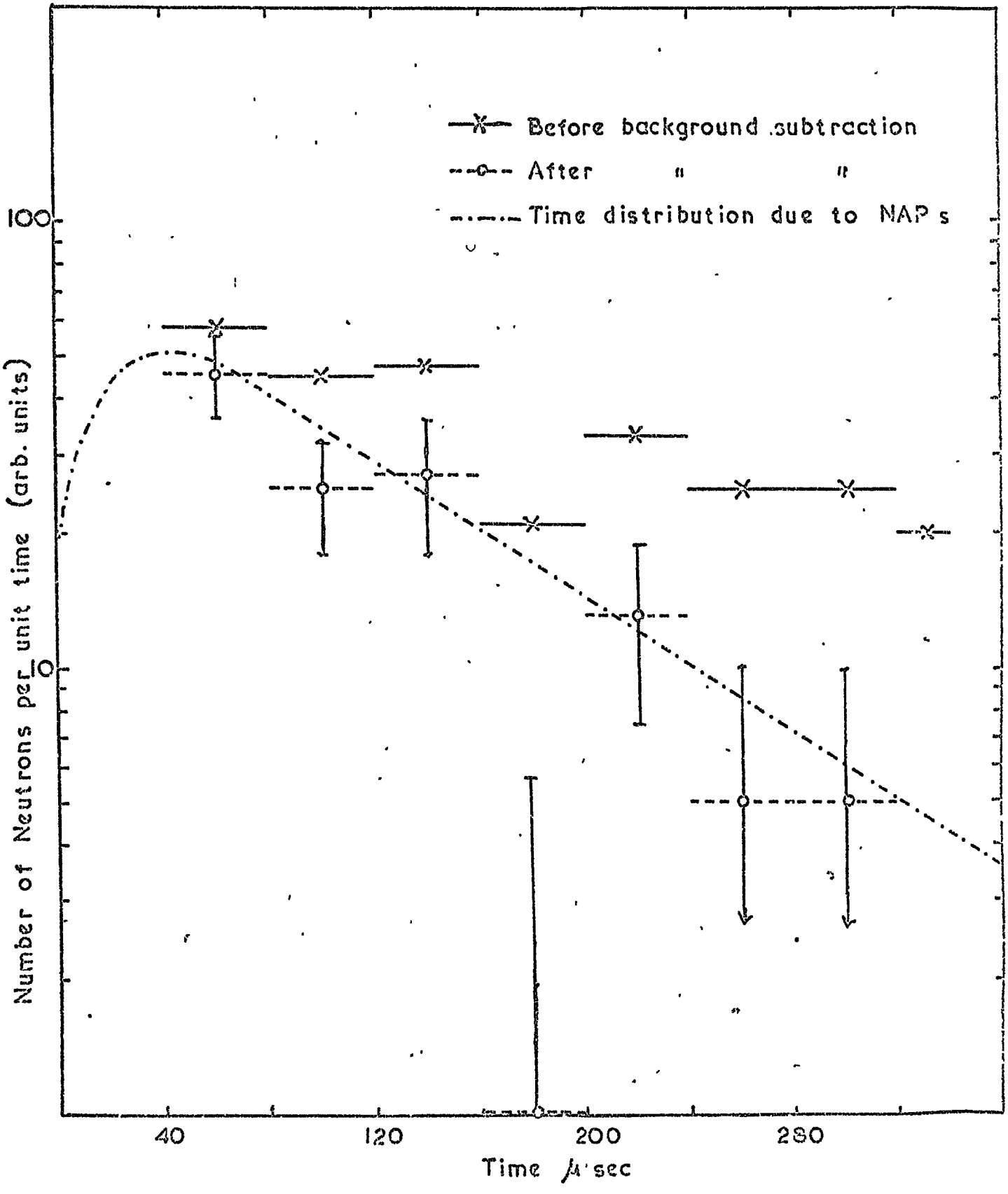

5-5 Discussion

The values of $\bar{\nu}\sigma$ measured by Allkofer et al. using the SIGY monitor should not be directly compared with those of Meyer et al. using the LIGY monitor because the same value of ϵf was used for both experiments. It has been demonstrated by Hatton (1971) that the efficiency appropriate to the centre region of the LIGY has been measured to be $\epsilon = 0.03$ whilst a comparison of the counting rates of the SIGY and LIGY indicate (see section 3-1.4) a relative average efficiency for the whole surface of the SIGY of 0.022. The efficiency appropriate to the experimental measurements of Allkofer et al. will admittedly be slightly higher than this if, as is likely, the muons interacted towards the centre of the monitor but it is very unlikely that the efficiency is as high as 0.03. Since the precise correction depends on a knowledge of the acceptance of the spectrograph and this is not known, the value of 0.03 could be considered as an over-estimate by about 20-30%. Using the value of gating efficiency given by Hatton and Tomlinson (1968) f = 0.64 (c.f. f = 0.70 quoted by Allkofer et al) we get $\epsilon f \lesssim 0.019$, which will increase $\bar{\nu}\sigma$ by at least 8%. These corrected values would no longer give a very good fit to any of the calculated curves in fig. 5.3.

The $\bar{\nu}\sigma$ values obtained by Meyer et al. are also too low by 8% due to the overestimating of f so that these; if corrected, would agree better with curve I in figure 5.3.

The values of $\bar{\nu}\sigma$ for both experiments (corrected for the over-estimation of f) are shown in figure 5.8 together with the values calculated in this experiment.

The values obtained in the present experiment are generally mid-way between these two similar previous experiments and agree well with the theoretical prediction. The errors shown are the statistical errors not only due to the neutrons produced by the interactions but also the errors

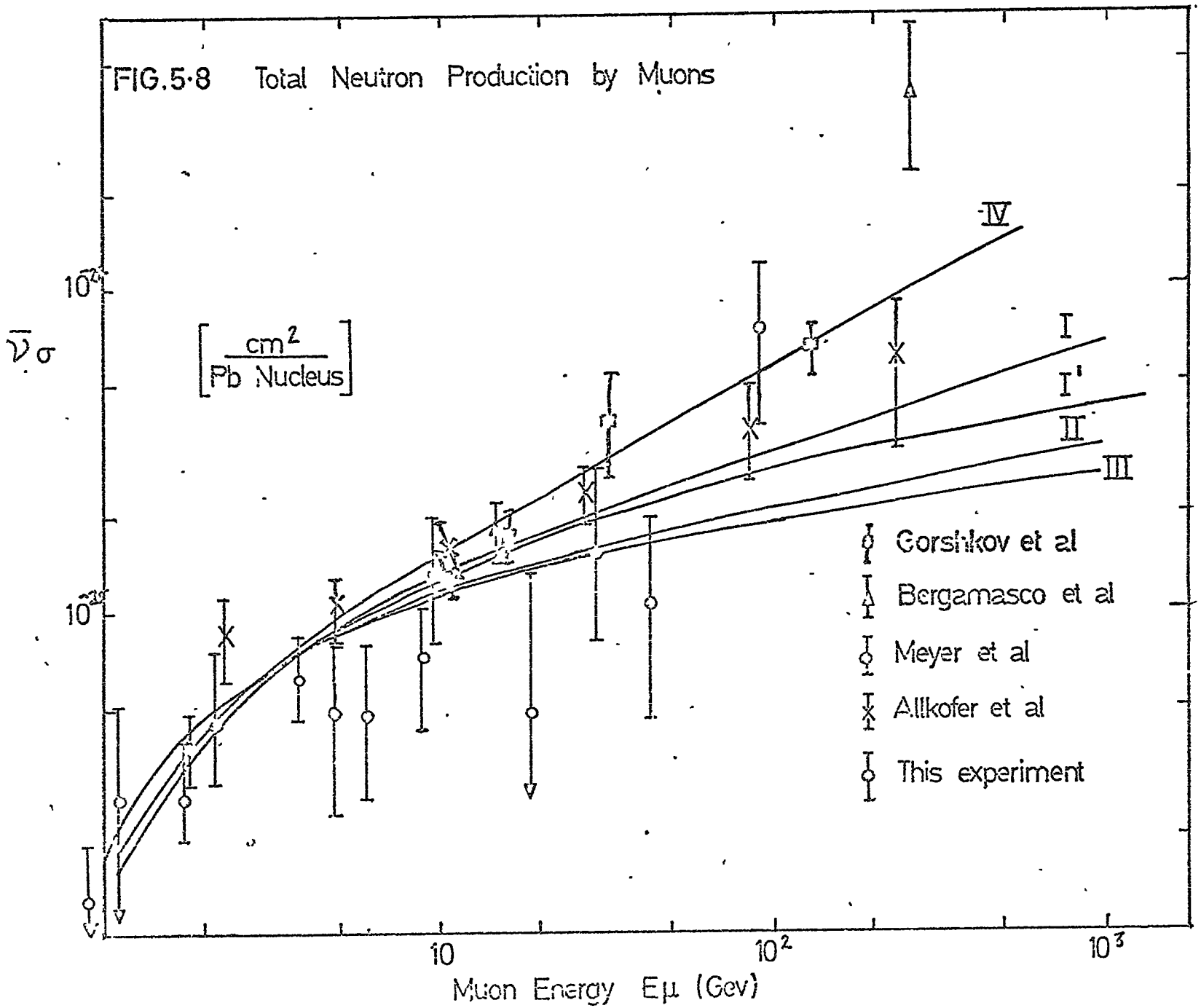
FIG.5·8 Total Neutron Production by Muons
$\bar{\nu}\sigma$
$\left[\frac{cm^2}{Pb\ Nucleus}\right]$
10^{-24}
10^{-25}
IV
I
I'
II
III
Gorshkov et al
Bergamasco et al
Meyer et al
Allkofer et al
This experiment
10
10^2
10^3
Muon Energy Eμ (Gev)

due to the subtraction of accidental neutrons. In spite of these large statistical uncertainties in $\bar{\nu}\sigma$, it would be difficult to reconcile the results of Allkofer et al.'s experiment with those of others if there was a systematic increase in $\bar{\nu}\sigma$ of 30% as a result of a lower neutron detection efficiency for the SIGY. However, it should be remembered that no direct measurement of this monitor's efficiency has been made and so a certain amount of doubt exists about it.

It might be expected that all these values should be slightly higher than the theoretical curves because the theoretical curves are based on a vanishingly small producer thickness and where the contribution to $\bar{\nu}$ from the extra-nuclear cascade which develops, in general, in a finite producer-thickness, is negligible. Further, $\bar{\nu}$ should increase with the producer thickness and this is confirmed by the results in table 5.2 which show that $\bar{\nu}$ for the DIGY (t = 270 g cm^{-2}) is about twice that for the SIGY (t = 150 g cm^{-2}).

This result is in contrast to that obtained by Bergamasco et al. using an even thicker producer (t = 390 g cm^{-2}), but the statistical errors are very large. Although some increase in $\bar{\nu}$ would be expected as the producer thickness increases, the increase measured in this experiment, relative to the results of Allkofer et al., is rather larger than expected from the comparison of neutron production by NAPs in the LIGY and DIGY monitors (see fig. 4.5). This suggests that either some events have been mis-classified in the present experiment or the difference is a statistical fluctuation. The probability of the latter possibility is estimated to be about 20%

The problem lies in the multiplicity distributions of the two experiments; either the present experiment has too few low multiplicity events or that of Allkofer et al. has too many high multiplicity events. Neither alternative is easy to understand and it is not possible to

compare meaningfully the two multiplicity distributions because of their large statistical errors. In particular, though, the discrepency cannot be explained in terms of production of neutrons by NAPs in the present experiment because this would increase relatively the higher multiplicities. Consequently if the average neutron multiplicity increases with thickness by as much as is suggested by the present experiment, it would be difficult to reconcile the results for $\bar{\nu}\sigma^-$ of the present experiment with those of the shielded and underground experiments, which are generally higher.

It can be seen in fig. 5.8 that $\bar{\nu}\sigma^-$ for the two unshielded experiments (this experiment and that of Meyer et al.) is generally lower than for the shielded ones. The unshielded experiments differ from the others in their use of only negative muons. In Allkofer et al.'s experiment positive muons account for about 50% more produced neutrons than the negative muons, compared with 30% which would be expected assuming a charge ratio of 1.3 and identical cross sections. Although it has been suggested (e.g. Osborne et al., 1973) that an anisotropy exists between the electro-magnetic interactions of positive and negative muons, the data summarised here are of such limited statistical significance, to contribute little to this conclusion.

The presence of the high background count rate of the monitors in the two unshielded experiments presents a serious problem, causing a substantial number of "accidental" events and consequent statistical errors which are not present in the shielded experiment. Also, there is a significant probability in both experiments of classifying an NAP as an interacting muon.

It would be expected therefore that the experiment of Allkofer et al. is more reliable than the others, it s only major source of error being in the choice of efficiency which may have resulted in $\bar{\nu}\sigma^-$ being systematically underestimated by 30%. Although this would raise the experimental points

significantly above the calculated values, it might be expected that if an allowance was made for neutron production in the extra-nuclear cascade, the calculated values of $\bar{\nu}\sigma$ would increase slightly and so restore better agreement with this experiment.

At high muon energies another factor becomes important; the variation of neutron detection efficiency with muon energy. An attempt was made to allow for this by Bergamasco et al. but no allowance was made by Allkofer et al.. Using the values of $\langle\epsilon_{evap}\rangle$ and $\langle\epsilon_{flat}\rangle$ appropriate to the SIGY (using $\epsilon(E_n)$ given by Pearce and Fowler 1964) we get from equation 5.4, $\langle\epsilon\rangle \approx 0.027$ at $E_\mu \approx 250$ GeV

where $\langle\epsilon_{evap}\rangle = 0.031$

and $\langle\epsilon_{flat}\rangle = 0.005$

i.e. a decrease of about 10% from the efficiency at 1 GeV. An alternative estimate for this decrease can be made from fig. 2.12.

Assuming that the neutrons from a 250 GeV muon (which will produce about 50 neutrons on average) have a similar energy spectrum to a 5 GeV NAP (being that which will also produce about 50 neutrons) the decrease in efficiency from $E_\mu \approx 1$ GeV to 250 GeV should be about 10%. This agrees with the estimate made by Bergamasco.

If Allkofer et al.'s high energy values of $\bar{\nu}\sigma$ are corrected for this effect the general slope of their data would agree better with Bergamasco et al.'s predicted curve IV and better agreement would be obtained with the underground measurements.

5-6 Conclusions

At low energies all the experiments give values of $\bar{\nu}\sigma$ which agree generally with each other, within the statistical errors, although the results of Allkofer et al. may be systematically too low by a significant amount due to the overestimation of the neutron detection efficiency of the SIGY monitor.

However, close investigation of $\bar{\nu}$, the average number of neutrons produced per interaction, suggests larger differences between the experimental results of Allkofer et al. and the present work which should be manifested in $\bar{\nu}\sigma^-$ also. The present experiment using an intermediate thickness of lead producer is estimated to produce twice as many neutrons per interaction as either the thin or thick lead producer experiments of Allkofer et al. and Bergamasco et al. respectively, although the statistical errors are large. Since the increase is only significant at the 20% level, this result is rather inconclusive.

The values of $\bar{\nu}\sigma^-$ measured in the present work and the experiment of Meyer et al. are generally lower than the others. Although this could be because of a lower interaction cross-section for negative muons than for positive muons, the possibility of it s having arisen from an experimental bias cannot be ruled out given the large corrections necessary in these two experiments to remove the effect of neutrons produced by NAPs.

The results of Allkofer et al. appear to constitute the most reliable data on the variation of $\bar{\nu}\sigma^-$ with energy over the range 2 to 250 GeV, having smaller statistical errors and not needing the large corrections mentioned above. There is evidence that at lower energies these data would significantly overestimate $\bar{\nu}\sigma^-$ if the most probable value of neutron detection efficiency of the SIGY is used (which would increase $\bar{\nu}\sigma^-$ at all energies by about 30%) and so it is possible that a systematic error may cause $\bar{\nu}\sigma^-$ to be overestimated over the whole energy range. This is not consistent though with the high energy measurements underground which are significantly higher than those of Allkofer et al. although the Allkofer et al. values may be too low by about 10% due to the fall in neutron detection efficiency with muon energy. However, although there

is doubt about the absolute values of $\bar{\nu}\sigma$ measured by Allkofer et al., the increase with energy is reasonably consistent with the results of the other experiments at the low and high energy limits.

Compared with the theoretical prediction, the results of the present experiment for the variation of $\bar{\nu}\sigma$ in the low energy region where direct neutron production by knock-on electrons is dominant reinforce the general agreement of the other experimental results in this region.

It has been pointed out that if an allowance is made for the change in neutron detection efficiency in the experiment of Allkofer et al., their results for the variation of $\bar{\nu}\sigma$ towards higher energies could give better agreement with the theoretical prediction of Bergamasco et al..

CHAPTER SIX

THE USE OF A NEUTRON MONITOR IN EAS

6-1 Introduction

This work originates from the suggestion by Hughes and Marsden (1966) that the neutron multiplicity distribution measured with a monitor could give information about the energy spectra of the NAPs producing the neutrons. Hughes and Marsden demonstrated that the multiplicity distribution measured by the LIGY monitor when exposed to the sea level flux of cosmic rays, could be accounted for by making a realistic assumption about the (relatively unknown) sea level neutron energy spectrum. It was deduced that a unique relationship existed between the incident energy spectrum and the produced multiplicity distribution so that monitoring the changes in the multiplicity distribution would give information about the time variations of the sea level neutron spectra and, in turn, the primary spectrum. In particular, the changes in the primary spectrum above 15 GeV and up to 200 GeV would be reflected in measurable changes in the rate of high multiplicities.

Latitude surveys of neutron monitors, reviewed by Hatton (1971), have demonstrated that increases in the average multiplicity indeed occur as the average primary energy increases, but that the changes are rather small due to the fluctuations in the extra-nuclear cascades in the atmosphere (Kodama and Ohuchi, 1968) which cause changes in parts of the primary spectrum to have an affect over a wide range of multiplicities.

The results of Shen (1968) confirmed that the monitor, in principle, could be used to detect changes in the sea level NAP spectra at energies well above that encountered by Hughes and Marsden and that the sensitivity to changes in the shape of the spectra can

be increased by increasing the producer thickness.

A monitor has been designed specifically for monitoring the low energy primary spectrum using the multiplicity distribution (Nobles et al. 1967). The monitor, called the Lockheed multiplicity monitor, has a thickness of t = 2.5 inelastic interaction lengths, or more than three times that of the SIGY or NM64. The efficiency was very high on account of the large number of BF_3 counters employed and the use of bismuth and reactor-grade graphite for producer and moderator respectively, both of which have relatively low thermal neutron capture cross-sections. The effective area presented to the cosmic ray flux was very small ($\sim 0.3\ m^2$ compared with $\sim 7m^2$ for the NM64) and so the sea level counting rate was also considerably low, and the usefulness in time variations studies has been rather limited. However, substantial changes in the multiplicity distribution during short term variations in the primary spectrum have been recorded, and changes in the slope of the spectrum have been estimated by Nobles et al. (1969).

As pointed out by Shen, this extension in the use of neutron monitors is limited in the cosmic ray beam by the sharply falling NAP energy spectrum, and the poor energy resolution associated with the broad exponential distribution of the produced neutrons and slow increase of average produced multiplicity with energy. However in EAS the NAP energy spectrum has a lower value of slope compared with that found in time variations studies, and therefore the lack of energy resolution should not constitute such a limitation. In EAS however, neutron monitors have almost entirely been used for NAP detection only, e.g. Danilova (1964); Chatterjee et al. (1963).

Exceptions to this are Hughes and Marsden (1966) who operated a standard IGY monitor in conjunction with a shower selection device and measured the average neutron multiplicity $\bar{m}$ for various ranges

of density of shower particles. They found that $\bar{m}$ remained roughly constant over the range of density 5 to 50 particles per square meter.

More recently, three NM64 monitors have been used by Böhm et al. (1970) and van Staa et al. (1973) to measure multiplicities recorded in EAS of size 10^4 to 5.10^6 particles and at core distances between 2 and 100m. Due to the large sensitive area of their neutron monitors, they were not able to identify the multiplicity produced by each NAP but they were able to roughly predict the variation of mean NAP energy with core distance, which decreased monotonically (with the average multiplicity) for increasing core distance.

A measurement in EAS of the multiplicity distribution has been made by Hook et al. (1970) using a monitor very similar to the one used in the present experiment. The shape was shown to agree with that expected for the shape of an NAP energy spectrum given by Greisen (1960) for a core distance of $r \approx 5$m. However it would appear that the agreement is rather fortuitous because the calculation used the neutron production multiplicities given by Shen which are almost certainly overestimates (see chapter 4).

In the work of Hook et al. a spectrograph situated over the monitor was used to simultaneously record, visually, the particle density. It was found that the average multiplicity was constant at about 2.2 over a wide range of particle densities, in agreement with Hughes and Marsden but that at the highest density measurement ($\sim$ 150 particle per m^2) near the shower core, the average multiplicity increased to 4. This was interpreted as being possibly due to the hard spectrum of NAPs in the core region. However, according to Böhm et al. the electron-photon component will make a significant contribution to the neutron yield, especially in the core region. Also, the high probability of recording

more than one NAP in the same EAS is a problem in using the multiplicity distribution for derivation of energy spectra.

In this chapter, the monitor response in large EAS is considered using the results of computer simulations of the EAS development to give fairly realistic energy spectra of NAPs, muons and electrons incident on a monitor situated in an EAS array, so that the usefulness of monitors in this type of experiment can be assessed.

At the present time, agreement between model calculations of the development of EAS and experimental data is based on important assumptions about the nature of ultra-high energy interactions and of the primary radiation. Whilst it would be hoped that the response of a monitor in EAS will give information about this, it is not the direct concern of this work. Rather, the aim is to use the models to investigate the sensitivity of the monitor response to changes in certain important factors affecting the development of the shower, and the accuracy of measurements of this response. These factors are the primary mass and the depth in the atmosphere of the first interaction of primary particles, the latter of which is considered to be responsible for large fluctuations in the properties of showers initiated by protons.

Monitors with different values of producer thickness and neutron detection efficiency are considered in order to optimise the design of devices for use in EAS studies.

To estimate the statistical accuracy of the monitor response from the expected absolute frequency of "useful" showers within the range of a monitor, the shower collection characteristics of an actual array must be used. In the present work the array considered is that located at Haverah Park which is described by Tennent (1968).

6-2 The Derivation of the Monitor Response to NAPs in EAS

6-2.1 The Multiplicity Distribution

Shen (1968) has shown that the multiplicity distribution $M(m)$ of detected neutrons due to a flux of NAPs incident on a neutron monitor can be related to the energy spectrum of the NAPs by

$$M(m) = \sum_{\bar{E}_s} f(m,\bar{E}_s)\, N(\bar{E}_s)\, \Delta E_s \qquad 6.1$$

where $$f(m,\bar{E}_s) = A_\alpha(\bar{E}_s)\exp(-\alpha(\bar{E}_s)\, m) \qquad 6.2$$

is the probability of an NAP of average energy $\bar{E}_s$ giving a detected neutron multiplicity m;

and $$A_\alpha(\bar{E}_s) = \exp(\alpha(\bar{E}_s)) - 1 \qquad 6.3$$

is the normalization constant so that

$$\sum_{m=1}^{\infty} f(m,\bar{E}_s) = 1 \ ;$$

and $N(E_s)$ is the differential energy spectrum of NAPs.

$\bar{E}_s$ is defined as $\int_{\Delta E_s} E_s\, N(E_s)\, dE_s$ where

ΔE_s is broad enough so that $f(m,\bar{E}_s)$ is approximately an exponential function of m.

As pointed out by Shen, $f(m,\bar{E}_s)$ is not necessarily a single exponential due to the production of evaporation neutrons from many nuclei in the extra-nuclear cascade. However, Shen showed that the average $f(m,\bar{E}_s)$ in a range ΔE_s could be closely approximated to a double exponential and this has been confirmed by the results of the present work (chapter 4). For the purposes of this investigation, $f(m,\bar{E}_s)$ has been assumed to be a single exponential over similar energy ranges to those used in Chapter 4. The results of Chapter 4 also indicate that the average neutron multiplicity $\bar{m}$ for pions (probably the principle NAP component in large EAS) may be lower than that for protons (the

principle source of neutrons in the work described in Chapter 4). It has been assumed, following Shen, that the neutron production by pions is the same as that by protons.

The measured neutron multiplicity distribution resulting from a number of EAS incident on a neutron monitor will only correspond to the calculated distribution in equation 6.1 if the multiplicities of neutrons from each NAP can be separately identified. If, for example, the detected multiplicities arise from two NAPs, each characterised by a single exponential probability distribution of multiplicities, then the resulting distribution of multiplicities will be of the characteristic double exponential form described by equation 4.11. In general, if there are D simultaneously incident NAPs interacting in the neutron monitor, the probability of ν neutrons being produced is given by Böhm et al. (1970) as:-

$$I(\nu) = \prod_{i=1,D} e^{-a_i \nu_i} (1 - e^{-a_i}) \qquad 6.4$$

where $\sum_{i=1,D} \nu_i = \nu$

so that the measured multiplicity (m) distribution is

$$q(m;t) = \sum_{\nu=m}^{\infty} \binom{\nu}{m} (\epsilon f)^m (1-\epsilon f)^{\nu-m} \prod_{i=1,D} e^{-a_i \nu_i} (1-e^{-a_i}) \qquad 6.5$$

Clearly, this $I(\nu)$ function introduces severe complications in the predicting of the detected multiplicity distribution, and great care must therefore be taken when measuring the multiplicity distributions in EAS to -

(a) minimise the chance of more than one NAP interacting in the monitor simultaneously, and

(b) try to identify each extra-nuclear cascade by either an auxiliary apparatus or by individual hodoscoping of the

neutron detectors to resolve the spatial distribution of detected neutrons.

The probability of m neutrons being detected from one NAP in a monitor of thickness t and efficiency ϵf is

$$q(m;t,\epsilon f) = \sum_{\bar{E}_s > E_{th}} p(m;t,\epsilon f,\bar{E}_s)\ N(\bar{E}_s)\ i(t)\Delta E_s \qquad 6.6$$

where $i(t)$ is the probability of the NAP interacting in the thickness t of monitor $= (1 - e^{-t/\lambda})$ assuming t is less than the range of the NAP where λ is the inelastic interaction length;

$N(\bar{E}_s)\ \Delta E_s$ is the probability of the NAP having an energy in the range of width ΔE_s and mean $\bar{E}_s$

and $$\sum_{\bar{E}_s = 0}^{\infty} N(\bar{E}_s)\Delta E_s = 1$$

where E_{th} is the low energy threshold (i.e. the energy required to penetrate the reflector of the monitor);

and p is the probability of an NAP of energy $\bar{E}_s$ producing m detected neutrons, given by

$$p(m;t,\epsilon f,\bar{E}_s) = \left[1 - \exp(-a(t,\epsilon f,\bar{E}_s))\right] \exp\ (-a(t,\epsilon f,\bar{E}_s)\ m) \qquad 6.7$$

where $$\sum_{m=0}^{\infty} p = 1$$

and $$a = \log \left[\frac{1}{\bar{\nu}(\bar{E}_s)\epsilon f} + 1 \right]$$

Assuming a Poissonian distribution in the positions of the NAPs over the plane containing the monitor as assumed by Böhm et al., the limiting density D_m below which the probability of a monitor of area $A = 10m^2$ having two or more NAPs incident on it simultaneously is less than 1% or 10%, is given by

$$P(x>1) = 1 - \sum_{x=0,1} \frac{(D_m A)^x}{x!} \exp(-D_m A) = .01, .1 \qquad 6.8$$

whence $D_m \sim 10^{-2}$ and $5.10^{-2} m^{-2}$ respectively.

In the case of a $1m^2$ monitor (or a larger one with a spatial resolving power of $1m^2$), these limiting densities are

$$D_m \sim 10^{-1} \text{ and } 5.10^{-1}m^{-2} \text{ respectively.}$$

Thus for average NAP densities D less than D_m, the multiplicity distribution for N_s showers incident over the monitor of area A is given by

$$P(m;t,\epsilon f) = N_s.D.A.q\ (m;t,\epsilon f) \qquad 6.9$$

and this distribution will have an average multiplicity

$$\bar{m} = \frac{\sum_{m=1}^{\infty} P(m;t,\epsilon f)\ m}{\sum_{m=1}^{\infty} P(m;t,\epsilon f)} \qquad 6.10$$

6-2.2 The Neutron Yield Per Shower

For NAP densities above this limit D_m (e.g. near the core of the EAS) the monitor may still be usefully operated as an energy absorbing device. The only quantity of interest would be the average number of neutrons detected per shower; the actual shape of the multiplicity distribution being of little relevence in view of the uncertain form of the production spectrum (equation 6.4).

The average number of neutrons detected per incident NAP is

$$\langle m \rangle = \sum_{m=1}^{\infty} q(m;t,\epsilon f)\ m \qquad 6.11$$

and the average number of neutrons detected per shower by a monitor of area A is

$$n = \langle m \rangle\ D.A \qquad 6.12$$

where D is the number of NAPs per unit area with energy E_s above zero.

6-2.3 The Sensitivity of Response to the NAP Energy Spectrum

A neutron monitor has an NAP energy threshold of about 100 MeV (Hatton, 1971) and the approximate median energy of NAPs contributing to the counting rate in the cosmic ray beam at sea level is typically

150 MeV. A consequence of the sharply falling cosmic ray NAP spectrum at this energy and the relatively slow rise in $\bar{\nu}(E_s)$, (see fig. 2.6) is that the range of E_s contributing to the counting rate is small and so measurements of variations in the counting rate essentially give information on changes in the NAP spectrum at energies just above the threshold.

Following the suggestion that the multiplicity distribution of detected neutrons can give information at higher energies, the median energy $\hat{E}_s(m)$ of NAPs contributing to a detected multiplicity m in the LIGY has been calculated by Hughes and Marsden, and Hatton, for this spectrum. They showed that $\hat{E}_s(m)$ increased monotonically with m from 0.12 GeV for m = 1 to 3.5 GeV for m = 6. The upper limit of the energy range to which multiplicity measurements are sensitive is dependent on the statistical limitations of the higher multiplicities. In time variations studies for example, this limit is determined by the length of time of a given variation.

In studies of EAS, the median energy contributing to the detected evaporation neutrons is almost certain to be higher due to the higher average NAP energy found in a shower environment. For a given monitor, the upper energy limit will be determined by the frequency of detected showers, the density of NAPs in the showers and partly by the shape of the NAP energy spectrum.

In order to estimate the approximate sensitivity of the multiplicity distribution to changes in the shape of the NAP spectrum. Calculations have been made (Dixon et al., 1971) of the variation of $\bar{m}$ with the exponent γ_I of the integral NAP energy spectrum (given by $N(>E_s) = \text{const.}\ E_s^{-\gamma_I}$; $E_s > 1$ GeV), for a typical neutron monitor. The results are shown in fig. 6.1. It is seen that for these simplified spectra, the variation of the average measured multiplicity reflects the change in slope of the

FIG. 6·1

The dependence of $\bar{m}$ on slope of spectrum of incident particles.

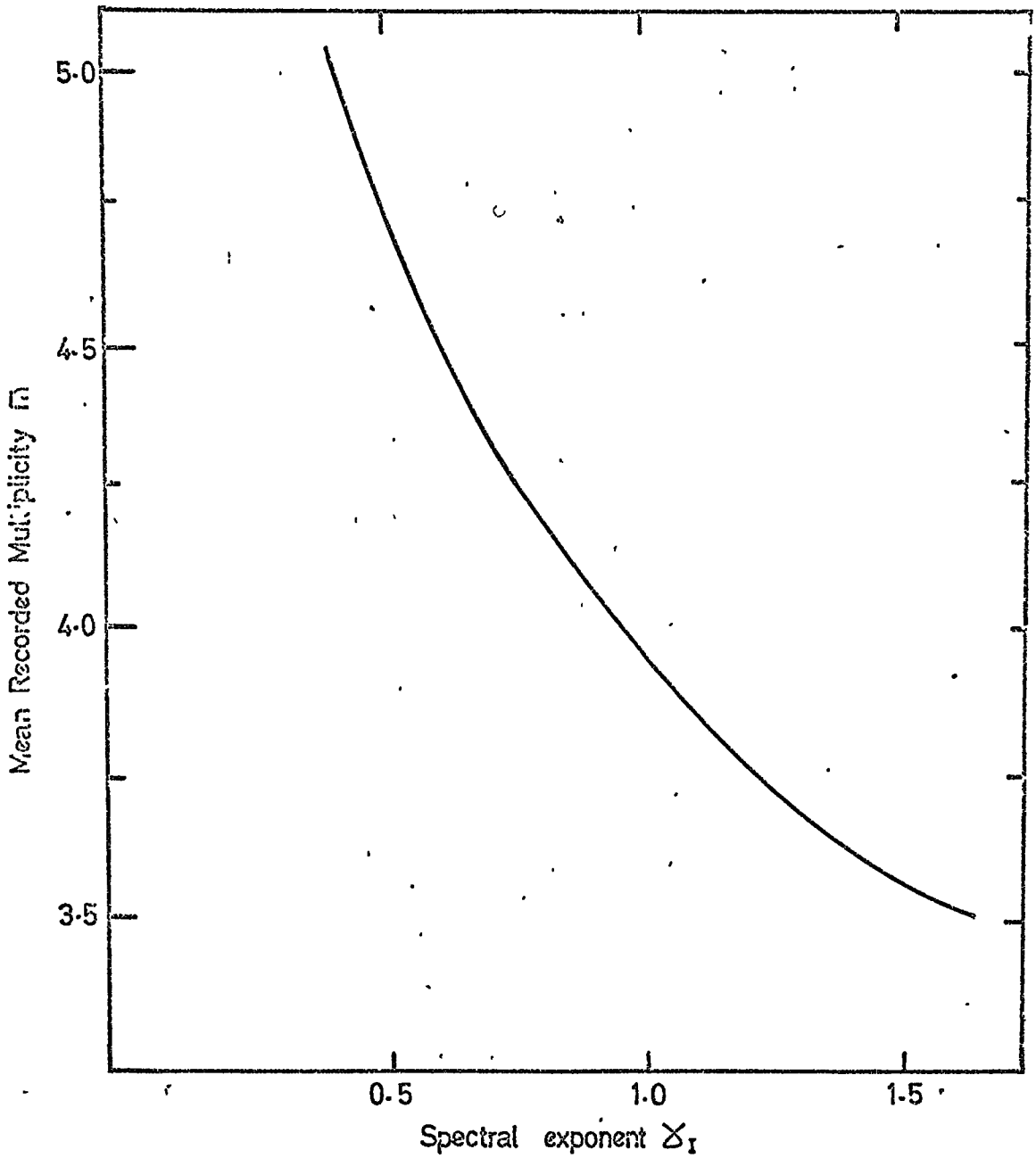

spectra to a marked degree.

To investigate the effects of fine structure in the spectrum, the multiplicity distributions have been calculated for the spectra shown in fig. 6.2. where the $N(>E_s)$ const. $E_s^{-1.0}$ spectrum has been perturbed in four places in turn (a-d). The five resulting multiplicity distributions are shown in fig. 6.3.

It can be seen that changes in the spectrum at low energies, a few GeV, are reflected in the multiplicity distribution over a wide range of multiplicities and the changes at higher energies have far less effect. This is due to the relatively large contribution to all multiplicities from the low energy part of the spectrum.

As a result it is possible that the multiplicity distribution could only be used to measure the slope of the energy spectrum in the range 1-10 GeV; studies at higher energies requiring statistical samples which are orders of magnitude larger in size.

It should be remembered that this spectrum represents a very unrealistic contribution from charged NAPs with energy around 1 GeV. In reality the spectrum flattens off at low energies due to ionization losses, and this will increase the sensitivity of the multiplicity distribution to the spectral shape at higher energies. The effect of this and the statistical limitations will be dealt with later on when more realistic spectra are considered.

6-3 NAPs in EAS Initiated by Primaries of Energy 10^{17}eV

6-3.1 Introduction

The EAS model calculations used in this work (Dixon et al.1973) cover a wide range of primary particle energy $E_I(10^{14}$-10^{17}eV) and atomic mass number and predict the numbers and energies of electrons, muons, nucleons and pions arriving at sea level at various distances from the core of the shower.

FIG. 6·2

THE PERTURBATIONS IN THE NAP ENERGY SPECTRUM

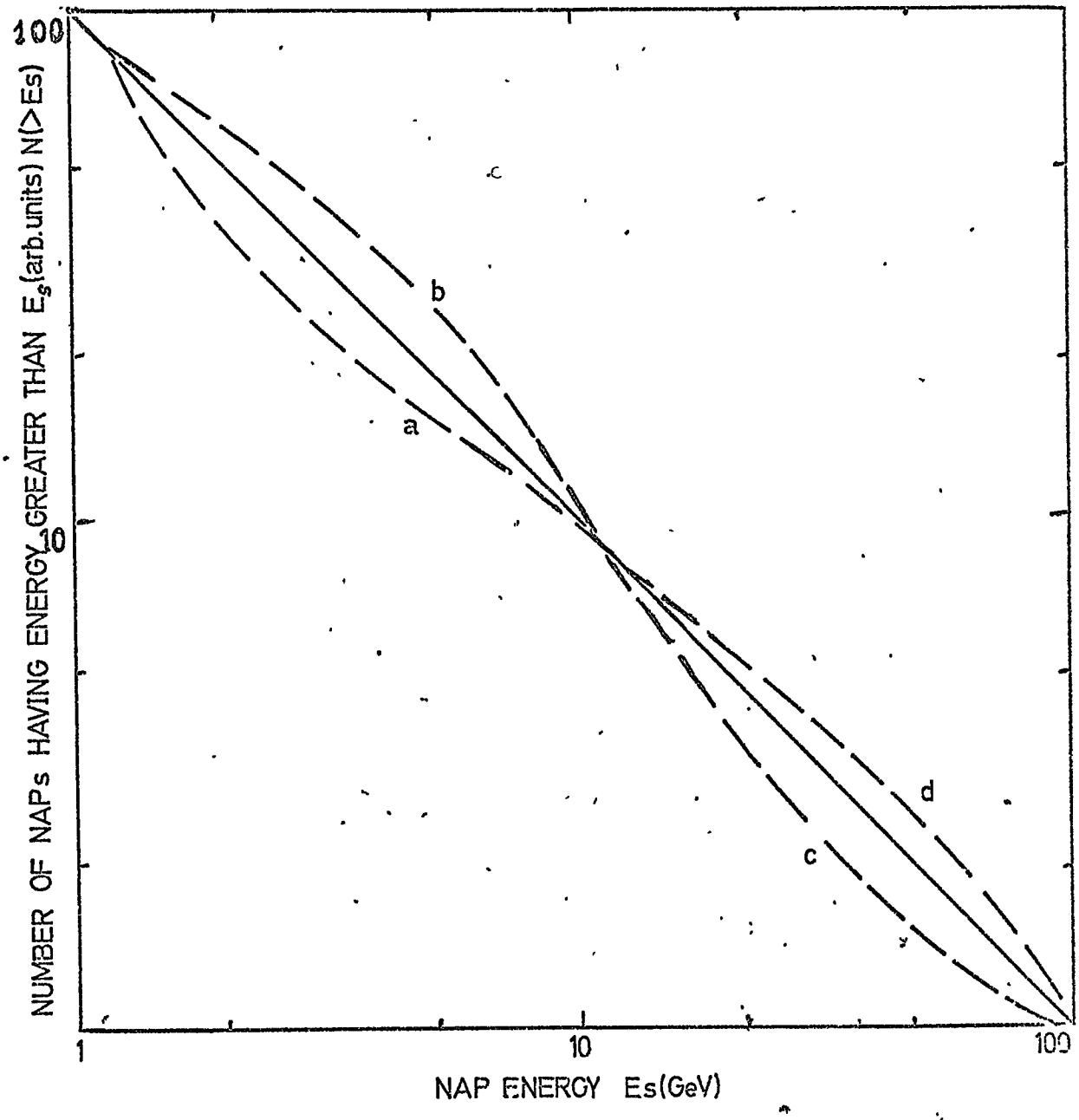

FIG. 6·3

THE NEUTRON MULTIPLICITY DISTRIBUTION DUE TO PERTURBED ENERGY N.A.P. SPECTRA.

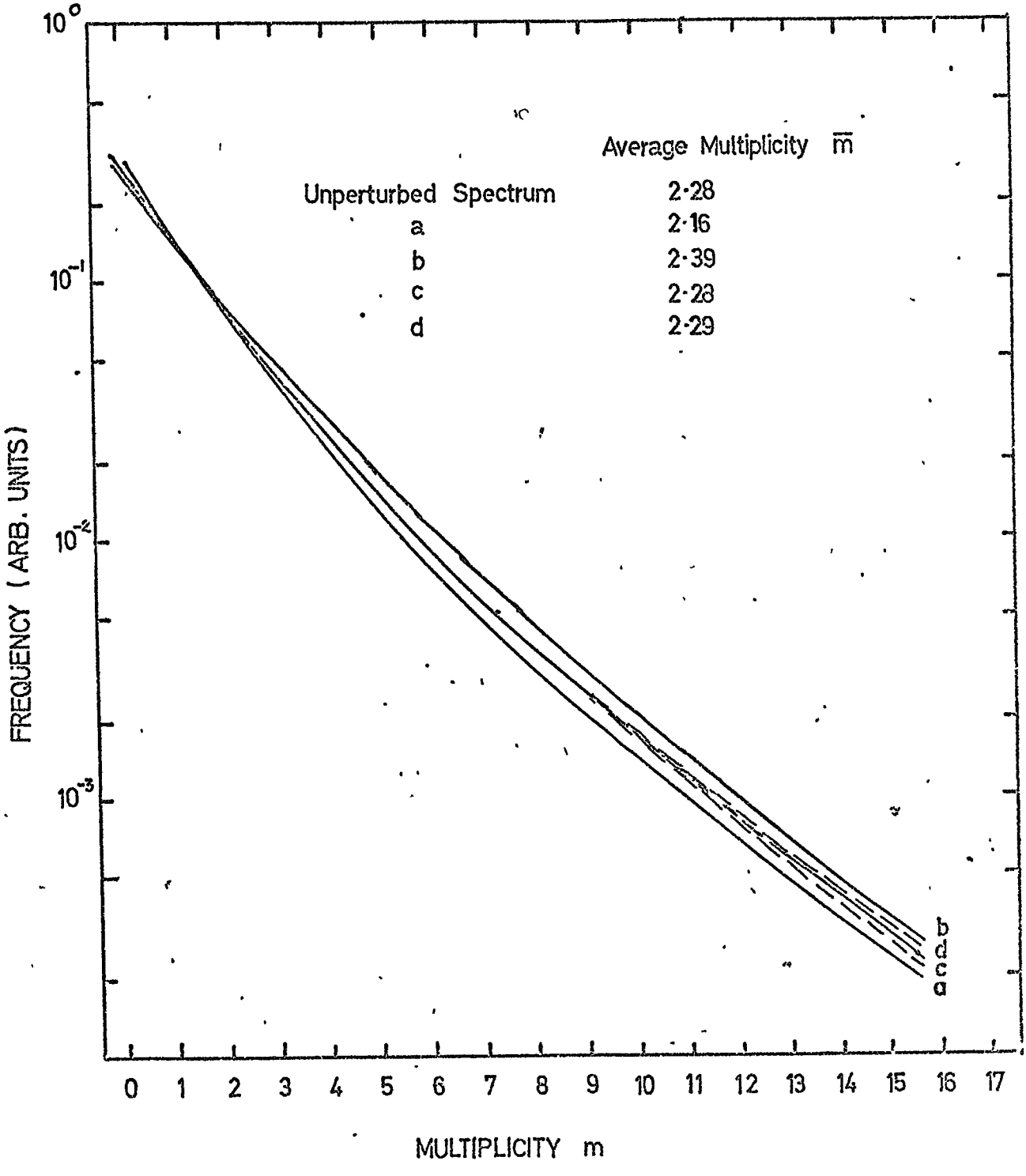

Since all these components of EAS can contribute to the production of neutrons in a monitor, these calculations can be used to estimate the relative yield of neutrons from each component. The results of Dixon et al. (1973) and some measurements by Kellerman and Towers (1970) of photons in showers of high energy have been used to estimate the average number of neutrons produced in a monitor. The monitor has been assumed to be one interaction length thick (200g cm^{-2} of lead) with an area of $10m^2$ and a neutron detection efficiency of 0.03. The calculation of the number of produced neutrons is based on equation 6.12. The data for neutron production by NAPs and muons were obtained from the present work, whilst those for neutrons produced by electrons and photons was estimated by assuming, after Böhm et al. that the neutron yield is proportional to the energy flow of the electron-photon component, normalised to the accelerator result of Bathow et al. (1966).

In agreement with Böhm et al. these results indicated that the electron-photon component is responsible for a very considerable proportion of the neutrons produced and also that stopping negative muons and fast interacting muons give significant contributions at the larger distances from the core. The absolute number of neutrons produced by NAPs is encouragingly high near the core but falls off rapidly at the larger distances. It would appear from this rough estimation that NAP studies will be seriously hampered by the presence of the electron-photon component (and perhaps the muon component as well) unless special precautions are taken to minimise these effects (by the use of an absorbing layer above the monitor, for example). The effect of this contamination and the means by which it may be minimised will be considered in more detail later on in conjunction with a study of the design of a neutron monitor for EAS studies.

The average energy spectra of pions calculated by Dixon et al. and shown in figs. 6.4,5 and 6 (curve A) for various distances from the core of a vertical shower initiated by a 10^{17}eV proton, show that both the average energy of the spectrum and the number of pions increases as R decreases. Following the results shown in fig. 6.1 it would be expected that this would be reflected in a neutron multiplicity distribution of higher average $(\bar{m})$.

The probability of detecting a multiplicity m from a pion of energy $\bar{E}_s$

$$q_{\bar{E}_s}(m;t,\varepsilon f) = p(m;t,\varepsilon f, \bar{E}_s)\, N(\bar{E}_s)\, i\,(t)$$

in a typical monitor is indicated in fig. 6.7 for the two spectra (A) given in figs. 6.4 and 6.6. It appears that the majority of the neutrons are produced by pions in a relatively narrow energy range centred on about 10 GeV, and that pions with energies below 1 GeV do not strongly contribute to the multiplicity distribution. This has been regarded as justification for neglecting them in this work.

The median energy for a detected multiplicity m at 50m increases from 6 GeV when m = 1, through 14 GeV when m = 10, 23 GeV when $m \approx 20$, to 50 GeV when $m \tilde{\sim} 30$. The statistical accuracy of multiplicity measurements decreases as the multiplicity increases and eventually sets an upper limit on the energy range. This limit is determined by the frequency of showers that are recorded over a given lnegth of time, and in order to assess the usefulness of the monitor in this context, it is important to estimate the absolute frequency of NAPs incident on a monitor giving rise to recorded neutrons in conjunction with a signal indicating the detection of a shower by a large EAS array.

It is apparent from figs. 6.4,5 and 6 that the lateral distribution of pions in the shower falls sharply with radial distance R. In view of the large areas over which these showers are detected, and the severe

FIG. 6.4

INTEGRAL PION SPECTRUM AT 50m FROM THE CORE OF A 10^{17}eV SHOWER AT SEA LEVEL

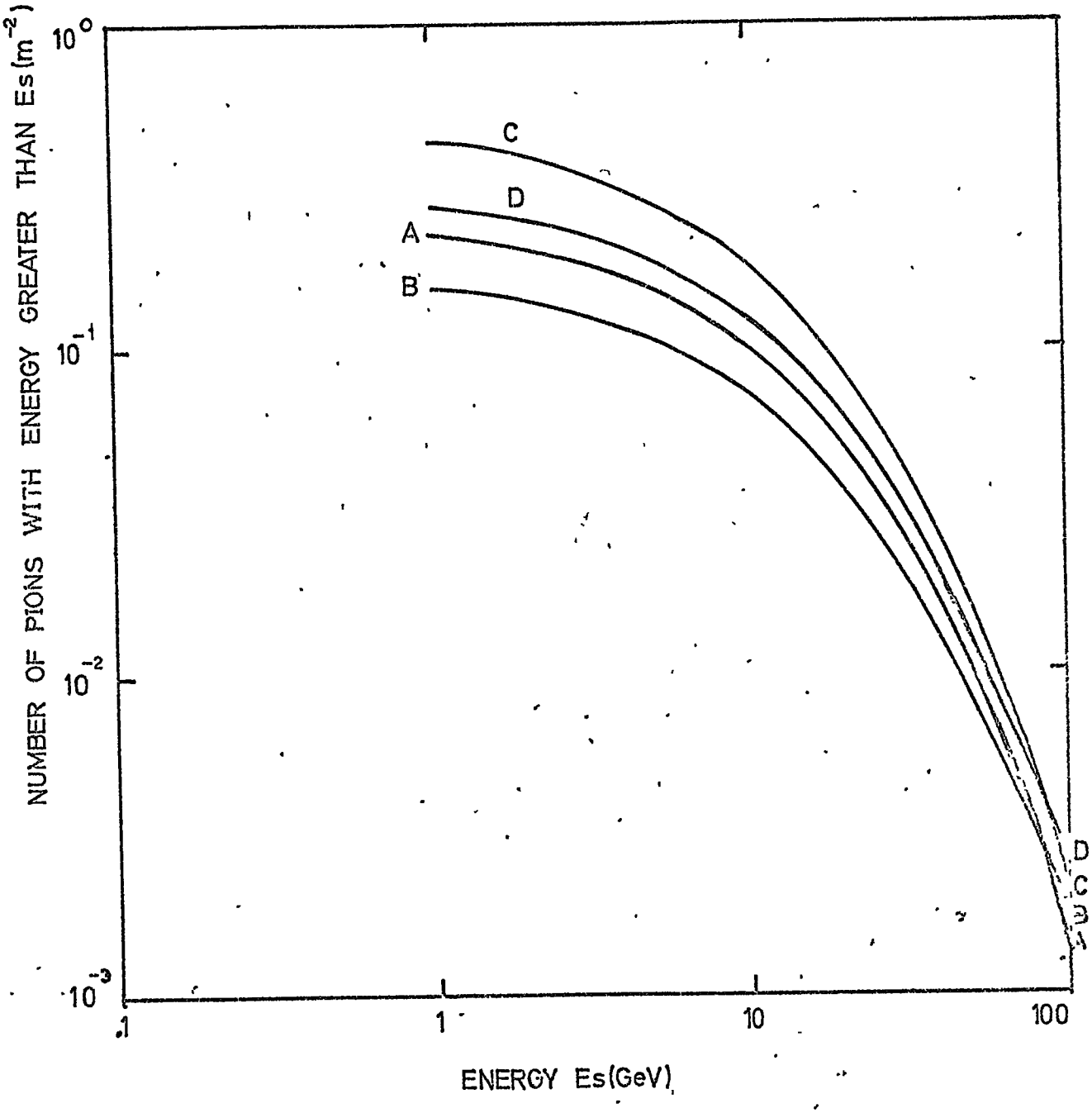

FIG. 6.5

INTEGRAL PION SPECTRUM AT 100m FROM THE CORE OF A 10^{17}eV SHOWER AT SEA LEVEL

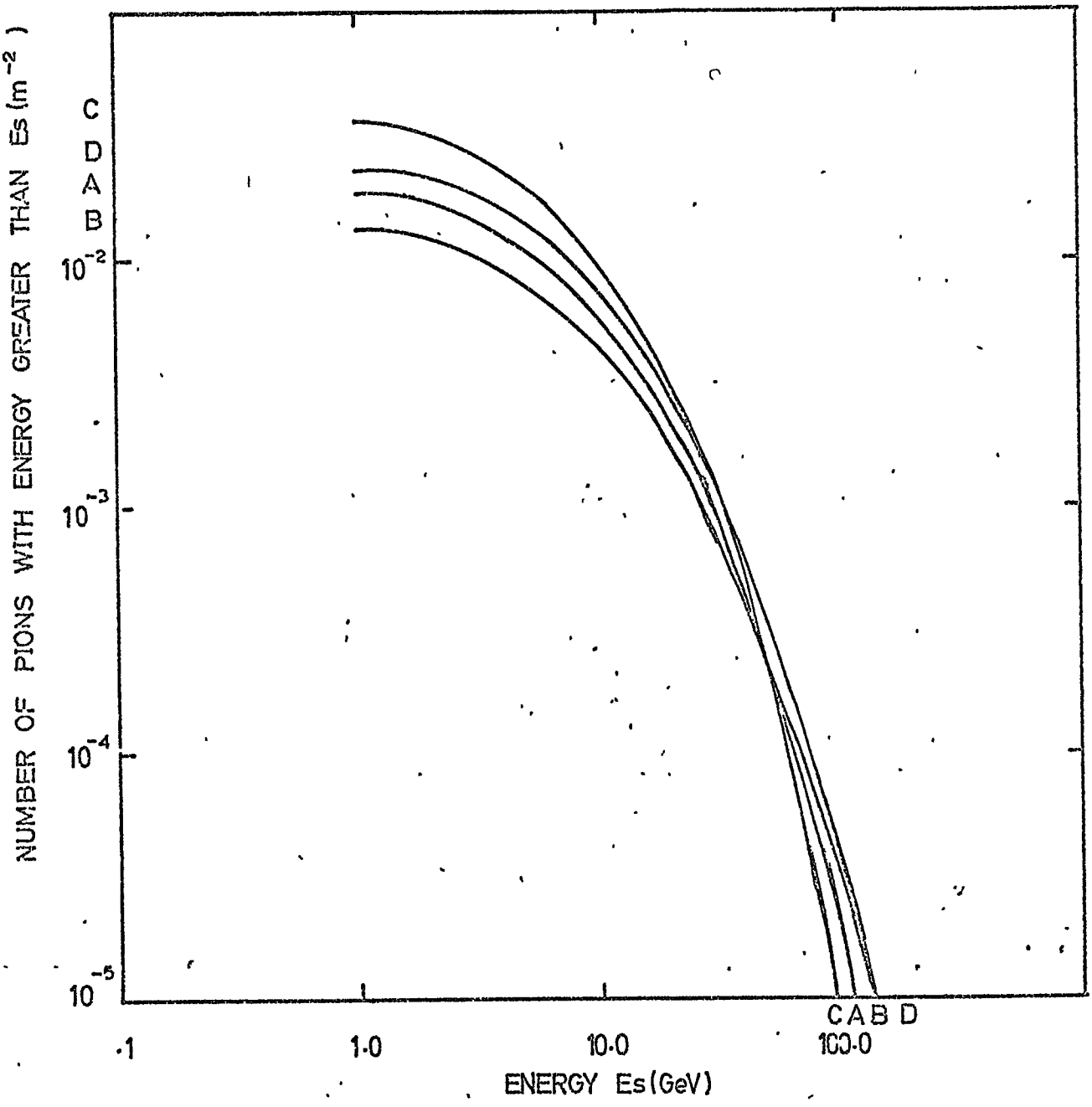

Fig.6.6

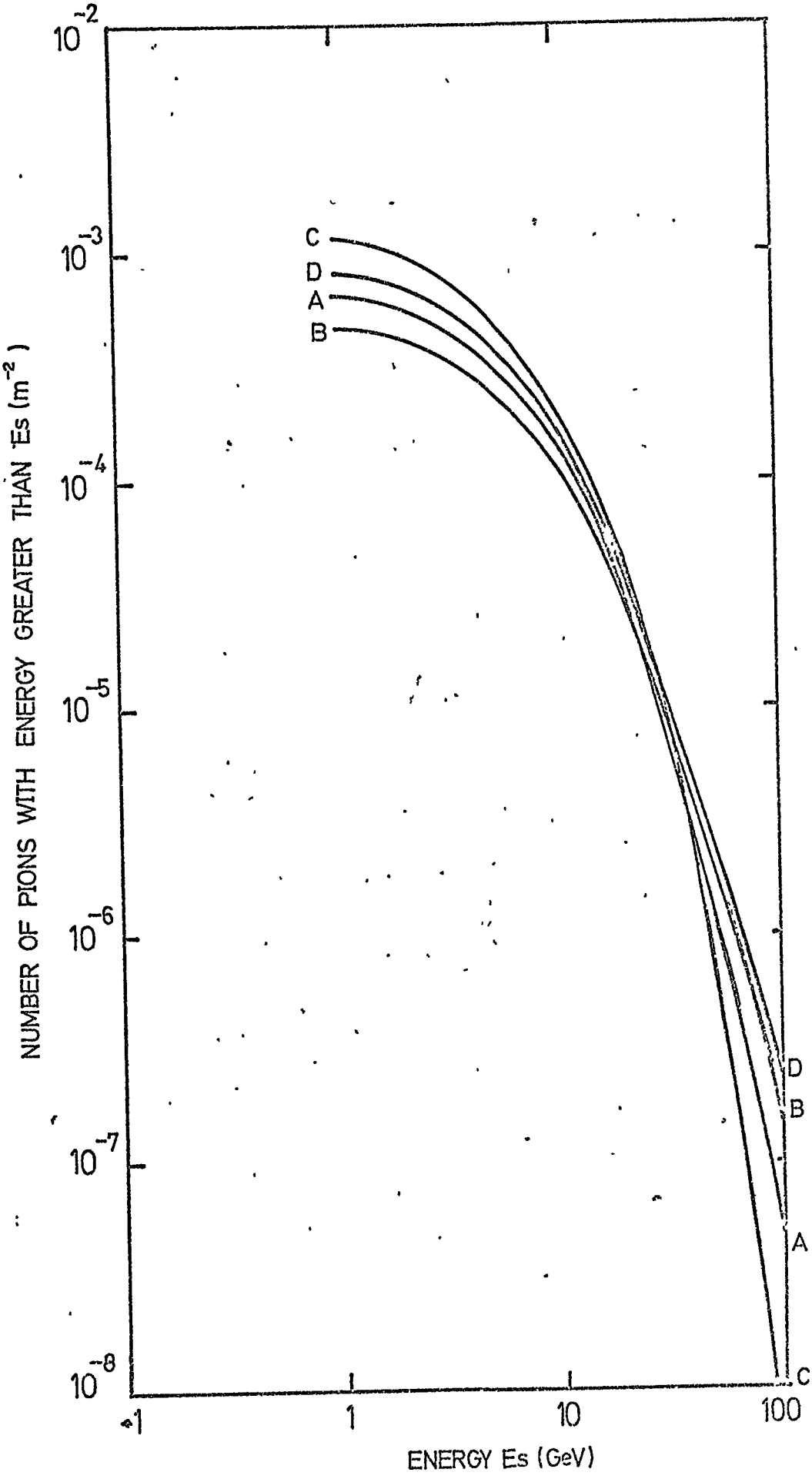
INTEGRAL PION SPECTRUM at 200m FROM
THE CORE OF A 10^{17} eV SHOWER at SEA LEVEL
NUMBER OF PIONS WITH ENERGY GREATER THAN Es (m^{-2})
10^{-2}
10^{-3}
10^{-4}
10^{-5}
10^{-6}
10^{-7}
10^{-8}
C
D
A
B
D
B
A
C
1
1
10
100
ENERGY Es (GeV)

FIG.6-7

PROBABILITY OF A DETECTED MULTIPLICITY m BEING DUE TO NAP OF ENERGY $\overline{Es}$

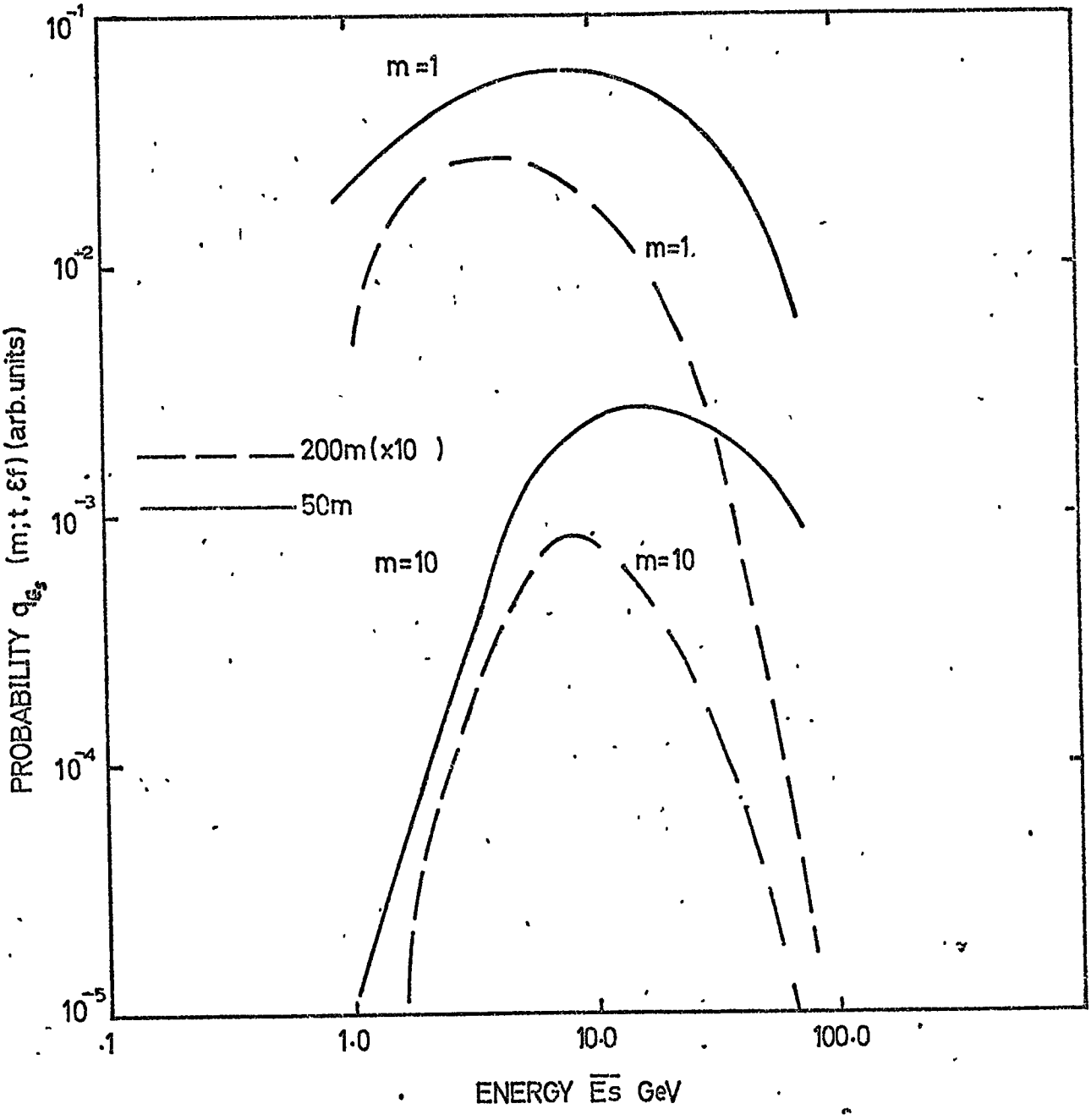

statistical limitations of studies of large EAS, it is important to establish the range of R, if any, which will give a large enough yield of neutrons to justify the use of a monitor. Studies at large R will be limited by the low flux of pions whilst those at small R will be limited by the small rate of showers. Since the useful, intermediate range depends on the frequency and distribution of detected showers across the detection array, it will be necessary to specify the geometry of the array. In the next section the possibilities of using a monitor in the Haverah Park array will be considered in more detail.

6-3.2 The Haverah Park EAS Array

Four deep water cerenkov detectors of area $34m^2$ provide the basic means of detecting showers initiated by primary particles of energy of about 10^{17}eV. The array trigger requirement is a coincidence between the detector located at the centre of an equilateral triangle plus at least any two of the other detectors located 500m away at the apexes of the triangle. Other tanks provide additional information about the particle densities and assist in the accurate location of the core of the shower and estimation of the primary particle energy. A detailed description of this array and the mode of shower analysis has been given by Tennent (1968).

The probability P(R) of a detected analysable shower having energy greater than about 10^{17}eV falling in a range of R has been estimated from Machin (1972) using a geographical plot of the core locations of a large number of showers recorded over a number of years at Haverah Park. Since the rate of these showers is about three per day the number of useful showers falling within a range of distance R from the monitor per year can be simply calculated. The number of detected neutrons per year due to pions ($>$ 1 GeV) incident on the typical $10m^2$ monitor, from showers falling within this range has been estimated and the results shown in table 6.1.

Table 6.1

The Neutron Yield due to Pions at Various radial distances at Haverah Park

Radial Distance Range R meters	Probability of Incidence of a Shower	Neutron Yield by pions per year
< 50	0.05	$\gtrsim 150$
50 - 150	0.14	35
150 - 250	0.10	1
250 - 350	0.10	10^{-1}
350 - 450	0.12	10^{-2}
450 - 550	0.16	-
550 - 1000	0.33	-

The upper limit of R can be seen to be around 100m. The lower limit of R for useful measurements will be determined by the error in core location in thearea in which the monitor is situated, and has been taken here as 50m. (Although the present core location accuracy is ±25m, future improvements may reduce this to ± 5m).

6-3.3 The Energy Spectra of NAPs - Model Calculations

In investigating the neutron monitor response to EAS, substantial use has been made of the EAS simulations of Dixon et al.(1973). A full description of this model is given in recent papers (Dixon et al.(1973), Dixon, Waddington and Turver (1973) and Dixon and Turver (1973)).

The model basically consists of two parts. The first deals with the primary particle interactions and the creation of all the pions in nuclear induced interactions using the Monte Carlo method, whilst the second takes the resulting matrix of pion energies and heights of production in the atmosphere and follows the development of the resulting pion, electron and muon components, down to sea level by a step by step procedure allowing for ionization losses. The predictions of this model include the general 3-D characteristics of the pions greater than 1 GeV at sea level. In view of the limited range in radial distance R that will yield useful results from neutron monitor studies, results of the EAS simulations will only be given here for three values of R at 50m, 100m and 200m.

No allowance has been made in the model for nucleon/anti-nucleon production in a high energy interaction. Such nucleon/anti-nucleon production could account for up to 30% of the energy available for particle production (Grieder, 1970). The effect of this important modification will be considered later.

6-3.4 The General Characteristics of the Simulated Showers

In the absence of nucleon/anti-nucleon production, and with the assumption that all secondary particles produced in nuclear interactions

are pions all but A of the NAPs in each shower are pions. Thus, it is assumed that any neutrons produced in nuclear interactions in the atmosphere give a negligible contribution to the NAPs at sea level. Since neutrons are primarily responsible for the "background" count rate of neutron monitors, this is an important assumption to make and consitutes perhaps the greatest limitation to the application of the simulation data to the present work.

A comparison of results for the average showers produced by primary particles of two masses and an energy $E_I = 10^{17}$eV is shown in figs. 6.4,5 and 6 (curves A and D). It is seen that the pion spectra from the heavy incident nucleus (for which A = 56) have almost exactly the same shapes as those from protons, although the absolute numbers of pions are slightly higher.

The showers have been chosen from a large sample to reflect the average development to be expected. It is well known that the form of the proton-induced shower at sea level is particularly sensitive to the depth of maximum cascade development which in turn reflects fluctuations in the depth of first interaction. Also shown (curves B and C) are the spectra resulting from two substantial fluctuations in this depth. The actual values of the depth (measured in g cm^{-2} from the top of the atmosphere) and corresponding depths t at shower maximum (the depth at which the number of particles in the shower, mainly electrons, reaches its maximum during the atmospheric development) are given in Table 6.2. Since about 10% of the showers interact within 10 g cm^{-2} and the same greater than 200 g cm^{-2}, the relative frequency of showers B or C relative to the average is approximately 0.1.

It can be seen that the absolute number of pions greater than

Table 6.2

The Fluctuations of the Proton Induced Showers

Shower Type	Depth of First interaction $g\ cm^{-2}$	Depth of Shower maximum $g\ cm^{-2}$
A	98	700
B	13.5	600
C	270	850

1 GeV fluctuates by a factor of about 100% at all radial distances.

The late developing shower (curve C) is characterised by a relatively large number of pions at low energy and a somewhat low number at high energy. The opposite is the case for the early developing shower (curve B).

6-3.5 Comparison with Experimental Measurements and other Calculations

In view of the many uncertainties in any model of the development of EAS, it is important to determine to what extent the predictions represent accurately the real showers.

The total pion energy spectrum for shower A (approximately normalised to a 10^{16}eV shower) is compared in fig. 6.8 with some measurements of NAP spectra above 10 GeV compiled by Tanahashi (1970) and a low energy measurement of Chatterjee et al. (1963). It is seen that above 10 GeV although the shape is in reasonable agreement, the predicted absolute intensity is too high by a factor of five. However there is very good agreement with the low energy point.

Included in fig. 6.8 are some results of a model of Grieder (1970) which includes some anti-nucleon production and gave the best overall fit to the available experimental data. These overestimate the NAP intensity even more, although the shape is in good agreement. Other results of this model indicate that the anti-nucleon production process causes an increase in numbers of NAPs so the NAP intensities predicted by Dixon et al. would not be expected to fall when an allowance for anti-nucleon production is included. It would also seem that although the fraction of nucleons in the NAP component increases dramatically with anti-nucleon production, the shape of the NAP energy spectrum above 10 GeV would not necessarily be altered greatly.

The steeper slope of the combined experimental data between 1 and 10 GeV implies a larger contribution from NAPs with energy below 1 GeV

FIG. 6.8

TOTAL INTEGRAL NAP SPECTRUM OF A 10^{16} eV SHOWER AT SEA LEVEL

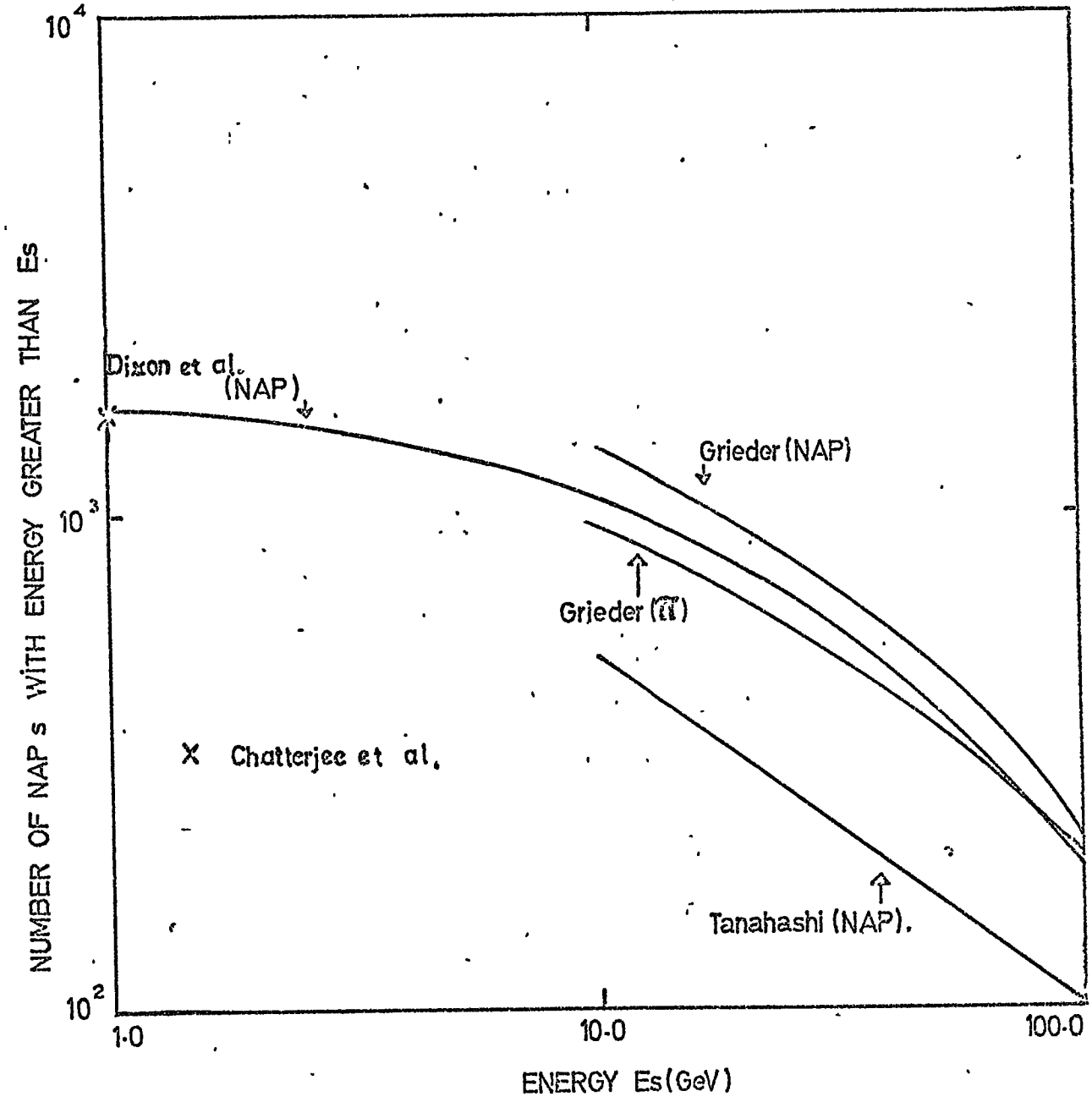

than predicted by the model.

In fact the experiment of Chatterjee et al. used neutron monitor type devices which would have had an energy threshold of about 100 MeV, so it is possible that the mean NAP energy has been overestimated. In this case the measured slope would give better agreement but extend to lower NAP energies, whilst the absolute intensity at 1 GeV would be lower than that predicted by the model.

The difference in slope could be qualitatively understood in terms of a neutral component of NAPs (neutrons) produced either by nucleon/anti-nucleon pair production or by inelastic pion-air nuclei interactions in the form of intra-nuclear cascade products. This component could give an important contribution to the NAPs in the low energy region where ionization losses of charged particles play an important role.

The multiplicity distributions detected by three NM64 monitors of total area 21 m^2 in showers of typical size 10^5 particles have been used to derive the lateral distribution and lateral energy distribution of NAPs and the relationship between the total number of NAPs and shower size (Böhm et al. 1970). Their measured lateral distribution (a relationship not strongly dependent on model parameters) for showers of size 10^5 particles is compared with Dixon et al.'s calculations for 10^{15}eV showers in fig. 6.9. It seems that at this lower energy the predicted absolute number of particles is underestimated although the shape of the lateral distribution for radial distances $R > 10m$, is in good agreement.

However, Böhm et al cohsidered their measurements to be over-estimates of the NAP intensity on account of neutron production by the electron-photon component. Their measurement may also have a contribution from NAPs less than 1 GeV.

FIG. 6-9

THE LATERAL DISTRIBUTION OF NAP s IN A SHOWER (SIZE = 10^5 PARTICLES)

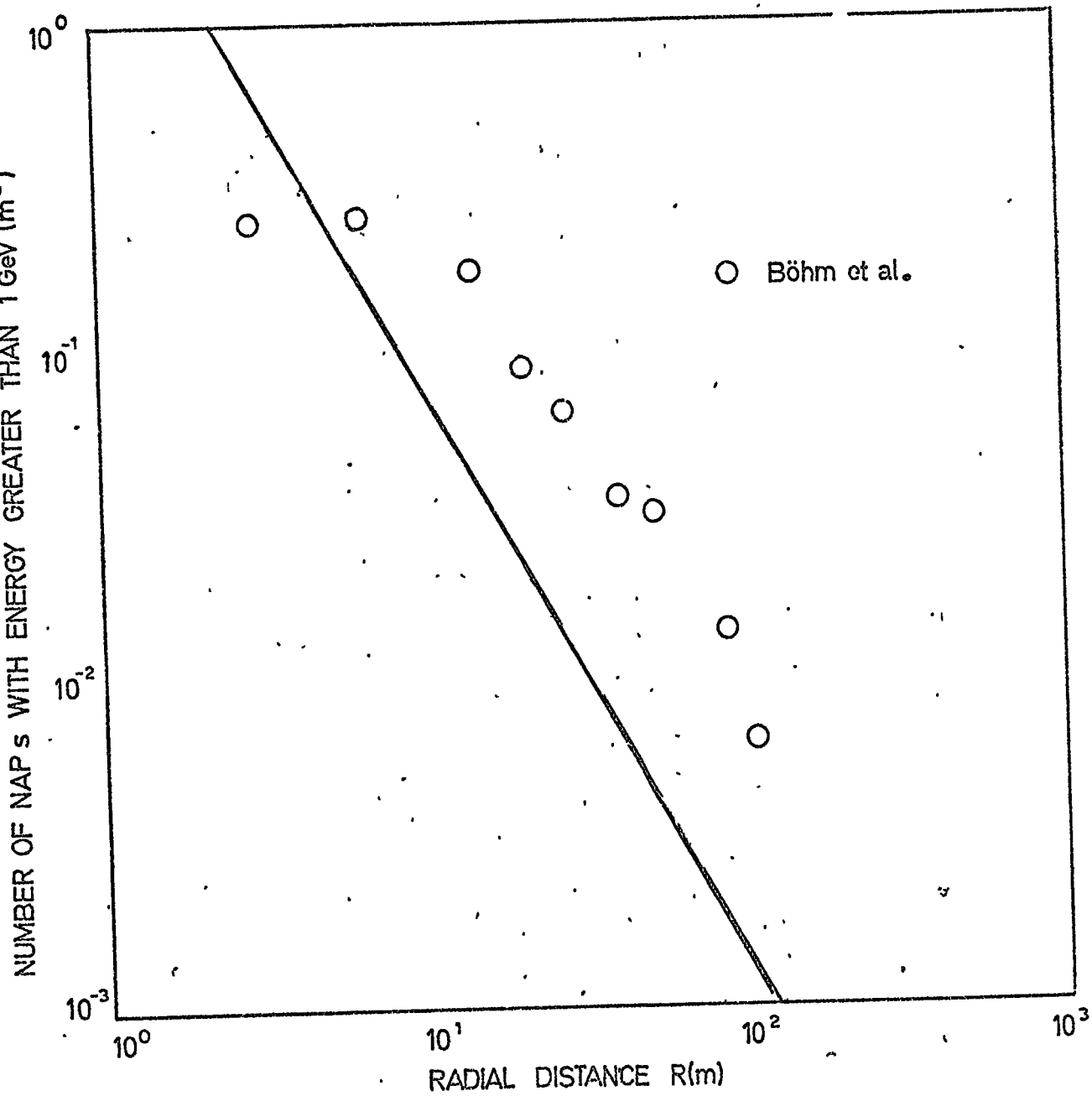

Further, as pointed out by Hook (1972) there are difficulties in comparing measurements of showers (of a given average size) with predictions (for the energy of primary particle that produces, on average the same shower size) due to the large fluctuations which occur in the shower development.

Thus it would appear that the model of Dixon et al., inspite of the simplifying assumptions concerning the development of the NAP component is capable of reproducing the broad features of the NAPs above 1 GeV at sea level. It should be noted however, thatthere is evidence of the predicted absolute intensity of NAPs being too high and the slope of the NAP energy spectrum being too flat, with a low energy cut-off that is too high.

6-4. The Monitor Response in EAS of Energy 10^{17}eV

6-4.1 Introduction

In the previous section it has been established that a monitor placed in the Haverah Park EAS array should produce a significant yield of neutrons due to pions of energy a few GeV. Also, the variation of median pion energy appropriate to a multiplicity m, has been estimated for the NAP spectra calculated by Dixon et al..

It has been demonstrated that the model of Dixon et al. gives a reasonable description of the shapes of the NAP energy spectra at least above 10 GeV and the lateral distribution at sea level although the absolute intensity of NAPs may be overestimated. The model also indicates that the electron-photon component may give a considerable contribution to the neutron yield. However, the model suffers from the ignoring of low energy neutrons which could give a significant yield of evaporation neutrons in a monitor.

The uncertainty in absolute value of $\bar{m}$ for pions mentioned in section 6-2.1, further compounds the problems not only of estimating

the absolute intensity of NAPs but also the slope of their energy spectrum γ_1. However since the variation of $\bar{m}$ with energy for pions, neutrons and protons above 1 GeV should be similar, it would seem justifiable to use this model and the available information on neutron production by protons, to investigate the changes in the monitor response due to different NAP spectra at sea level due to fluctuations in development, and different primary particle masses.

This section attempts to answer the following questions for a variety of monitor designs.

(1) Given that $\bar{m}$ is expected to increase with smaller spectral slope γ_I can thedifferences in γ_I predicted by Dixon et al. for showers A - D be resolved with the likely statistical errors of $\bar{m}$ after collecting say, one year's data?

(2) What is the maximum energy of NAP about which information can be obtained from measurements of multiplicity distributions during one year?

(3) Can measurements of n, the neutron yield per shower, be used for either definitive measurements of, say, the degree of fluctuation of each shower, or giving useful information about the differences in say, the average fluctuations of different samples of showers?

The multiplicity distribution of detected neutrons $p(m;t,\epsilon f)$ attributable to distinct NAPs and the average number of detected neutrons per shower n attributable to all the NAPs incident simultaneously on the monitor have been calculated for the spectra of pions at sea-level in showers shown as A, B and C in figs. 6.4,5 and 6, resulting from primary protons of energy 10^{17}eV, and the spectra shown as D in the case of showers initiated by primary particles of mass $M_I = 56$, of the same energy.

Four basic designs of monitor were considered representing the combinations of two values of thickness (one and two NAP inelastic interaction lengths) and two values of efficiency (0.03 and 0.06); these are the sort of values which could be realised in practice using the IGY-and NM64 type monitors. The area of the monitor was assumed to be $10m^2$ in all cases. The results are summarised in Table 6.3

6-4.2 The Multiplicity Distribution

The multiplicity distributions corresponding to showers A and D each resulting from 100 showers falling 50m from the t = 2, ϵf = 0.06 monitor are shown in fig. 6.10. This sample of showers would require about one year to be collected using the Haverah Park array and therefore constitutes the typical size of statistical sample which may be investigated. It can be seen that the shape of the multiplicity distribution is not particularly sensitive to this large variation in primary mass and that the primary mass could not be identified even with the thick, high efficiency monitor, using one year's data and neglecting all systematic errors.

The effect on the multiplicity distributions of fluctuations in the proton induced shower is shown in fig. 6.11 where showers A, B and C have been assumed to fall 50m from the t = 2, ϵf = 0.06 monitor with relative frequencies 1.0 : 0.1: 0.1 respectively. These results show that the multiplicity distribution would be more able to reveal information about these fluctuations although not even the high efficiency/thick monitor would give results that approach statistical significance.

Define m_{max} for a given multiplicity distribution corresponding to a given NAP spectrum incident on a given monitor, as that multiplicity for which the expected number of events with multiplicity greater than m_{max} attributable to single NAPs per year, is say ten. Then the median

Table 6.3 The Neutron Yield per Shower (n) and Average Multiplicity ($\bar{m}$) - Summary of Results.

Design of Monitor: Thickness t (inel. int. length)			2		2		1		1	
Design of Monitor: Efficiency ϵf			0.03		0.06		0.03		0.06	
Shower Type	Radial Distance R (m)	Number of showers in sample	n	$\bar{m}$	n	$\bar{m}$	n	$\bar{m}$	n	$\bar{m}$
A	50	100	12±1.5	7.74±0.76	24±2.8	13.2±1.2	3.1±0.43	3.29± 0.30	6.2±0.82	5.50±0.51
B	50	10	8.5±4.1	7.91±3.1	17±7.4	13.5±4.6	2.2±1.1	3.31±1.2	4.3±2.2	5.56±2.1
C	50	10	21±6.2	7.12±1.6	43±11	12.2±2.5	5.9±1.8	3.20±0.68	12±3.5	5.32±1.1
D	50	100	15±1.7	7.73±0.69	30±3.1	13.2±1.0	3.8±0.47	3.28±0.27	7.6±0.91	5.49±0.46
A	100	100	0.80±0.35	6.32±2.2	1.6±0.65	11.0±3.5	0.24±0.12	3.13±1.0	0.49±0.22	5.21±1.7
B	100	10	0.58	6.48	1.2±1.8	11.3±81	0.17	3.16	0.35	5.26
C	100	10	1.4±1.4	5.85±5.8	2.8±2.6	10.2±9.1	0.45±0.49	3.05±3.9	0.89±0.93	5.05±5.5.
D	100	100	0.99±0.39	6.31±2.0	2.0±0.72	11.0±3.1	0.30±0.13	3.13±0.92	0.60±0.24	5.19±1.5
A	200	100	0.023	5.33	0.046	9.28	0.008	2.98	0.016	4.90
B	200	10	0.017	5.53	0.034	9.67	0.006	3.02	0.012	4.98
C	200	10	0.038	5.00	0.076	8.67	0.014	2.91	0.027	4.76
D	200	100	0.029	5.45	0.058	9.51	0.010	3.00	0.020	4.94

Note: All the errors quoted are the standard deviations resulting from the assumed sample sizes.

FIG. 6·10

The Detected Multiplicity Distribution due to NAP s in EAS.

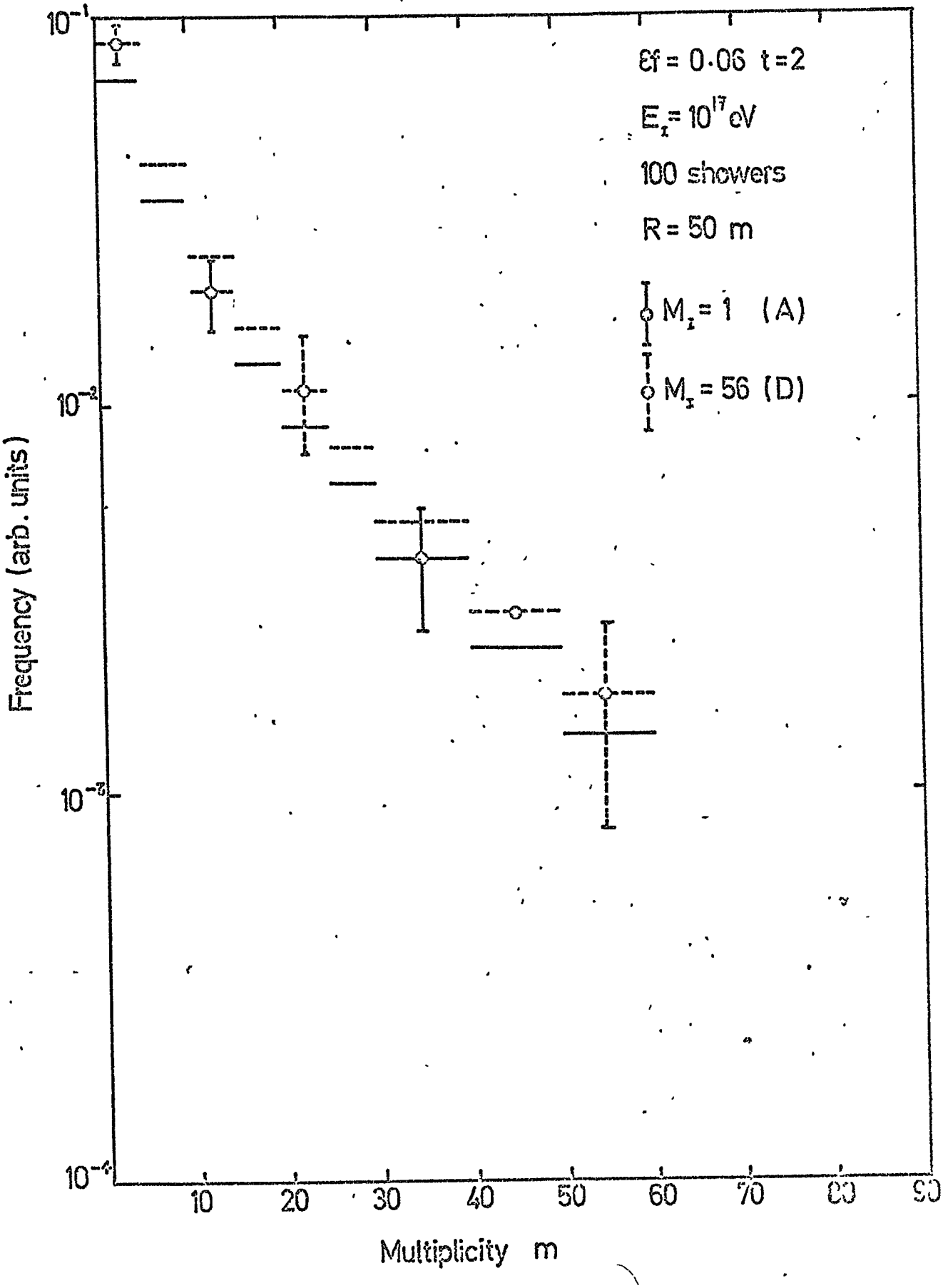

FIG. 6.11

The Detected Multiplicity Distribution due to NAP s in EAS.

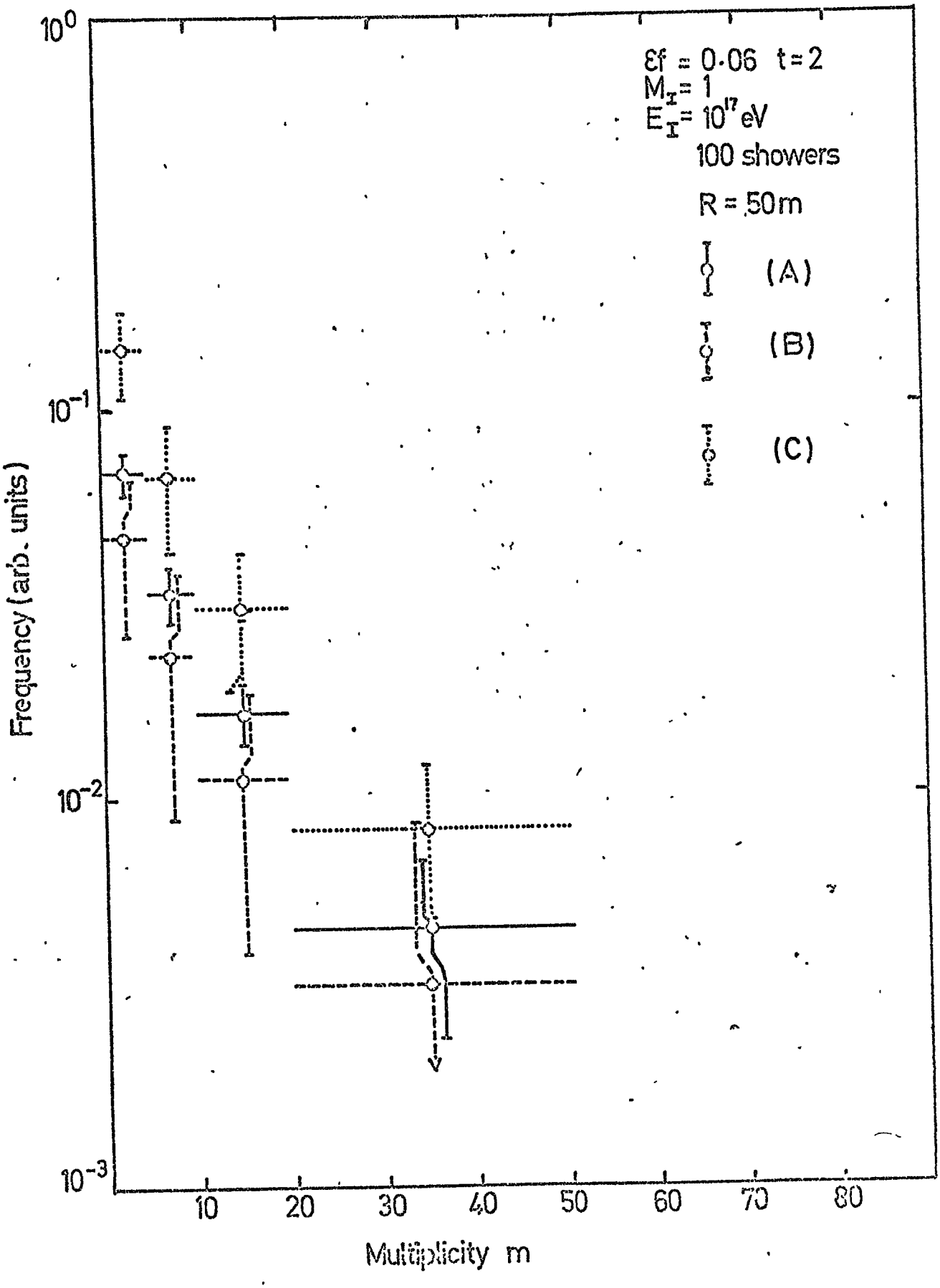

energy E_{max} corresponding to m_{max} is a measure of the maximum energy to which the multiplicity distribution is sensitive. Calculations indicate that E_{max} increases from $\sim$12 GeV to $\sim$20 GeV for an increase in thickness from t = 1 to 2, at both efficiencies, for spectrum A in fig. 6.4, corresponding to $m_{max} \approx 9$ for the t = 1, ϵf = 0.03 monitor and $m_{max} \approx 48$ for the t = 2, ϵf = 0.06 monitor.

The corresponding values of E_{max} for the different multiplicity distributions caused by fluctuations in the proton showers (curves C and B in fig. 6.4) are lower than this on account of the larger statistical errors, and are ~8 and $\sim$10 GeV respectively for the t $\doteq$ 1 and 2 monitors.

This it appears that the size of the statistical errors would limit the information about the shape of the energy spectrum of NAPs in these showers to energies less than 20 GeV. Further, the differences in spectral shape in this energy range predicted by Dixon et al. for the two primary masses and the fluctuations in development are too small to be resolved by the designs considered here.

The errors in $\bar{m}$ calculated for the four monitor designs can be used to estimate from fig. 6.1, the error in the slope of the integral NAP spectrum (assuming that the slope can be considered as constant over the sensitive energy range, 1 - 10 GeV or so) which gives the best fit to the multiplicity distribution recorded over one year ignoring potentially large systematic errors due to electron-photon contamination etc., assumptions about the neutron production spectrum (including the absolute value of $\bar{\nu}$) and the monitor efficiency. This error for the 50m spectrum is about $\pm$ 30% for all four designs considered here.

6-4.3 The Neutron Yield per Shower

The neutron yield per shower n, is slightly higher for shower

D than for shower A at all radial distances considered (see fig.6.12) reflecting the higher absolute intensity of pions (≥1 GeV) predicted by the model for the showers initiated by the heavy primary particles. However the errors are too large to enable definitive measurements to be made of individual showers to distinguish between the A and D spectra.

The neutron yield shows greater variations for the fluctuations in development of the showers initiated by primary protons (curves B and C in fig. 6.12) again reflecting the absolute intensity of pions above 1 GeV, but the standard deviations are still too large to enable definitive measurements.

The similarity in spectral shapes A-D causing arelatively constant mean measured multiplicity per incident NAP enables the neutron monitor to be used as a NAP density measuring device over a range of radial distances R from the shower core.

Rewriting equation 6.11, we have the number of NAPs per unit area above ~1 GeV given by

$$D = \frac{n}{\langle m \rangle A} = \frac{n}{\epsilon f \bar{\nu} i(t) A} \qquad 6.13$$

If we assume a single exponential production spectrum averaged over the sensitive energy range, then this becomes

$$D = \frac{n}{(\bar{m}-1) i(t) A}$$

Such an assumption may be justified given that the distributions in figs. 6.10 and 11 follow a reasonably straight line up to m_{max}, although this is partly because it was assumed in their derivation that $f(m,\bar{E}_s)$ (E_s averaged over a few GeV) was of this form. If this assumption is not found to be valid, it should be possible to obtain a meaningful estimate of D by extrapolating the detected multiplicity distribution back to zero (see fig. 4.2) thus obtaining the total number of interacting NAPs including those producing no detected

NUMBER OF NEUTRONS DETECTED PER SHOWER BY A $10m^2$ MONITOR

FIG. 6.12

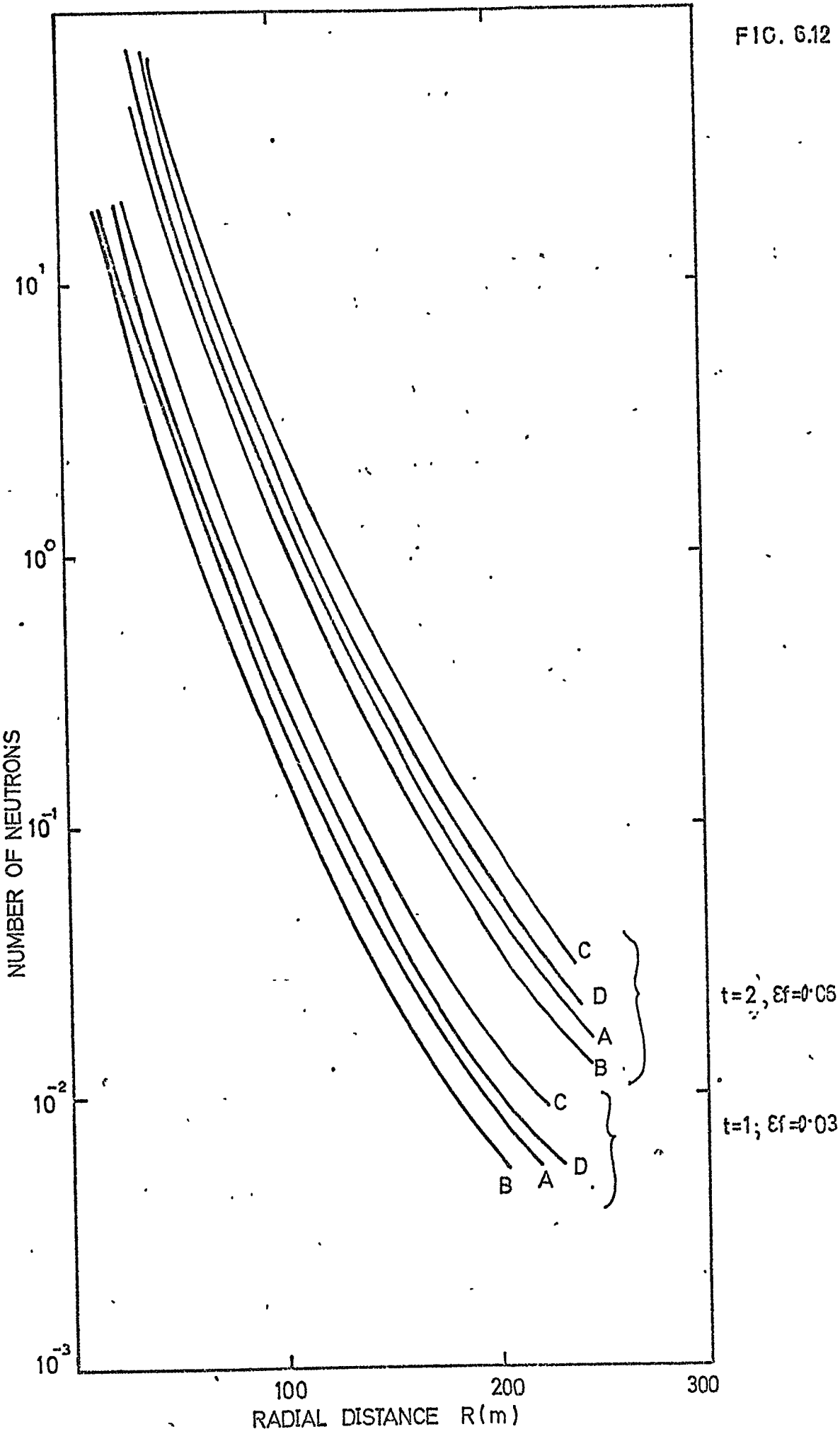

neutrons and hence $\langle m \rangle$.

If equation 6.13 is evaluated for samples of showers, of a given size, whose cores fall in various bands R, R + ΔR of radial distance from the monitor, the radial density distribution of NAPs will be obtained. The absolute intensity will be uncertain to the error in the form of the production spectrum averaged over all NAP energies contributing to n.

Thus, although the errors in n are too large to allow meaningful definitive measurements on individual showers, such an analysis on a sample of showers which is thought to have, say, developed late in the atmosphere, or be due to a heavy primary, can give an independent test of this hypothesis by the estimated relative changes in the NAP density. In particular, the results in table 6.3 indicate that the measured difference from the mean NAP density of the early and late developing showers at radial distances of about 50m would be statistically significant above the 50% level for all the monitors considered here, for the expected yearly sample sizes.

Of great importance at short radial distances ($\lesssim$ 50m) is the ability to identify neutrons from single NAP interactions (in order to evaluate $\langle m \rangle$)and to measure the position of the shower core accurately. At 50m, the probability of more than 1 NAP falling simultaneously on an area of $1m^2$ is about 10% for the shower represented by curve C in fig. 6.4 so that showers falling at distances less than this are liable to give a significant probability of producing "unresolved" neutrons. The core location accuracy is probably of even greater importance. From fig. 6.12 it can be seen that an error of $\pm$ 5m in core location (that expected from an "improved" Haverah Park array) leads to an error in n of 25% at 50m. The present array with its core location error ($\pm$ 25m) would lead to an error in n of about 100%

and would thus be of little use in NAP studies.

It has been demonstrated earlier that the model of Dixon et al. may be seriously in error in predicting the nucleon/anti-nucleon composition of the NAP component. Since the work of Grieder (1970) indicates that the shape of the NAP energy spectrum is rather insensitive to assumptions made about nucleon/anti-nucleon production, the average measured multiplicity $\bar{m}$ for NAPs should also be insensitive to these assumptions provided that the average multiplicity $\bar{\nu}$ produced by the various NAP components are very similar. Given that $\bar{\nu}$ has been assumed to be that measured for protons in the present work, and $\bar{\nu}$ for neutrons should be almost identical to that for protons above 1 GeV according to Shen (1968), the only additional source of uncertainty is due to the anti-nucleons which are present in slightly less numbers than the nucleons at sea level and about 15% of the total number of NAPs, according to Grieder. However, it would not be expected that an anti-nucleon annihilation reaction of a few GeV in the producer of a neutron monitor and producing a few pions with energy of about 1 GeV would result in a value of $\bar{\nu}$ very different to that resulting from an average strong interaction of a nucleon of the same energy. Therefore the effect on $\bar{m}$ of this modification in the EAS model would not be very great. However, if as suggested earlier, neutrons of energies less than 1 GeV give an important contribution to the NAP spectrum the predicted average measured multiplicity could become sensitive to the assumptions about anti-nucleon production because $\bar{\nu}$ for neutrons is considerably higher than that for protons or pions in this energy region.

In the absence of a model that takes account of this low energy component it is difficult to accurately estimate its effect. Certainly it would increase the total neutron yield and lower the average

multiplicity $\bar{m}$, in addition to reducing the statistical errors in these quantities, thus enabling the showers investigated here to be resolved more easily.

6-4.4 The Design of Monitor

As pointed out by Shen and Hatton, an increase in thickness t of producer will increase the sensitivity of the multiplicity distribution to changes in the NAP energy spectrum by making $\bar{\nu}$ a more rapidly changing function of energy and will also bias the monitor towards higher NAP energies.

The results in table 6.3 confirm that the thicker monitor is more able to resolve the differences in $\bar{m}$ between the various spectra and show that the corresponding increase in efficiency has less effect. Also, the high energy bias has been demonstrated in section 6-4.2 where it was found that a t = 2 monitor would respond to NAPs up to about 20 GeV compared with 12 GeV for the t = 1 monitor. An increase in t also increases the probability of an NAP's detection by increasing both the probability i (t) of its interacting and (by increasing $\bar{\nu}$) the probability of it s producing at least one detected neutron. All these factors are important if the monitor is to be used as an energy spectrometer based upon multiplicity measurements. Even when the monitor is only to be used as an NAP detector, the increase in detection probability of a thicker monitor is to be desired also. The upper limit of t = 2 (chosen in this work because of the lack of calculations of $\bar{\nu}(E_s)$ for thicknesses greater than this) would therefore appear to be highly desirable.

An increase in thickness of the producer of a conventional IGY type monitor from t = 1 to 2 would reduce the monitors efficiency through the reduction in solid angle subtended by the counter/moderator to the producer, unless the monitor were designed to compensate for this by increasing the number of counters.

An obvious alternative method of increasing t is to place two monitors on top of each other; in this way the t = 2, ϵf = 0.06 design parameters could be approached using two NM64 monitors.

In order to maintain the spatial resolving power of the monitor, it would be necessary to individually hodoscope the counters as in the DIGY monitor described in this work. It was shown in fig. 4.1 that a negligible number of neutrons were detected 40cm beyond the point of interaction measured across the monitor, so that it is feasible to expect a resolution of 1 m^2 by accepting neutrons from any, say, five adjacent counters.

In view of the fact that the electron-photon component of EAS can give rise to considerable neutron production, it is important to take steps to minimise it s effect. Approximate calculations have been made of the neutron yield due to electrons and photons in a 10^{17}eV shower at various distances from the shower core of a monitor protected by a layer of lead of thickness 10 radiation lengths (5cm). The calculations of Messel and Crawford (1969) give the yield of secondary electrons and photons of various energies at various depths of absorber for various energies of incident electrons and photons. These have been used, weighted with the incident spectra calculated by Dixon et al. and measured by Kellerman and Towers to obtain the residual flux of electrons and photons of various energies emerging beneath the absorber. The resulting neutron yield from secondary electrons and photons has then been estimated assuming approximate values for the track length of photons (produced by secondary electrons) and the photonuclear cross-section-neutron multiplicity product. It was found that the neutron yield due to electrons and photons fell to less than 0.2% of that calculated for the unshielded monitor for all core distances, and that this resulting

yield was due to 10-20 MeV photons produced by 200-500 MeV incident electrons and photons. This indicates that in practice a smaller amount of absorber would be sufficient to reduce the effect of electrons and photons, and that the outer thermaliser-reflector may in some cases be sufficiently thick to serve the purpose. In the case considered above, the NAP flux would be reduced by the absorber by less than 25%.

6-5 Conclusions

The results of calculations have shown that the expected neutron yield in a $10m^2$ monitor of established design, due to 10^{17}eV showers recorded for example by the Haverah Park array in one year is too small to enable the measured multiplicity distribution to be used to resolve the differences in shape of the NAP energy spectra in showers predicted by Dixon et al. for two widely differing primary particle masses, and for the fluctuations in development expected if the primaries are protons.

It has also been shown that the total neutron yield per shower for these monitors of surface area $10m^2$, cannot be used for meaningful definitive measurements of individual showers due to the large statistical errors. However, this yield per shower, measured over a number of showers, can be used in conjunction with the measured multiplicity distribution to measure the NAP density changes at various distances from the core caused by the fluctuations in development of proton initiated showers and could assist in identifying the mass of the primary particle that initiates the showers.

Further, the response of a monitor could also give significant information about the accuracy of various EAS models such as the one used here, by measuring the absolute NAP flux and the slope of

the integral energy spectrum in this region to within a statistical error of 30%, although uncertainties in the neutron production spectrum of pions will increase the systematic uncertainties in both quantities.

In particular, the prediction of the present model that there is a negligible flux of NAPs below 1 GeV could be tested. Any such flux would tend to raise the neutron yield per shower whilst lowering the average multiplicity.

The calculations have confirmed that an increase in the monitor's producer thickness improves the energy resolution but that the high density of NAPs in 10^{17}eV showers requires individual hodoscoping of the counters, and a small amount of absorber ($\sim$10 radiation lengths of lead) may be necessary to remove the effects of the electron-photon component.

CHAPTER SEVEN

SUGGESTIONS FOR FURTHER WORK

7-1 The Mechanism of Neutron Production

The results of the present work demonstrate that it is only possible to reconcile the theoretically predicted response of a monitor to protons and pions with that measured, by making a number of fairly critical assumptions relating to intra-nuclear cascade theory, interaction mean free paths, and the energy and number spectra of evaporation particles produced in the monitor, particularly above about 10 GeV where the derivation of the response of the monitor is based on a relatively crude extrapolation from results of emulsion experiments.

This implies two important points.

(a) At the present time, experiments to investigate nuclear physics problems using monitors are bound to give limited information compared with "thin target" experiments such as that of MacDonald et al. (1965) using controlled beams of particles incident on devices with high neutron detection efficiencies, which are relatively insensitive to the neutron energy, and where extra-nuclear cascade effects can be ignored.

(b) For meaningful interpretation of certain neutron monitor measurements of a given cosmic ray component it will be necessary to have a sound empirical knowledge of the response of the monitor to that component. For example, in EAS work the lack of information on neutron production by pions is a particular problem. If monitors were to be used for accurate measurements of, say, the shape of the NAP energy spectrum, it would be necessary to calibrate them in a beam of pions with various energies at an accelerator machine.

7-2 The use of monitors in EAS - Calculations

Although the results of the present work indicate that the use of a monitor to measure changes in the shape of the NAP energy spectrum in large EAS may not yield fruitful results, there remains the possibility that

(a) this conclusion is significantly in error because of errors in the model of the development of EAS (particularly at low NAP energies) and (b) in smaller EAS there may be more favourable conditions for the use of a monitor in this way (in that the statistical errors associated with the more frequent showers are likely to be smaller than those found in the present work).

This would suggest that further work needs to be carried out on deriving the very low energy NAP component in EAS both large and small, and incorporating the interaction of this component with the monitor in a similar way to the method of Hatton (1971) in deriving the total counting rate of monitors, and possibly in accordance with the philosophy of Hillas (1970) in deriving the monitor response as part of the EAS calculation. An important ingredient in any such treatment would be a realistic treatment of the interaction of the electron-photon (and possibly muon) component with the monitor.

Although neutron monitors have been used extensively for NAP detection in EAS there appears to be conflicting information about the nature and energy of the detected NAPs, and of the effect of the electron-photon component, thus limiting the usefulness of the results of such work. It would be hoped that measurements of the multiplicity distribution could, in conjunction with the theoretical approach mentioned above, help the development of a clearer understanding of the NAP component at low energies.

7-3 The Use of Monitors in EAS - Experimental Work

It has been demonstrated that even in the absence of such detailed knowledge, a monitor could be used to help identify fluctuations in the NAP flux due to the shower development, providing that the shape of the NAP energy spectrum remains more or less constant (as appears to be the case from calculations in large EAS) so that the uncertainty in the NAP energy is relatively unimportant. This suggests that an experimental study along these lines could give useful results even in the absence of more refined modelling techniques.

Compared with other NAP detectors, neutron monitors are simple to build, and can be operated for long periods with minimal attention; and these factors may offset their lack of energy resolution. Recent work by Quang et al.(1973)demonstrates that the use of a form of concrete (made of SiO_2) to act as both producer and thermaliser in monitors may offer a cheaper alternative to the more usual materials, a factor of great importance when trying to cover large areas within an EAS array.

REFERENCES

Allkofer, O.C. and Andresen, R.D., (1968), Nucl. Phys. B8, 402.

Allkofer, O.C., Carstensen, K. and Dau, W.D., (1971), Proc. 12th Int. Conf. on Cosmic Rays, Hobart, 4, 1314.

Antipov, Yu. M., et al. (1971), Phys. Letters, 34B, 2, 164.

Baba, H., (1970), Nucl. Phys. A, 159, 625.

Barashenkov, V.S., Maltsev, V.M. and Mikhul, E.K., (1961), Nucl. Phys., 24, 642.

Barashenkov, V.S. and Abdinov, O.B., (1969), Joint Institute for Nuclear Research Report No. JINR-P2-4568. (Unpublished).

Barashenkov, V.S., Gudima, K.K., and Toneev, V.D., (1970), Sov. J. Nucl. Phys., 10, 436.

Barashenkov, V.S., Ilinov, A.S. and Toneev, V.D., (1971), Sov. J. Nucl. Phys., 13, 422

Barrett, P.H., Bollinger, L.M., Cocconi, G., Eisenberg, Y. and Greisen, K., (1952), Rev. Mod. Phys. 24, 133.

Barton, J.C. and Gaines, P.J., (1970), Proc. 11th Int. Conf. on Cosmic Rays, Acta, Phys. Hung. 29, Suppl. 4, 411.

Bathow, G. et al. (1966), DESY, report No. 66/13.

Bercovitch, M., Carmichael, H., Hanna, G.C. and Hincks, E.P., (1960), Phys. Rev., 119, 412.

Bergamasco, L., (1970), Nuovo Cim. B, 66, 120.

Bergamasco, L., Costa, S., and Picchi, P., (1973), Nuovo Cim. A, 13 403.

Bertini, H.W., (1963), Phys. Rev. 131, 1801.

Bertini, H.W., (1965), Phys. Rev. 138, AB2

Bertini, H.W., (1969), Phys. Rev. 188 , 1711

Bertini, H.W., and Guthrie, M.P., (1971), Nucl. Phys. A,169, 670.

Bertini, H.W., (1972), Phys. Rev. C, 6, 631.

Böhm, E, Fritze, R., Roose, J.U., Samorski, M., Staubert, R., and Trümper, J., (1970), Act. Phys. Hung., 29, Suppl. 3, 487.

Brooke, G. and Wolfendale, A.W., (1964), Proc. Phys. Soc. 83, 843.

Caldwell, D.O., Elings, V.B., Heese, W.P., Jalm, G.E., Morrison, R.J., Murphy, F.V. and Yount, D.E., (1969), Phys. Rev. Letters, 23, 1256.

Castagnoli, C., Picchi, P. and Srimaglio, S., (1967), Nucl.Phys., 87, 641.

Chatterjee, B.K., Murthy, G.T., Naranan, S., Sreekantan, B.V., Srinivasa, M.V., (1963), Proc. 8th Int. Conf. on Cosmic Rays, Jaipur, 4, 227.

Cocconi, G., Cocconi-Tongiorgi, V. and Widgoff, M., (1950), Phys. Rev., 79, 768.

Cocconi, G. and Cocconi-Tongiorig, V., (1951), Phys. Rev., 84, 29.

Coxell, H. and Wolfendale, A.W., (1961), Nuovo Cim., 21, 7.

Daiyasu, K., Kobayakawa, K., Murota, T. and Nakano, T., (1962), J. Phys. Soc. Japan, 17, 344.

Danilova, T.V., Denisov, E.V. and Nikol'ski, S.I., (1964), Sov. Phys. (JETP), 19, 1056.

De Pagter, J. and Sard, R.D. (1960), Phys. Rev., 118, 1353.

Diggory, I.S., Dixon, H.E., Earnshaw, J.C., Hook, J.R., Jenkins, I.A., Maslin, G.C., O'Donnell, B.D., Orford, K.J., and Turver, K.E., (1971), Proc. 12th Int. Conf. on Cosmic Rays, Hobart, 3, 1236.

Dixon, H.E., Jenkins, I.A., Mamidzhanian, A.E., Maslin, G.C$_R$, and Turver, K.E., (1971), Proc. 12th Int. Conf. on Cosmic Rays, Hobart, 4, 1643.

Dixon, H.E., Earnshaw, J.C., Hook, J.R., Hough, J.J., Smith, G.J., Stephenson, W., and Turver, K.E., (1973), To be published in the Philosophical Transactions of the Royal Society.

Dixon, H.E., Turver, K.E., and Waddington, C.J., (1973). To be published in the Philosophical Transactions of the Royal Society.

Dixon, H.E., and Turver, K.E., (1973), To be published in the Philosophical Transactions of the Royal Society.

Dostrovsky, I., Rabinowitz, P., and Bivins, R., (1958), Phys. Rev. 111, 1659.

Evseev, V., Kozlowski, T., Roganov, V., and Woitkowska, J., (1970), Proc. of the 3rd Int. Conf. on high energy Physics and nuclear structure, New York, U.S.A., 157.

Fenton, A.G., Fenton, K.B., and Rose, D.C., (1958), Canad. J. Phys., 36, 824.

Fraser, J.S., Green, R.E., Hilborn, J.W., Milton, J.C.D., Gibson, W.A., Gross, E.E., and Zucker, A., (1965), AED-CONF-65-288-9.

Gardener, M., Jones, D.G., Taylor, F.E., and Wolfendale, A.W., (1962)., Proc. Phys. Soc., 80, 697.

Geiger, K.W., (1956), Canad. J. Phys. 34, 288

George, E.P. and Evans, J., (1950), Proc. Phys. Soc. A, 63, 1248.

Giacomelli, G., (1970), Progress in Nuc. Phys., 12, 2, 77.

Gilat, J. and Grover, J.P., (1971), Phys. Rev. C, 3, 734.

Gorshkov, G.V. and Zyabkin, V.A., (1971), Sov. J. Nucl. Phys., 12, 187.

Gorshkov, G.V., Zyabkin, V.A., and Yakovlen, R.M., (1971), Sov. J. Nucl. Phys., 13, 450.

Greisen, K., (1960), Ann. Rev. Nucl. Sci., 10, 63.

Grieder, P.F.K., (1970), Acta. Phys. Hung., 29, Suppl. 3, 563-568.

Hagge, D.E., Baijal, J.S., Diaz, J.A., Kaplan, S.N., and Pyle, R.V., (1964), Bull. Am. Phys. Soc., 9, 725.

Harding, J.F., Lattimore, S. and Perkins, D.H., (1949), Proc. Roy. Soc. A, 196, 325.

Harman, C.V. and Hatton, C.J., (1968), Canad. J. Phys. 46, S1052.

Hatton, C.J., (1971), Prog. in Elem. Part. and Cosmic Ray Phys. X, 1.

Hatton, C.J. and Carmichael, H., (1964), Canad. J. Phys. 42, 2443.

Hatton, C.J. and Tomlinson, E.V., (1968), Nuovo Cim. B, 53, 63.

Hayman, P.J. and Wolfendale, A.W., (1962), Proc. Phys. Soc., 80, 710.

Hess, W.N., (1959), Annals, of Phys., 2, 115.

Hicks, D.A., Ise, J., and Pyle, R.V., (1956), Phys. Rev., 101, 1016.

Hillas, A.M. (1970), Acta. Phys. Hung., 29, Suppl. 3, 344.

Hodgson, R.J.W., Murdoch, H.S., and Rathgeber, H.D., (1968), Can. J. Phys., 46, 373.

Hook, J.R., Maslin, G.C, Orford, K.J., and Turver, K.E., (1970), Acta. Phys. Hung., 29, Suppl. 3, 475.

Hook, J.R., Jenkins, I.A., and Turver, K.E., (1971), Proc. 12th, Int. Conf. on Cosmic Rays, Hobart, 4, 1429.

Hook, J.R., (1972), Ph.D Thesis, University of Durham. U.K.

Hughes, E.B., (1961), Ph.D. Thesis, University of Leeds, U.K.

Hughes, E.B., Marsden, P.L., Brooke, G., Meyer, M.A., and Wolfendale, A.W., (1964), Proc. Phys. Soc., 83, 239.

Hughes, E.B., and Marsden, P.L., (1966), J. Geophys. Res., 71, 1435.

Jameel, M., (1965), Nuovo Cim., 36, 1066.

Kaplan, S.N., Moyer, B.J., and Pyle, R.V., (1958), Phys. Rev., 112, 968.

Kellermann, E.W. and Towers, L., (1970), J. Phys. A, 3, 284-295.

Kessler, P., (1960), Nuovo Cim., 17, 809.

Kodama, M. and Ohuchi, T., (1968), Canad. J. Phys., 46, S1090.

Le Couteur, K.J., (1950), Proc. Phys. Soc., A, 63, 259.

Le Couteur, K.J., (1952), Proc. Phys. Soc., A, 65, 718.

Machin, A.C., (1972), Ph.D Thesis, University of Durham, U.K.

McDonald, B., Diaz, J.A., Kaplan, S.N., and Pyle, R.V., (1965), Phys. Rev., 139, 5B, 1253.

Messel, H. and D.F. Crawford, (1969), Electron Photon Shower Distribution Tables, Pergamon Press Ltd.

Metropolis, N., Bivins, R., Storm, M., Turkevich, A., Miller, J.M., and Freidlander, G., (1958a), Phys. Rev., 110, 185.

Metropolis, N., Bivins, R., Storm, M., Miller, J.M., Freidlander, G., and Turkevich, A., (1958b), Phys. Rev., 110, 204.

Meyer, H., Teucher, M.W. and Lohrmann, E., (1963), Nuovo Cim., 28, 1399.

Meyer, M.A., Wolfendale, R.W., Hughes, E.B., and Marsden, P.L., (1964), Proc. Phys. Soc., 83, 253.

Nobles, R.A., Alber, R.A., Hughes, E.B., Newkirk, L.L. and Walt, M., (1967), J. Geophys. Res., 72, 3817.

Nobles, R.A., Hughes, E.B. and Wolfson, C.J., (1969) J. Geophys. Res., 74, 6459

Newton, T.D., (1956), Canad. J. Phys., 34, 804.

Osborne, A.R., Abdel-Monem, M.S., Benbrook, J.R., Sheldon, W.R., Duller, N.M., and Green, P.J., (1973), 13th Int. Conf. on Cosmic Rays, Denver, 3, 2042.

Owen, B.G. and Wilson, J.G., (1951), Proc. Phys. Soc. A, 64, 417.

Pearce, R.M. and Fowler, A.G., (1964), J. Geophys. Res., 69, 4451.

Powell, C.F., Fowler, R.H., Perkins, D.H., (1959), "The Study of Elementary Particles by the Photographic Method", (London).

Primakoff, H., (1955), Proceedings of the 5th Rochester Conference, 174.

Quang, T.T., Fenton, A.G., and Fenton, K.B., (1973), Proc. 13th Int. Conf. on Cosmic Rays, Denver, 4, 2796.

Ramamurthy, V.S., Kapoor, S.S., Kataria, S.K., (1970), Phys. Rev., Letters, 25, 386.

Roos, C.E., and Peterson, V.Z., (1961), Phys. Rev., 124, 1610.

Rossi, B., (1956), High Energy Particles (New York: Prentice Hall Inc.)

Serber, R., (1947), Phys. Rev., 72, 1114.

Shen, M.L., (1967), Nucl. Phys., B, 3, 77.

Shen, M.L., (1968), Suppl. Nuovo Cim., 4, 1177.

Simpson, J.A., (1948), Phys. Rev., 73, 1389.

Simpson, J.A., (1949), Echo Lake Conf. on Cosmic Rays, 175.

Simpson, J.A., Fonger, W., and Treiman, S.B., (1953), Phys. Rev., 90, 93.

Simpson, J.A., (1957), Ann. IGY., (London:Pergamon Press), part VII.

Skyrme, D.M., (1962), Nucl. Phys. 35, 177.

Tanahashi, G., (1970), Private communication to P.F.K. Grieder (1970).

Tennent, R.M., (1960), Prog. in Cosmic Ray Physics, V, 367.

Tennent, R.M., (1968), Can. J. Phys., 46, 1.

Treiman, S.B. and Fonger, W., (1952), Phys. Rev., 85, 364.

van Staa, R., Aschenbach, B., Böhm, E., and Cachon, A., (1973), Proc. 13th Int. Conf. on Cosmic Rays, Denver, 4, 2676.

Vasil'kov, R.G., Govorkov, B.B., Goldanskii, V.J., Kon'shin, V.A., Lupandin, O.S., Matusevich, E.S., Pimenov, B.A., Prokhorov, S.S., and Tsypin, S.G., (1968), Sov. J. Nucl. Phys., 7, 64.

Webber, W.R., (1962), Prog. in Elem. Part. and Cosmic Ray Physics, VI, 77.

Weisskopf, V.F., (1937), Phys. Rev., 52, 295.

West, D. and Wood, E., (1971), Canad. J. Phys., 49, 15, 2061.

Wheeler, J.A., (1949), Rev. Mod. Phys., 21, 133.

A C K N O W L E D G E M E N T S

Many people have contributed in some way to the production of this thesis including Professor G.D. Rochester F.R.S. who provided the laboratory facilities of the physics department; Dr. K.E. Turver, who as my supervisor has given valued guidance; Messrs. A.M. Bevils, J. Blackburn, I.S. Diggory, H. Davison, H.E. Dixon, J.C. Earnshaw, J.R. Hook, W. Leslie, K.J. Orford, T. Richardson and N.S. Storer who as colleagues played various invaluable and mainly arduous roles; and Mrs. D.A. Anson for the typing.

All of the above mentioned people are sincerely thanked.

The work was funded by a Science Research Council research studentship.